PHYSICAL AND BIOLOGICAL PROPERTIES OF SYNTHETIC POLYCATIONS IN ALGINATE CAPSULES

PHYSICAL AND BIOLOGICAL PROPERTIES OF SYNTHETIC POLYCATIONS IN ALGINATE CAPSULES

By RACHELLE MELANIE KLEINBERGER, B.Sc.

A Thesis Submitted to the School of Graduate Studies in Partial Fulfillment of the Requirements for the Degree Doctor of Philosophy of Science

McMaster University DOCTOR OF PHILOSOPHY OF SCIENCE (2017) Hamilton, Ontario (Chemistry and Chemical Biology)

TITLE: Physical and Biological Properties of Synthetic Polycations in Alginate Capsules

AUTHOR: Rachelle Melanie Kleinberger, B.Sc. (McMaster University)

SUPERVISOR: Professor Harald D. H. Stöver

NUMBER OF PAGES: xxvii, 218

Lay Abstract

The treatment of enzyme deficiency disorders by cell transplantation is limited by the immune attack of foreign tissue in absence of immunosuppressants. Cells protected in an encapsulation device has shown promise. Poly-L-lysine, a widely used membrane material in these protective capsules, binds to the anionic gel entrapping living cells because it is highly cationic. The high cationic charge is difficult to hide causing the immune system to build tissue around the capsule, preventing the encapsulated cells from exchanging nutrients and therapeutic enzymes. This thesis aims to replace poly-L-lysine by synthesizing a series of more biocompatible materials of decreasing cationic charge. These materials were studied for the ability to support tissue growth and form stable capsules. The membrane strength was measured using an aspiration method validated for these types of capsules. Reducing the cationic charge of the materials increased the biocompatibility of the capsule membrane but also made for weaker membranes.

Abstract

The use of cell transplantation to treat enzyme deficiency disorders is limited by the immune response targeted against foreign tissue or the use of life-long immunosuppressants. Hiding cells from the immune system in an encapsulation device is promising. Cells encapsulated within an anionic calcium alginate hydrogel bead are protected through a semi-permeable membrane formed by polycation, poly-L-lysine (PLL). A final layer of alginate is added to hide the cationic PLL surface but this has proved to be difficult creating capsules which are prone to fibrotic overgrowth, blocking exchange of nutrients, waste and therapeutic enzymes through the capsule. For long term applications these capsules need to be both biocompatible and mechanically robust.

This thesis aims to address the biocompatibility issue of high cationic surface charge by synthesizing polycations of reduced charge using N-(3-aminopropyl)methacrylamide hydrochloride (APM) and N-(2-hydroxypropyl)methacrylamide (HPM) and study the associated mechanical properties of the capsules using micropipette aspiration. Micropipette aspiration was applied and validated for alginate based capsules (gel and liquid core) to quantify stiffness.

Varying ratios of APM were used to control the overall charge of the polycations formed while HPM was incorporated as a neutral, hydrophilic, nonfouling comonomer. The molecular weight (MW) was controlled by using reversible addition-fragmentation chain transfer (RAFT) polymerization. The biocompatibility of these polymers was tested by cell adhesion and proliferation of 3T3 fibroblasts onto APM/HPM copolymer functionalized surfaces and by solution toxicity against C2C12 myoblasts. The ability for

the APM/HPM copolymers to bind to alginate and form capsules was also assessed, along with the integrity and stiffness of the capsule membrane with or without additional covalent cross-linking by reactive polyanion, poly(methacrylic acid-co-2-vinyl-4,4-dimethylazlactone) (PMV60).

Thermo-responsive block copolymers of N-isopropylacrylamide (NIPAM) and 2-hydroxyethylacrylamide (HEA) were also synthesized as potential drug delivery nanoparticles, showing control over micelle morphology with varying NIPAM to HEA ratios.

Acknowledgements

I would like to express my endless gratitude to my supervisor, Professor Harald D.H. Stöver. He has been such a great mentor and leader, giving me support, guidance and many opportunities to reach my potential. He has influenced the scientist I am today, which is not limited to my research capabilities/experience but he has also nurtured my professional development and personal growth. Thank you for your encouragement and advice in all those pursued opportunities. I really appreciate being a member of your group.

I would also like to thank my committee members Dr. Kari Dalnoki-Veress and Dr. Michael Brook for their enthusiasm and valuable insight towards my project. Thanks for enriching my knowledge of polymer physics and chemistry and being positive coaches.

I thank past and current group members for their friendship and support. Thank you Padraic Foley, Dr. Jeffrey Li, Dr. Jafar Mazumdar, Dr. Casandra Gardner, Sara Mohajeri, Jennifer Anderson, Samantha Ros, Alison Stewart, Jing Zhao, Yuqing Zhao, Christal Zhou, Sheilan Sinjari, Shanna Shi and Allison Abdilla. I would also like to kindly thank Dr. Nick Burke for his constant encouragement, advice and teaching moments about technical lab work, experimental design and fundamental polymer chemistry. Thank you for all the time you have taken to help me and answer countless amounts of questions. It has been a privilege to work with you.

I would like to thank the members of the NSERC CREATE-IDEM program for their helpful advice, consultations and bringing a new perspective. I would also like to thank the NSERC CREATE-IDEM and Discovery Grants for funding.

Thank you to Marnie Timleck and Marcia Reid in the electron microscopy facility for showing me how to troubleshoot microscope issues and sample preparation. I would also like to thank Drs. Gonzalo Hortelano, Heather Sheardown and Todd Hoare for access to their facilities and equipment, allowing me to expand my research in cell-polymer interactions and thermo-responsive polymer self assembly.

I thank all my friends for their support and friendship but especially Samantha Ros for being there to listen and make working after hours more fun and less lonely. I would like to thank my parents, Gottfried and Remy Kleinberger, for their loving support (emotional and financial), raising me and making sure I never was hungry. My brother Friedi Kleinberger, thanks for being interested (or at least pretending to be interested) whenever I talked about my work. A warm thank you to Adam Leontowich for his encouragement, love, patience, and being someone I could rely on while I achieve my goals.

Table of Contents

List of Figures

Chapter 1

Chapter 2

List of Schemes

List of Tables

List of all Abbreviations and Symbols

Abbreviations

2 h	2 hour gelling bath wash
2 m	2 minute gelling bath wash
AA	Acrylic acid
A beads	Calcium alginate beads
ACN	Acetonitrile
ADH	Adipic acid dihydrazide
AIBN	Azobisisobutyronitrile
AF	Aminofluorescein
AFM	Atomic force microscopy
ANOVA	Analysis of variance
AP	Alginate-PLL
APA	Alginate-PLL-alginate
APM	N-(3-aminopropyl)methacrylamide hydrochloride
APTES	3-aminopropyltriethoxysilane
ATRP	Atom transfer radical polymerization
BCS	Bovine calf serum
CaAlg	Calcium alginate
CHES	(N-cyclohexyl-)2-aminoethanesulfonic acid
CTA	Chain transfer agent
CTP	4-cyanopentanoic acid dithiobenzoate
DLS	Dynamic light scattering
DMA	Dimethylacrylamide

DMEM	Dulbecco's modified eagle's medium
DMP	2-(dodecylthiocarbonothioylthio)-2-methylpropionic acid
DMPA	2,2-dimethoxy-2-phenylacetophenone
DP	Degree of polymerization
EDC	1-ethyl-3-(3-(dimethylamino)-propyl)carbodiimide
EDTA	Ethylenediaminetetracetic acid
FBR	Foreign body response
FBS	Fetal bovine serum
FITC	Fluorescein isothiocyanate
G	Guluronic acid
GPC	Gel permeation chromatography
GS	Washing procedure to AP capsules first with gelling bath, then saline
HEA	2-hydroxyethylacrylamide
HEPES	4-(2-hydroxyethyl)piperazine-1-ethanesulfonic acid
HPM	N-(2-hydroxypropyl)methacrylamide
ICP-MS	Inductively coupled plasma mass spectrometry
kDa	Kilodalton
kPa	Kilopascal
LCST	Lower critical solution temperature
M	Mannuronic acid
MAA	Methacrylic acid
MEHQ	Monomethyl ether hydroquinone
MES	2-(N-morpholino)ethanesulfonic acid sodium salt
MW	Molecular weight

MWCO	Molecular weight cut-off
NIPAM	N-isopropylacrylamide
NMR	Nuclear magnetic resonance
$pAPM_{X-Y}$	Poly(APM-co-HPM) where X represents the mol% of APM and Y is the MW in kDa
$pAPM_{X}r$	RbITC labeled poly(APM-co-HPM)
PBS	Phosphate buffered saline
PDADMAC	Poly(diallyldimethylammonium chloride)
PDI	Polydispersity index
PDL	Poly-D-lysine
PEC	Polyelectrolyte complex
PEG	Polyethyleneglycol
PEI	Poly(ethylenimine)
PEO	Polyethylene oxide
PLL	Poly-L-lysine
PLL*f*	FITC labeled PLL
PLL*r*	RbITC labeled PLL
PLO	Poly-L-ornithine
PMCG	Polymethylene-co-guanidine
PMM	Poly(methyl vinyl ether-*alt*-maleic anhydride)
PMV0	Fully hydrolyzed PMV60
PMV60	Poly(MAA-co-VDMA), containing ~60% VDMA
PMV60*f*	Aminofluorescein labeled PMV60
PVA	Polyvinylalcohol

PVAm	Polyvinylamine hydrochloride
RAFT	Reversible addition-fragmentation chain transfer
RbITC	Rhodamine B isothiocyanate
SS	Washing procedure to AP capsules of 2 consecutive saline washes
*t*BA	*Tert*-butyl acrylate
TEM	Transmission electron microscopy
THPC	Tetrakis(hydroxymethyl)phosphonium chloride
TNF-α	Tumor necrosis factor - alpha
TRP	Temporarily reactive polyanion
UP MVG	Ultra pure medium viscosity high G
V-501	4,4'-azobis(4-cyanopentanoic acid)
VDMA	2-vinyl-4,4-dimethylazlactone
WHO	World Health Organization

Symbols

α	PLL polymerized by reaction of the amino group on the α carbon of lysine (In this thesis, this form of PLL can be assumed when α is not specified)
Ɛ	PLL polymerized by reaction of the amino group on the Ɛ carbon of lysine
n	Number of replicates
M_n	Number average molecular weight
M_n^{theo}	Theoretical number average molecular weight
$[M]_o$	Initial monomer concentration
$[I]_o$	Initial initiator concentration
$[CTA]_o$	Initial chain transfer agent concentration
MW_{CTA}	Molecular Weight of the chain transfer agent
MW_m	Molecular weight of the monomer
x	Length of tongue drawn into the pipette
x_o	Length of tongue protruding into the pipette if the applied pressure differential is 0
P_1	Pressure inside the micropipette
P_2	Pressure of the suspending medium
T	Membrane/surface tension
R_p	Inner radius of the micropipette
R_c	Radius of the microcapsules
ΔP	Pressure differential $(P_2 - P_1)$
E	Young's modulus
Φ	Wall function
ΔV	Volume change

Declaration of Academic Achievement

Chapters 2-5 of this thesis include research projects containing multiple authors. The contributions of my work to each of these chapters are declared below.

Chapter 2

I, Rachelle M. Kleinberger (RMK) designed the experiments with guidance from Dr. H. D. H. Stöver (HDHS) and Dr. N. A. D. Burke (NADB). RMK performed all the experiments except the determination of Ca^{2+} concentration by ICP-MS, which was determined by Kevin Ferguson in the Occupational and Environmental Health Laboratory. RMK processed the data using suggestions from Dr. K. Dalnoki-Veress (KDV). RMK analyzed the data and wrote the manuscript. Edits to the manuscript were performed by NADB, KDV and HDHS.

Chapter 3

RMK designed the work for this chapter with help from NADB and HDHS. RMK performed all experiments. Christal Zhou (CZ) helped perform the cell attachment and proliferation studies under RMK's supervision. RMK processed and analyzed the data, as well as wrote the manuscript. Edits to the manuscript were provided by NADB and HDHS for publication.

Chapter 4

RMK designed the work for this chapter with help from NADB and HDHS. PMV60 was designed and developed by Dr. Casandra M. Gardner and the modified

procedure which RMK used was developed by NADB and Shivanthi Sriskandha. Some of the batches of PMV60 were provided by Shivanti, while other batches were provided by RMK. RMK performed all other experiments. RMK processed and analyzed the data, as well as wrote the manuscript, with edits provided by NADB and HDHS for publication.

Chapter 5

RMK, with help from NADB, developed the fundamental design. RMK carried out all the experimental work, and wrote the manuscript. TRH helped in designing the block copolymer dimensions and the cross-linking chemistry, and is currently guiding their study for use as controlled release materials. NADB and HDHS helped with interpretation and editing of the manuscript for publication.

CHAPTER 1

Introduction

1.1. Concept of cell encapsulation

Applications using the entrapment of live cells for bioreactors,[1] protein/enzyme delivery,[2,3] or vaccination[4] can be achieved through ionotropic gelation of sodium alginate at physiological conditions. Cells dispersed in sodium alginate are dropped into a calcium chloride containing bath forming anionic, hydrogel beads. Further coating the beads by electrostatic complexation with cationic poly-L-Lysine (PLL) forms capsule membranes having tunable and reduced permeability. One major application for these capsules is encapsulation of hybridoma cells in bioreactors for large scale production of monoclonal anti-bodies. The high molecular weight anti-bodies are trapped within the capsule, while lower molecular weight proteins are free to escape through the membrane. After sufficient cell growth and anti-body production, the capsules are washed and broken for anti-body isolation. This encapsulation device has successfully increased the purity of the anti-body isolated as well as reduced the volume of solutions and time needed to isolate industrial scale quantities.[1]

Cell encapsulation has also been proposed for direct treatment of disease. The obvious advantage to encapsulation of active enzymes and living cells over conventional delivery of enzymes, as first described in 1964 and 1966 by Chang,[5,6] is continuous generation, supply and regulatory feedback, with immune-protection. In these applications the concept of size exclusion of anti-bodies through a semi-permeable alginate-polycation

membrane is also used, but in this case to exclude anti-bodies from the cell containing capsule, thus being able to immuno-isolate living cells implanted into a host (Figure 1.1). This concept was first demonstrated by Lim and Sun in 1980 as a treatment for diabetes, by the encapsulation of pancreatic islets and their implantation into mice, which showed normalized glucose levels past two weeks.[3] Since this work, application of such capsules for treatment of disease has also continued to be of particular interest, but not limited to, Hemophilia B,[7] Lysosomal storage disorders,[8] and cancer.[9] Although alginate-PLL capsules provide well tolerated encapsulation conditions and tunable permeability, the long term use of these cell encapsulation devices *in vivo* faces additional challenges such as poor cell and host compatibility of polycationic materials, which can reduce encapsulated cell viability and cause foreign body response (FBR) to implanted capsules, and poor mechanical integrity.

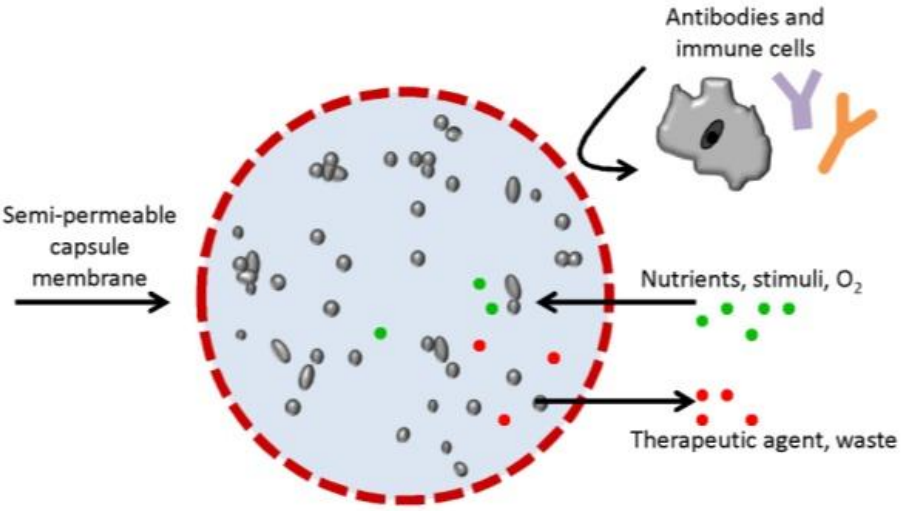

Figure 1.1: Cells encapsulated in alginate-PLL capsules.[10]

1.2. Alginate gellation

Alginate is a naturally occurring carbohydrate polymer extracted from brown algae. It contains two carbohydrate monomer units known as guluronic acid (G) and mannuronic acid (M), structured in homoblocks of G and M units and in blocks of alternating G and M units (Figure 1.2).[11] The ratio of G to M units and the length of the blocks is highly dependent on the source of alginate[12] and thus there can be large variability in the alginate composition. Since the mechanism of gellation with Ca^{2+} is co-operative, forming junctions of ionic cross-links with G blocks in an egg-box structure,[13] the molecular weight (MW), the ratio of G to M, and the length of these blocks is important for the properties of the resultant gel.[14,15] Calcium alginate gels formed with higher G content and longer G blocks result in more porous, stiffer gels that are more resistant to Na^{+}/Ca^{2+} exchange and dissolution, than those gelled with lower G content.[14] Enhanced binding of Ca^{2+} to high G alginate and the reduced shrinkage upon gellation compared to high M alginates leads to capsule formation with reduced islet cellular protrusions.[16] Thus, intermediate to high G alginates are often used to form alginate beads. Although the G content is determined from the source and tissue of the algae it is extracted from,[12] the G content of the alginate can be tuned using mannuronan-C-5 epimerase,[15,17] giving additional control over gelling and mechanical properties.[15,17,18]

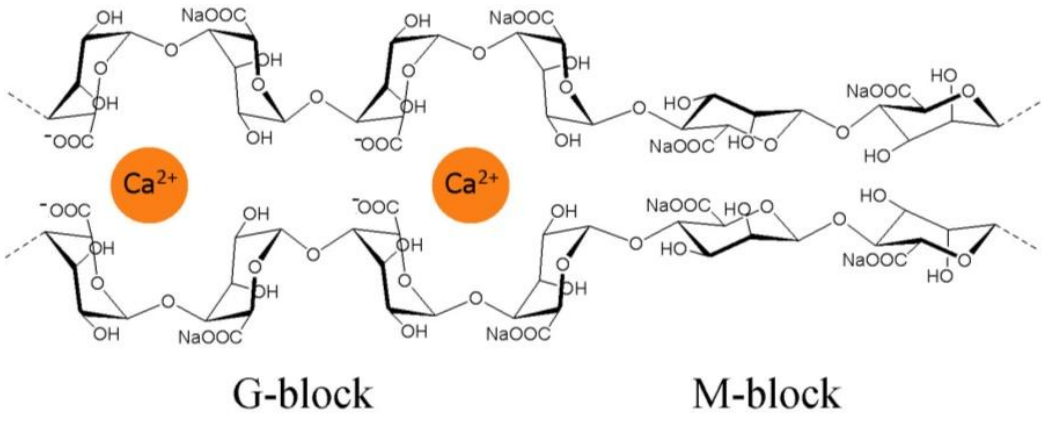

Figure 1.2: Structure of alginate, comprised of G and M residues and the binding of Ca^{2+}.[12]

In addition to the alginate composition, properties of alginate beads can also be modified by the nature of the gellation solution, which affect the concentration gradient and distribution of alginate gelled across the bead. Factors that affect the rate of gellation and diffusion of alginate during gellation, producing more homogenous beads are higher M content, higher MW, increased $CaCl_2$ concentration and increased ionic strength with competing monovalent cations, such as sodium.[19,20] These can be important in controlling the permeability[21] of the alginate gel and the long-term integrity of the resultant polycation coated alginate capsule.[22]

Another approach to maintain alginate bead integrity and reduce osmotic swelling and bead dissolution is the use of other higher affinity divalent cations less likely to exchange with sodium, such as strontium or barium.[18,23] Using barium has shown to increase the stability of alginate gel beads to swelling in saline but only for alginate beads containing high G residues.[18] This was suggested as an approach to increase bead stability

to divalent metal cation exchange with sodium and reduce bead swelling. The use of high levels of soluble barium causes toxicity concerns but due to the much higher affinity of Ba^{2+} to alginate, only low levels of Ba^{2+} (1 mM) are needed in the presence of Ca^{2+} (50 mM) to gel alginate and decrease bead swelling while keeping Ba^{2+} leakage below the World Health Organization (WHO) approved level.[24] While leakage of Ca^{2+} still occurs, some swelling of these Ba^{2+}/Ca^{2+} gel beads is observed but is greatly reduced.[18] Permeability of these Ca^{2+}/Ba^{2+} alginate beads remains a concern,[18] still requiring use of polycation membrane formation.

Due to the advantages of alginate, it has become one of the most widely used biomaterials because it is naturally abundant, highly hydrated and easy to gel, making this process relatively simple and biotolerable to entrap living cells and use for implantable materials. However, since alginate is biological derived, strict purification protocols are required due to the presence of biological contaminants of proteins, endotoxins and polyphenols, which stimulate immune response.[25,26,27]

1.3. PLL–alginate capsule membrane formation, properties and immune response

Calcium alginate beads gelled from intermediate or high G alginates require a polycation coating to reduce the permeability and maintain immuno-isolation after the Ca^{2+} has been fully exchanged with Na^{+}. PLL is the most commonly studied polycation for creating membranes on alginate beads. The Alginate-PLL-Alginate (APA) capsule is formed by coating an alginate bead with PLL then again alginate in a layer-by-layer fashion. Inconsistent *in vivo* results showing lower immune response to APA capsules

formed from high G[28,29] or low G[30,31,32,33,34] alginates created the debate over which alginate is more immunogenic. However, once it was realized that unpurified alginates illicit immune responses[25,26,27,32] and that the biotolerability of APA capsules was also very sensitive to minor procedural changes[29,32,33,35,36,37,38,39] during production, there has been a call for descriptive standardized protocols to reduce variation between research labs.[10,40] The interaction of PLL with alginate is highly dependent on the PLL reaction conditions. The resultant membrane can be adjusted by increasing the coating time, concentration, temperature of the coating solution and the MW of the polycation.[22,39,41,42,43,44] This often results in different membranes which will have varying immunological properties, permeability and capsule strength. The MW of PLL can influence its rate of diffusion into the alginate bead, PLL bridging, and affecting the amount bound and membrane thickness, as well as the molecular weight cut-off (MWCO),[43,44] integrity, swelling and mechanical properties[39,41,43,44] of the capsule membrane. The most commonly used PLL has MW of 17– 24 kDa.[39,43] Increasing the concentration and the incubation time of PLL will increase the amount bound and therefore increase mechanical properties, capsule stability to swelling and rupture[22,39,41,44] and decrease permeability.[42,44]

Tuning the permeability of the APA capsule is important for keeping large immune molecules (IgG is ~150 kDa) out but allow for exchange of small molecules, like food, waste, therapeutic enzyme and oxygen.[43] Pore size will influence the MWCO of the membrane by controlling the size of the solute able to pass the membrane. Diffusion of a solute through the membrane is governed by the size, 3D configuration and charge, not

just the molecular weight of the solute.[45] Thus, testing membranes for IgG (~150 kDa) diffusion, should be performed directly with IgG or with model molecules (such as dextran) of the same viscosity radius not MW.[45,46]

Permeability of the capsules is often described by the MWCO due to pore size and also the rate of diffusion of a solute through the membrane. On a molecular level, this restriction occurs due to increasing the diffusion path length of the solute through the membrane by blockage due to polymer chains within the membrane. Interactions of the polymer with the solvent interface create hydrodynamic drag to diffusing solutes.[40] Other intermolecular bonds between polymer membrane and solute will also affect the rate of diffusion through the membrane. Hydrogen bonds, hydrophobic interactions, ionic bonds with the diffusing solute to the polymer provide additional resistance to diffusion through the membrane while repulsive forces (ie. polymer and solute both of anionic charge) can reduce diffusion into the capsule but increase the rate of diffusion out of the anionic alginate bead.[12,21,40,47] These effects on diffusion through the membrane will also vary locally due to heterogeneity of the pore size in the membrane.[40]

As mentioned above, the permeability of APA capsules can be controlled by adding and adjusting the PLL membrane using different MW, coating concentration or time due to more material and/or thicker membranes affecting the pore size and diffusion path length. Coating additional bi-layers of PLL and alginate with the same MW generally show the same permeability and mechanical strength equivalent to coating a single bi-layer for the same total incubation time.[48] This likely leads to similar membrane thickness and pore size.

Often the same properties which control the MWCO also control the mechanical properties of the capsule. Using mixed MW PLL coating solutions or building up multi-layered capsule using different MW PLL can help tailor specific properties.[44,48]

The resulting properties of the PLL membrane are not only dependent on the PLL itself, but also the interaction of the polycation with the underlying alginate, which can vary depending on the nature of the alginate gel. While alginate beads formed from high M alginates tend to form weaker alginate gel beads, they also have more anionic residues available to bind polycations to the surface[41] forming a capsule wall which is less permeable than capsules formed with high G alginates.[22] The reduced interaction of the PLL layer with the high G alginate beads[41] forms capsules more likely to induce immune response.[32,33] The nature of the PLL-alginate bead interaction can also be altered by increasing the number of surface anionic residues on the alginate hydrogel using higher concentrations of alginate or formation of beads with inhomogenous alginate distribution.[22,41]

The binding of PLL is also influenced by the type of cation used to gel the alginate. Sr is harder to displace than Ca, so it is harder to bind PLL to Sr alginate beads. Additionally, exchange of Ca with Na prior to coating with PLL can help increase PLL binding to Ca alginate beads.[41] It is also important to realize that there is competition between divalent ions and PLL with alginate, and the relative strength of the binding of these divalent ions can affect the subsequent stability of the PLL bound in the membrane, leading to PLL shedding.[41] However, reduced PLL binding due to high affinity gelling ions within the core will still experience reduced capsule swelling and increased stability

against capsule rupture due to the more resistant gel core,[22] but have shown to also be less biocompatible due to poorer neutralization of PLL's cationic charge by Ba alginate beads.[34]

The size of capsule is determined from the size of the underlying alginate bead and can have important impact on the function of the encapsulation device. Larger capsules of 800 μm diameter were shown to have less islet cellular protrusions compared to 500 μm capsules and therefore initiate a lower host immune response.[36] While there is less chance with slightly larger capsules (~800 μm in diameter compared to 500 μm) to form incomplete capsules due to cellular protrusions, higher viscosity solutions and high G content can help reduce this problem.[16] Lower access to oxygen and nutrients in the peritoneal cavity due to poor vascularisation causes necrotic islet death within the capsule, thus other sites are encouraged[49] but has been limited by size constraints.[50] Thus, if cellular protrusions can be limited, using smaller capsules of about 315 μm allow lower capsule volume and the possibility for intravascular liver implants[50] closer to blood supply and better insulin response time.[51] While smaller empty APA capsules were shown to have increased biocompatibility,[37] the effect of capsule size on biocompatibility is not independent of membrane formation and the resultant properties. Reducing alginate bead size increases the surface to volume ratio, affecting the membrane formation process and permeability. Smaller alginate beads are more sensitive to the PLL coating concentrations/conditions, requiring narrow disperse beads to make reproducible capsule properties.[52] Thus, it is important to realize that direct application of coating methods to different size alginate beads could result in capsules of different biocompatibility or

mechanical properties due to differences in the resultant PLL membrane. Although smaller capsules are encouraged for maximum O_2 diffusion,[53] recent experiments has sparked debate on the ideal size of implanted biomaterials. The opposite trend was observed in islet containing barium-alginate beads, which showed more fibrotic overgrowth for 500 μm beads compared to larger >1500 μm beads.[54]

1.4. Alternative polycations to replace PLL

Regardless of the numerous ways to control the properties of the PLL membrane, many studies have concluded the foreign body reaction to APA capsules *in vivo* is due to the PLL in the membrane. Uncoated alginate beads (without PLL) did not evoke immune response or were less immunogenic than those coated with PLL.[29,30,32,34,38,55] Further investigation into the immunogenity of the PLL layer showed that host response is due to PLL penetration through the final layer of alginate[56] and formation of a more hydrophobic complex membrane.[34] The PLL in the membrane induces fibrosis or proteolytic degradation by binding of immunoglobins[57] and proteins,[58] activation of complement and inflammation,[58,59] macrophage activation and release of cytokines such as tumor necrosis factor- alpha (TNF-α),[55,60] and causing cellular necrosis.[55]

There are many attempts in the literature to increase the biocompatibility of the APA capsule. A common approach is to functionalize the PLL with polyethylene glycol (PEG) to make the surface of the capsule anti-fouling. Grafting PEG onto PLL amine units or terminally (di-block copolymers) has been effective in reducing immune response to these materials by preventing protein adhesion, however forming robust capsules using

these PEG functionalized PLLs is problematic and can require the use of an additional, underlying PLL layer.[61,62] Incorporation of an anti-fouling surface has also been pursued by covalent attachment of PEG or polyvinylalcohol (PVA) directly onto pre-formed AP capsules.[63]

Alternate polypeptides have been investigated, such as less hydrophobic poly-L-ornithine (PLO)[34,64,65,66] or polyarginine[58] which has been shown to interact with anionic hydrogel beads differently compared to PLL.[67] Even other configurations of polylysine have been investigated, such as α-poly-D-lysine (α-PDL)[22,64,65] or Ɛ-PLL.[68] Capsules formed with PDL on high G alginate beads were found to illicit much higher immune response even though both capsules had similar degree of swelling and ruptured capsules by explosion assay.[64] Lower permeability was also found for capsules formed with PDL instead of PLL.[22,52] Capsules formed from Ɛ-PLL were less swollen than capsules formed with α-PLL of similar MW.[68]

Others have tried to replace PLL with other polycations such as lower charge density and naturally sourced chitosan. Membrane formation, capsule integrity and strength are also dependent on MW, type of alginate, coating time, etc.,[69,70] however due to solubility limitations, typical coating procedures are performed at reduced pH (around 5-6), which may not be favorable conditions for certain cell types. Reduced MW chitosan can increase solubility at higher pH and can form capsules using modified procedures.[71]

Common synthetic polycations have also been investigated such as poly(ethylenimine) (PEI),[72] poly(diallyldimethylammonium chloride) (PDADMAC),[72]

polyvinylamine hydrochloride (PVAm).[73] Polymethylene-co-guanidine (PMCG) membrane formation with alginate and cellulose sulfate has shown some promise *in vivo* and can be tuned for optimized conditions.[74,75] Others have synthetically designed polycations of various charge densities and hydrophilicities using ter-polymers of dimethylaminoethyl methacrylate, methyl methacrylate and 2-hydroxy-ethyl methacrylate.[76] Additionally, there are current investigations into a combinatorial library of reduced charged poly(β-amino alcohol) polycations,[77] polyampholytes[78] and charge-shifting polycations.[79]

Due to a non-specific host response caused by injury during implantation,[80] the use of APA capsules containing anti-inflammatory and immunosuppressing drugs, such as dexamethasone, have shown that the temporary use of these drugs can reduce the foreign body response and is a possible alternative to long-term immune suppression.[81] For sustained released, hydrophobic core micelles, containing dexamethasone, are also currently under investigation for co-encapsulation with islets for cell encapsulation therapies.[82]

Recently, the search for drug-free anti-inflammatory Ba alginate beads by high throughput screening of chemically modified alginates suggests that immune response to alginate beads could be lowered by incorporation of triazole containing modifications.[83]

1.5. Mechanical properties of capsules

Alginate beads and alginate based microcapsules have been tested by various methods to assess their mechanical properties. The strength of capsules is often described from a percentage of broken capsules from explosion assays due to osmotic pressure[84] or shaking capsules in the presence of glass beads.[85] However, when 100% of capsules pass or fail, or further understanding of the nature of the material is needed, other techniques have been explored. Mainly, these methods include determination of local surface properties by atomic force microscopy (AFM),[86] bulk properties quantified as modulus,[87,88,89,90] force at defined deformation,[14,65,91,92] or bursting deformation, force, work[48,86,92,93] from uni-axial compression, or rheology[87] and application of centrifugal forces from a spinning drop apparatus.[94,95] From these methods, it was previously determined that calcium alginate beads exhibit plastic deformation due to the rupture of ionic cross-links.[88,89] Alginate beads were also shown to exhibit viscoelastic behavior, seen by relaxation experiments and rate dependent behavior due to water loss and/or intrinsic viscoelastic properties of the gel.[88,90,92,93] Thus, modulus and bursting force determined from these methods are rate dependent[88,92] and cannot be directly compared unless determined at high speeds[88] where viscous flow is negligible or using bursting work[96] instead of bursting force for capsules.

Aspiration is often used to measure the modulus or membrane tension of cells,[97] tissue,[98] and liquid or gel filled capsules[99,100] and has sparingly been used to determine the capsule stiffness of alginate gel capsules.[101] This technique has the advantage of easily being adopted into most labs using common equipment. A known pressure differential,

ΔP, is applied to a capsule with a known radius, R_c, using a micropipette of known radius, R_p, and the deformation, x, of the capsule into the pipette is measured (Scheme 1.1). Membrane tension, T, can be determined from aspiration of a liquid-filled capsule with a thin, semi-permeable membrane by applying Laplace's law (equation 1.1).[99] P_1 is the pressure within the micropipette and P_2 is the external pressure. Equation 1.1 is invalid if x is greater than R_p. However, in alginate beads, not all capsules have a thin membrane or a liquid core, and thus equation 1.1 cannot be applied.

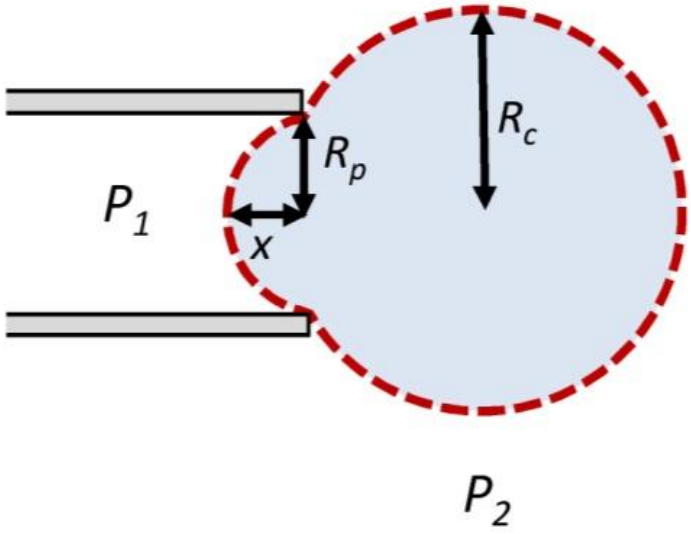

Scheme 1.1: Scheme of an aspirated capsule.[99]

(1.1) $\Delta P = P_2 - P_1 = 2T\left(\frac{2x}{x^2+R_p^2} - \frac{1}{R_c}\right)$ [99]

Young's modulus can be determined by aspiration of a homogenous bulk gel with a relatively small and thin walled pipette tip by modelling to a incompressible elastic or viscoelastic solid. Thus, application of equation 1.2 can be solved for a local Young's modulus, E, using a predetermined value for the wall function, ϕ (which is related to the pipette wall thickness). This model has been applied to endothelial cells which have been flattened by exposure to shear stresses. Application of this model assumes that the matrix being aspiration is a homogenous, isotropic, incompressible elastic half-space (Poisson's ratio of 0.5) which is much larger than the diameter of the pipette used for aspiration. There is no curvature of the sample being aspirated, *x* is purely due to normal loads and there is no shear stress in the membrane. It also requires that the deformations are small, linear and that wall thickness is thin with no adhesion of the capillary to the elastic medium. A thin walled pipette, in full contact with a flat sample from the inner radius to the outer radius, would require the wall parameter of 0.2-0.6 to accurately use the predetermined values. The wall parameter is determined by taking the difference between the outer and inner radius of the pipette and dividing it by the inner radius of the pipette.[102]

(1.2) $\Delta P = \left(\frac{2\pi E x}{3R_p}\right)\phi$ [102]

Aspiration of a flattened cell deviates from this model since the cell's internal structure is complex and the boundaries of the cell are not considered. Additionally, larger displacements were measured as small strains were difficult to measure however the cells deformed linearly even for x/R_p values greater than 1. It is also difficult to use an

ideal wall parameter of 0.2 (where both wall function models behave the same) because a wall parameter of at least 0.4 is more practical to form.[102]

Accordingly, A beads and APA capsules would not fit this model as they are heterogeneous, compressible, viscoelastic in nature and could lose water.[90,92] Additionally, the bead and capsules are spherical and would require much larger capsules compared to the capillary diameter to be approximated as a flat half-space.

Since the size of the radius of the pipette governs the depth of sample measured,[98] the radius of the pipette compared to the capsules can be controlled to look at local or whole capsule properties even though equation 1.2 is not necessarily applicable to elastic spheres when the pipette radius is not proportionally small.

The strength or modulus of alginate beads and capsules is dependent on the amount of G ratio, the type of gelling cation, the presence of a polycation membrane and its thickness. Alginate beads are more brittle[89,93] and stiff when made with alginates of higher G content,[14,89,93] and with more strongly bound ions,[18,89] due more ionic cross-links or stronger cross-linking. The addition of a capsule membrane can contribute to increase the overall stiffness of the capsule[92,95] and reduce the viscoelastic response seen by relaxation experiments.[92] However liquefaction of the gel core has shown a large reduction in strength of the capsules.[65] The integrity of the capsule membrane can be tuned by increasing polycation coating time and concentration.[48,65,95] However, the resistance to compression is dependent on the ratio of polycation membrane thickness to capsule size because thick membranes can touch during deformation causing capsule

rupture at lower deformations regardless of an increase in strength/rigidity of having a thick membrane.[92,96]

1.6. Increase of mechanical properties with Covalent Cross-linking

Many groups have used covalent cross-linking to increase the mechanical strength of APA and analogous capsules. Adding covalent cross-links to the membrane can also alter the permeability of the capsule membrane. Increased degree of cross-linking is associated with more dense membranes and reduced pore size, leading to slower diffusion through the membrane.[103,104]

PLL and other polycations containing primary amines (eg. chitosan, PVAm) allow multiple strategies for covalent cross-linking. Common amine reactive small molecules have been employed such as, 1-ethyl-3-(3'-dimethyl aminopropyl) carbodiimide (EDC),[103] genipin,[105] glutaraldehyde,[103] tolylene 2,4-diisocyanate,[106] tetrakis(hydroxymethyl)phosphonium chloride (THPC).[79]

Photo-cross-linking of methacrylated glycol chitosan membranes in the presence of small molecule photo-initiators has shown increased capsule stability by reduced swelling.[107] However, reactive small molecules often pose a toxicity concern to encapsulated cells. Polymeric photo-cross-linkers, such as pre-modified polycations, α-phenoxycinnamylidene-acetylated poly (allylamine)[108] and N-5-azido-2-nitrobenzoyloxysuccinimide functionalized PLL[109] have also been investigated to covalent cross-link the capsule membrane and do not require additional small molecule initiators.

Reactive polyanions such as poly[methacrylic acid-co-2-(methacryloyloxy)ethyl acetoacetate],[110] can be used to covalently cross-link the membrane by taking advantage of fast electrostatic complexation to increase the concentration of reactive groups, aiding in covalent bond formation.[111] Temporarily reactive polyanions (TRPs) have been developed to prevent covalent binding of surface proteins by hydrolysis of amine reactive groups and thus reducing host immune response. TRPs such as partially hydrolyzed poly(methyl vinyl ether-alt-maleic anhydride) (PMM)[112] and poly(2-vinyl-4,4-dimethylazlactone-co-methacrylic acid) (PMV)[113] show promising biotolerability.[114]

Covalent cross-linking of alginate based capsules is not only restricted to the membrane. Reactive polyanions from poly[methacrylic acid-co-2-(methacryloyloxy)ethyl acetoacetate] can also be used for forming core cross-linked capsules using reduced MW PLL.[115] There are many other ways of forming covalent, core cross-linked hydrogels, that do not necessarily rely on amine functionality from the membrane and can range from but not limited to photo-cross-linking polymerizations[116] or complementary reactive polymers within the hydrogel.[117,118,119] These include "click' reactions, such as Cu(I) catalyzed azide-alkyne Huisgen cycloaddition,[118] thiol-ene approaches,[120] and Diels-Alder.[121]

1.7. Purpose and context of this thesis

This thesis develops methods to increase the biocompatibility of alginate based capsules by replacing PLL with reduced charge polycations to create more hydrophilic membranes with reduced cationic surface charges. Using polycations with reduced cationic charge to increase biocompatibility of these capsules presents the challenge of

adequate binding of these polycations in the alginate bead and therefore, capsule and membrane stability is a concern. Capsule and membrane stability refers to the ability of the capsule and membrane respectively, to resist changes such as swelling, rupture or disintegration by a stimulus such as Na^{+}/Ca^{2+} exchange. More specifically, mechanical stability refers to capsule resistance to an external mechanical force and chemical stability refers to capsule resistance to chemical challenges such as ionic strength or pH changes. Thus, in order to increase or maintain sufficient mechanical properties of these capsules, covalent cross-linking of the membrane was investigated.

The following thesis starts with characterizing alginate beads and APA capsules by micropipette aspiration. Using a relatively large micropipette, the stiffness of whole capsules, including contributions from both shell and core, could be quantified.

The alginate beads and APA capsules aspirated are visco-elastic in nature, permeable and compressible. This requires that application of micropipette aspiration is performed at the same rate for each sample and assumes that any intrinsic rate dependent behavior such as viscoelastic flow and water loss contributes to the apparent stiffness and is not manufactured by the experiment but is influenced by the properties of the beads/capsules, allowing direct comparison between samples.

No model is applied here and the apparent stiffness measured is a sum of stretching, bending and shear deformation of the membrane and core, translation of the capsule into the capillary as well as volume loss due to compression. Beads and capsules are assumed to have equivalent interaction/friction with the capillary and only beads and capsules that

were freely released when returned to $\Delta P=0$ where used. Capsule compositions which showed adhesion to the capillary (by needing a positive ΔP to eject the capsule from the capillary after aspiration or remained attached to the pipette) were assumed to have a large difference in the weighting of the variables contributing to the stiffness and were not compatible by this method. Thus, this method is limited as it does not deal with these individual components which is rich with information. To help identify different contributions of the stiffness from the gel core and the membrane, the alginate core is liquefied with sodium citrate to reveal the membrane properties in the absence of a gel core.

When the spherical shape of a capsule is considered, the ratio of the capillary to the sphere can have some effect. Larger capsules will experience more stretching and changes in curvature at the capsule boundary while under aspiration where as much smaller capsules aspirated with the same capillary diameter will experience less change in curvature and more translational motion into the capillary. For largely different capsule sizes, these effects could cause greater x due to greater translation if the capillary diameter is very large, making smaller capsules appear less stiff than if aspirated by a smaller capillary.[122]

This technique was validated and used to study the apparent stiffness of alginate beads and capsules as a function of reduced gellation in the capsule core due to Na^+/Ca^{2+} exchange during capsule aging modelled by successive washing steps. The effect of the PLL membrane stiffness as a result of different washing procedures was also investigated,

showing that Ca^{2+} facilitated redistribution of the polycation membrane reduces the density of the membrane and the resultant membrane stiffness.

This thesis also addresses the biocompatibility issues associated with APA capsules due to the high cationic charge in the shell causing cytotoxicity to encapsulated cells and immune rejection by the host due to exposed PLL in the capsule membrane. Polycations of reduced charge density were prepared using N-(3-aminopropyl)methacrylamide (APM) and N-(2-hydroxypropyl)methacrylamide (HPM) by reversible addition-fragmentation chain transfer (RAFT) polymerization to control MW. APM was chosen due to its ability to provide cationic charge and is of similar structure to lysine. HPM was chosen as a neutral biocompatible comonomer used to reduce the charge density along the linear polymer backbone. Within this thesis, the term "charge density" is used to describe the monomeric cationic charge ratio within the polymer chain and does not necessarily describe quantitatively the cationic charge within a volume, due to extension or relaxation of the polymer coil.

Polycation interaction with alginate was studied as a function of charge density and MW. The membrane thickness increased with reduced charge density, MW and Ca^{2+} redistribution. The biocompatibility of these polycations were tested through solution toxicity, and by assessment of cell adhesion and proliferation on polycation modified surfaces. The results showed lower cell toxicity, cell adhesion and proliferation with reduced charge density polycations. Intermediate charge density polycations showed a compromise between reducing biocompatibility but still having enough charge density to adequately interact with alginate beads.

Capsules formed from intermediate charge density polycations were studied and compared against APA capsules, whereby the integrity/stability of the capsules were assessed using mechanical and chemical tests. These capsules showed that they are largely less stable compared to APA capsules and prone to greater capsule swelling, rupture or disintegration on liquefaction of the gel core. To increase the stability of these capsules, capsule membranes were covalently cross-linked using reactive polyanion PMV, which has been previously synthesized in our lab. The resulting properties of cross-linking these capsules with PMV was tested for stability, permeability and membrane stiffness. PMV cross-linking was determined to be dependent on the amine content and MW which also affects polycation in-diffusion. Cross-linking was shown to enhance intermediate charge density polycations if MW is sufficiently high and the distribution of polycation is concentrated. The membrane stiffness of such capsules is low but can be increased by increasing the number of layers in the capsule membrane.

RAFT polymerization was also performed to prepare thermo-responsive micelles which may be useful in encapsulating hydrophobic drugs, such as dexamethasone. Poly(N-isopropylacrylamide) (p(NIPAM)) is a thermo-responsive polymer that is soluble in water below its lower critical solution temperature (LCST) of about 32 °C. Upon heating above its LCST, the polymer phase separates due to hydrophobic regions desolvating from water.[123] In this thesis p(NIPAM) was synthesized with 10 % acrylic acid (AA) and chain extended with varying lengths of p(2-hydroxyethylacrylamide) (p(HEA)) to form a series of block-co-polymers. Synthesis and characterization of the thermo-responsive micelles formed from the self assembly of p((NIPAM-*co*-AA)-*b*-

HEA) block copolymers above the LCST were studied. Micelles were also covalently cross-linked using EDC chemistry with the available AA groups. Micelle size and morphology was governed by the relative length of the hydrophobic to hydrophilic blocks,[124,125] which is important to control effective entrapment or release of micelle particles from the alginate capsules.[82]

1.8. References

[1] Posillico, E. G. *Biotechnology* **1986,** *4,* 114–117.
[2] Wheatly, M. A.; Chang, M.; Park, E.; Langer, R. *J. Appl. Polym. Sci.* **1991,** *43*, 2123 – 2135.
[3] Lim, F.; Sun, A. M. *Science* **1980,** *210*, 908–910.
[4] Gomez-Vargas, A.; Rosenthal, K. L.; McDermott, M. R.; Hortelano, G. *Vaccine* **2004,** *22*, 3902–3910.
[5] Chang, T. M. S. *Science* **1964,** *146*, 524–525.
[6] Chang, T. M. S.; MacIntosh, F. C.; Mason, S. G. *Can. J. Physiol. Pharmacol.* **1966,** *44*,115–128.
[7] Liu, H. W.; Ofosu, F. A.; Chang, P. L. *Hum.Gene Ther.* **1993,** *4,* 291–301.
[8] Ross, C. J. D.; Bastedo, L.; Maier, S. A.; Sands, M. S.; Chang, P. L. *Hum. Gene Ther.* **2000,** *11,* 2117–2127.
[9] Cirone, P.; Bourgeois, J. M.; Austin, R. C.; Chang, P. L. *Hum. Gene Ther.* **2002,** *13,* 1157–1166.
[10] Orive, G.; Hernández, M. A.; Gascón, A. R.; Calafiore, R.; Chang, T. M. S.; De Vos, P.; Hortelano, G.; Hunkeler, D.; Lacík, I.; Shapiro, A. M. J.; Pedraz, J. L. *Nat. Med.* **2003,** *9,* 104–107.
[11] Haug, A.; Larsen, B.; Smidsrød, O. *Acta Chem. Scand.* **1967,** *21,* 691–704.
[12] Smidsrød, O.; Skjåk-Bræk, G. *Trends Biotechnol.* **1990,** *8,* 71–78.
[13] Grant, G. T.; Morris, E. R.; Rees, D. A.; Smith, P. J. C.; Thom, D. *FEBS Lett.* **1973,** *32,* 195–198.
[14] Martinsen, A.; Skjåk-Bræk, G.; Smidsrød, O. *Biotechnol. Bioeng.***1989,** *33,* 79–89.
[15] Skjåk-Bræk, G.; Smidsrød, O.; Larsen, B. *Int. J. Biol. Macromole.* **1986,** *8,* 330–336.
[16] De Vos, P.; De Haan, B.; Wolters, G. H. T.; Van Schilfgaarde, R. *Transplantation* **1996,** *62,* 888–893.
[17] Mørch, Y.A.; Holtan, S.; Donati, I.; Strand, B.L.; Skjåk-Bræk, G. *Biomacromolecules* **2008,** *9,* 2360–2368.
[18] Mørch, Y. A.; Donati, I.; Strand, B. L.; Skjåk-Bræk, G. *Biomacromolecules* **2006,** *7,* 1471–1480.
[19] Skjåk-Bræk, G.; Grasdalen, H.; Smidsrød, O. *Carbohydr. Polym.* **1989,** *10,* 31–54.

[20] Thu, B.; Skjåk-Bræk, G.; Micali, F.; Vittur, F.; Rizzo, R. *Carbohydr*. *Res*. **1997,** *297,* 101–105.
[21] Martinsen, A.; Storrø, I.; Skjåk-Bræk, G. *Biotechnol*. *Bioeng*. **1992,** *39,* 186–194.
[22] Thu, B.; Bruheim, P.; Espevik,T.; Smidsrød, O.; Soon-Shiong, P.; Skjåk-Bræk, G. *Biomaterials* **1996,** *17,* 1069–1079.
[23] Haug, A.; Smidsrød O. *Acta Chem*. *Scand*. **1970,** *24,* 843–854.
[24] Mørch, Y. A.; Qi, M.; Gundersen, P. O. M.; Formo, K.; Lacik, I.; Skjåk-Break, G.; Oberholzer, J.; Strand, B. L. *J*. *Biomed*. *Mater*. *Res*., *Part A* **2012,** *100,* 2939–2947.
[25] Orive, G.; Hernández, R. M.; Gascón, A. R.; Pedraz, J. L. *Biomacromolecules* **2005,** *6,* 927–931.
[26] Dusseault, J.; Tam, S. K.; Ménard, M.; Polizu, S.; Jourdan, G.; Yahia, L.; Hallé, J. P. *J*. *Biomed*. *Mater*. *Res*., *Part A* **2006,** *76A,* 243–251.
[27] De Vos, P.; De Haan, B. J.; Wolters, G. H. J.; Strubbe, J. H.; Van Schilfgaarde, R. *Diabetologia***1997,** *40,* 262–270.
[28] Soon-Shiong, P.; Otterlie, M.; Skjåk-Bræk, G.; Smidsrød, O.; Heintz, R.; Lanza, R. P.; Espevik, T. *Transplant*. *Proc*. **1991,** *23,* 758–759.
[29] Vandenbossche, G. M. R.; Bracke, M. E.; Cuvelier, C. A.; Bortier, H. E.; Mareel, M. M.; Remon, J. P. *J*. *Pharm*. *Pharmacol*. **1993,** *45,* 115–120.
[30] King, A.; Sandler, S.; Andersson, A. *J*. *Biomed*. *Mater*. *Res*. **2001,** *57,* 374–383.
[31] Clayton, H. A.; London, N. J. M.; Colloby, P. S.; Bell, P. R. F.; James, R. F. L. *J*. *Microencapsul*. **1991,** *8,* 221–233.
[32] De Vos, P.; De Haan, B.; Van Schilfgaarde, R. *Biomaterials* **1997,** *18,* 273–278.
[33] DeVos, P.; De Haan, B. J. Van Schilfgaarde, R. *Transplant*. *Proc*. **1998,** *30,* 492–493.
[34] Tam, S. K.; Bilodeau, S.; Dusseault, J.; Langlois, G.; Hallé, J. P.; Yahia, L. H. *Acta Biomater*. **2011,** *7,* 1683–1692.
[35] Hsu, B. R. S.; Ho, Y. S.; Fu, S. H.; Huang, Y. Y.; Chiou, S. C.; Huang, H.S. *Transplant*. *Proc*. **1995,** *27,* 3227–3231.
[36] De Vos, P.; De Haan, B.; Pater, J.; Van Schilfgaarde, R. *Transplantation* **1996,** *62,* 893–899.
[37] Robitaille, R.; Pariseau, J. F.; Leblond, F. A.; Lamoureux, M.; Lepage, Y.; Hallé, J.P. *J*. *Biomed*. *Mater*. *Res*. **1999,** *44,* 116–120.
[38] King, A.; Strand, B.; Rokstad, A. M.; Kulseng, B.; Andersson, A.; Skjåk-Bræk, G.; Sandler, S. *J*. *Biomed*. *Mater*. *Res*., *Part A* **2003,** *64A,* 533–539.
[39] Ma, X.; Vacek, I.; Sun, A. *Artif*. *Cells Blood Substit*. *Immobil*. *Biotechnol*. **1994,** *22,* 43–69.
[40] De Vos, P.; Bučko, M.; Gemeiner, P.; Navrátil, M.; Švitel, J.; Faas, M.; Strand, B. L.; Skjåk-Bræk, G.; Mørch, Y. A.; Vikartovská, A.; Lacík, I.; Kolláriková, G.; Orive, G.; Poncelet, D.; Pedraz, J. L.; Ansorge-Schumacher, M. B. *Biomaterials* **2009,** *30,* 2559–2570.
[41] Thu, B.; Espevik, T.; Smidsrød, O.; Soon-Shiong, P.; Skjåk-Bræk, G. *Biomaterials* **1996,** *17,* 1031–1040.
[42] Vandenbossche, G. M. R.; Van Oostveldt, P.; Demeester, J.; Remon, J. P. *Biotechnol*. *Bioeng*. **1993,** *42,* 381–386.

[43] Goosen, M. F. A.; O'Shea, G. M.; Gharapetian, H. M. ; Chou, S.; Sun, A. M. *Biotechnol*. *Bioeng*. **1985,** *27,* 146–150.
[44] King, G. A.; Daugulis, A. J.; Faulkner, P.; Goosen, M. F. A. *Biotechnol*. *Prog*. **1987,** *3,* 231–240.
[45] Robitaille, R.; Leblond, F. A.; Bourgeois, Y.; Henley, N.; Loignon, M.; Hallé J. P. *J*. *Biomed*. *Mater*. *Res*. **2000,** *50,* 420–427.
[46]Briššová, M; Petro, M.; Lacík, I.; Powers, A. C.; Wang, T. *Anal*. *Biochem*. **1996,** *242,* 104–111.
[47] Stockwell, A. F.; Davis, S. S.; Walker, S. E. *J*. *Control*. *Release* **1986,** *3*,167–175.
[48] Gugerli, R.; Cantana, E.; Heinzen, C.; Von Stockar, U.; Marison, I. W. *J*. *Microencapsul*. **2002,** *19,* 571–590.
[49] De Vos, P.; Van Straaten, J. F. M.; Nieuwenhuizen, A. G.; de Groot, M.; Ploeg, R. J.; De Hann, B. J.; Van Schilfgaarde, R. *Diabetes* **1999,** *48,* 1381–1388.
[50] Leblond, F. A.; Simard, G.; Henley, N.; Rocheleau, B.; Huet, P. M.; Hallé, J. P. *Cell Transplant*. **1999,** *8,* 327–337.
[51] Chicheportiche, D.; Reach, G. *Diabetologia* **1988,** *31,* 54–57.
[52] Strand, B. L.; Gåserod, O.; Kulseng, B.; Espevik, T.; Skjåk-Bræk, G. *J*. *Microencapsul*. **2002,** *19,* 615–630.
[53] Schrezenmeir, J.; Kirchgessner, J.; Gerö, L.; Kunz, L. A.; Beyer, J.; Mueller-Klieser, W. *Transplantation* **1994,** *57,* 1308–1314.
[54] Veiseh, O.; Doloff, J. C.; Ma, M.; Vegas, A. J.; Tam, H. H.; Bader, A. R.; Li, J.; Langan, E.; Wyckoff, J.; Loo, W. S.; Jhunjhunwala, S.; Chiu, A.; Seibert, S.; Tang, K.; Hollister-Lock, J.; Aresta-Dasilva, S.; Bochenek, M.; Mendoza-Elias, J.; Wang, Y.; Qi, M.; Lavin, D. M.; Chen, M.; Dholakia, N.; Thakrar, R.; Lacík, I.; Weir, G. C.; Oberholzer, J.; Greiner, D. L.; Langer, R.; Anderson, D. G. *Nat*. *Mater*. **2015,** *14,* 643–652.
[55] Strand, B. L.; Ryan, L.; In't Veld, P.; Kulseng, B.; Rokstad, A. M.; Skjåk-Bræk, G.; Espevik, T. *Cell Transplant*. **2001,** *10,* 263–275.
[56] Tam, S. K.; Dusseault, J.; Polizu, S.; Ménard, M.; Hallé, J.P.; Yahia, L. *Biomaterials* **2005,** *26,* 6950–6961.
[57] Tam, S. K.; de Haan, B. J.; Faas, M. M.; Hallé, J. P.; Yahia, L.; de Vos, P. *J*. *Biomed*. *Mater*. *Res*., *Part A* **2009,** *89A,* 609–615.
[58] Van Raamsdonk, J. M.; Cornelius, R. M.; Brash, J. L.; Chang, P. L. *J*. *Biomater*. *Sci*. *Polym*. *Ed*. **2002,** *13,* 863–884.
[59] Rokstad, A. M.; Brekke, O.; Steinkjer, B.; Ryan, L.; Kolláriková, G.; Strand, B. L.; Skjåk-Bræk, G.; Lacík, I.; Espevik, T.; Mollnes, T. E. *Acta Biomater*. **2011,** *7,* 2566–2578.
[60] Juste, S.; Lessard, M.; Henley, N.; Ménard, M.; Hallé, J. P. *J*. *Biomed*. *Mater*. *Res*., *Part A* **2005,** *72A,* 389–398.
[61] Sawhney, A. S.; Hubbell, J. A. *Biomaterials* **1992,** *13,* 863–870.
[62] Spasojevic, M.; Paredes-Juarez, G. A.; Vorenkamp, J.; de Haan, B. J.; Jan Schouten, A.; de Vos, P. Reduction of the inflammatory responses against alginate-poly-L-lysine microcapsules by anti-biofouling surfaces of PEG-b-PLL diblock copolymers. *PLoS ONE*

[Online] **2014,** *9*, e109837.
http://journals.plos.org/plosone/article?id=10.1371/journal.pone.0109837 (accessed Apr 1, 2015)
[63] Kung, M. I.; Wang, F. F.; Chang, Y. C.; Wang, Y. J. *Biomaterials* **1995,** *16,* 649–655.
[64] Ponce, S.; Orive, G.; Hernandez, R.; Gascon, A. R.; Pedraz, J. L.; de Haan, B. J.; Faas, M. M.; Mathieu, H. J. de Vos, P. *Biomaterials* **2006,** *27,* 4831–4839.
[65] De Castro, M.; Orive, G.; Hernández, R. M.; Gascón, A. R.; Pedraz, J. L. *J. Microencapsul*. **2005,** *22,* 303–315.
[66] Darrabie, M. D.; Kendall, W. F., Jr.; Opara, E. C. *Biomaterials* **2005,** *26,* 6846–6852.
[67] Bysell, H.; Malmsten, M. *Langmuir* **2009,** *25,* 522–528.
[68] Ma, Y.; Zhang, Y.; Liu, Y.; Chen, L.; Shen, L.; Zhao, W.; Sun, G.; Li, N.; Wang, Y.; Guo, X.; Ma, X. *J. Biomed. Mater. Res., Part A* **2013,** *101A,* 1265–1273.
[69] Gåserod, O.; Smidsrød, O.; Skjåk-Bræk, G. *Biomaterials* **1998,** *19,* 1815–1825.
[70] Gåserod, O.; Sannes, A.; Skjåk-Bræk, G. *Biomaterials* **1999,** *20,* 773–783.
[71] Bartkowiak, A.; Hunkler, D. *Ann. N. Y. Acad. Sci*. **1999,** *875,* 36–45.
[72] Schneider, S.; Feilen, P. J.; Slotty, V.; Kampfer, D.; Preuss, S.; Berger, S.; Beyer, J. Pommersheim, R. *Biomaterials* **2001,** *22,* 1961–1970.
[73] Wang, F. F.; Wu, C. R.; Wang, Y. J. *Biotechnol. Bioeng*. **1992,** *40,* 1115–1118.
[74] Wang, T.; Lacík, I.; Brissová, M.; Anilkumar, A. V.; Prokop, A.; Hunkler, D.; Green, R.; Shahrokhi, K.; Powers, A. C. *Nature* **1997,** *15,* 358–362.
[75] Bartkowiak, A.; Canaple, L.; Ceausoglu, I.; Nurdin, N.; Renken, A.; Rindisbacher, L.; Wandrey, C.; Desvergne, B.; Hunkeler, D. *Ann. N. Y. Acad. Sci*. **1999,** *875,* 135–145.
[76] Wen, S.; Xiaonan, Y.; Stevenson, W. T. K. *Biomaterials* **1991,** *12,* 374–384.
[77] Minglin, M.; Liu, W. F.; Hill, P. S.; Bratlie, K. M.; Siegwart, D. J.; Chin, J.; Park, M.; Guerreiro, J.; Anderson, D.G. *Adv. Mater*. **2011,** *23,* H189–H194.
[78] Dubey, A.; Burke, N. A. D.; Stöver, H. D. H. *J. Polym. Sci., Part A: Polym. Chem*. **2015,** *53*, 353–365.
[79] Ros, S.; Burke, N. A. D.; Stöver, H. D. H. *Macromolecules* **2015,** *48,* 8958−8970.
[80] Robitaille, R.; Dusseault, J.; Henley, N.; Desbiens, K.; Labrecque, N.; Hallé, J.P. *Biomaterials* **2005,** *26,* 4119–4127.
[81] Bünger, C. M.; Tiedenbach, B.; Jahnke, A.; Gerlach, C.; Freier, Th.; Schmitz, K. P.; Hopt, U. T.; Schareck, W.; Klar, E.; de Vos, P. *Biomaterials* **2005,** *26,* 2353–2360.
[82] Velluto, D.; Manzoli, V.; Tomei, A. A. Development and evaluation of self-assembled biomaterials to maximise the function of conformal encapsulation of pancreatic islets in type 1 diabetes. In *Book of Abstracts*, Proceedings of the 10th World Biomaterials Congress. Montreal, Canada, May 17–22, 2016; P.0259, 1283.
[83] Vegas, A. J.; Veiseh, O.; Doloff, J. C., Ma, M.; Tam, H. H.; Bratlie, K.; Li, J.; Bader, A. R.; Langan, E.; Olejnik, K.; Fenton, P.; Kang, J. W.; Hollister-Locke, J.; Bocjenek, M. A.; Chiu, A.; Siebert, S.; Tang, K.; Jhunjhunwala, S.; Aresta-Dasilva, S.; Dholakia, N.; Thakrar, R.; Vietti, T.; Chen, M.; Cohen, J.; Siniakowicz, K.; Qi, M.; McGarrigle, J.; Lyle, S.; Harlan, D. M.; Greiner, D. L.; Oberholzer, J.; Weir, G. C.; Langer, R.; Anderson, D. G. *Nat. Biotechnol*. **2016,** *34,* 345–352.
[84] Van Raamsdonk, J. M.; Chang, P. L. *J. Biomed. Mater. Res*. **2001,** *54,* 264–271.

[85] Leblond, F. A.; Tessier, J.; Hallé, J.P. *Biomaterials* **1996,** *17,* 2097–2102.
[86] Lekka, M.; Sainz-Serp, D.; Kulik, A. J.; Wandrey, C. *Langmuir* **2004,** *20,* 9968–9977.
[87] LeRoux, M. A.; Guilak, F.; Setton, L. A. *J. Biomed. Mater. Res.* **1999,** *47,* 46–53.
[88] Wang, C. X.; Cowen, C.; Zhang, Z.; Thomas, C.R. *Chem. Eng. Sci.* **2005,** *60,* 6649–6657.
[89] Chan, E. S.; Lim, T. K.; Voo, W. P.; Pogaku, R.; Tey, B. T.; Zhang, Z. *Particuology* **2011,** *9,* 228–234.
[90] Nguyen, V. B.; Wang, C. X.; Thomas, C. R.; Zhang, Z. *Chem. Eng. Sci.* **2009,** *64,* 821–829.
[91] Yamagiwa, K.; Kozawa, T.; Ohkawa, A. *J. Chem. Eng. Jpn.* **1995,** *28,* 462–467.
[92] Zhao, L.; Zhang, Z. *Artif. Cells Blood Substit. Immobil. Biotechnol.* **2004,** *32,* 25–40.
[93] Mancini, M.; Moresi, M.; Rancini, R. *J. Food Eng.* **1999,** *39,* 369–378.
[94] Leick, S.; Hennin, S.; Degen, P.; Suter, D.; Rehage, H. *Phys. Chem. Chem. Phys.* **2010,** *12,* 2950–2958.
[95] Leick, S.; Kemper, A.; Rehage, H. *Soft Matter* **2011,** *7,* 6684–6694.
[96] Rehor, A.; Canaple, L.; Zhang, Z.; Hunkeler, D. *J. Biomed. Sci. Polym. Ed.* **2001,** *12,* 157–170.
[97] Hochmuth, R. M. *J. Biomech.* **2000,** *33,* 15–22.
[98] Aoki, T.; Ohashi, T.; Matsumoto, T.; Sato, M. Ann. Biomed. Eng. **1997,** *25,* 581–587.
[99] Jay, A. W. L.; Edwards, M. A. *Can. J. Physiol. Pharmacol.* **1968,** *46,* 731–737.
[100] Campillo, C.; Pépin-Donat, B.; Viallat, A. *Soft Matter* **2007,** *3,* 1421–1427.
[101] Roskiński, S.; Grigorescu, G.; Lewińska, D.; Ritzén, L. G.; Viernstein, H.; Teunou, E.; Poncelet, D.; Zhang, Z.; Fan, X.; Serp, D.; Marison, I.; Hunkeler, D. *J. Microencapsul.* **2002,** *19,* 641–659.
[102] Theret, D. P.; Levesque, M. J.; Sato, M.; Nerem, R. M.; Wheeler, L. T. *J. Biomech. Eng.* **1988,** *110,* 190–199.
[103] Chandy, T.; Mooradian, D. L.; Rao, G. H. R. *Artif. Organs* **1999,** *23,* 894–903.
[104] Ranganath, S. H.; Ling Tan, A.; He, F.; Wang, C.-H.; Krantz, W. B. *AIChE J.* **2011,** *57,* 3052–3062.
[105] Hongmei, C.; Ouyang, W.; Jones, M.; Metz, T.; Martoni, C.; Haque, T.; Cohen, R.; Lawuyi, B.; Prakash, S. *Cell Biochem. Biophys.* **2007,** *47,* 159–167.
[106] Sato, T.; Chiba, T.; Yoshinaga, K.; Kitajima, M.; Terashima, M. *J. Exp. Med.* **1988,** *155,* 271–274.
[107] Hillberg, A. L.; Oudshoorn, M.; Lam, J. B. B.; Kathirgamanathan, K. *J. Biomed. Mater. Res., Part B* **2015,** *103B*, 503–518..
[108] Lu, M. Z.; Lan, H.L.; Wang, F. F.; Chang, S. J.; Wang, Y. J. *Biotechnol. Bioeng.* **2000,** *70,* 479–483.
[109] Dusseault, J.; Leblond, F. A.; Robitaille, R.; Jourdan, G.; Tessier, J.; Ménard, M.; Henley, N.; Hallé, J. P. *Biomaterials* **2005,** *26,* 1515–1522.
[110] Shen, F.; Mazumder, M. A. J.; Burke, N. A. D.; Stöver, H. D. H.; Potter, M. A. *J. Biomed. Mater. Res., Part B* **2009,** *90B,* 350–361.
[111] Mohajeri, S.; Burke, N. A. D.; Stöver, H. D. H. *Polym. Degrad. Stab.* **2015,** *114*, 94–104.

[112] Gardner, C. M.; Burke, N. A. D.; Stöver, H. D. H. *Langmuir* **2010,** *26,* 4916–4924.
[113] Gardner, C. M.; Stöver, H. D. H. *Macromolecules* **2011,** *44,* 7115–7123.
[114] Gardner, C.M.; Potter, M. A.; Stöver, H. D. H. *J. Mater. Sci.: Mater. Med.* **2012,** *23*, 181–193.
[115] Mazumder, M. A. J.; Burke, N. A. D.; Shen, F.; Potter, M. A.; Stöver, H. D. H. *Biomacromolecules* **2009,** *10,* 1365–1373.
[116]Rokstad, A. M.; Donati, I.; Borgogna, M.; Oberholzer, J.; Strand, B. L.; Espevik, T.; Skjåk-Bræk, G. *Biomaterials* **2006,** *27,* 4726–4737.
[117] Private communication with Sara Alison Stewart and Dr. Harald D.H. Stöver, Department of Chemistry and Chemical Biology.
[118] Breger, J. C.; Fisher, B.; Samy, R.; Pollack, S.; Wang, N. S.; Isayeva, I. *J. Biomed. Mater. Res., Part B* **2015,** *103B,* 1120–1132.
[119] Gattás-Asfura, K. M.; Fraker, C. A.; Stabler, C. L. *J. Biomed. Mater. Res., Part A* **2011,** *99A,* 47–57.
[120] Lin, C.; Raza, A.; Shih, H. *Biomaterials* **2011,** *32,* 9685–9695.
[121] Nimmo, C. M.; Owen, S. C.; Shoichet, M. S. *Biomacromolecules* **2011,** *12,* 824–830.
[122] Haider, M. A.; Guilak, F. *J. Biomech. Eng.* **2002,** *124,* 586–595.
[123] Pelton, R. *J. Colloid Interface Sci.* **2010,** *348,* 673–674.
[124] Mayes, A. M.; Olvera de la Cruz, M. *Macromolecules* **1988,** *21,* 2543–2547.
[125] Zhang, L.; Eisenberg, A. *J. Am. Chem. Soc.* **1996,** *118,* 3168–3181.

CHAPTER 2

Systematic study of alginate-based microcapsules by micropipette aspiration and confocal fluorescence microscopy

Rachelle M. Kleinberger, Nicholas A. D. Burke, Kari Dalnoki-Veress, Harald D. H. Stöver. *Materials Science and Engineering C*. **2013**, *33*, 4295-4304. DOI: 10.1016/j.msec.2013.06.033

This chapter validates the use of micropipette aspiration to study the stiffness of alginate gel beads and APA capsules. The stiffness is measured for whole capsules with or without gel cores. Confocal microscopy shows the effect of Ca^{2+} facilitated redistribution of PLL in the membrane and the associated reduction of stiffness by aspiration.

Contributions: RMK designed the experiments with guidance from HDHS and NADB. RMK performed all the experiments except the determination of Ca^{2+} concentration by ICP-MS, which was determined by Kevin Ferguson in the Occupational and Environmental Health Laboratory. RMK processed the data using suggestions from KDV. RMK analyzed the data and wrote the manuscript. Edits to the manuscript were performed by NADB, KDV and HDHS.

2.1. Abstract

Micropipette aspiration and confocal fluorescence microscopy were used to study the structure and mechanical properties of calcium alginate hydrogel beads (**A** beads), as well as **A** beads that were additionally coated with poly-L-lysine (**P**) and sodium alginate (**A**) to form, respectively, **AP** and **APA** hydrogels. **A** beads were found to continue curing for up to 500 h during storage in saline, due to residual calcium chloride carried over from the gelling bath. In subsequent saline washes, micropipette aspiration proved to be a sensitive indicator of gel weakening and calcium loss. Aspiration tests were used to compare capsule stiffness before and after citrate extraction of calcium. They showed that the initial gel strength is largely due to the calcium alginate gel cores, while the long term strength is solely due to the poly-L-lysine–alginate polyelectrolyte complex (PEC) shells. Confocal fluorescence microscopy showed that calcium chloride exposure after PLL deposition led to PLL redistribution into the hydrogel bead, resulting in thicker but more diffuse and weaker PEC shells. Adding a final alginate coating to form **APA** capsules did not significantly change the PEC membrane thickness and stiffness, but did speed the loss of calcium from the bead core.

2.2. Introduction

Encapsulation of genetically engineered therapeutic cells has been proposed for treatment of several enzyme and hormone deficiency disorders, including diabetes [1], Parkinson's [2], and lysosomal storage disorders [3]. Encapsulation of allogeneic cells in a semi-permeable membrane can provide physical immune protection, and may enable long-term delivery of therapeutic peptides. The most common approach to cell

encapsulation involves embedding cells in a calcium alginate bead that is then coated with a polycation, commonly poly-L-lysine (PLL), to form a stable polyelectrolyte complex (PEC) shell to increase the stability, and tune the permeability, of the membrane [4].

These beads are usually further coated with alginate in order to hide the PLL from the host's immune system, resulting in capsules known as alginate/ PLL/alginate or **APA** capsules [4]. A recent study by Tam et al. suggests that the final layer of alginate does not significantly alter the outer composition of the membrane, casting doubt on the need for this final alginate coating [5].

The properties of **APA** capsules depend significantly on the type and concentration of alginate, PLL and gelling ion (typically calcium) used, as well as on the protocols used for their preparation and storage. Capsules can fail in their immune-protective role in a number of ways, which may include mechanical rupture, loss of the outer alginate coating followed by fibrotic overgrowth [6], and even degradation of alginate by redox processes or hydrolysis [7].

A key issue is the loss of calcium through exchange with, *e.g.*, sodium [8–10], leading to bead swelling [10], decreased gel modulus [11], and even rupture of the **APA** membrane [4].

Improved understanding and control of capsule properties are key challenges in the field, and have led to calls for greater standardization between different labs [12].

Many novel approaches to create covalently crosslinked capsules still use calcium alginate and polycations, such as PLL [13–16].

Tissue-like capsule stiffness and long-term mechanical integrity [17] are critical for successful transplantation of encapsulated therapeutic cells, as well as for related use of these gels in stem cell differentiation and regenerative medicine [18–21].

The mechanical stability of **APA**-type capsules has often been studied using ensemble pass/fail screening for the fraction of intact capsules following exposure to hypotonic media [15, 22], or shaking with glass beads [23]. The thickness of the membrane formed by the PLL–alginate PEC has been used to indicate capsule strength in some studies [4, 24] though at times the strongest capsules were reported to be those having a thin shell formed using higher molecular weight (MW) PLL [24]. In other studies, swelling ratios were used as an indicator of strength [4,25].

Mechanical tests of single alginate capsules have been carried out using atomic force microscopy (AFM) [26], compression testing [11, 17, 27–32], rheology [11], and deformation by centrifugal forces [33,34]. AFM measurements mainly provide information about local surface properties [26], while compression tests provide information about the whole bead from the analysis of Young's modulus [30], viscoelastic properties [35,36], and bursting forces [17, 36,37].

Micropipette aspiration is a common technique for studying mechanical properties of cells [38–40] and small semi-permeable capsules [41–44]. The application of this

method to larger, alginate-based capsules is rare, despite the simplicity of the technique and the quantitative information that can be extracted. Hunkeler and coworkers made limited use of aspiration to measure the membrane tension of capsules composed of an alginate/cellulose sulfate core coated with polymethylene-co-guanidine [45].

This paper describes a simple yet sensitive aspiration-based test of capsule stiffness, its validation and use to study the properties of model capsules as a function of preparation and storage conditions. Confocal microscopy was used to determine capsule morphology, in particular shell thickness, through the use of fluorescein labeled PLL.

2.3. Experimental

2.3.1. Materials

Sodium alginate (Pronova UP MVG, batch: BP-0908-01) was purchased from Novamatrix (Sandvika, Norway). Poly-L-lysine hydrobromide (PLL, M_n 15–30 kDa), fluorescein isothiocyanate (FITC) and HEPES sodium salt from Sigma-Aldrich (Oakville, ON Canada), and sodium chloride and calcium chloride from Caledon Laboratories (reagent grade, Georgetown, ON), were used as received. Trisodium citrate dihydrate (AnalaR) was purchased from EMD Chemicals (Gibbstown, NJ, USA) and was used as received. Sodium hydroxide and hydrochloric acid stock solutions (0.1 or 1.0 M) were purchased from LabChem (Pittsburgh, PA, USA).

2.3.2. PLL fluorescent labeling

FITC-labeled PLL, PLL*f*, was prepared as described earlier [16]. Briefly, PLL (HBr form, 99.5 mg, 0.48 mmol lysine) was dissolved in 0.2 M $NaHCO_3$ buffer (pH 9)

and 1.0 mg (0.0026 mmol) of FITC dissolved in N,N-dimethylformamide was added. The PLL*f* was purified by dialysis and isolated by freeze-drying (64.5 mg, 82% HCl form) with a labeling degree of 0.61%, determined from the maximum absorbance at 495 nm, using the absorption coefficient of free FITC of 77,000 M^{-1} cm^{-1} [46]. The extinction coefficient of PLL*f*, was 2.67 $mL \cdot cm^{-1} \cdot mg^{-1}$, measured at 495 nm.

2.3.3. Preparation of calcium alginate beads (A beads)

A solution of sodium alginate (5–10 mL, 1 wt.%) in saline was filtered (0.2 μm) and then extruded into 60 mL of gelling bath consisting of de-ionized water containing 1.1 wt.% $CaCl_2$ (100 mM) and 0.45 wt.% NaCl (77 mM), reflecting a 12–24 molar excess of Ca^{2+} over carboxylates. Extrusion was done at a rate of 0.5 mL/min, using a syringe pump and a flat-tipped 27 G needle fitted inside a 1 mm diameter tube that provided an annular airflow of 3–4 L/min. This airflow was adjusted to generate narrow disperse calcium alginate beads (**A** beads) with mean diameters of 500 to 600 μm, and standard deviations of about 50 μm. After extrusion was complete, the beads were kept in the gelling bath for another 10 min before being transferred into fresh gelling bath solution (using a 3:10 volume ratio of settled bead suspension to wash solution) for an additional 10 min, and before moving on to coating or aging experiments as described below. All solutions were pre-cooled to 4 ^{o}C and the gelling bath was placed in an ice bath during bead formation. The beads have smooth surfaces, and equatorial / axial aspect ratios not exceeding 1.1.

2.3.4. Preparation of AP and APA capsules

AP beads were prepared by adding 10 mL of 0.05 wt.% PLL or PLL*f* in saline (pH 7.0–7.5) to 3.0 mL of settled, freshly prepared **A** beads. After 6 min with occasional swirling, the supernatant was removed, and the as-formed beads washed a) once with fresh gelling bath and once with saline or b) twice with saline. Each wash took 2 min unless stated otherwise. Supernatant from coating and washing steps were analyzed for residual PLL*f* content using UV/Vis.

APA capsules were prepared by adding 1.67 mL of 0.03% sodium alginate to 0.5 mL of settled **AP** beads for 4 min, with occasional swirling. The resulting **APA** capsules were washed twice with saline for 2 min. All washing steps involved a 3:10 volume ratio of settled beads to coating/washing solution.

2.3.5. Monitoring the effects of storage/washing conditions on A and AP beads

Freshly prepared **A** beads and **AP** capsules were stored in saline (154 mM NaCl) at 4, 20 and 40 ºC. All washing steps used a volume ratio of settled beads to washing solution of 3:10. Beads were monitored by microscopy and aspiration at room temperature, in a small amount of their own supernatant. Supernatants were monitored for Ca^{2+} content using ICP-MS.

2.3.6. Citrate treatment

Sodium citrate (5 mL, 70 mM) and settled **AP** or **APA** capsules (0.5 mL) were mixed at room temperature for 5 min before the supernatant was removed and the settled,

liquid filled capsules were washed once with saline (1.67 mL).

2.3.7. Micropipette aspiration (Scheme 2.1):

A borosilicate disposable micropipette with an inner diameter of 290 μm and an outer diameter of 1120 μm (Fisher Scientific) was attached to a 10 mL glass buret (0.5 cm inner diameter, 65 cm length) using flexible Tygon tubing, forming a U-tube filled with water. A number of capillary tips from one batch were examined by optical or scanning electron microscopy (TESCAN VP SEM) and were found to have smooth, circular openings and near identical inner diameters of 291 ± 2 μm.

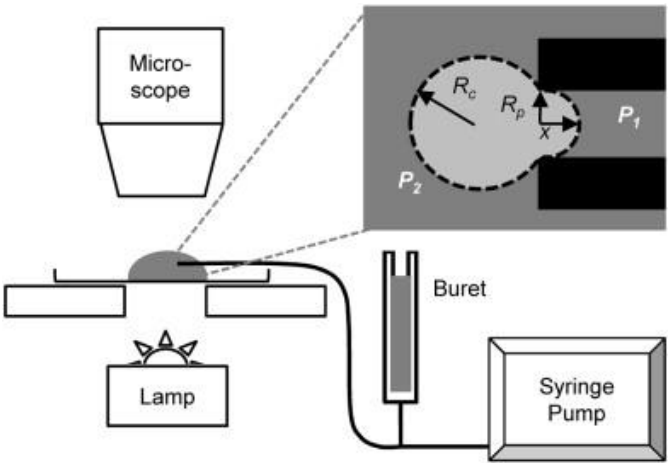

Scheme 2.1. Setup for micropipette aspiration

A syringe pump (NE-1600, New Era Pump Systems™) connected to the Tygon tubing *via* a Y-shaped connector allowed automated control of the height of the water column and hence the pressure differential. About 0.25–0.50 mL of a suspension of capsules in their own storage supernatant (unless indicated otherwise) was placed on a flat, hydrophobic polystyrene dish located on the stage of an Olympus BH2-UMA optical

microscope. Capsules were captured on the open end of the capillary while applying a negative pressure differential of 0.75 nN/μm^2 (equivalent to 0.75 kPa). Once a capsule was captured, the water column was lowered to 3.75 kPa at a rate of 0.75 kPa/min. The rate of change of applied pressure differential was constant for all capsules aspirated, allowing for direct comparison between the viscoelastic beads and capsules. Images of the aspirated capsule were taken every minute in transmission mode. The length of projection of the capsule into the capillary was measured using ImageJ software and plotted against the pressure differential. Measurements were conducted in triplicate, using a new capsule for each aspiration series.

2.3.8. Microscopy

Optical and fluorescence images of capsules were collected with an Olympus BX51 microscope equipped with a Q-Imaging Retiga EXi camera and ImagePro software. Average capsule diameters were determined from measurements of a minimum of 60 capsules.

Confocal microscopy images of **AP** or **APA** capsules prepared using PLL*f* were obtained with a Zeiss LSM510 confocal laser scanning microscope equipped with argon and HeNe lasers, operated with Zeiss LSM510 software, or on a Nikon Eclipse 90i upright microscope equipped with a Nikon C2 confocal head, an argon multi-line laser and NIS-Elements viewer software. The extent of PLL*f* diffusion into the capsules, or membrane thickness, was determined by the full width at half height of 36 μm-wide line profiles across equatorial confocal sections, generated using ImageJ software.

2.3.9. Characterization of coating/washing solutions

Supernatant solutions containing PLL*f* were analyzed by UV–Vis spectroscopy (Cary 50 Bio) following dilution in 35 mM HEPES buffer (pH 7.8) such that the $A_{495} < 1$. The A_{495} value was used to calculate the concentration of PLL*f*, using the PLL*f* extinction coefficient of 2.67 $mL \cdot cm^{-1} \cdot mg^{-1}$ described above.

Some gelling and washing solutions were analyzed for Ca^{2+} content using inductively coupled plasma-mass spectrometry (ICP-MS, PerkinElmer ELAN 6100 with ELAN software) performed by the Occupational and Environmental Health Laboratory at McMaster. Samples were prepared for ICP-MS by dilution with 1% HNO_3 (trace metal grade) to bring the calcium concentration within the calibration range of 0.2–10 ppm.

2.3.10. Statistics

All values are reported and graphed as mean ± standard deviation, with significant differences determined from Student's *t*-test analysis between two groups and one-way ANOVA with a Bonferroni post hoc analysis for comparison of more than two groups. Significance was determined for $p < 0.05$.

2.4. Results and Discussion

Micropipette aspiration has been used extensively to study the mechanical properties of cells [38–40], and thin walled capsules [41–44]. It involves using a micropipette to apply a pressure differential to the wall of a captured cell or capsule, and visually measuring the length of the tongue aspirated into the pipette as a function of

applied pressure differential. The cell or capsule is often modeled as a liquid droplet, or an elastic or viscoelastic solid. In the case of liquid droplets, the surface tension, T, is described by the inset of Scheme 2.1 and the corresponding Eq. (1), where P_1 is the pressure inside the micropipette, P_2 is the pressure of the suspending medium, R_p is the inner radius of the micropipette, R_c is the radius of the microcapsule, and x is the length of the tongue drawn into the pipette. Eq. (1) is only valid when x is less than R_p [41].

$$P_2 - P_1 = 2T\{[2x/(x^2+R_p^2)] - [1/R_c]\} \quad (1)$$

The membrane tension of liquid-filled capsules with thin, semi-permeable membranes can be obtained by an application of Laplace's law, which describes the stretching deformation of a membrane caused by an applied pressure differential. This model however, does not account for any bending stresses due to finite wall thicknesses, or for the presence of a cohesive gel core that would resist deformation [41].

Cells and capsules with gel cores, are usually modeled as incompressible elastic or viscoelastic solids by applying the homogenous half-space model. Eq. (2) can be used to determine Young's modulus for such samples, provided that the inner diameter of the capillary R_p is much smaller than the diameter of the sample aspirated [47].

$$\Delta P = (2\pi Ex/3R_p)\phi \quad (2)$$

Here, $\Delta P = P_2 - P_1$ is the applied pressure differential, and E is Young's modulus of the capsule. ϕ is the wall function, a term with some dependence on the capillary wall

thickness. Eq. (2) requires a thin-walled pipette having a small inner diameter compared to the capsule diameter [47], and only measures the local surface modulus or requires a homogenous sample.

The present study uses aspiration capillaries with an inner diameter approximately 1/2 of the initial capsule diameter, to study the stiffness of both hydrogel beads and capsules and hence Eq. (2) cannot be strictly applied. However, the relatively large radius of the capillary is advantageous, because it provides information on the mechanical properties of the entire bead which are the main interest in capsule applications. Given the relatively large capillary inner diameter, a plot of deformation, normalized to the pipette radius $(x - x_o)/R_p$ *versus* pressure differential (ΔP), reflects a combination of core and membrane properties.

This work studies the initial **A** beads formed by gelling sodium alginate droplets with calcium chloride, as well as the **AP** and **APA** capsules formed by subsequent coatings with PLL, and finally alginate. This approach to capsule formation was originally developed by Lim and Sun [1] and remains the basis for most cell encapsulation procedures [15,16]. The term *bead* is used to reflect the gel nature of the entire as-formed **A** spheres, while with **AP** and **APA,** the term *capsule* indicates the presence of a PEC shell around the gel or liquid core.

Despite the recognition that calcium loss that may occur by exchange with sodium during preparation and storage, there remain significant differences in how different laboratories prepare and handle such capsules [48,49]. One aim of this paper is to detail how subtle variations in preparation and storage conditions can influence the structure

and the mechanical properties of these hydrogel beads and capsules.

2.4.1. Micropipette aspiration applied to calcium alginate type

Fig. 2.1 illustrates primary aspiration data for seven **A** beads with diameters ranging from 564 to 710 μm. These particular beads had been stored in saline, and were transferred into fresh saline just prior to testing. Fig. 2.1 shows a linear increase in the non-dimensional strain $(x - x_o)/R_p$ with increasing pressure differential, for each bead. The deformation $(x - x_o)$ was determined from the length of the projection into the capillary, x, minus x_o, the length of the tongue projecting into the capillary at zero pressure differential resulting from the natural curvature of the beads. x_o was determined from the x-intercept of ΔP *versus* x plots since beads could not be captured at $\Delta P = 0$. The slopes (pressure differential, ΔP, *versus* $(x - x_o)/R_p$) describe the stiffness of the beads, where the differences in the slope are attributed to random scatter in the sample stiffness rather than a function of bead size (see Fig. 2A.1 in the Supporting information for a plot of stiffness *vs*. bead diameter). Thus, the average stiffness of these beads was measured to be 15.5 ± 1.3 kPa.

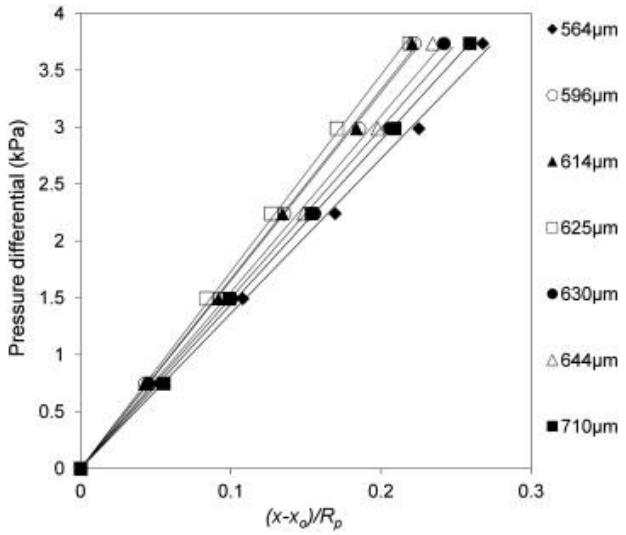

Fig. 2.1 Pressure differential (ΔP) versus normalized deformation $(x - x_o)/R_p$ for **A** beads with diameters from 564 to 710 µm.

The stiffness of **A** beads and **AP** capsules, determined from this method are equivalent within experimental error for different capillaries of the same inner diameter. The *slope* of the linear aspiration curves reflects the beads' overall stiffness, which may include contributions from:

1) stretching and bending stress of the membrane during deformation [41], and

2) deformation of the gel core, including water-loss from core compression.

Data points were rejected when the projection into the pipette exceeded the inner radius of the pipette. In such cases images were collected more frequently at low pressure differentials to ensure an adequate number of data points with $x < R_p$.

Fig. 2.2 shows aspiration curves for **A** beads that had been treated to zero and three saline washes (one bead each). These aspiration curves show how stiffness decreases with successive saline washes, reflecting weakening of the calcium alginate gel due to calcium loss.

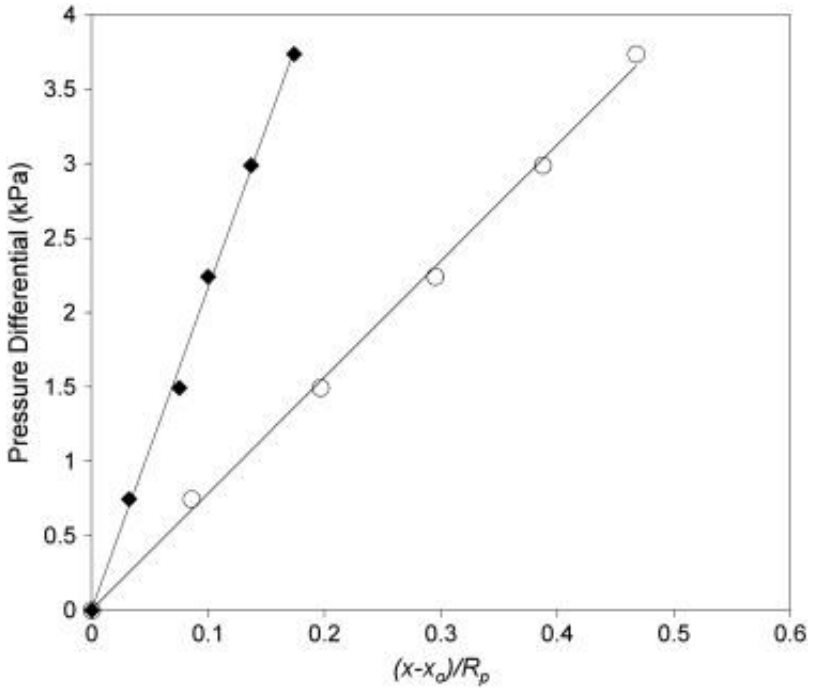

Fig. 2.2 Aspiration plots for individual calcium alginate beads as formed (◆) and washed three times with saline (○). The aspiration curves are linear fits to the data points.

2.4.1.1. Mechanical properties of calcium alginate-based beads

The properties of the calcium alginate beads are affected by the concentration and MW of the alginate, as well as the ratio and distribution of its guluronic (G) and mannuronic acid (M) units. Higher G/M ratio alginates produce stiffer gels with better mechanical integrity [50]. Also important are the type and concentration of the gelling ion (typically Ca^{2+}, as well as Sr^{2+} or Ba^{2+}), the presence of other ions such as sodium in the

gelling solution, and the gelling time and temperature. Divalent cations with higher affinities for alginate, such as Sr^{2+} and Ba^{2+} lead to formation of inhomogeneous beads (dense shell, diffuse core), while the addition of non-gelling ions such as sodium to the gelling bath, leads to beads with increased homogeneity [9,51]. Bead properties can continue to change with storage, especially due to Ca^{2+} loss [9,50,52].

Treatment of **AP** and **APA** capsules with citrate has often been done in the past to extract calcium and liquefy the cores [16,31,53]. This process will remove contributions of stiffness arising from the calcium alginate gel core and the calcium alginate portion of the shell, and leave only the PLL–alginate PEC component of the shell.

Less well appreciated is the significant effect of washing steps during preparation on the structure and strength of the alginate-based capsules. Hsu et al. found that omitting a saline wash prior to PLL coating led to stronger APA capsules with denser shells and higher in *vivo* integrity [54]. Ma et al., using calcium lactate instead of calcium chloride in their gelling bath, and omitting washing with CHES ((N-cyclohexyl-)2-aminoethanesulfonic acid) solution after PLL coating, obtained more robust capsules, as determined by the percentage of intact capsules after explantation [24].

In this work, the calcium alginate beads were prepared by gelling a 1% solution of Pronova UP MVG alginate in a bath containing 100 mM $CaCl_2$ and 77 mM NaCl. The alginate solution had a viscosity of about 200–250 cP, which is thought to be ideal for bead preparation [55]. The gelling solution contains sodium chloride at concentrations

often used to generate "homogeneous" beads, with less pronounced core–shell morphology [15,16,51,56].

All solution changes were carried out using volume ratios of settled beads to new solution of 3:10. The initial gelling bath contains an excess of Ca^{2+} to alginic acid units (12-to-24-fold depending on amount of alginate gelled), and ICP-MS analysis of the gelling bath after bead formation revealed little change in the Ca^{2+} concentration. The subsequent transfer into saline reduces the calcium concentration from 100 mM to about 20 mM, reflecting a roughly 1:4 ratio of solution remaining in interstitial and pore volume in the settled beads, to new solution.

2.4.1.2 Effect of gelling time and temperature on stiffness of A beads

One common variable in the literature is the total gelling time of **A** beads, comprised of the time needed to form a batch of beads plus an additional 5–30 min in gelling bath to allow the last-formed beads to cure [50]. Longer exposure to the gelling solution can further strengthen the gel, but may be detrimental to encapsulated cells. Velings reported that at least 10 h is needed to fully stabilize calcium alginate beads stored in 50–330 mM calcium chloride solutions containing a total ionic strength of 1 M adjusted by addition of sodium chloride [57].

The **A** beads in this study were prepared during 10 to 20 min of extrusion time and stored in this initial gelling bath for an additional 10 min. They were then transferred to a fresh gelling solution for 10 min, and finally transferred into saline and stored at 4 °C.

Fig 2.3 shows an increase in stiffness of the resulting **A** beads from 13.2 ± 0.3 kPa for as-formed beads, to a plateau of about 34.4 ± 2.0 kPa after 500 h. This slow curing may involve additional crosslinking due to the approximately 20 mM Ca^{2+} still present in the saline storage solution, as well as annealing of existing calcium alginate crosslinks facilitated by the sodium chloride present [56,57].

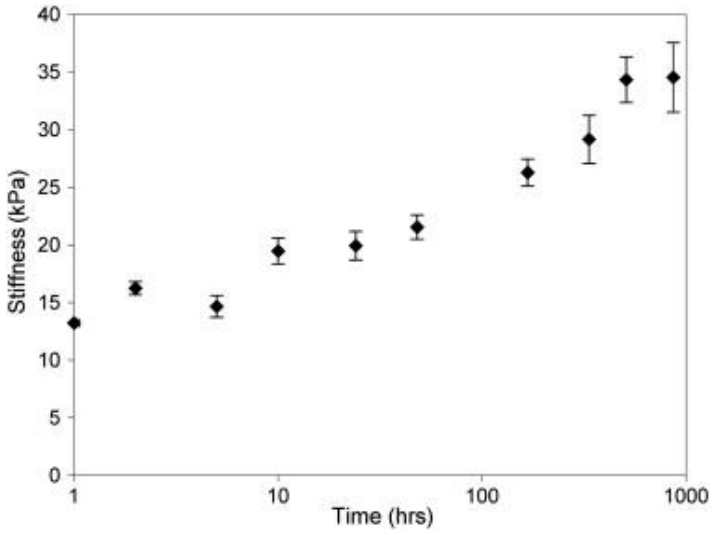

Fig. 2.3 Stiffness of **A** beads during storage in the first saline wash at 4 °C. Stiffness was measured at 20 °C.

Serp et al. found that heating **A** beads in 11 mM Ca^{2+} led to smaller, denser, and stiffer beads, with these effects becoming more pronounced as the temperature was increased from 50 to 130 °C [58]. Temperatures used for **A** beads containing cells usually just range from 4 to 37 ^{o}C [59–61].

To explore the effect of temperature on curing behavior in this more narrow

temperature range, **A** beads washed once with saline were stored at 4, 20 and 40 ^{o}C, and their stiffness monitored over one week. The stiffness of all beads increased with time as expected from Fig. 2.3, with a negligibly higher curing rate at higher temperatures (see Fig. 2A.2 in the Supporting information).

2.4.1.3. Effect of additional saline washes on stiffness and swelling of A beads

Additional wash cycles with saline should further reduce the Ca^{2+} concentration in the supernatant and cause Ca^{2+} loss from the beads in exchange for sodium, leading to both swelling and decreased stiffness. Bead swelling during saline washes is often used as a measure of the stability of alginate-based beads and capsules [4,24].

Serp et al. observed no swelling of calcium alginate beads when $[Na^{+}]/[Ca^{2+}]$ in solution was less than 20, though changes to mechanical properties were already noticed at $[Na^{+}]/[Ca^{2+}]$ greater than 5 [62]. Similarly, two other groups reported swelling of high G calcium alginate beads for $[Na^{+}]/[Ca^{2+}]$ ratios exceeding 20 [63] or 30 [28], and found this ratio to vary with alginate composition (G/M ratio) [28,63].

ICP-MS was used in the present work to measure $[Ca^{2+}]$ in the supernatant following successive saline washes of **A** beads, using 3:10 volume ratios of settled beads to saline wash solution.

Fig. 2.4 shows $[Ca^{2+}]$ dropping rapidly from 100 mM in the gelling bath to 2.9 mM after the third wash, and then descending more slowly as bound Ca^{2+} was released into the supernatant.

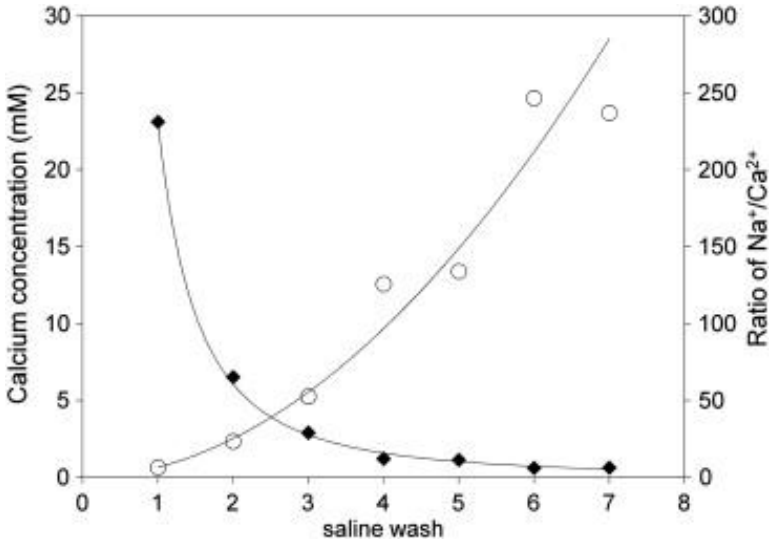

Fig. 2.4 $[Ca^{2+}]$ and $[Na^{+}]/[Ca^{2+}]$ in supernatant during successive saline washes of **A** beads. (◆): $[Ca^{2+}]$; (○): $[Na^{+}]/[Ca^{2+}]$

Fig. 2.5 compares the diameter and stiffness during these successive saline washes. It had previously been shown that calcium alginate gels stored in saline containing 1.8 mM $CaCl_2$ and 0.15 M NaCl decreased in strength over the first 15 h [11]. As a result, beads were stored for a minimum of 20 h after each saline wash before carrying out these measurements.

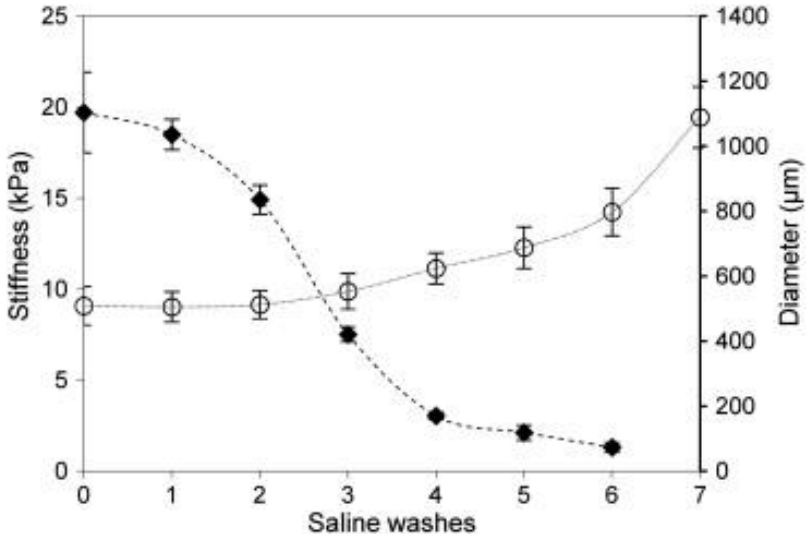

Fig. 2.5 Stiffness (◆) and diameter (○) of **A** beads as function of the number of saline washes.

The first saline wash did not affect stiffness or bead diameter. This appears to be consistent with previous data by Morch et al., carried out using slightly different washing protocols [9]. As mentioned above, the presence of about 20 mM of calcium in the first saline wash is sufficient to maintain the gel strength.

After the second saline wash, the calcium concentration is reduced to ~6.5 mM ($[Na^+]/[Ca^{2+}]$ ratio of 24) and the stiffness decreased significantly compared to the starting alginate bead ($p < 0.05$ by Student's *t*-test). In contrast, the bead diameter only started to increase at the third saline wash compared to the starting mean diameter ($p < 0.001$), where the $[Na^+]/[Ca^{2+}]$ exceeded 30. Stiffness decreased and diameter increased until the seventh wash, at which point the beads were at the brink of failure and could not be aspirated without rupture.

These data suggest that aspiration is a much more sensitive probe for bead strength and calcium loss, than measurement of bead diameters.

In contrast to the above saline-washed **A** beads, **A** beads washed with gelling bath showed slight increases in stiffness (see Fig. 2A.3 in the Supporting information), likely because of ongoing annealing of the gel, rather than further calcium uptake. The average stiffness (31 ± 6 kPa) after two or more washes (48 h in 100 mM calcium chloride) was greater than or equal to the stiffness of 34 ± 2 kPa reached after approximately 500 h in 20 mM calcium chloride (Fig. 2.3).

2.4.2. Stiffness of AP capsules as a function of coating protocol

The calcium alginate beads (**A**) used in cell encapsulation are usually coated with a polycation such as PLL. The resulting PLL–alginate PEC shell reduces capsule permeability, and increases capsule mechanical stability. The nature of this PEC shell depends on G/M ratio, calcium alginate porosity, PLL MW and concentration [4,24,52], and ionic strength and type of ions present in the medium [4]. Lower MW PLL can penetrate more deeply into the bead to form a thicker shell, while higher MW PLL leads to thinner shells. Similarly, increasing the PLL coating time and concentration can increase the thickness of the membrane [24,49], the amount of PLL bound [4] and the strength of the capsule [52].

Vandenbossche et al. studied the MW cut-off and PLL distribution in **APA** capsules as a function of PLL coating time and concentration and suggested that in order to reduce variability between batches, PLL should be allowed to react with calcium

alginate until completion, *e.g.* for 30 min at 40 ^{o}C, for a PLL concentration of 0.1% (w/v) [48]. With an eye to maximize eventual cell viability, a more conservative coating protocol was used in the present study (0.05% PLL for 6 min at 4 °C) [15,16,64–67]. Coating conditions were kept constant, and stiffness measured by aspiration was used to determine the effects of different washing protocols after PLL coating.

2.4.2.1. Effect of washing solution on AP capsules

Different protocols in the literature describe washing capsules with saline [5,48,51,54,68–70], or gelling bath [15,16], following PLL coating. To the best of our knowledge the effect of calcium on PLL distribution and associated mechanical properties in **AP** capsules has not yet been reported. Calcium alginate beads will bind more chitosan from coating solutions containing calcium chloride, rather than saline. This effect was attributed to calcium specifically rather than differences in ionic strength and thought to be due to a greater porosity of the alginate beads facilitating chitosan loading [71].

The present study hence explores the effect of different saline and calcium chloride treatments, on swelling, stiffness and PLL distribution of **AP** and **APA** capsules.

2.4.2.2. Effect of calcium exposure on AP capsules

AP capsules were washed with a) saline for 2 min, b) gelling solution for 2 min, or c) gelling solution for 2 h, before being transferred to saline. The three types of capsules are denoted as $\mathbf{AP^{SS}}$, $\mathbf{AP^{GS}_{2\ m}}$ and $\mathbf{AP^{GS}_{2\ h}}$, respectively, where SS, $GS_{2\ m}$ and $GS_{2\ h}$ denote their washing histories.

UV/Vis analysis of the combined coating and first washing supernatants showed that all three capsules bound similar amounts (84–86%) of the PLL*f* from the coating solutions.

Fig. 2.6a compares the stiffness of the three capsules. The **AP^{SS}** capsules have a stiffness (23 ± 2 kPa) comparable to those of the **A** beads (25 ± 2 kPa after 24 h of storage). It appears that the formation of the PEC shell in the **AP^{SS}** capsules offsets any weakening of the calcium alginate gel upon exposure to saline during coating and washing. The **AP$^{GS}_{2\ m}$** (42 ± 4 kPa) and **AP$^{GS}_{2\ h}$** (45 ± 4 kPa) were significantly stiffer than **AP^{SS}** capsules which is mainly attributed to these capsules retaining the strength of their calcium alginate gel cores. ICP-MS revealed that the **AP^{SS}** capsule experienced Ca^{2+} levels of about 2.5 mM in the second saline wash. In contrast, the **AP$^{GS}_{2\ m}$** and **AP$^{GS}_{2\ h}$** capsules have 20 mM Ca^{2+} in their storage solution, and hence the strength of the calcium alginate gel is maintained or even increased by extended curing.

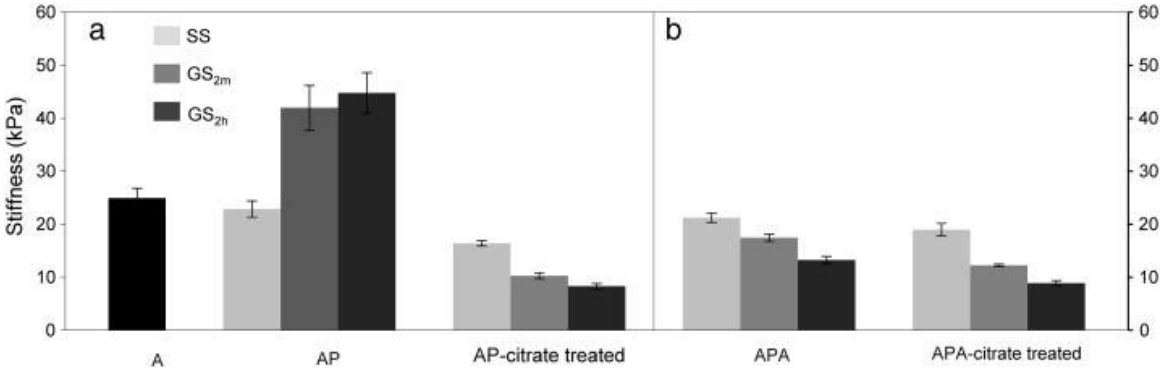

Fig. 2.6 The effect of different washing protocols on the stiffness of a) **AP** and b) **APA** capsules, both as formed, and following treatment with citrate to fully dissolve the calcium alginate cores. SS, $GS_{2\ m}$ and $GS_{2\ h}$ correspond to washing in saline (2 min) or gelling bath wash for (2 min or 2 h), respectively, followed by storage in saline.

The capsule diameters are consistent with the differences in stiffness showing marginally larger mean diameter for $\mathbf{AP^{SS}}$ capsules (544 ± 45 μm) compared to the $\mathbf{AP^{GS}}_{2\ m}$ and $\mathbf{AP^{GS}}_{2\ h}$ capsules (524 ± 39 μm and 518 ± 38 μm, respectively). While the differences in diameter between the $\mathbf{AP^{SS}}$ capsules and either $\mathbf{AP^{GS}}$ capsule ($p < 0.01$ by ANOVA) are statistically significant, the absence of overlap of the standard deviations in stiffness measurements illustrates the greater signal/noise of the aspiration data.

As mentioned above, stiffness measurements using intermediate diameter capillaries reflect properties of both gel cores and PEC shell. To distinguish between these contributions, the three capsule types were treated with sodium citrate to remove Ca^{2+} and liquefy the core.

The citrate-treated $\mathbf{AP^{SS}}$ capsules (Fig. 2.6a) showed only a moderate further decrease in stiffness, attributed to removal of bound Ca^{2+} from the core and shell.

In contrast, citrate treatment led to a large decrease in stiffness for both $\mathbf{AP^{GS}}$ capsules, reflecting the large role of calcium in stiffening these capsules before citrate treatment. Of special interest is that both types of $\mathbf{AP^{GS}}$ capsules had lower stiffness than $\mathbf{AP^{SS}}$ capsules following citrate treatment (Fig. 2.6a), indicating that post-PLL gelling bath washes may only temporarily strengthen the capsules. These results are consistent with recent analogous observations where PLL-alginate capsule walls were found to be softer than those of calcium alginate [34].

While the relative degree of capsule swelling is often used to assess capsule

strength, swelling caused by citrate treatment of these particular capsules proved to be an unreliable indicator of relative capsule strength. The three types of capsules, swelled by small, and similar amounts (about 15–20 ± 10%) upon citrate treatment, while showing quite different capsule stiffness ($p < 0.01$ for all citrate treated **AP** capsules).

Confocal microscopy revealed that gelling bath washes allow the initially bound PLL*f* to redistribute further into the capsules (Fig. 2.7). While in $\mathbf{AP}^{\mathbf{SS}}$ capsules the PLL*f* shell was 9.2 ± 0.9 μm thick, washing with gelling bath led to PLL*f* shell thicknesses of 26 ± 2 μm for $\mathbf{AP}^{\mathbf{GS}}{}_{\mathbf{2\ m}}$ and 46 ± 4 μm for $\mathbf{AP}^{\mathbf{GS}}{}_{\mathbf{2\ h}}$. Subsequent citrate-treatment caused little change in PLL*f* shell thicknesses, at 10 ± 1, 27 ± 1 and 51 ± 3 μm, respectively, lending confidence that aspiration measurements of these hollow capsules reveal the contribution of the PEC shell to the overall stiffness of the earlier, composite capsules that still had calcium alginate gel components in the core and shell contributing to stiffness.

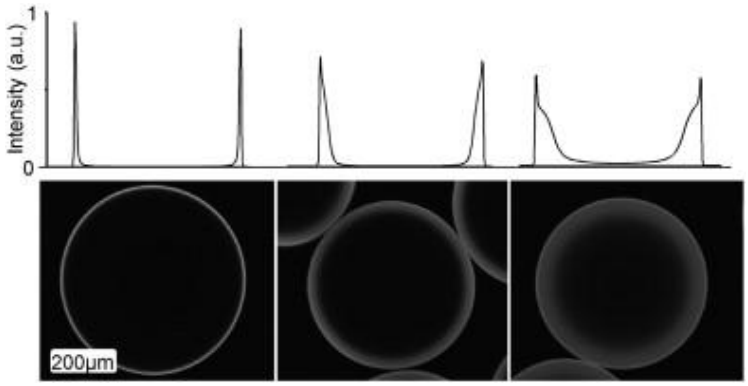

Fig. 2.7 Line profiles (top) and equatorial confocal images (bottom) showing the distribution of PLL*f* in $\mathbf{AP}^{\mathbf{SS}}$ (left), $\mathbf{AP}^{\mathbf{GS}}{}_{\mathbf{2\ m}}$ (middle) and $\mathbf{AP}^{\mathbf{GS}}{}_{\mathbf{2\ h}}$ (right) capsules.

Previous studies have observed the migration of polycations in capsules and found

that it can be facilitated by the presence of divalent metal ions such as Ca^{2+}. Strand et al. noticed slow changes to PLL distribution in **AP** capsules during storage in saline containing 1 mM $CaCl_2$, leading to a doubling of the shell thickness over two weeks, with no further changes over two years [51]. Gåserød et al. found dramatic differences in the rate, location and extent of chitosan binding, depending on the Ca^{2+} content of the coating solution [71,72]. Higher [Ca^{2+}] in the coating solution led to increased in-diffusion, more chitosan bound and greater capsule strength. While higher ionic strength was thought to facilitate chitosan in-diffusion, the rate and extent of chitosan binding were greater in the presence of $CaCl_2$ than for NaCl solutions of the same ionic strength. Enhancement of cooperative Ca^{2+}–alginate binding, sometimes referred to as egg box structures, and the resulting increased porosity, was believed to be important.

Thu et al. reported that the presence of 12 mM Ca^{2+} or Sr^{2+} in the supernatant caused the release of PLL from **AP** capsules into the surrounding solution during three weeks of storage [4]. It appears that most of the PLL*f* migration in the capsules studied here takes place within the hydrogel rather than into the supernatant, as confirmed by the presence of only trace amounts of PLL*f* in washing solutions determined by UV–Vis analysis.

In the current work, all three types of capsule bind similar amounts of PLL but the different washing procedures cause different radial distributions. The high charge density of PLL is thought to lead to a "hit and stick" mechanism, causing PLL to initially bind preferentially to surface regions [4,73]. Higher ionic strength and, in particular, Ca^{2+} in

the washing solution, can weaken the interactions between PLL and alginate, allowing PLL to diffuse further into the gel. This results in thicker but lower density PEC shells that are less stiff once the calcium alginate component is removed by citrate or, equivalently, multiple saline washes as described below. In addition to affecting capsule strength, the differing shell morphologies might influence the permeability and biocompatibility of the membranes. The sensitivity of capsule structure to slight variations in preparation details (*e.g.*, washing) may help to explain why capsules made with apparently similar procedures can perform quite differently.

The rate at which the PLL*f* moved further into the **AP** capsules was examined by tracking the shell thickness and stiffness over time for capsules stored in gelling bath (100 mM Ca^{2+}, 77 mM Na^{+}) and first saline wash (~20 mM Ca^{2+}, 154 mM Na^{+}) (Fig. 2.8), respectively. The shells of capsules stored in ~20 mM Ca^{2+} thicken from about 25 to 30 μm over 30 min, and then more slowly to 35 μm after 13 h. The capsules stored in 100 mM Ca^{2+} show a much faster increase in shell thickness, reaching 75 μm after 18 h.

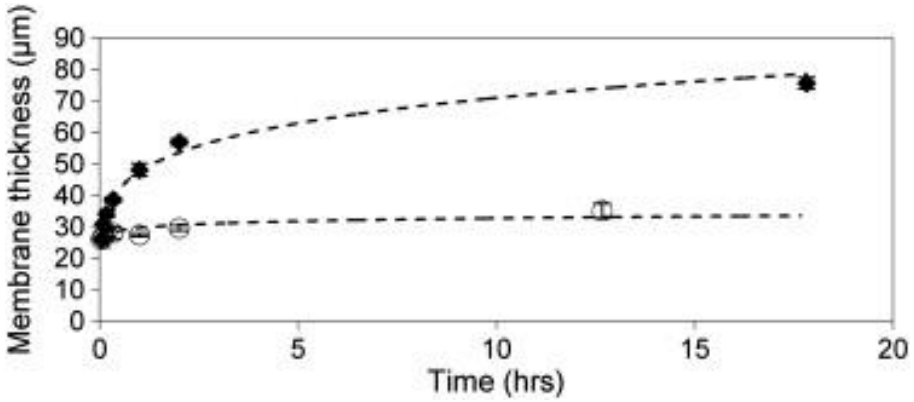

Fig. 2.8 Thickness of PLL*f* shell as function of storage time in (◆) gelling bath ([Ca^{2+}] = 100 mM) or (○) saline ([Ca^{2+}] = 20 mM).

The above **AP** capsules, stored in 100 mM Ca^{2+} for 2 min to 18 h, were treated with citrate to liquefy the core, and then tested by aspiration. Citrate-treatment is used here to mimic the replacement of calcium with sodium during multiple saline washes, or indeed during incubation and implantation. Fig. 2.9 shows that the PEC shells become both thicker and more compliant with increasing storage time in 100 mM Ca^{2+}.

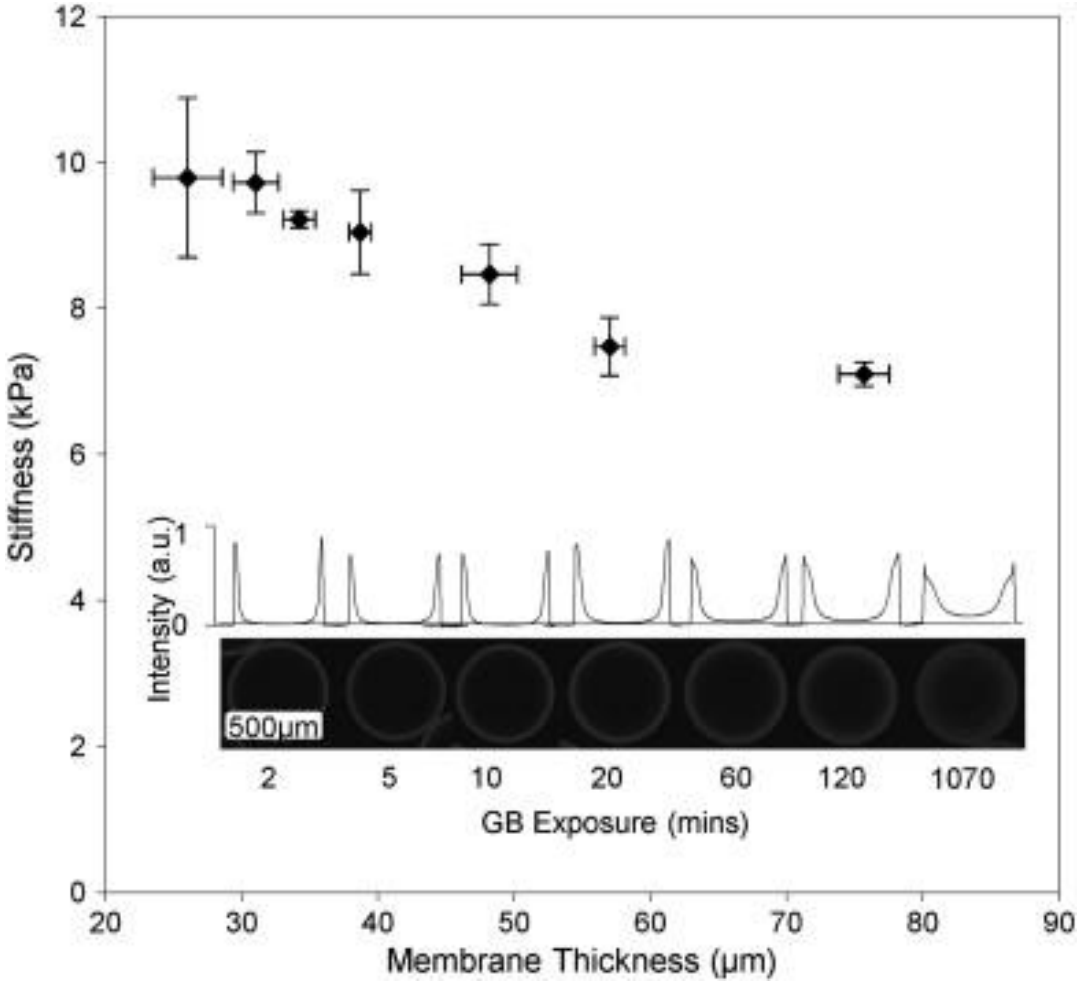

Fig. 2.9 Stiffness of citrate-treated **AP** capsules *versus* membrane thickness, for **AP** beads stored in gelling solution for 2 min to 18 h. The inset shows the corresponding confocal images and line profiles, before citrate treatment.

These results confirm that storage in gelling bath following PLL coating can increase short-term gel stiffness, but can compromise long-term strength of the capsules, by weakening the PLL–alginate PEC shell that is responsible for long-term integrity.

As mentioned above, calcium alginate gels weaken when exposed to saline solutions with [Ca^{2+}] of ~6.5 mM. A similar process will occur *in vivo* because of the low serum Ca^{2+} levels of about 1 mM. Both treatments with chelating agents such as citrate, and exposure to saline, are often used to mimic this process. Fig. 2.10 compares the stiffness for $\mathbf{AP^{GS}_{2\ h}}$ capsules treated using both methods. The resulting capsules showed increasing compliance with successive saline washes, until after six washes the stiffness levels off at a value corresponding to that of the citrate-treated **AP** capsules. These results show the rapid weakening of the gel core that occurs in solutions with low calcium levels and demonstrate that the alginate–PLL PEC shell is responsible for the long-term strength of such capsules.

$\mathbf{AP^{GS}_{2\ h}}$ capsules treated with citrate or seven saline washes experienced 18 and 6% swelling, respectively, even though both treatments lead to a three-fold decrease in stiffness (Fig. 2.10). This again highlights the ability of aspiration to detect changes in mechanical properties despite a comparative lack of swelling.

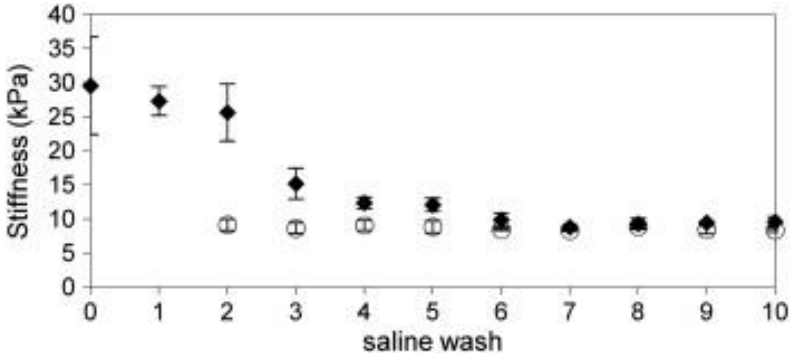

Fig. 2.10 Stiffness for (◆) untreated and (○) citrate-treated $\mathbf{AP^{GS}_{2\ h}}$ capsules as a function of saline washes.

2.4.3. APA capsules: The effect of the final alginate coating

A final coating of alginate is often applied to **AP** capsules to improve the biocompatibility by covering the PLL, however, there is debate about the need for this step [4,5]. The effect of the final alginate coating on the mechanical and structural properties of **AP** capsules was hence examined by aspiration, optical and confocal microscopy.

$\mathbf{AP^{SS}}$, $\mathbf{AP^{GS}_{2\ m}}$ and $\mathbf{AP^{GS}_{2\ h}}$ beads were coated with 0.03% sodium alginate for 4 min to form the corresponding $\mathbf{AP^{SS}A}$, $\mathbf{AP^{GS}_{2\ m}A}$ and $\mathbf{AP^{GS}_{2\ h}A}$ beads, respectively. These were washed once with saline and stored in a second saline solution for 24 h before testing.

The stiffness of these three types of **APA** capsules differs significantly (Fig. 2.6b) with $\mathbf{AP^{SS}A}$ capsules stiffer than $\mathbf{AP^{GS}A}$ capsules ($p < 0.01$ of all **APA** capsule types). $\mathbf{AP^{SS}}$ capsules showed no apparent change after coating with alginate ($p > 0.05$), while

both types of **AP^{GS}A** capsules were substantially weaker than their **AP^{GS}** precursors ($p < 0.01$).

Exposure to the final alginate solution and subsequent saline washes apparently causes significant loss of Ca^{2+} from the **AP^{GS}** capsules. In contrast, **AP^{SS}** beads, which already had little core gel strength prior to the final alginate coating, show little change in this step. Once the gel in the core is weakened by Ca^{2+} loss and the contribution of the shell to capsule strength becomes more important, the less diffuse shells of **AP^{SS}** capsules compared to **AP^{GS}** leads to greater stiffness.

It was found that the **AP^{GS}A** capsules have a slightly thinner PEC membranes compared to their **AP^{GS}** precursors (19 ± 1 μm and 36 ± 3 μm *vs*. 26 ± 2 μm and 46 ± 4 μm for **AP$^{GS}_{2\ m}$A** and **AP$^{GS}_{2\ h}$A** respectively), likely because the **APA** capsules have less exposure to significant Ca^{2+} concentrations. ICP-MS showed 20 mM Ca^{2+} in the **AP$^{GS}_{2\ m}$** supernatant, compared to 2 mM in the **AP$^{GS}_{2\ m}$A** supernatant, allowing continuing PLL in-diffusion in the **AP$^{GS}_{2\ m}$** capsules during storage, in contrast to the **AP$^{GS}_{2\ m}$A** capsules. Thus, coating with alginate can reduce calcium levels below those needed for further PLL in-diffusion, and thus indirectly affects PLL distribution in the **AP$^{GS}_{2\ m}$A** capsules by stopping PLL migration during storage.

Washing with a calcium-containing solution such as gelling bath following PLL coating has been done in the past to ensure a highly crosslinked gel core. It can also increase the amount of surface alginate bound to the capsule surface. This is thought to be due to the creation of an outer calcium alginate gel layer, formed using calcium escaping

from the core of the capsule. However, this surface gel is not stable and about 80% was lost after 24 h of storage in saline, presumably due to calcium loss [4]. Thus, modifying **APA** capsule formation procedures can result in structural changes to the PEC shell and should be acknowledged.

2.4.3.1. Effect of citrate treatment on APA capsules

All three types of **APA** capsules were treated with citrate to dissolve any residual calcium alginate gel and determine the effect, if any, of the final layer of alginate on PEC shell stiffness. **AP^{SS}A** capsules showed a small change in stiffness after citrate treatment (Fig. 2.6b), indicating the presence of at most a weak gel core in the precursor capsules. Citrate treatment gave a more pronounced decrease in stiffness for **AP$^{GS}_{2\ m}$A** and **AP$^{GS}_{2\ h}$A** capsules (Fig. 2.6b), reflecting the presence of more gel in these cores ($p < 0.05$ on respective **APA** capsules before and after citrate treatment).

AP^{SS}A diameters increased by 3% after citrate treatment compared to 13% for both **AP$^{GS}_{2\ m}$A** and **AP$^{GS}_{2\ h}$A** capsules, consistent with more calcium crosslinking in the gel cores for the **AP^{GS}A** capsules. The earlier loss of Ca^{2+} from **AP^{SS}A** capsules may also allow some alginate to escape from the capsules, reducing the osmotic pressure experienced during subsequent citrate treatment.

Capsules stored in their original saline supernatant show little change to the mechanical properties over a period of 6 weeks (Fig. 2.11). It is worth noting that any initial differences in strength between the **AP** and **APA** membranes within a capsule type tended to disappear with time (see Fig. 2.11), suggesting slow restructuring of the PEC

membrane. The final alginate coat hence seems to not significantly contribute to the mechanical properties of **APA** capsules.

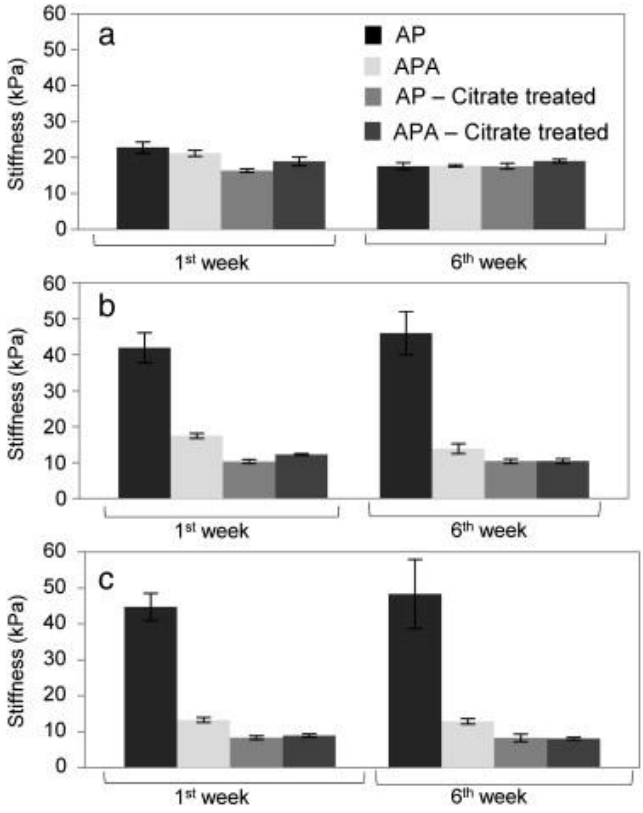

Fig. 2.11 Stiffness of untreated and citrate-treated **AP** and **APA** capsules during the first and sixth week of storage for a) $\mathbf{AP^{SS}A}$, b) $\mathbf{AP^{GS}{}_{2\,m}A}$ and c) $\mathbf{AP^{GS}{}_{2\,h}A}$.

The situation may be more complex *in vivo* where encapsulated cells and the host may deposit materials, both within the capsules, and on the capsule surface. These biological processes will themselves be sensitive to the composition of the capsule. A recent study by Gardner et al. [74] found that **APA** capsules explanted after six weeks in mice were stronger than the initial capsules or those that had been incubated for six weeks *in vitro* as measured by a chemical challenge (citrate/high pH). This behaviour was attributed to the deposition of cells and proteins on the outer capsule surface.

Preliminary aspiration experiments with these same capsules conducted during the current work indeed revealed that they had become stronger (stiffer) during implantation. **APA** capsules (empty or cell containing) showed an increase in stiffness after six weeks of implantation while control **APA** capsules incubated *in vitro* showed little change in stiffness. The measurements on explanted capsules were complicated by fibrotic overgrowth. Some capsules showed a large degree of fibrotic overgrowth and only capsules with minimal cellular deposits were tested. In addition, a poly(ethylene oxide) coated capillary was used to reduce interactions between protein and cellular deposits on the capsules, and the micropipette tip. We are currently developing cross-linked capsules with improved anti-fouling properties, and will carry out further studies on these in the future.

The current work illustrates that aspiration can serve as a rapid and sensitive tool for revealing changes to the capsule surface both *in vitro* and in biological environments. Overall, the present work may help our understanding of the complex behavior of such hydrogel capsules throughout their lifetime (preparation, coating, implantation), and may serve as a starting point for further, cell and animal-based studies.

2.5. Conclusion

Micropipette aspiration is a useful tool for understanding the mechanical properties of **A, AP** and **APA** beads and capsules, providing sensitivity in measurements yet being a rapid and simple technique. The calcium alginate core provides most of the initial mechanical strength in these hydrogels, while the PEC membrane dominates long-

term stability, due to calcium loss from **AP** and **APA** capsules. The mechanical properties of this membrane depends on the coating process in several ways: gelling bath washes following the PLL deposition redistributes this polycation further into the capsule, resulting in a thicker, and, at least at the present PLL concentrations, more compliant PEC membrane. The final alginate coating speeds calcium loss from the gel core, but does not seem to affect final membrane mechanical properties.

Supplementary data to this article can be found in the Chapter 2 Appendix (section 2.8).

2.6. Acknowledgements

We would like to thank the Natural Sciences and Engineering Research Council of Canada (NSERC) for funding, and Kevin Ferguson of OEHL at McMaster University for determination of Ca^{2+} content by ICP-MS.

2.7. References

[1] F. Lim, A.M. Sun, Microencapsulated islets as bioartificial endocrine pancreas, Science. 210 (1980) 908–911.
[2] T. Yasuhara, T. Shingo, K. Muraoka, M. Kameda, T. Agari, Y. W. Ji, H. Hayase, C. V. Borlongan, I. Date, Neurorescue effects of VEGF on a rat model of Parkinson's disease, Brain Research. 1053 (2005) 10–18.
[3] C.J.D. Ross, L. Bastedo, S.A. Maier, M.S. Sands, P.L. Chang, Treatment of a lysosmal storage disease, mucopolysaccharidosis VII, with microencapsulated recombinant cells, Hum. Gene Ther. 11 (2000) 2117–2127.
[4] B. Thu, P. Bruheim, T. Espevik, O. Smidsrød, P. Soon-Shiong, G. Skjåk-Bræk, Alginate polycation microcapsules. 1. Interaction between alginate and polycation, Biomaterials. 17 (1996) 1031–1040.
[5] S. K. Tam, S. Bilodeau, J. Dusseault, G. Langlois, J.P. Hallé, J.H. Yahia, Biocompatibility and physicochemical characteristics of alginate-polycation microcapsules, Acta Biomaterialia. 7 (2011) 1683–1692.

[6] B.L. Strand, L. Ryan, P.J. Veld, B. Kulseng, A.M. Rokstad, G. Skjåk-Bræk, T. Espevik, Poly-L-lysine induces fibrosis on alginate microcapsules via the induction of cytokines, Cell Transplant. 10 (2001) 263–275.
[7] H.K. Holme, L. Davidsen, A. Kristiansen, O. Smidsrød, Kinetics and mechanism of depolymerization of alginate and chitosan in aqueous solution, Carbohydr. Polym. 73, (2008) 656–664.
[8] S. Saitoh, Y. Araki, R. Kon, H. Katsura, M. Taira, Swelling/deswelling mechanism of calcium alginate gel in aqueous solutions, Dent. Mater. J. 19 (2000) 396–404.
[9] Y. A. Mørch, I. Donati, B.L. Strand, G. Skjåk-Bræk, Effect of Ca^{2+}, Ba^{2+} , and Sr^{2+} on alginate microbeads, Biomacromolecules, 7 (2006) 1471–1480.
[10] X. Wang, H. G. Spencer, Calcium alginate gels: Formation and stability in the presence of an inert electrolyte, Polymer. 39 (1998) 2759–2764.
[11] M.A. LeRoux, F. Guilak, L.A. Setton, Compressive and shear properties of alginate gel: effects of sodium ions and alginate concentration, J. Biomed. Mater. Res. 47 (1999) 46–53.
[12] P. de Vos, M. Bukco, P. Gemeiner, M. Navrátil, J. Švitel, M. Faas, B.L. Strand, G. Skjåk-Bræk, Y.A. Mørch, A. Vikartovská, I. Lacík, G. Kolláriková, G. Orive, D. Poncelet, J.L. Pedraz, M. B. Ansorge-Schumacher, Multiscale requirements for bioencapsulation in medicine and biotechnology, Biomaterials. 30 (2009) 2559–2570.
[13] J. Dusseault, F.A. Leblond, R. Robitaille, G. Jourdan, J. Tessier, M. Ménard, N. Henley, J.P. Hallé, Microencapsulation of living cells in semi-permeable membranes with covalently cross-linked layers, Biomaterials. 26 (2005) 1515–1522.
[14] H. Chen, W. Ouyang, B. Lawuyi, S. Prakash, Genipin cross-linked alginate-chitosan microcapsules: Membrane characterization and optimization of cross-linking reaction, Biomacromolecules. 7 (2006) 2091–2098.
[15] F. Shen, M.A.J. Mazumder, N.A.D. Burke, H.D.H. Stöver, M.A. Potter, Mechanically enhanced microcapsules for cellular gene therapy, J. Biomed. Mater. Res. Part B: Appl. Biomater. 90B, (2009) 350–361.
[16] C.M. Gardner, N.A.D. Burke, H.D.H. Stöver, Cross-linked microcapsules formed from self-deactivating reactive polyelectrolytes, Langmuir. 20 (2010) 4916–4924.
[17] R. Gugerli, E. Cantana, C. Heinzen, U. von Stockar, I.W. Marison, Quantitative study of the production and properties of alginate/poly-L-lysine microcapsules, J. Microencapsulation, 19 (2002) 571–590.
[18] A.J. Engler, S. Sen, H.L. Sweeney, D.E. Discher, Matrix elasticity directs stem cell lineage specification, Cell. 126 (2006) 677–689.
[19] T. Yeung, P.C. Georges, L.A. Flanagan, B.M. Miguelina, M. Funaki, N. Zahir, W. Ming, V. Weaver, P.A. Janmey, Effects of substrate and stiffness on cell morphology cytoskeletal structure, and adhesion, Cell Motil. Cytoskeleton. 60, (2005) 24–34.
[20] S.Y. Tee, J. Fu, C.S. Chen, P.A. Janmey, Cell shape and substrate rigidity both regulate cell stiffness, Biophys. J. 100, (2011) L25–L27.
[21] D.E. Discher, P.A. Janmey, Y.L. Wang, Tissue cells feel and respond to the stiffness of their substrate, Science. 310 (2005) 1139–1143.

[22] J.M. Van Raamsdonk, P.L. Chang, Osmotic pressure test: A simple, quantitative method to assess the mechanical stability of alginate microcapsules, J. Biomed. Mater. Res. 54 (2001) 264–271.
[23] F.A. Leblond, J. Tessier, J.P. Hallé, Quantitative method for the evaluation of biomicrocapsule resistance to mechanical stress, Biomaterials. 17 (1996) 2097–2102.
[24] X. Ma, I. Vacek, A. Sun, Generation of alginate-poly-L-lysine-alginate (APA) biomicroscopies- The relationship between the membrane strength and the reaction conditions, Art. Cells, Blood Subs., and Immob. Biotech. 22 (1994) 43–69.
[25] X. Liu, W. Xue, Q. Lin, W. Yu, Y. Fu, X. Xiong , X. Ma, Swelling behaviour of alginate–chitosan microcapsules prepared by external gelation or internal gelation technology, Carbohydr. Polym. 56, (2004) 459–464.
[26] M. Lekka, D. Sainz-Serp, A.J. Kulik, C. Wandrey, Hydrogel microspheres: Influence of chemical composition on surface morphology, local elastic properties, and bulk mechanical characteristics, Langmuir. 20 (2004) 9968–9977.
[27] K. Yamagiwa, T. Kozawa, A. Ohkawa, Effects of alginate composition and gelling conditions on diffusional and mechanical properties of calcium-alginate gel beads, J. Chem. Eng. JPN. 28 (1995) 462–467.
[28] A. Martisen, G. Skjåk-Bræk, O. Smidsrød, Alginate as immobilization material. 1. Correlation between chemical and physical-properties of alginate gel beads, Biotechnol. Bioeng. 33 (1989) 79–89.
[29] M. Mancini, M. Moresi, R. Rancini, Mechanical properties of alginate gels: empirical characterisation, J. Food Eng. 39 (1999) 369–378.
[30] C.X. Wang, C. Cowen, Z. Zhang, C.R. Thomas, High-speed compression of single alginate microspheres, Chem. Eng. Sci. 60, (2005) 6649–6657.
[31] M. De Castro, G. Orive, R.M. Hernández, A.R. Gascón, J.L. Pedraz, Comparative study of microcapsules elaborated with three polycations (PLL, PDL, PLO) for cell immobilization, J. Microencapsulation. 22 (2005) 303–315.
[32] E.S. Chan, T.K. Lim, W.P. Voo, R. Pogaku, T.B. Tey, Z. Zhang, Effect of formulation of alginate beads on their mechanical behavior and stiffness, Particuology. 9 (2011) 228–234.
[33] S. Leick, S. Henning, P. Degen, D. Suter, H. Rehage, Deformation of liquid-filled calcium alginate capsules in a spinning drop apparatus, Phys. Chem. Chem. Phys. 12 (2010) 2950–2958.
[34] S. Leick, A. Kemper, H. Rehage, Alginate/poly-L-lysine capsules: mechanical properties and drug release characteristics, Soft Matter. 7 (2011) 6684–6694.
[35] V.B. Nguyen, C.X. Wang, C.R. Thomas, Z. Zhang, Mechanical properties of single alginate microspheres determined by microcompression and finite element modeling, Chem. Eng. Sci. 64 (2009) 821–829.
[36] L. Zhao, Z. Zhang, Mechanical characterization of biocompatible microspheres and microcapsules by direct compression, Art. Cells, Blood Subs., and Immob. Biotech. 32 (2004) 25–40.
[37] A. Rehor, L. Canaple, Z. Zhang, D. Hunkeler, The compressive deformation of multicomponent microcapsules: Influence of size, membrane thickness, and compression speed, J. Biomater. Sci. Polymer Ed. 12 (2001) 157–170.

[38] R.M. Hochmuth, Micropipette aspiration of living cells, J. Biomech. 53 (2000) 15–22.
[39] W.R. Jones, H. Ping Ting-Beall, G.M. Lee, S.S. Kelley, R.M. Hochmuth, F. Guilak, Alterations in the Young's modulus and volumetric properties of chondrocytes isolated from normal and osteoarthritic human cartilage, J. Biomech. 32 (1999) 119–127.
[40] M. Sato, D.P. Theret, L.T. Wheeler, N. Ohshima, R.M. Nerem, Application of the micropipette technique to the measurements of cultured porcine aortic endothelial cell viscoelastic properties, ASME J. Biomech. Eng. 112 (1990) 263–268.
[41] A.W.L. Jay, M.A. Edwards, Mechanical properties of semipermeable capsules, Can. J. Physiol. Pharmacol. 46 (1968) 731–737.
[42] K. Olbrich, W. Rawicz, D. Needham, E. Evans, Water permeability and mechanical strength of polyunsaturated lipid bilayers, Biophys. J. 79 (2000) 321–327.
[43] H. Baumler, G. Artmann, A. Voigt, R. Mitlohner, B. Neu, H. Kiesewetter, Plastic behaviour of polyelectrolyte microcapsules derived from colloid templates, J. Microencapsulation, 17 (2000) 651–655.
[44] C. Campillo, B. Pepin-Donat, A. Viallat, Responsive viscoelastic giant lipid vesicles filled with a poly(N-isopropylacrylamide) artificial cytoskeleton, Soft Matter, 3 (2007) 1421–1427.
[45] S. Rosiński, G. Grigorescu, D. Lewińska, L.G. Ritzén, H. Viernstein, E. Teunou, D. Poncelet, Z. Zhang, X. Fan, D. Serp, I. Marison, D. Hunkeler, Characterization of microcapsules: recommended methods based on round-robin testing, J. Microencapsulation. 19 (2002) 641–659.
[46] R.P. Haugland, Handbook of Fluorescence Probes and Research Products, ninth ed., Molecular Probes, Eugene, 2002, pp. 55.
[47] D.P. Theret, M.J. Levesque, M. Sato, R.M. Nerem, L.T. Wheeler, The application of a homogeneous half-space model in the analysis of endothelial cell micropipette measurements, J. Biomechan. Eng. 110 (1988) 190–199.
[48] P. De Vos, B.J. de Haan, R. Van Schlifgaard, Is it possible to use the standard alginate-PLL procedure for production of small capsules? Transplant. Proc. 30 (1998) 492–493.
[49] G.M. Vandenbossche, P.V. Oostveldt, J. Demeester, J.P. Remon, The molecular-weight cutoff of microcapsules is determined by reaction between alginate and polylysine, Biotechnol. Bioeng. 42 (1993) 381–386.
[50] O. Smidsrød, G. Skjåk-Bræk, Alginate as immobilization matrix for cells, Trends Biotechnol. 8 (1990) 71–78.
[51] B.L. Strand, Y.A. Morch, T. Espevik, G. Skjåk-Bræk, Visualization of alginate-poly-L-lysine-alginate microcapsules by confocal laser scanning microscopy, Biotechnol. Bioeng. 82 (2003) 386–394.B.
[52] B. Thu, P. Bruheim, T. Espevik, O. Smidsrod, P. Soon-Shiong, G. Skjåk-Bræk, Alginate polycation microcapsules. 2. Some functional properties, Biomaterials. 17, (1996) 1069–1079.
[53] A.M. Sun, G.M. O'Shea, Microencapsulation of living cells- A long-term delivery system, J. Controlled Release. 2 (1985) 137–141.

[54] B.R. Hsu, Y.S. Ho, S.H. Fu, Y.Y. Huang, S.C. Chiou, H.S. Huang, Membrane compactness affects the integrity and immunoprotection of alginate-poly-L-lysine-alginate microcapsules, Transplant. Proc. 27 (1995) 3227–3231.
[55] D.B. Seifert, J.A. Phillips, Production of small, monodispersed alginate beads for cell immobilization, Biotechnol. Prog. 13 (1997) 562–568.
[56] G. Skjåk-Bræk, H. Grasdalen, O. Smidsrød, Inhomogenous polysaccharide ionic gels, Carbohydr. Polym. 10 (1989) 31–54.
[57] N.M. Velings, M.M. Mestdagh, Physicochemical properties of alginate gel beads, Polym. Gels Networks. 3 (1995) 311–330.
[58] D. Serp, M. Mueller, U. von Stockar, I.W. Marison, Low-temperature electron microscopy for the study of polysaccharide ultrastructures in hydrogels. II. Effect of temperature on the structure of Ca^{2+}-alginate beads, Biotechnol. Bioeng. 79 (2002) 253–259.
[59] C. Young, P.D. Rekha, W. Lai, A.B. Arun, Encapsulation of plant growth-promoting bacteria in alginate beads enriched with humic acid, Biotechnol. Bioeng. 95 (2006) 76–83.
[60] N. Wang, G. Adams, L. Buttery, F.H. Falcone, S. Stolnik, Alginate encapsulation technology supports embryonic stem cells differentiation into insulin-producing cells, J. Biotechnol. 144 (2009) 304–312.
[61] H.L. Ma, S.C. Hung, S.Y. Lin, Y.L. Chen, W.H. Lo, Chondrogenesis of human mesenchymal stem cells encapsulated in alginate beads, J. Biomed. Mater. Res. Part A. 64A, (2003) 273–281.
[62] D. Serp, E. Cantana, C. Heinzen, U. von Stockar, I. W. Marison, Characterization of an encapsulation device for the production of monodisperse alginate beads for cell immobilization, Biotechnol. Bioeng. 70 (2000) 41–53.
[63] J. Vorlop, J. Klein, New developments in the field of cell immobilization-formation of biocatalysts by ionotropic gelation, in: F.M. Lafferty (Ed.), Enzyme Technology, Springer-Verlag, Heidelberg, 1983, pp. 219–235.
[64] M.F.A. Goosen, G.M. O'Shea, H.M. Gharapetian, S. Chou, A. Sun, Optimization of microencapsulation parameters-semipermeable microcapsules as a bioartificial pancreas, Biotechnol. Bioeng. 27 (1985) 146–150.
[65] A. Safley, H. Cui, S. Cauffiel, C. Tucker-Burden, C.J. Weber, Biocompatibility and immune acceptance of adult porcine islets transplanted intraperitoneally in diabetic NOD mice in calcium alginate poly-L-lysine microcapsules versus barium alginate microcapsules without poly-L-lysine, J. Diabetes Sci. Technol. 2 (2008) 760–767.
[66] G.M. Lee, B.O. Palsson, Simplified method of making alginate-polylysine microcapsules for hybridoma cell culture using RPMI 1640 medium, Biotechnol. Tech. 4 (1990) 341–344.
[67] H.A. Clayton, N.J.M. London, P.S. Colloby, P.R.F. Bell, R.F.L. James, The effect of capsule composition on the biocompatibility of alginate-poly-L-lysine capsules, J. Microencapsulation. 8 (1991) 221–233.
[68] M.H. Ottøy, O. Smidsrød, Swelling of poly-L-lysine and chitosan-coated superswelling sodium-alginate gel beads, Polymer Gels and Networks. 5 (1997) 307–314.

[69] A. King, B. Strand, A. Rokstad, B. Kulseng, A. Andersson, G. Skjåk-Bræk, S. Sandler, Improvement of the biocompatibility of alginate/poly-L-lysine/alginate microcapsules by the use of epimerized alginate as a coating, J. Biomed. Mater. Res. Part A. 64A (2003) 533–539.
[70] H.A. Hobbs,W.F. Kendall, M. Darrabie, E.C. Opara, Prevention of morphological changes in alginate microcapsules for islet xenotransplantation, J. Investig. Med. 49 (2001) 572–575.
[71] O. Gåserød, O. Smidsrød, G. Skjåk-Bræk, Microcapsules of alginate-chitosan -I- A quantitative study of the interaction between alginate and chitosan, Biomaterials. 19 (1998) 1815–1825.
[72] O. Gåserød, A. Sannes, G. Skjåk-Bræk, Microcapsules of alginate-chitosan. II. A study of capsule stability and permeability, Biomaterials. 20 (1999) 773–783.
[73] G. Maurstad, Y. A. Mørch, A.R. Baush, B.T. Stokke, Polyelectrolyte layer interpenetration and swelling of alginate-chitosan multilayers studied by dual wavelength reflection interference contrast microscopy, Carbohydr. Polym. 71 (2008) 672–681.
[74] C.M. Gardner, M.A. Potter, H.D.H. Stöver, Improving covalent cell encapsulation with temporarily reactive polyelectrolytes, J. Mater. Sci.-Mater. Med. 23 (2012) 181–193.

2.8. Appendix

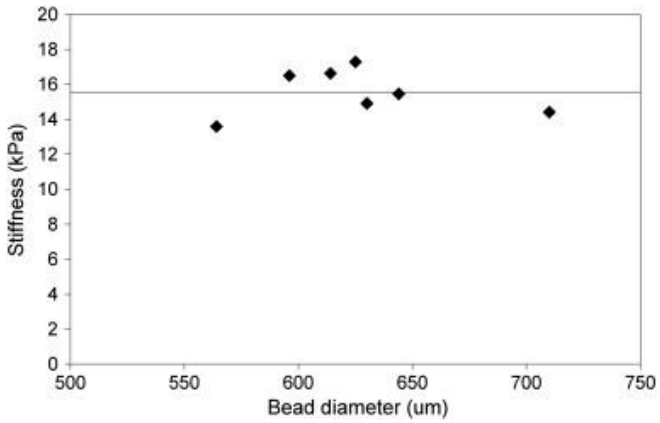

Fig. 2A.1 The stiffness of calcium alginate beads as a function of bead diameter where the solid line marks the average stiffness.

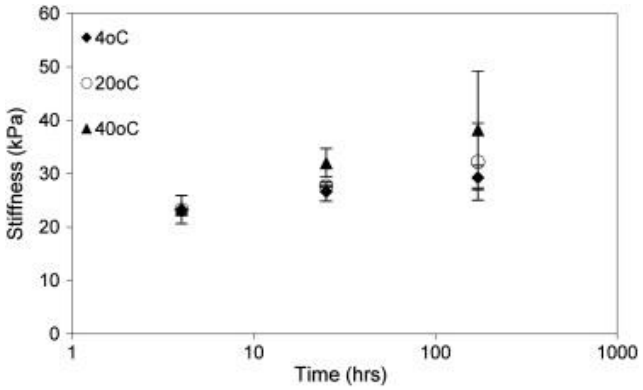

Fig. 2A.2 The stiffness of calcium alginate beads stored in saline at different temperatures. Measurements were performed at 20 ^{o}C.

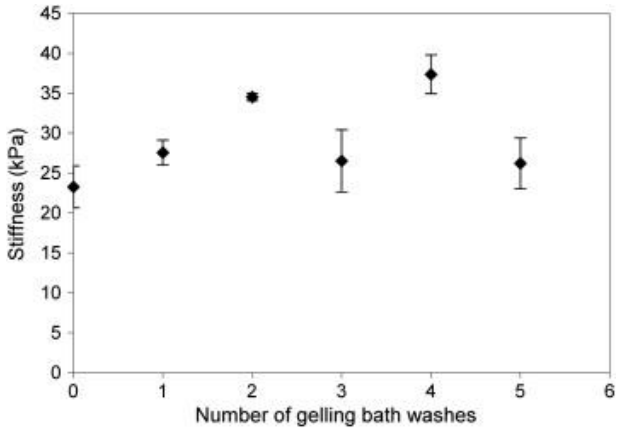

Fig. 2A.3 The stiffness of calcium alginate beads washed in gelling bath.

CHAPTER 3

Synthetic polycations with controlled charge density and molecular weight as building blocks for biomaterials

Rachelle M. Kleinberger, Nicholas A. D. Burke, Christal Zhou, Harald D. H. Stöver.
Journal of Biomaterials Science, Polymer Edition. **2016**, *27*, 351-369.
http://www.tandfonline.com/doi/full/10.1080/09205063.2015.1130407

This chapter shows the synthesis and characterization of APM/HPM copolymers using RAFT polymerization with 75, 50, 25 and 10% APM. The binding of these polycations with alginate in solution or to alginate beads was investigated. The biocompatibility of these polycations is assessed by solution toxicity and cell attachment to polycation modified surfaces. Higher charge density polycations bound better to alginate but also showed higher cell attachment to polymer modified surfaces. Low cell attachment and proliferation onto substrates modified with low charge density polycations was due to reduced fouling surfaces and not toxicity, as observed by high biocompatibility to cells in solutions.

Contributions: RMK designed the work for this chapter with help from NADB and HDHS. RMK performed all experiments. CZ helped RMK perform the cell attachment and proliferation studies under RMK's supervision. RMK processed and analyzed the data, as well as wrote the manuscript, with edits from NADB and HDHS.

3.1. Abstract

A series of polycations prepared by RAFT copolymerization of N-(3-aminopropyl)methacrylamide hydrochloride (APM) and N-(2-hydroxypropyl)methacrylamide, with molecular weights of 15 and 40 kDa, and APM content of 10–75 mol%, were tested as building blocks for electrostatically assembled hydrogels such as those used for cell encapsulation. Complexation and distribution of these copolymers within anionic calcium alginate gels, as well as cytotoxicity, cell attachment, and cell proliferation on surfaces grafted with the copolymers were found to depend on composition and molecular weight. Copolymers with lower cationic charge density and lower molecular weight showed less cytotoxicity and cell adhesion, and were more mobile within alginate gels. These findings aid in designing improved polyelectrolyte complexes for use as biomaterials.

3.2. Introduction

Cell encapsulation may in future enable cell-based treatments of enzyme and hormone deficiency disorders such as insulin-dependent diabetes,[1] Parkinson's disease [2], and lysosomal storage disorders.[3] This approach involves enclosing cells that express a therapeutic peptide such as insulin, in an immunoisolating hydrogel matrix prior to transplantation into patients, avoiding the need for immunosuppressing agents. The best-known capsule types are based on a calcium alginate gel core coated with poly-L-lysine (PLL) and a final layer of alginate (referred to as Alginate/PLL/Alginate or APA capsules).[4] The resulting alginate/PLL polyelectrolyte complex in the shell reduces the permeability of the capsule to immune system components [4,5] such as

immunoglobulins or antibodies, and prolongs cell and capsule survival beyond the loss of calcium to the host.[6–8]

Recent studies show instances of poor host compatibility in these hydrogel capsules that are mainly attributed to the PLL. Exposed PLL can stimulate macrophages to produce TNF-α,[9,10] induce inflammation [11], and bind more immunoglobulins.[12,13] Hallé showed that some of the PLL is exposed on the surfaces of APA capsules,[14] enhancing host cell adhesion.[15] As well, some types of encapsulated cells are sensitive to PLL in the coating solution.[9,16]

Our group recently showed that reactive synthetic polyanions can be used to decrease the undesired net cationic charge density remaining on such capsule surfaces.[17]

A more fundamental approach to mitigate concerns with the use of polycations such as PLL is to replace PLL with lower charge density polycations. Sawhney and Hubbell grafted polyethyleneglycol (PEG) onto PLL in order to reduce its net charge density.[18] They observed reduced protein and complement binding, and less fibrotic overgrowth; however, the membrane required an additional, initial PLL layer for reduced permeability and stability. Chaikof and co-workers also developed PLL-*g*-PEG copolymers that tried to balance electrostatic binding ability with cell cytotoxicity.[19,20] De Vos and co-workers recently prepared calcium alginate capsules coated with PLL-*b*-PEG diblock polymers that showed less fibrotic overgrowth compared to APA capsules, though requiring 50 h incubation with PLL-*b*-PEG to form an effective anti-fouling layer.[21]

While PEG serves well in mitigating host reactions, there is interest in alternate hydrophilic polymers.[22–24] Poly(N-(2-hydroxypropyl)methacrylamide) (HPM) and analogs have shown good biocompatibility [25,26] and have been suggested as a replacement for PEG.[22]

N-(3-aminopropyl)methacrylamide hydrochloride (APM) was selected as the cationic monomer in this study due to its similarity in structure to PLL, and to its ability to copolymerize with HPM using RAFT conditions, similar to those recently reported.[27–29] Polymers containing APM have been previously used in numerous applications including layer-by-layer [30] and bulk hydrogel [31] cellular scaffolds, antimicrobial polymers [32], and bioconjugation.[28,29]

We describe here synthetic, controlled charge density copolymers of HPM and APM. These synthetic copolymers are modeled in part after chitosan, a natural, low-charge density cationic polysaccharide, with HPM serving as a neutral hydrophilic co-monomer to provide anti-fouling properties.

As cationic charge density and molecular weight (MW) strongly affect cytotoxicity as well as polycation binding to polyanions such as calcium alginate,[4,5,33–36] we used reversible addition- fragmentation chain transfer (RAFT) copolymerization, a controlled radical polymerization, to prepare APM/HPM copolymers with four co-monomer ratios and two molecular weights, balancing electrostatic binding ability against cytotoxicity (Scheme 1). In particular, polycations with high MW and reduced charge density (lower APM content) were expected to form alginate complexes with better cytocompatibility compared to PLL.

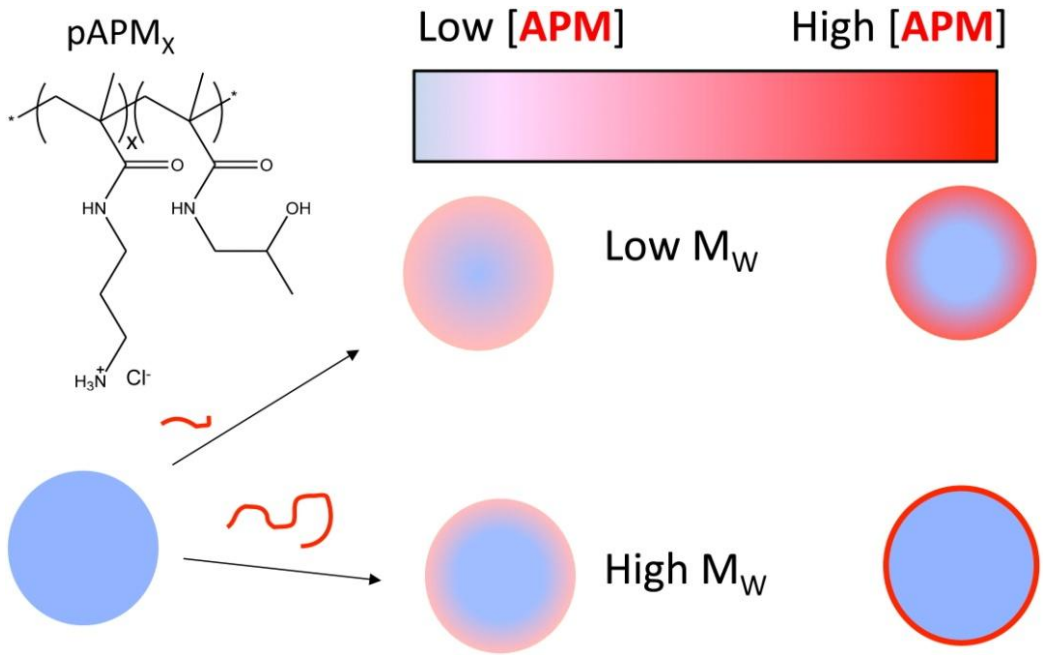

Scheme 3.1. Anticipated distribution of pAPM$_X$ copolymers in CaAlg beads as a function of charge density (mol fraction APM) and molecular weight.

The polycations are identified as pAPM$_{X–Y}$, where *X* represents the mol% APM and *Y* is the MW in kDa. The interaction of these polycations with calcium alginate gel beads and with mammalian cells was examined to assess their suitability as replacements for PLL in alginate-type capsules, and possibly other hydrogel films and matrices.

3.3. Experimental

3.3.1. Materials

Sodium alginate (Pronova UP MVG, batch #: BP-0908–01) was purchased from Novamatrix (Sandvika, Norway). Poly-L-lysine hydrobromide (PLL, M_n 15–30 and 40–60 kDa), Poly(methyl vinyl ether-*alt*-maleic anhydride) (PMM, *M*n ≈ 80,000 g/mol), rhodamine B isothiocyanate (RbITC), HEPES sodium salt, 4-cyanopentanoic acid

dithiobenzoate (CTP), and 4,4′-azobis(4-cyanopentanoic acid) (V-501) and 3-aminopropyltriethoxysilane (APTES, ≥98%) were purchased from Sigma–Aldrich (Oakville, ON Canada), and HPLC grade water, acetonitrile, reagent-grade dioxane, sodium chloride, and calcium chloride from Caledon Laboratories (reagent grade, Georgetown, ON) were used as received. APM hydrochloride and HPM were purchased from Polysciences (Warrington, PA) and were used as received. Dulbecco's modified Eagle's medium (DMEM, high glucose, pyruvate), Fetal bovine serum (qualified, Canada origin), alamarBlue® Cell Viability Reagent, Penicillin–Streptomycin (10,000 U/mL), 0.25% Tryspin–EDTA (1X) phenol red, and TryPLE^{TM} Express Enzyme (1X) were obtained from Invitrogen (Burlington, ON), and Bovine calf serum (USA origin) was obtained from Sigma–Aldrich. C2C12 *Mus musculus* myoblasts (CRL-1772) and NIH/3T3 *Mus musculus* fibroblasts (CRL-1658) were obtained from ATCC.

3.3.2 General RAFT polymerization procedure

RAFT co-polymerizations of APM and HPM with 4-cyanopentanoic acid dithiobenzoate (CTP) as RAFT agent and 4,4′-azobis(4-cyanopentanoic acid) (V-501) as initiator were carried out in a 2:1 water/dioxane mixture. The ratio of $[CTP]_o$:$[V\text{-}501]_o$ was kept at 1:0.33, and $[M]_o$:$[CTP]_o$ ratios of 130:1 or 330:1 were used to target the low and high MW polymers, respectively. The monomer concentration was 2 or 4 M, respectively. A typical reaction is as follows:

APM (1.18 g, 6.60 mmol), HPM (0.320 g, 2.23 mmol), CTP (18.9 mg, 0.0676 mmol), and V-501 (6.20 mg, 0.0221 mmol) were dissolved in 4.5 mL of 2:1 (v/v) water:dioxane. The reaction mixture was purged with N_2 for 45 min at room temperature

and then immersed in an oil bath at 70 °C for 5 h. The polymerization proceeded under positive N_2 pressure, and aliquots of the reaction mixture were removed periodically with a N_2-purged needle and syringe. The crude reaction mixture was analyzed by GPC and ^{1}H NMR (600 MHz) to determine the MW, polydispersity index (PDI), and conversion. The conversion of both monomers was determined by comparing the integrations of the vinylic ^{1}H NMR peaks at 5.7 and 5.5 ppm (APM and HPM) to the combined CH peak of monomeric and polymeric HPM (4.0 ppm). The remaining polymer was isolated from the reaction mixture by precipitation in acetone and collected by centrifugation. The polymer was dried under vacuum overnight, yielding a pink powder. The conversion for this reaction was 66%, with 656 mg polymer isolated. Typical reaction conversions and polymer yields were 65–80%.

Copolymer composition was determined by ^{1}H NMR analysis of the isolated polymers dissolved in D_2O. The area of the peak at 4.0 ppm (1H from HPM) was compared with the area of the signals at 3.0–3.4 ppm (4H from APM + 2H from HPM).

The MW (M_n) of the copolymer after precipitation was additionally determined by ^{1}H NMR (Bruker 600 MHz, 1024 scans) by comparing the end-group signal at 7.9 ppm (2H) with the polymeric HPM signal at 4.0 ppm (1H). The theoretical MW (M_n^{theo}) was calculated using Equation (1).[37]

$$M_n^{theo} = \frac{[M]_0}{[CTA]_0} \times MW_m \times \text{conversion} + MW_{CTA} \qquad (1)$$

$[M]_o$ and $[CTA]_o$ are the initial concentrations of the monomer (APM + HPM) and chain transfer agent, MW_m and MW_{CTA} are the molecular weights of the monomers

(weighted average) and chain transfer agent, and conversion is obtained from ^{1}H NMR analysis of the reaction mixture at the end of the polymerization.

3.3.3. Removal of sulfur-containing chain ends

The dithiobenzoate chain ends were removed by reacting $pAPM_X$ copolymers (0.574 g, 0.0387 mmol chain end) with a 20:1 M excess of V-501 (0.219 g, 0.781 mmol) in 5.4 mL of 2:1 water:dioxane for 24 h at 75 °C after purging with N_2 for 45 min. The polymers were precipitated in acetone and isolated by centrifugation. ^{1}H-NMR spectra (600 MHz, 1024 scans) confirmed the removal of the end-groups by disappearance of the signal for the aromatic protons at 7.9 ppm. The polymers were then dialyzed against de-ionized water and isolated by freeze-drying to yield 0.371 g (65%). This reaction was performed similarly for all compositions and molecular weights with typical recoveries of the copolymer following end-group removal of 65–85%.

3.3.4. GPC

The MW of $pAPM_X$ copolymers were determined by gel permeation chromatography consisting of a Waters 515 HPLC pump, Waters 717 plus Autosampler, three columns (Waters Ultrahydrogel-120, -250, -500; 30 cm × 7.8 mm; 6 μm particles), and a Waters 2414 refractive index detector. The columns were maintained at 35 °C. Samples were eluted at a flow rate of 0.8 mL/min in a 0.5 M acetic acid/0.5 M sodium acetate buffer pH = 4.8 mobile phase. The system was calibrated using narrow-dispersed PEG standards (Waters, Mississauga, ON).

3.3.5. Alginate–polycation complexation

Model complexation experiments were performed at 154 and 377 mM NaCl concentrations. Polycations were dissolved at 0.5 wt% in saline with pH adjusted at 7.0–7.5. Sodium alginate solution at 0.5 wt% was prepared in saline. All solutions were filtered through 0.45-μm filters. Polycation solutions (0.5 mL) were placed in vials and varying volumes of sodium alginate solution were added to give a 1:1 ratio of COO^- to NH_3^+. For experiments at 377 mM NaCl, a 1.49 M NaCl stock solution was added to 0.5 mL of polycation in saline such that the final NaCl concentration would be 377 mM upon addition of the correct volume of sodium alginate solution to achieve a 1:1 ratio of COO^- to NH_3^+. Samples were observed by optical microscopy.

3.3.6. Fluorescent labeling of PLL and $pAPM_X$

PLL and $pAPM_X$ copolymers were fluorescently labeled with RbITC. For example, $pAPM_{75–15}$ (HCl form, 0.12 g, 0.71 mmol monomer units) was dissolved in 12 mL of 0.20 M $NaHCO_3$ buffer (pH 9) before adding 1.9 mg (0.0035 mmol) RbITC dissolved in 0.76 mL N,N-dimethylformamide. The solution was stirred overnight and then dialyzed in 3.5 kDa MW cut-off cellulose dialysis tubing (Spectrum Laboratories) for four days with at least daily changes of 4 L of de-ionized water, until no rhodamine or DMF could be detected in the dialysate by UV/Vis spectroscopy, using a Cary 50 Bio UV/Vis spectrometer. The sample was isolated by freeze-drying to yield 0.10 g $pAPM_{75–15}$ RbITC (76% yield). The extinction coefficient of this labeled polymer was 0.32 mL cm^{-1} mg^{-1}, measured at 560 nm in 21 mM HEPES buffer (pH 7.5), corresponding to a labeling degree of 0.070 mol%, and a labeling efficiency of 14% based on the absorption

coefficient of free RbITC of 8.7 × 104 M^{-1} cm^{-1} at 560 nm. The labeling reaction was performed on all $pAPM_X$ copolymers and PLL (15–30 and 40–60 kDa), resulting in extinction coefficients of 0.31–0.45 mL cm^{-1} mg^{-1}, labeling degrees of 0.062–0.089 mol%, and labeling efficiencies of 13–19%.

3.3.7. Preparation of calcium alginate beads

Calcium alginate beads (CaAlg beads) were prepared as previously described.[38] Briefly, a solution of sodium alginate (5–10 mL, 1 wt%) in saline was filtered (0.2 μm) and then extruded through a flat-tipped 27 G needle into 60 mL of aqueous gelling bath solution containing 1.1 wt% $CaCl_2$ (100 mM) and 0.45 wt% NaCl (77 mM), at a rate of 0.5 mL/min. An annular coaxial airflow of 3–4 L/min was adjusted to control CaAlg bead diameter (approx. 0.5 ± 0.05 mm). The beads were kept in the gelling bath for another 10 min after extrusion, then transferred into a fresh gelling bath solution for additional 10 min (using a 3:10 volume ratio of settled bead suspension to wash solution). All solutions were pre-cooled to 4 °C and the gelling bath was placed in an ice bath during bead formation to mimic conditions used during actual cell encapsulations.

3.3.8. Coating alginate beads

CaAlg beads were coated with 0.1 wt% PLL or APM/HPM copolymers in saline (pH 7.0–7.5) for 6 min. The beads were washed with either saline or gelling bath for 2 min followed by a final saline wash. The beads were coated or washed in a 3:10 ratio of beads to coating or washing solutions and stored in the final saline wash at 4 °C.

3.3.9. Confocal microscopy

Confocal microscopy of fluorescently labeled capsules was carried out on a Zeiss LSM510 confocal laser scanning microscope equipped with argon and HeNe lasers, operated with Zeiss LSM510 software. The extent of $pAPM_X$ diffusion into the capsules, or membrane thickness, was determined by the full width at half height of 10-pixel-wide (36 μm) line profiles across equatorial confocal sections of three capsules, generated using ImageJ software. Confocal microscopy was performed within 1–4 days of capsule formation.

3.3.10. Cell viability tests using alamarBlue assay

C2C12 myoblasts were cultured in DMEM supplemented with 10% FBS in the presence of 5% CO_2, 95% air with 100% humidity at 37 °C in a water-jacketed incubator. Cells were plated into tissue culture-treated 24 well polystyrene plates at 50,000 cells/well in 1 mL of media. Cells were incubated overnight to allow for attachment. The media was then removed and cells were washed with PBS. Cells were incubated with 250 μL of polymer solutions in phosphate buffered saline pH = 7.4 (PBS) added to cells with 300 μL of serum free media for total polymer concentrations of 0.01, 0.1, and 1 mg/mL for 20 h at 37 °C with experiments done in triplicate. alamarBlue (55 μL) was added to each of the wells and incubated for another 3 h. The fluorescence of the reduced alamarBlue was measured by exciting at 560 nm and measuring the emission at 590 nm on a Synergy 4 Plate reader from BioTek. Cell viability was determined from the relative alamarBlue conversion of a positive control treated without polycation.

3.3.11. Cell attachment and proliferation tests

Glass bottom black-walled 96 well plates (In vitro Scientific) were washed with 95% ethanol and dried under an air stream prior to coating with a 2 v/v% solution of APTES in 95% ethanol at pH 4.5 for 2 min, washed with 95% ethanol, dried under air, and cured overnight. The wells were coated with 0.1 w/v% poly(methyl vinyl ether-*alt*-maleic anhydride) (PMM) in acetonitrile (ACN) for 5 min and washed with ACN. Polycation solution in de-ionized water (pH 8–9) was added to each well and allowed to react overnight before washing with de-ionized water and drying. Some well bottoms were further coated with PMM as above, then hydrolyzed overnight in 35 mM HEPES buffer pH 7.8 overnight. The plates were then soaked in PBS and stored in a refrigerator for 3–11 days before use. All aqueous solutions were filtered with 0.2-μm membrane prior to addition to well. Prior to use, the plates were sterilized with 70% ethanol for 30 min and washed with PBS. Certain wells were then coated with 0.03 wt% alginate in saline for 5 min and washed twice with saline. The resulting plate contains surfaces of (a) polycation, (b) polycation/alginate, and (c) polycation/PMM for each polycation composition and MW. The control wells do not have polycation, but only the layer of hydrolyzed PMM bound to the APTES-functionalized glass. NIH/3T3 fibroblasts were seeded with 2500 cells/well in DMEM supplemented with 10% BCS for three days before observing cell morphology with optical microscopy and cell viability with alamarBlue. The alamarBlue assay was conducted by replacing the media with 100 μL of media containing 10% of the alamarBlue reagent and then incubating the samples for 4.5 h. The results represent three individual experiments, each done in triplicate.

3.3.12. Statistics

All values are reported and graphed as mean ± standard deviation, with significant differences determined by one-way ANOVA with Games-Howell *post hoc* analysis. Significance was determined for $p < 0.05$.

3.4. Results and discussion

Our aim was to prepare polycations with reduced charge density, but similar MWs compared to the 15–30 and 40–60 kDa PLL commonly used with alginate beads.[4,5,36] Hence, APM/ HPM copolymers with 10, 25, 50, and 75 mol% APM, and M_n of 15 and 40 kDa (DP of 90 and 240) were targeted by RAFT copolymerization.

RAFT polymerization using CTP as chain transfer agent and V-501 as initiator in aqueous acetate buffer at pH 5.0–5.2 has been reported for HPM [27] and APM,[28] and for HPM with 5–10 mol% APM.[29] Narain [39,40] and McCormick [41] have used a water/dioxane mixture to polymerize APM by RAFT, also using CTP and V-501. Aqueous and mixed aqueous/organic solutions are useful as APM is not soluble in many organic solvents in its acid form.

In the current work, attempts to use aqueous acetate buffer (pH = 4.8–5.2) showed poor CTP solubility at higher CTP or APM concentrations. It appears that HPM, but not APM, helps solubilize CTP in purely aqueous media, and as a result, a 2:1 (v/v) water:dioxane mixture was used in all reactions.

Although a buffer was not used in the current work, the water/dioxane mixtures were acidic because APM was used as the hydrochloride salt. This slightly acidic medium helps minimize both aminolysis and hydrolysis of the dithioester group of CTP.[42]

RAFT copolymerization of APM and HPM to form $pAPM_{75–15}$ using a 2:1 water:dioxane solvent mixture was followed by ^{1}H NMR (Figure 3A.1) and GPC. It showed a linear first-order kinetic plot up to 75–80% conversion (Figure 3.1), as well as linear growth of M_n with conversion and low PDI (Figure 3.2). Similar results were seen with other monomer compositions (Figures 3A.2) except that the observed M_n values fell further from the expected values as the HPM content of the copolymer increased. This is likely because the GPC mobile phase, 1 M aq. acetate buffer, pH 4.8,[40] chosen for its compatibility with APM homopolymer and high APM copolymers, was not an ideal solvent for copolymers with high HPM content.

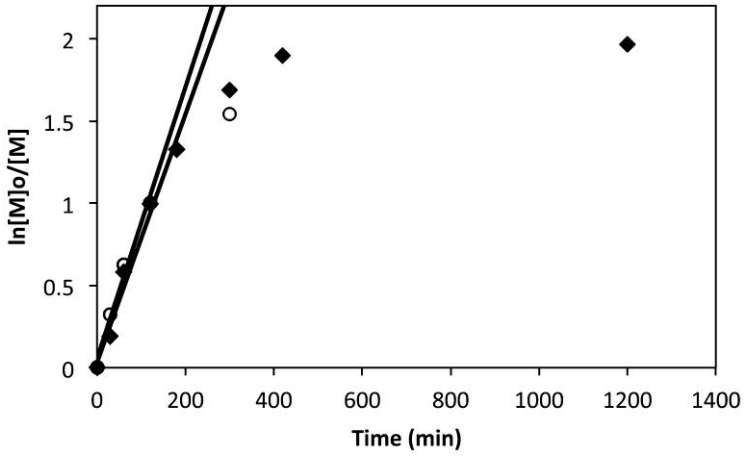

Figure 3.1. Pseudo-first-order kinetic plot for RAFT polymerization of $pAPM_{75}$ copolymers with monomer:CTP ratio of (♦) 130:1 and (O) 330:1.

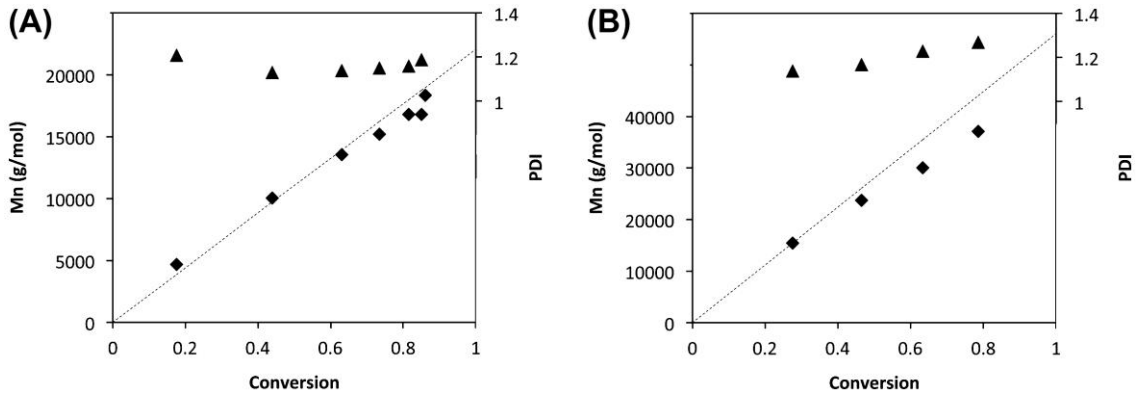

Figure 3.2. (♦) Experimental M_n and (▲) PDI vs. Conversion plots for RAFT copolymerization of $pAPM_{75}$ with a M:CTP ratio of (A) 130:1 and (B) 330:1 in 2:1 water:dioxane. The dotted line represents the theoretical M_n. Experimental M_n and PDI were estimated by aqueous GPC and conversion was determined by ^{1}H NMR (600 MHz).

The initial pH of the polymerization mixtures was between 2 and 3, which Liu et al. showed was suitable for RAFT polymerization of monomers like APM using CTP because it ensures complete protonation of the amine and CTP hydrolysis is slow.[43] The relative consumption of the two monomers, and hence the composition of the copolymer formed, was monitored throughout the polymerization by ^{1}H NMR, and showed only marginal drift (Figure 3A.3).

Preparative copolymerizations containing 10, 25, 50, and 75 mol% APM were carried out using monomer:CTP ratios of 130:1 and 330:1 which would result in DPs of about 90 and 240, corresponding to 15 and 40 kDa, respectively, at ~70% conversion. The properties of these $pAPM_X$ copolymers prepared by RAFT are described in Table 3A.1. The MWs were determined by both NMR end-group analysis (Figure 3A.4) and aqueous GPC (Figures 3A.5 and 3A.6). End-group analysis showed MWs consistently above the expected values, which is attributed to some hydrolysis of the dithiobenzoate

end-group during polymerization/purification. Aqueous GPC tended to show values lower than expected, especially for HPM-rich copolymers as mentioned above. NMR analysis indicated that the final copolymers had compositions very close to the feed ratios, in agreement with the relative rates of comonomer incorporation described earlier (Figure 3A.3).

Thus, RAFT copolymerization was successfully used to prepare two sets of APM/HPM copolymers having M_n of about 15 and 40 kDa and dispersities of 1.2–1.3, each with 10, 25, 50, and 75 mol% APM.

3.4.1. End-group removal by reaction with free radicals

The hydrophobic dithiobenzoate end-group in as-formed RAFT polymers can impact solubility, is prone to hydrolyze to an undesirable thiol end-group, and increases the cytotoxicity of pHPM.[44] We thus replaced the dithioester end-groups with 4-cyanopentanoic acid groups, by reaction with excess radical initiator.[29] Complete exchange of the end-groups was confirmed by disappearance of the characteristic dithiobenzoate peaks in the 7.5– 8.0 ppm region of the NMR spectrum (Figures 3A.7). GPC analysis (Figures 3.3 and 3A.6) showed a slight shoulder on the high MW side of many chromatograms after end-group removal, indicating that there had been some polymer–polymer termination, reflected in a marginal increase in dispersity (Table 3A.1).

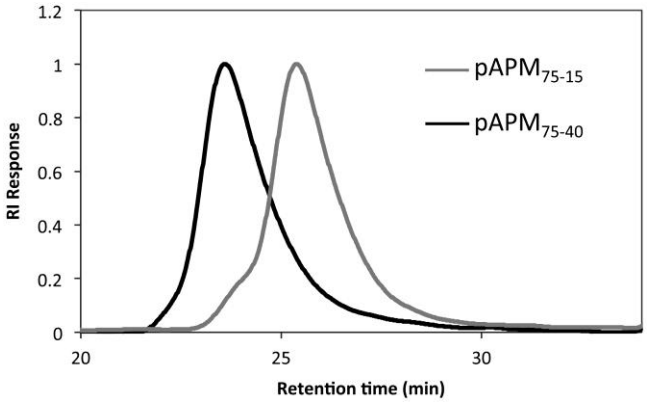

Figure 3.3. GPC chromatograms of the $pAPM_{75}$ copolymers after end-group exchange by treatment with excess initiator.

The change of end-group decreased the elution time (increased apparent MW) of the polymers (Table 3A.1, Figures 3A.5, and 3A.6). The effect was most pronounced for the polymer with lowest MW and APM content ($pAPM_{10–15}$), where, after end-group replacement, the apparent M_n increased from 4.55 to 10.8 kDa, a MW much more in line with expected values. This is in agreement with the GPC mobile phase (1 M acetate, pH 4.8) not being an ideal solvent for copolymers with low APM content, a problem exacerbated by the presence of the hydrophobic dithiobenzoate group.

3.4.2. Interaction of polycations with sodium alginate and with CaAlg beads

Polycation/alginate complexation was explored using optical microscopy (Figure 3.4), by mixing alginate and 40 kDa polycations at a 1:1 charge ratio at pH 7 in either isotonic saline (154 mM NaCl) or 377 mM NaCl, which has the same ionic strength as the gelling bath used in forming CaAlg beads (100 mM $CaCl_2$, 77 mM NaCl). The lower the MW, 15 kDa polycations behaved similarly (images not shown).

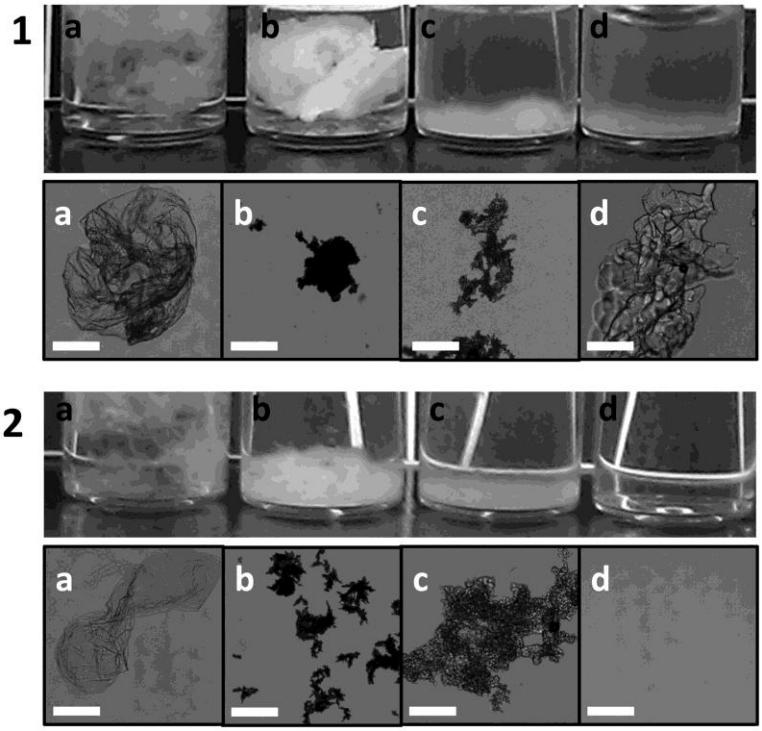

Figure 3.4. Polycation–alginate complexes formed in (1) 154 mM and (2) 377 mM NaCl solutions for (a) PLL 40–60 kDa, (b) $pAPM_{75–40}$, (c) $pAPM_{50–40}$, and (d) $pAPM_{25–40}$. White scale bars represent 500 μm. Complexes with $pAPM_{10–40}$ were soluble under all conditions used here (not shown).

No macroscopic phase separation was seen when combining the lowest charge density $pAPM_{10–40}$ with sodium alginate in either 377 mM NaCl or in isotonic saline. Similarly, $pAPM_{25–40}$ did not show macroscopic phase separation in 377 mM NaCl, but did form a mixture of transparent gels and liquid complex coacervate droplets with alginate in isotonic saline.

PLL (40–60 kDa) and $pAPM_{50–40}$ gave marginally translucent films and precipitates that became more transparent with increase in ionic strength.

$PAPM_{75–40}$ gave a solid precipitate with high contrast to the surrounding solution in both saline and 377 mM NaCl, consistent with low water contents and strong binding.

These observations confirm the expected trend toward weaker polyelectrolyte complexation and higher water content, with increase in ionic strength or lower APM content.

The specific distribution of the polycations used in, e.g., capsule membranes requires careful consideration: exposure of polycation at the capsule surface can trigger an immune response,[14,15] while polycations penetrating deeply into cell-containing gels may harm the encapsulated cells while not enhancing capsule integrity or controlling permeability.

Accordingly, CaAlg beads were coated with fluorescently labeled versions of the polycations, and both the extent of binding and the distribution of the polycations within the capsules were assessed by confocal fluorescence microscopy. In addition, the effect of two commonly used capsule-washing protocols on polycation binding and distribution was examined.

Confocal microscopy images of capsules coated with the polycations and washed twice with isotonic saline are shown in Figure 3.5, while capsules washed once with gelling bath (100 mM $CaCl_2$; 77 mM NaCl) and then once with saline are shown in Figure 3.6. Figures 3.5 and 3.6 were reproduced in the supplementary information showing multiple capsules (refer to Figures 3A.8 and 3A.9). Line profiles, normalized to the same detector gain, are shown in Figure 3A.10, and were used to determine the membrane thickness as defined by the full width at half height. The areas under the line profiles gave an indication of the relative amounts of polycation bound.

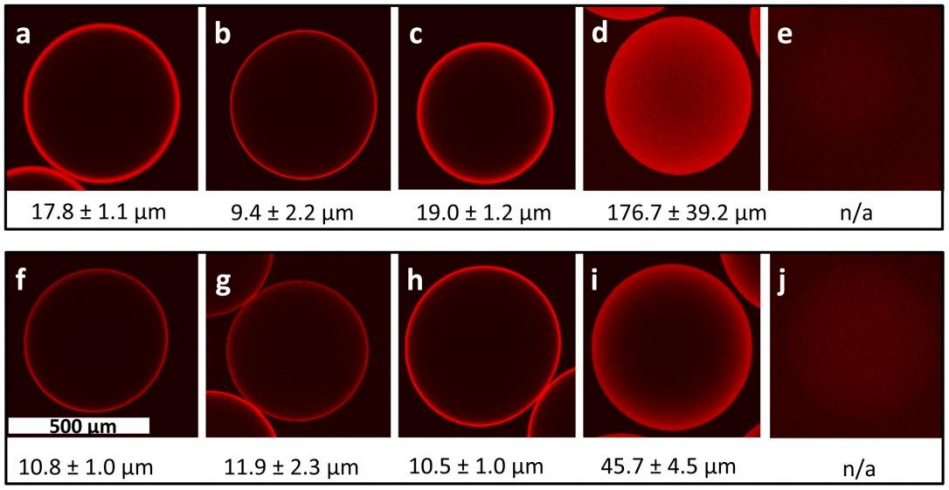

Figure 3.5. Confocal cross-sectional images showing the distribution of RbITC-labeled polycations in CaAlg beads coated with: (a) PLL 15–30 kDa, (b) $pAPM_{75–15}$, (c) $pAPM_{50–15}$, (d) $pAPM_{25–15}$, (e) $pAPM_{10–15}$, (f) PLL 40–60 kDa, (g) $pAPM_{75–40}$, (h) $pAPM_{50–40}$, (i) $pAPM_{25–40}$, and (j) $pAPM_{10–40}$. Beads were washed twice with saline after polycation coating. The shell thickness as determined from full widths at half height of line profiles (Figure 3A.10) is shown below each image. Confocal images were taken at different detector gains.

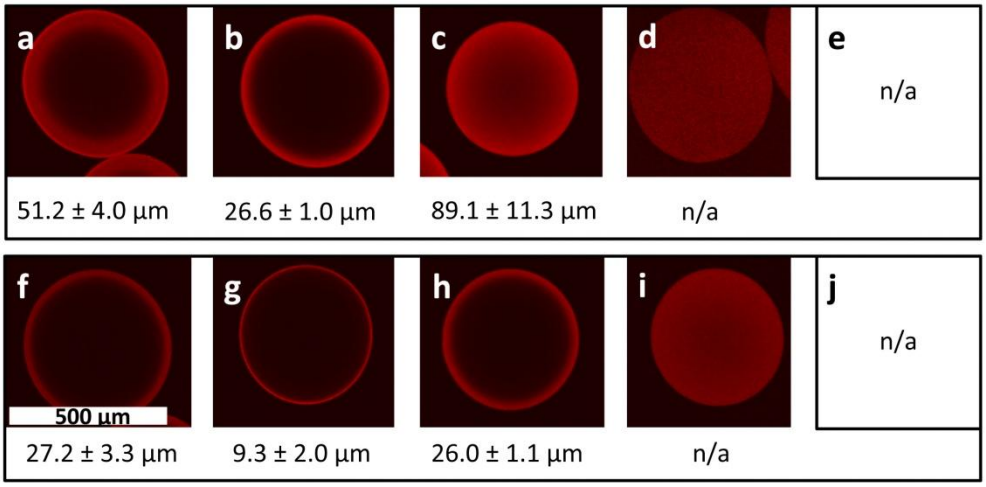

Figure 3.6. Confocal cross-sectional images showing the distribution of RbITC-labeled polycations in CaAlg beads: (a) PLL 15–30 kDa, (b) $pAPM_{75–15}$, (c) $pAPM_{50–15}$, (d) $pAPM_{25–15}$, (e) $pAPM_{10–15}$, (f) PLL 40–60 kDa, (g) $pAPM_{75–40}$, (h) $pAPM_{50–40}$, (i) $pAPM_{25–40}$, and (j) $pAPM_{10–40}$. Beads were washed once with gelling bath and once with saline. The shell thickness as determined from full widths at half height of line profiles (Figure 3A.10) is shown below each image. Confocal images were taken at different detector gains.

Polycations with higher MW and charge density were largely restricted to the capsule surface, reflecting strong electrostatic binding to alginate. The lower MW polycations diffused more deeply into the calcium alginate bead, with the low MW $pAPM_{25–15}$ becoming distributed evenly throughout the bead (Figure 3.5(d)). The two polycations containing 10 mol% APM content were not bound at all.

Calcium and sodium ion concentrations are also known to affect the binding of polycations to CaAlg beads, affecting gel porosity, polycation hydrodynamic volume, and weakening polyelectrolyte complexation.[4,38,45–47] We similarly observed here that washing with the calcium chloride-based gelling bath promoted in-diffusion of the polycation (see Figure 3.6 and 3A.10). Washing with Ca^{2+} after polycation coating can thus help redistribute polycations with high charge density/MW further into the alginate beads, creating thicker membranes and potentially less undesirable polycation exposure at the bead surface (Figure 3A.10).

PLL 15–30 and 40–60 kDa have the highest charge density of the polymers studied, but in terms of in-diffusion, behave more like $pAPM_{50–15}$ and $pAPM_{50–40}$, respectively (Figure 3.5(a) and (f), Figure 3.5(c) and (h), and Figure 3A.11). This is in agreement with other studies that showed higher degrees of in-diffusion of PLL compared to other polycations, when coating CaAlg beads [47,48] or other anionic hydrogels.[49] For example, PLL was found to diffuse more deeply into polyacrylate hydrogels than polyhistidine and polyarginine of the same MW, which was attributed to differences in chain conformation, the nature of the cationic group, and hydrophobicity.

Based on the polycation distribution in the CaAlg beads studied here, the most promising polycations for membrane formation include $pAPM_{50–15}$, $pAPM_{50–40}$, or $pAPM_{25–40}$ (saline washes), as well as $pAPM_{75–15}$ with a gelling bath wash. In the next section, we explore the compatibility of these polycations with model cells.

3.4.3. Polycation cell and host compatibility

Surgical implantations always trigger a local immune response to the injury, which is exacerbated if the implant binds proteins and host cells.

Although the general cytotoxicity of polycations including PLL is reduced in the presence of alginate,[9] other polyanions [33], and serum proteins,[50] some cell types may still be affected by the polycations used in the coating process.[9] Polycation cytotoxicity is attributed to the disruption of cell membrane, releasing cellular components [33,34,51] and causing necrosis,[9] which can lead to chronic inflammation.[52]

Chaikof examined the effect of PLL-*g*-PEG on the viability of islet clusters using Live-Dead staining after exposure to 80 μM (~1 mg/mL) polycation solutions for 40 min. Unmodified PLL was shown to disrupt the cell membranes leading to internalization of the polycation and 20% cell survival. Conversely, grafting 40% of the lysine units with 200 Da PEG gave a polycation that remained on the cell surface and showed 100% cell viability.[19]

Our approach involves diluting the charge density on the polycation by copolymerization of the amine-functional APM with an uncharged hydroxy-functional

comonomer, HPM. Factors that will increase polycation cell membrane binding and rupture, include high charge density, high MW, branched structure, and chain flexibility.[33,34,51]

We used an alamarBlue assay to test viability of C2C12 myoblasts exposed to polycations in solution. In addition, we studied the binding of 3T3 fibroblasts to model surfaces grafted with the different polycations, as a proxy test for undesirable attachments of host cells to transplants.

3.4.4. Polycation cytotoxicity as measured by alamarBlue cell viability assay

C2C12 myoblasts were chosen for this assay because they stop dividing at confluence, a feature that has made them popular for cell encapsulation.[53] The cells were treated with polycations in serum-free media for 20 h at concentrations of 0.01, 0.1, and 1 mg/mL. Cell viabilities, defined as alamarBlue conversion relative to a control (Figure 3.7), show that cytotoxicity increased with polycation concentration, charge density, and MW.[33,34,51,54] Both high and low molecular weight PLL and $pAPM_{75}$ resulted in cessation of metabolic activity at all concentrations, except the lowest concentration. Viability improved with $pAPM_{50–15}$,and none of the low charge density polycations $pAPM_{25}$ and $pAPM_{10}$ show significant cytotoxicity, at all concentrations used. Pissuwan and co-workers have seen similar cytocompatibility with pHPM prepared by RAFT (CTP end-group removed), showing 100% viability for three different cell lines at 1000 μM (~0.14 mg/mL) after 24 h incubation.[44] The higher cytotoxicity of polycations with higher MW [34] is attributed to greater binding affinity for cell membranes [54] leading to increased membrane damage.[33,51]

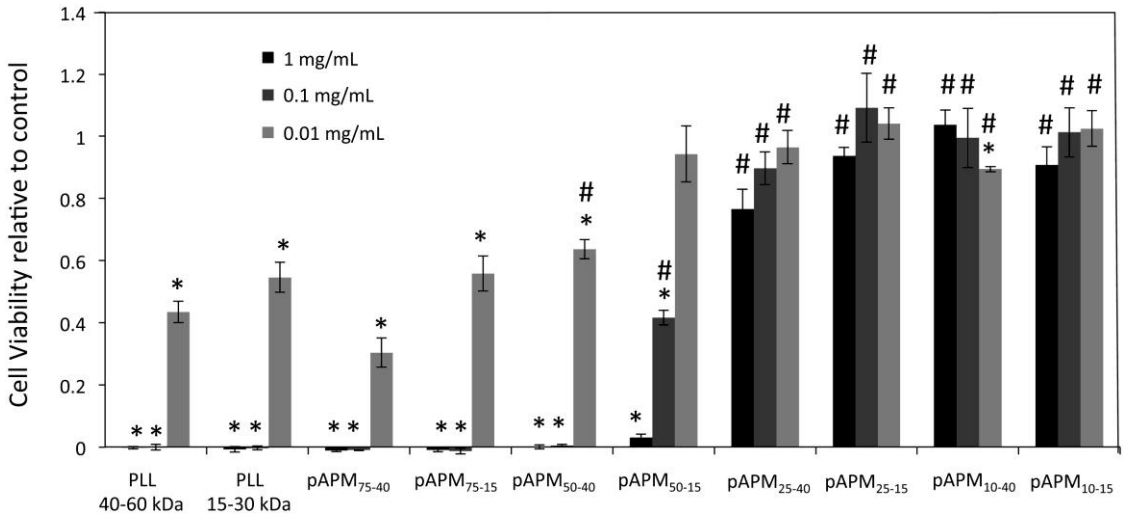

Figure 3.7. Cell viability relative to control after exposure of C2C12 myoblasts to polycations, assessed by alamarBlue assay. (*) and (#) markers indicate statistical significance ($p < 0.05$), as determined by ANOVA using Games-Howell *post hoc* analysis compared to the control ($n = 15$) (*) or to PLL of the same MW and concentration ($n = 3$) (#). Experiments were done in triplicate.

The cytotoxicity of polycations can also be assessed through their effects on cell morphology. For example, Fischer et al. saw that increased polycation toxicity for L929 mouse fibroblasts was accompanied by an increase in cell debris due to lysis, and loss of spindle shape due to detachment from the cell culture dish.[51] The effect of the dissolved polycations on the C2C12 cell morphology was also examined by optical microscopy (Figure 3A.12). As an adherent cell line, healthy C2C12 cells spread and remain attached to the tissue culture plate as seen in the control wells (Figure 3A.12d). However, cells that were exposed to polycations of increasing charge density became less likely to be attached to the culture plate and more likely to show a spherical rather than elongated morphology (Figure 3A.12).

3.4.5. Cell attachment and proliferation on polymer-modified substrates

High cationic charge densities (from pAPM or PLL) promote protein and cell binding, which can be useful in certain cell culture applications [31,55] but can lead to undesirable immune responses in transplanted biomaterials.

Hubbell found reduced binding of BSA, fibrinogen, complement, and cells on calcium alginate surfaces coated with PLL-g-PEO compared to PLL.[18] Similarly, Fairbanks found that pHPM gels were hydrophilic, non-cytotoxic, and had anti-fouling properties showing reduced fibronectin adsorption compared to tissue culture-treated polystyrene, and this prevented L929 mouse fibroblast attachment.[56]

We hence assessed the attachment and growth of NIH/3T3 cells over three days, on surfaces bearing different $pAPM_X$ copolymers. The polycations were covalently attached to a glass surface modified with APTES and an anhydride-containing polymer, poly(methyl vinyl ether-alt-maleic anhydride) (PMM). In some cases, the polycation layer was then coated with alginate or PMM. Cells were incubated in complete medium for three days with no change of medium to ensure that no unattached cells were lost. Attachment to the substrates was assessed by microscopy (PLL, $pAPM_{50}$, and $pAPM_{25}$ are shown in Figures 3.8 and $pAPM_{75}$ and $pAPM_{10}$ are shown in Figure 3A.13).

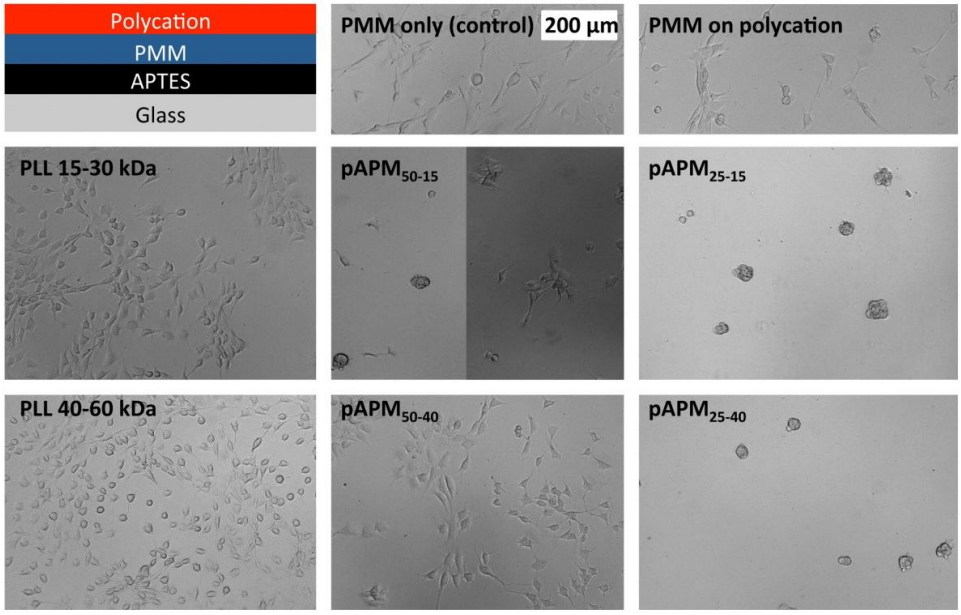

Figure 3.8. Representative optical microscopy images of NIH/3T3 cells on polycation-grafted glass after three days of incubation. The PMM-on-polycation image shows cell attachment on a $pAPM_{25–15}$ surface that was coated with PMM (anhydride form) and then hydrolyzed.

Greater cell attachment is seen for higher charge density polycations (PLL, $pAPM_{75}$) used as the top layer, for both MWs. Substrates coated with $pAPM_{50–15}$ show a mixture of well-spread attached cells (right half of image) and unattached spherical and clustered cells (left half of image). Adding an alginate layer on top of the polycation led to less cell attachment for both MWs of PLL- and $pAPM_{75}$-coated substrates (Figure 3A.14), but had no observable effect on cell morphology for polycations with 50 or less mol% APM.

Cells on PMM surfaces were well attached and spread-out. Slides coated with either MW $pAPM_{10}$ followed by PMM gave varied results, attributed to poor PMM binding to the $pAPM_{10}$.

NIH/3T3 fibroblasts are anchorage dependent,[57] and their attachment and proliferation on these surfaces was assessed by alamarBlue assay in multi-well plates (Figure 3.9). alamarBlue conversion was found to increase with the charge density of the polycations bound to the substrate (Figure 3A.15). A statistically significant positive linear trend was observed for both the 40 and 15 kDa series of polymers, ($p < 0.001$ and $p < 0.001$ respectively), showing a dependence of adherent cell activity on charge density after three days of proliferation. In addition, $pAPM_{50–15}$ and $pAPM_{75–15}$ showed minor, not statistically significant, increases of cell activity with MW.

The effect of an alginate final layer on cell growth was found to be minimal, in agreement with previous studies of APA capsules showing little ability of the final alginate layer to either bind effectively to or to hide the PLL.[14]

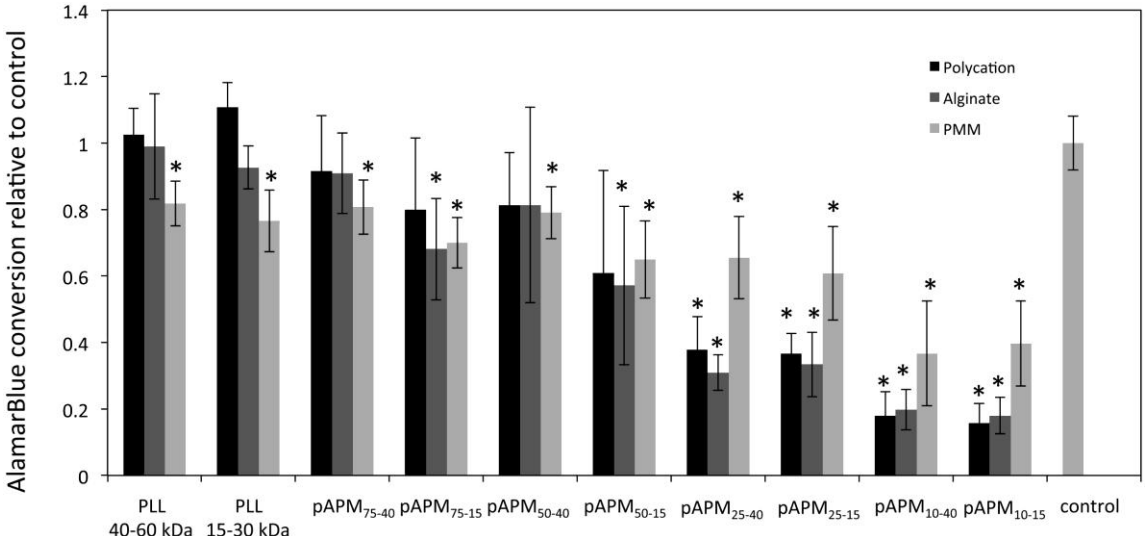

Figure 3.9. alamarBlue conversion relative to control of NIH/3T3 cells after three days of proliferation on polycation-modified glass, and on polycation-modifed glass additionally coated with alginate or PMM. Statistically significant difference to the control is marked by an '*' ($p < 0.05$ determined by ANOVA using Games-Howell *post hoc* analysis). The data points in the graph represent three individual experiments, each in triplicate ($n = 9$ for all, except $pAPM_{75–15}$, $pAPM_{75–15}$ with alginate on top, and $pAPM_{75–40}$, with PMM on top where $n = 8$).

PMM (anhydride form in acetonitrile) was coated onto the polycation layer and then hydrolyzed in order to assess cell attachment to a covalently bound polyanion. Cells showed significant attachment to all the PMM-coated polycation surfaces; however, they showed lower cell densities leading to lower alamarBlue conversion compared to control (PMM alone). This may result from incomplete binding of PMM to polycation surfaces from acetonitrile, in particular for $pAPM_{10}$ (15 and 40 kDa) substrates which showed the lowest cell attachment of the PMM-coated substrates.

The attachment and proliferation of cells on PMM surfaces was somewhat surprising since calcium alginate capsules with anionic surfaces, including PMM, often show reduced fibrotic overgrowth compared to capsules with a cationic surface.[17]

However, Ishihara and co-workers found that HeLa cells attached well onto polymer brushes that were highly anionic or cationic but not those that were zwitterionic (low net charge) because they fostered the greatest amount of fibronectin adhesion.[58] In the case of PLL (15–30 and 40–60 kDa) or $pAPM_{75}$ (15 and 40 kDa), adding a layer of PMM likely causes a switch from a highly cationic to highly anionic surface, which was still able to promote cell attachment. With low charge density polycations, covalent binding of PMM may result in a more highly charged, albeit anionic, surface that improves *in vitro* cell attachment for NIH/3T3.

Brafman et al. screened a variety of commercial polymers and found that PMM was a promising support for long-term self-renewal of human embryonic stem cells.[59] In their study, the growth media did not contain serum proteins, but they found that the production of extracellular proteins was higher than seen for cells grown on Matrigel, suggesting that the cells increased their rate of ECM production in response to the highly charged support.

The above experiments suggest $pAPM_{50–15}$ may be a suitable candidate for capsule membranes used in cells encapsulation, whereas copolymers with more than 50 mol% APM would be useful in cell scaffolds and those with less than 50 mol% APM would be useful for anti-fouling matrices. Further studies explore the physicochemical and mechanical properties of the polyelectrolyte complex membranes based on $pAPM_x$, explore covalent cross-linking to reinforce the polyelectrolyte complex membranes, and test the compatibility of $pAPM_x$-coated capsules with encapsulated cells and hosts.

3.5. Conclusions

A series of polycations with well-defined charge densities and MWs were prepared by RAFT copolymerization of APM with HPM, and investigated for use in alginate–polycation complexes. Polycations with higher charge density ($pAPM_{75–15}$, $pAPM_{75–40}$) formed stronger complexes with alginate and stronger cell attachment than those with lower charge density. The intermediate charge density copolymer $pAPM_{50–15}$ showed reduced fouling and cytotoxicity compared to high and low MW PLL and $pAPM_{75}$, yet still showed good membrane formation on calcium alginate capsules. The lowest charge density polycations (high and low MW $pAPM_{10}$ and $pAPM_{25}$) showed the best cytocompatibility, but bound only weakly to polyanions. Thus, the $pAPM_{50–15}$ copolymer emerged as a promising reduced cationic charge density alternative to PLL. If required, the mechanical robustness of such capsules may be increased through covalent cross-linking with reactive polyanions, and this approach is currently being explored.

Supplementary data to this article can be found in the Chapter 3 Appendix (section 3.10.).

3.6. Acknowledgments

We would like to thank NSERC (Discovery Grant and CREATE IDEM programs) for funding, and acknowledge Christine Di Cresce, Emilia Bakaic, Ivana Postic, and Bahareh Sayyar for their help with cell cultures and assays, Iwona Wenderska for helping with statistical analysis, and Dr. Heather Sheardown and Dr. Gonzalo Hortelano for providing access to their cell culture facilities.

3.7. Disclosure statement

No potential conflict of interest was reported by the authors.

3.8. Funding

This work was supported by the Natural Sciences and Engineering Research Council of Canada Collaborative Research and Training Experience Program - Integrated Development of Extracellular Matrices [grant RGPIN89661-11].

3.9. References

[1] Lim F, Sun AM. Microencapsulated islets as bioartificial endocrine pancreas. Science. 1980;210:908–910.
[2] Yasuhara T, Shingo T, Muraoka K, et al. Neurorescue effects of VEGF on a rat model of Parkinson's disease. Brain Res. 2005;1053:10–18.
[3] Ross CJD, Bastedo L, Maier SA, et al. Treatment of a lysosomal storage disease, mucopolysaccharidosis VII, with microencapsulated recombinant cells. Hum. Gene Ther. 2000;11:2117–2127.
[4] Thu B, Bruheim P, Espevik T, et al. Alginate polycation microcapsules I. Interaction between alginate and polycation. Biomaterials. 1996;17:1031–1040.
[5] Goosen MFA, O'Shea GM, Gharapetian HM, et al. Optimization of microencapsulation parameters: semipermeable microcapsules as a bioartificial pancreas. Biotechnol. Bioeng. 1985;27:146–150.
[6] Saitoh S, Araki Y, Kon R, et al. Swelling/deswelling mechanism of calcium alginate gel in aqueous solutions. Dent. Mater. J. 2000;19:396–404.
[7] Mørch YA, Donati I, Strand BL, et al. Effect of Ca^{2+}, Ba^{2+}, and Sr^{2+} on alginate microbeads. Biomacromolecules. 2006;7:1471–1480.
[8] Wang X, Garth Spencer HG. Calcium alginate gels: formation and stability in the presence of an inert electrolyte. Polymer. 1998;39:2759–2764.
[9] Strand BL, Ryan L, In't Veld P, et al. Poly-L-lysine induces fibrosis on alginate microcapsules via the induction of ctytokines. Cell Transplant. 2001;10:263–275.
[10] Juste S, Lessard M, Henley N, et al. Effect of poly-L-lysine coating on macrophage activation by alginate-based microcapsules: assessment using a new in vitro method. J. Biomed. Mater Res. 2005;72A:389–398.
[11] Rokstad AM, Brekke OL, Steinkjer B, et al. Alginate microbeads are complement compatible, in contrast to polycation containing microcapsules, as revealed in a human whole blood model. Acta Biomater. 2011;7:2566–2578.
[12] De Vos P, De Haan B, Van Schilfgaarde R. Effect of the alginate composition on the biocompatibility of alginate-polylysine microcapsules. Biomaterials. 1997;18:273–278.

[13] Tam SK, de Haan BJ, Faas MM, et al. Adsorption of human immunoglobulin to implantable alginate-poly-L-lysine microcapsules: effect of microcapsule composition. J. Biomed. Mater. Res. 2009;89A:609–615.
[14] Tam SK, Dusseault J, Polizu S, et al. Physicochemical model of alginate–poly-L-lysine microcapsules defined at the micrometric/nanometric scale using ATR-FTIR, XPS, and ToFSIMS. Biomaterials. 2005;26:6950–6961.
[15] Tam SK, Bilodeau S, Dusseault J, et al. Biocompatibility and physicochemical characteristics of alginate-polycation microcapsules. Acta Biomater. 2011;7:1683–1692.
[16] Rokstad AM, Holtan S, Strand BL, et al. Microencapsulation of cells producing therapeutic proteins: optimizing cell growth and secretion. Cell Transplant. 2002;11:313–324.
[17] Gardner CM, Potter MA, Stöver HDH. Improving covalent cell encapsulation with temporarily reactive polyelectrolytes. J. Mater. Sci.: Mater. Med. 2012; 23:181–193.
[18] Sawhney AS, Hubbell JA. Poly(ethylene oxide)-graft-poly(L-lysine) copolymers to enhance the biocompatibility of poly(L-lysine)-alginate microcapsule membranes. Biomaterials. 1992;13:863–870.
[19] Wilson JT, Krishnamurthy VR, Cui W, et al. Noncovalent cell surface engineering with cationic graft copolymers. J. Am. Chem. Soc. 2009;131:18228–18229.
[20] Wilson JT, Cui W, Kozlovskaya V, et al. Cell surface engineering with polyelectrolyte multilayer thin films. J. Am. Chem. Soc. 2011;133:7054–7064.
[21] Spasojevic M, Paredes-Juarez GA, Vorenkamp J, et al. Reduction of the inflammatory responses against alginate-poly-L-lysine microcapsules by anti-biofouling surfaces of PEG-b-PLL diblock copolymers. *PLoS ONE* [Internet]. 2014 [cited 2015 Sept 28];9. Available from: http://journals.plos.org/plosone/article?id=10.1371/journal.pone.0109837
[22] Sung HJ, Luk A, Murthy NS, et al. Poly(ethylene glycol) as a sensitive regulator of cell survival fate on polymeric biomaterials: the interplay of cell adhesion and pro-oxidant signaling mechanisms. Soft Matter. 2010;6:5196–5205.
[23] Ishida T, Kiwada H. Accelerated blood clearance (ABC) phenomenon upon repeated injection of PEGylated liposomes. Int. J. Pharm. 2008;354:56–62.
[24] Knop K, Hoogenboom R, Fischer D, et al. Poly(ethylene glycol) in drug delivery: pros and cons as well as potential alternatives. Angew. Chem. Int. Ed. 2010;49:6288–6308.
[25] Kopeček J, Šprincl L, Lím D. New types of synthetic infusion solutions. I. Investigation of the effect of solutions of some hydrophillic polymers on blood. J. Biomed. Mater. Res. 1973;7:179– 191.
[26] Kopeček J, Kopečková P. HPMA copolymers: origins, early developments, present, and future. Adv. Drug Deliv. Rev. 2010;62:122–149.
[27] Scales CW, Vasilieva YA, Convertine AJ, et al. Direct, controlled synthesis of the nonimmunogenic, hydrophilic polymer, poly(N-(2-hydroxypropyl)methacrylamide) via RAFT in aqueous media. Biomacromolecules. 2005;6:1846–1850.
[28] Alidedeoglu AH, York AW, Rosado DA, et al. Bioconjugation of D-glucuronic acid sodium salt to well-defined primary amine-containing homopolymers and block copolymers. J. Polym. Sci., Part A: Polym. Chem. 2010;48:3052–3061.

[29] York AW, Zhang Y, Holley AC, et al. Facile synthesis of multivalent folate-block copolymer conjugates via aqueous RAFT polymerization: targeted delivery of siRNA and subsequent gene suppression. Biomacromolecules. 2009;10:936–943.
[30] Goujon LJ, Hariharan S, Sayyar B, et al. Tunable hydrogel thin films from reactive synthetic polymers as potential two-dimensional cell scaffolds. Langmuir. 2015;31:5623–5632.
[31] Irwin EF, Gupta R, Dashti DC, et al. Engineered polymer-media interfaces for the long-term self-renewal of human embryonic stem cells. Biomaterials. 2011;32:6912–6919.
[32] Paslay LC, Abel BA, Brown TD, et al. Antimicrobial poly(methacrylamide) derivatives prepared via aqueous RAFT polymerization exhibit biocidal efficiency dependent upon cationic structure. Biomacromolecules. 2012;13:2472–2482.
[33] Morgan DM, Clover J, Pearson JD. Effect of synthetic polycations on leucine incorporation, lactate dehydrogenase release, and morphology of human umbilical vein endothelial cells. J. Cell Sci. 1988;91:231–238.
[34] Choksakulnimitr S, Masuda S, Tokuda H, et al. In vitro cytotoxicity of macromolecules in different cell culture systems. J. Control. Release. 1995;34:233–241.
[35] Gugerli R, Cantana E, Heinzen C, et al. Quantitative study of the production and properties of alginate/poly-L-lysine microcapsules. J. Microencapsul. 2002;19:571–590.
[36] Ma X, Vacek I, Sun A. Generation of alginate-poly-L-lysine-alginate (APA) biomicrocapsules: the relationship between the membrane strength and the reaction conditions. Artif. Cells, Blood Sub. Biotechnol. 1994;22:43–69.
[37] Moad G, Chiefari J, Chong YK, et al. Living free radical polymerization with reversible addition-fragmentation chain transfer (the life of RAFT). Polym. Int. 2000;49:993–1001.
[38] Kleinberger RM, Burke NAD, Dalnoki-Veress K, et al. Systematic study of alginate-based microcapsules by micropippette aspiration and confocal fluorescence microscopy. Mater. Sci. Eng. C. 2013;33:4295–4304.
[39] Ahmed M, Narain R. The effect of polymer architecture, composition, and molecular weight on the properties of glycopolymer-based non-viral gene delivery systems. Biomaterials. 2011;32:5279–5290.
[40] Deng Z, Bouchékif H, Babooram K, et al. Facile synthesis of controlled-structure primary amine-based methacrylamide polymers via the reversible addition-fragmentation chain transfer process. J. Polym. Sci., Part A: Polym. Chem. 2008;46:4984–4996.
[41] Li Y, Lokitz BS, McCormick CL. Thermally responsive vesicles and their structural "locking" through polyelectrolyte complex formation. Angew. Chem. Int. Ed. 2006;45:5792–5795.
[42] Thomas DB, Convertine AJ, Hester RD, et al. Hydrolytic susceptibility of dithioester chain transfer agents and implications in aqueous RAFT polymerizations. Macromolecules. 2004;37:1735–1741.
[43] Liu G, Shi H, Cui Y, et al. Toward rapid aqueous RAFT polymerization of primary amine functional monomer under visible light irradiation at 25°C. Polym. Chem. 2013;4:1176–1182.

[44] Pissuwan D, Boyer C, Gunasekaran K, et al. In vitro cytotoxicity of RAFT polymers. Biomacromolecules. 2010;11:412–420.
[45] Bartkowiak A, Hunkeler D. Alginate−Oligochitosan microcapsules: a mechanistic study relating membrane and capsule properties to reaction conditions. Chem. Mater. 1999;11:2486–2492.
[46] Strand BL, Mørch YA, Espevik T, et al. Visualization of alginate-poly-L-lysine-alginate microcapsules by confocal laser scanning microscopy. Biotechnol. Bioeng. 2003;82:386–394.
[47] Gåserød O, Smidsrød O, Skjåk-Bræk G. Microcapsules of alginate-chitosan I. A quantitative study of the interaction between alginate and chitosan. Biomaterials. 1998;19:1815–1825.
[48] Gåserød O, Sannes A, Skjåk-Bræk G. Microcapsules of alginate-chitosan II. A study of capsule stability ad permeability. Biomaterials. 1999;20:773–783.
[49] Bysell H, Malmsten M. Interactions between homopolypeptides and lightly cross-linked microgels. Langmuir. 2009;25:522–528.
[50] Sgouras D, Duncan R. Methods for the evaluation of biocompatibility of soluble synthetic polymers which have potential for biomedical use: 1-use of the tetrazolium-based colorimetric assay (MTT) as a preliminary screen for evaluation of *in vitro* cytotoxicity. J. Mater. Sci.: Mater. Med. 1990;1:61–68.
[51] Fischer D, Li Y, Ahlemeyer B, et al. In vitro cytotoxicity testing of polycations: influence of polymer structure on cell viability and hemolysis. Biomaterials. 2003;24:1121–1131.
[52] Schneider BL, Schwenter F, Pralong WF, et al. Prevention of the initial host immunoinflammatory response determines the long-term survival of encapsulated myoblasts genetically engineered for erythropoietin delivery. Mol. Ther. 2003;7:506–514.
[53] Li RH, Williams S, Burkstrand M, et al. Encapsulation matrices for neurotrophic factor-secreting myoblast cells. Tissue Eng. 2000;6:151–163.
[54] Singh AK, Kasinath BS, Lewis EJ. Interaction of polycations with cell-surface negative charges of epithelial cells. Biochim. Biophys. Acta. 1992;1120:337–342.
[55] McKeehan WL, Ham RG. Stimulation of clonal growth of normal fibroblasts with substrata coated with basic polymers. J. Cell Biol. 1976;71:727–734.
[56] Fairbanks BD, Thissen H, Maurdev G, et al. Inhibition of protein and cell attachment on materials generated from N-(2-Hydroxypropyl)acrylamide. Biomacromolecules. 2014;15:3259–3266.
[57] Tamada Y, Ikada Y. Fibroblast growth on polymer surfaces and biosynthesis of collagen. J. Biomed. Mater. Res. 1994;28:783–789.
[58] Ishihara K, Kitagawa T, Inoue Y. Initial cell adhesion on well-defined surface by polymer brush layer with varying chemical structures. ACS Biomater. Sci. Eng. 2015;1:103–109.
[59] Brafman DA, Chang CW, Fernandez A, et al. Long-term human pluripotent stem cell self-renewal on synthetic polymer surfaces. Biomaterials. 2010;31:9135–9144.

3.10. Appendix

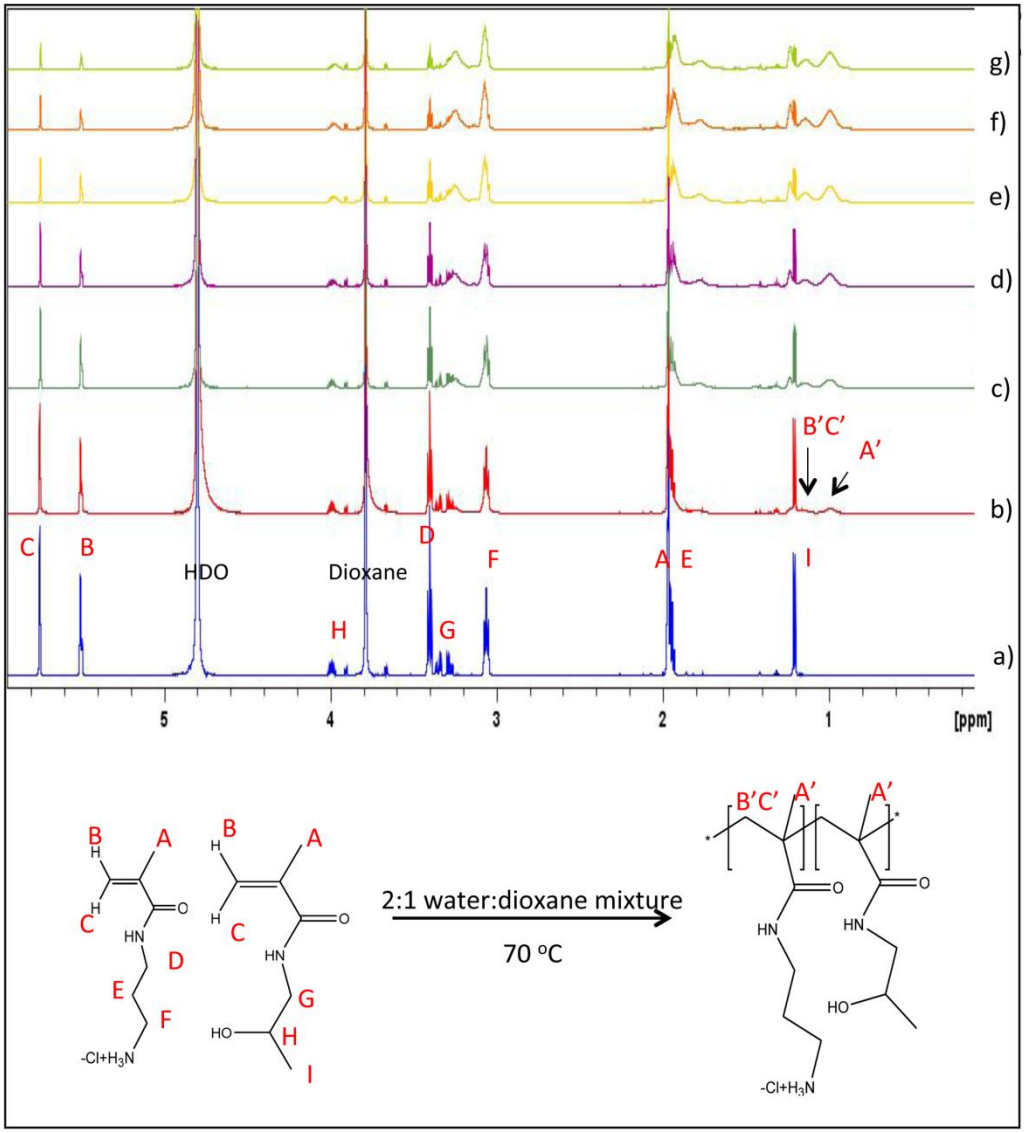

Figure 3A.1. ^{1}H NMR (600 MHz) spectra in D_2O at room temperature showing progress of $pAPM_{75}$ RAFT copolymerization after heating in a 70 °C oil bath for a) 0 h (0% conversion), b) 0.5 h (18% conversion), c) 1 h (44% conversion), d) 2 h (63% conversion), e) 3 h (74% conversion), f) 5 h (82% conversion), g) 7 h (85% conversion). M:CTP ratio = 130:1.

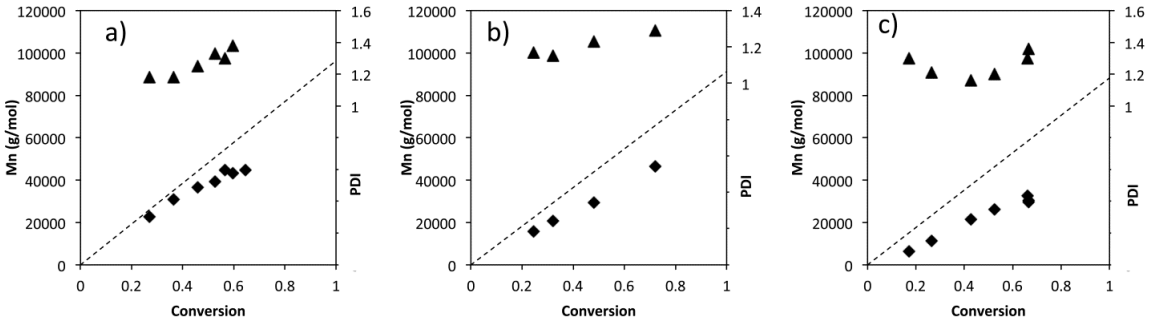

Figure 3A.2. Evolution of MW and PDI during RAFT polymerizations of a) $pAPM_{50}$ b) $pAPM_{25}$ c) $pAPM_{10}$ in 2:1 water: dioxane mixture. M:CTP ratio = 600:1. The experimental M_n (◆) is shown on the primary axis and the PDI (▲) is shown on the secondary axis. The dotted line represents the theoretical M_n.

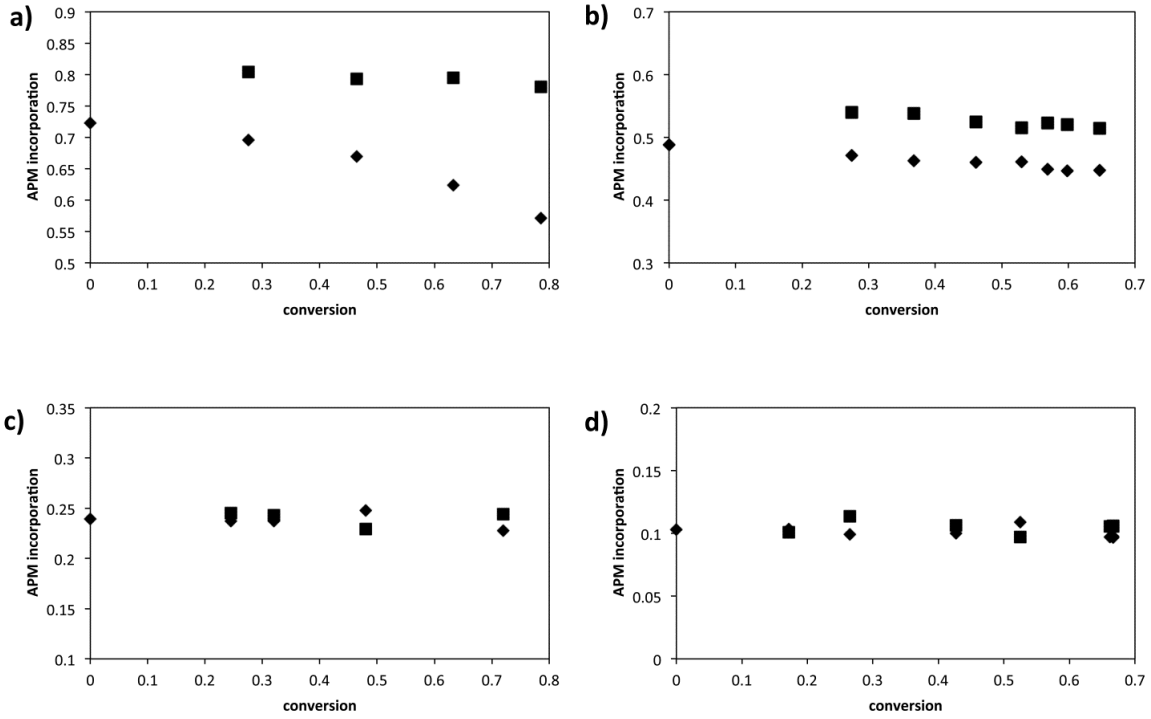

Figure 3A.3. Fraction of APM in monomer mixture (◆) and in copolymer (■) as a function of conversion for copolymerizations with a) $pAPM_{75}$ b) $pAPM_{50}$ c) $pAPM_{25}$ d) $pAPM_{10}$. M:CTP ratio = 330:1 for $pAPM_{75}$ and 600:1 for $pAPM_{50}$, $pAPM_{25}$ and $pAPM_{10}$.

Table 3A.1. Properties of $pAPM_X$ copolymers produced by RAFT polymerization

$[M]_o$:$[CTP]_o$:$[I]_o$ (APM:HPM)	%Conversion[a] (Isolated Yield)*	Composition APM:HPM[b]	Theoretical M_n (kDa); DP	M_n (kDa) (PDI)[c] GPC	M_n (kDa) NMR[d]
130:1:0.33 (75:25)	66 (66)	75:25	14.8; 85.8	14.4 (1.19)[c1] 17.7 (1.20)[c2]	19.5
130:1:0.33 (50:50)	70 (66)	51:49	14.9; 91.0	11.9 (1.23)[c1] 16.0 (1.23)[c2]	19.4
130:1:0.33 (25:75)	76 (73)	25:75	15.3; 98.8	8.33 (1.23)[c1] 14.1 (1.20)[c2]	20.3
130:1:0.33 (10:90)	67 (73)	9:91	13.0; 87.1	4.55 (1.35)[c1] 10.8 (1.23)[c2]	17.3
330:1:0.33 (75:25)	79 (83)	75:25	44.5; 261	32.3 (1.39)[c1] 33.3 (1.33)[c2]	49.5
330:1:0.33 (50:50)	74 (80)	51:49	39.5; 244	31.5 (1.25)[c1] 36.5 (1.29)[c2]	48.5
330:1:0.33 (25:75)	72 (78)	26:74	36.4; 238	24.0 (1.18)[c1] 30.0 (1.26)[c2]	49.2
330:1:0.33 (10:90)	69 (81)	10:90	33.7; 228	17.4 (1.17)[c1] 24.7 (1.21)[c2]	44.0

a) From NMR (600 MHz, 16 scans); b) From NMR (600 MHz, 1024 scans); c) From aqueous GPC of c1) crude samples, c2) after end-group removal; d) From end-group analysis by NMR (600 MHz, 1024 scans) on samples isolated by precipitation prior to end group removal.

*Polymer yield was determined from the amount of recovered polymer compared to the amount expected based on the reaction conversion.

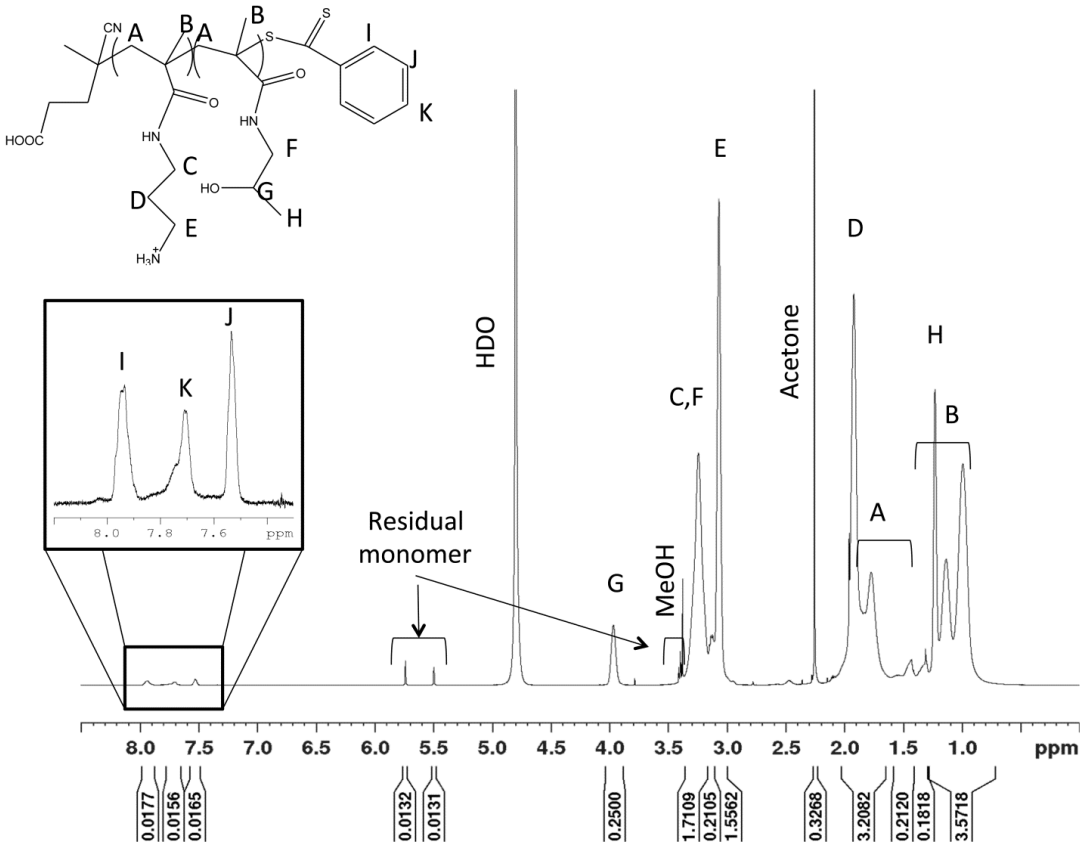

Figure 3A.4. ^{1}H NMR (D_2O, 600 MHz, 1024 scans) of $pAPM_{75\text{-}15}$ before end-group removal. Acetone signal arises from solvent used to isolate polymer following polymerization.

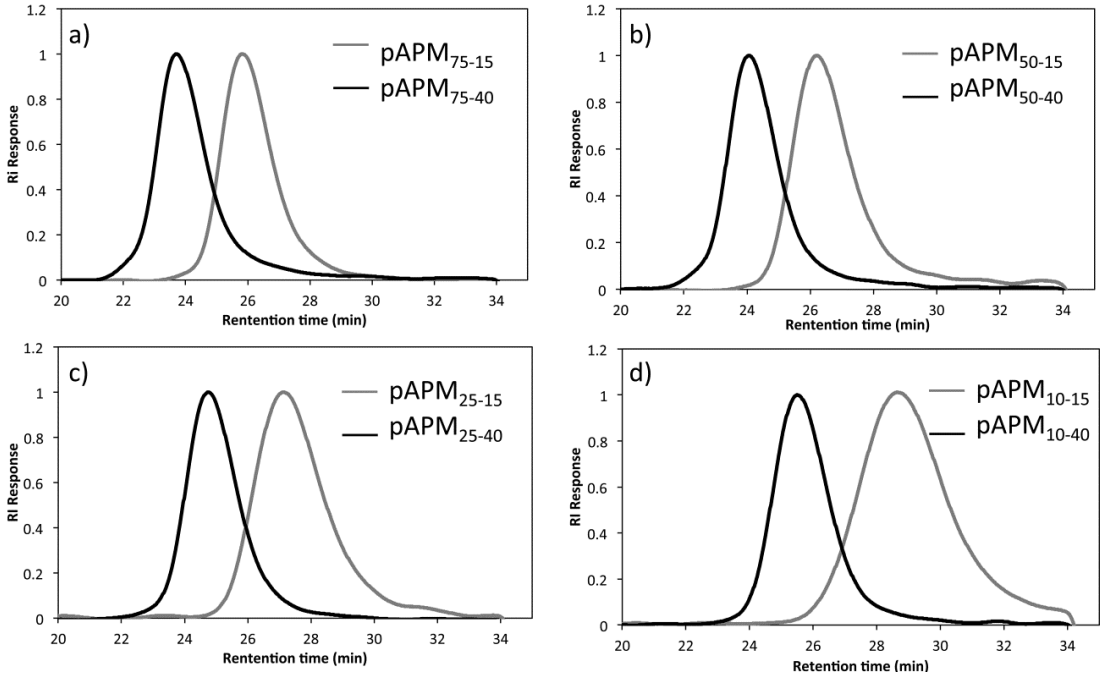

Figure 3A.5. GPC chromatograms of crude a) $pAPM_{75}$, b) $pAPM_{50}$, c) $pAPM_{25}$, d) $pAPM_{10}$ copolymers

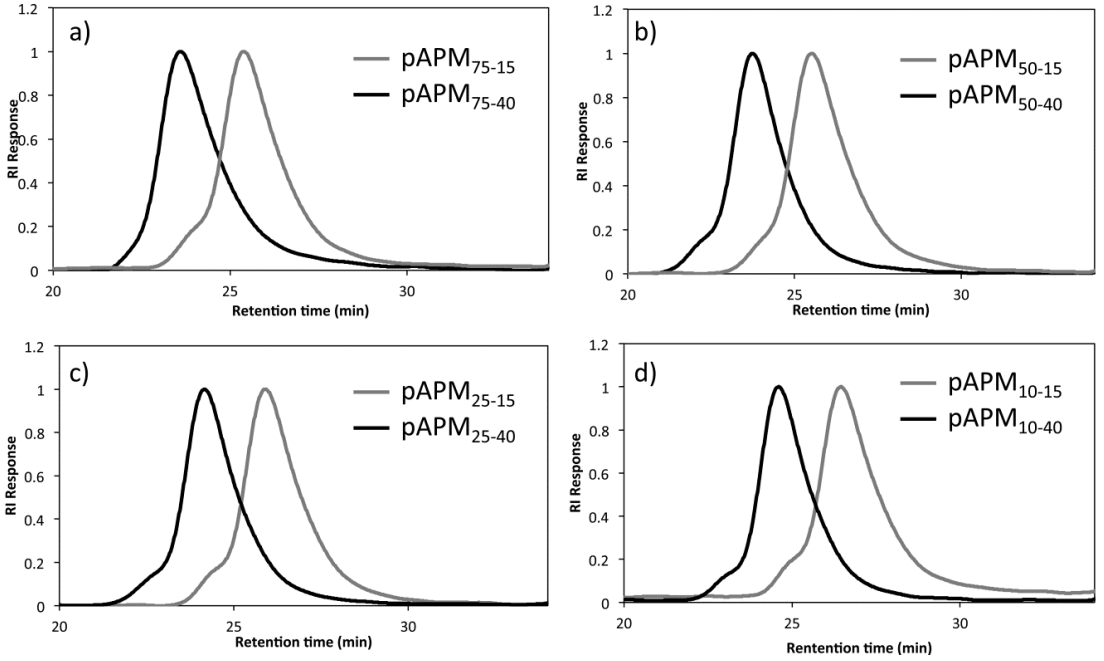

Figure 3A.6. GPC chromatograms of the a) $pAPM_{75}$, b) $pAPM_{50}$, c) $pAPM_{25}$, d) $pAPM_{10}$ copolymers after end-group removal. High MW shoulder indicates a small degree of polymer-polymer coupling.

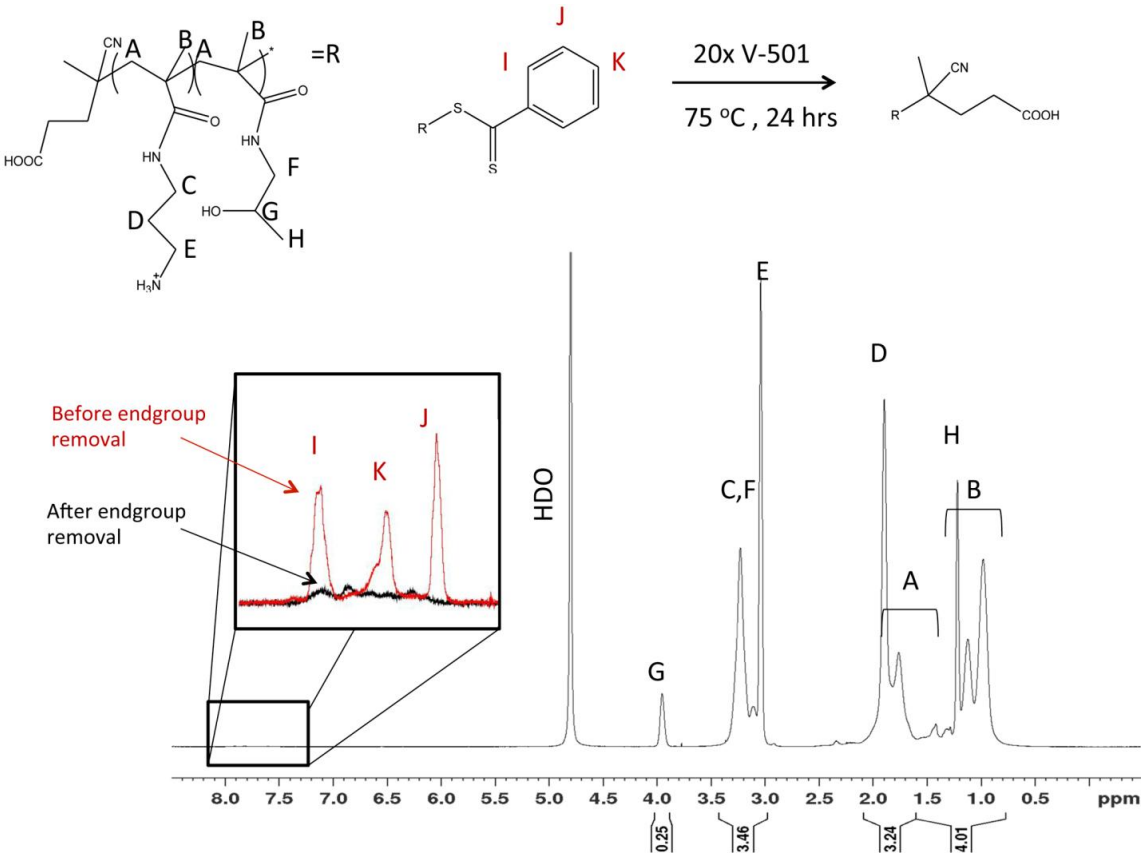

Figure 3A.7. ^{1}H NMR (D_2O, 600 MHz, 1024 scans) of $pAPM_{75\text{-}15}$ after end-group removal.

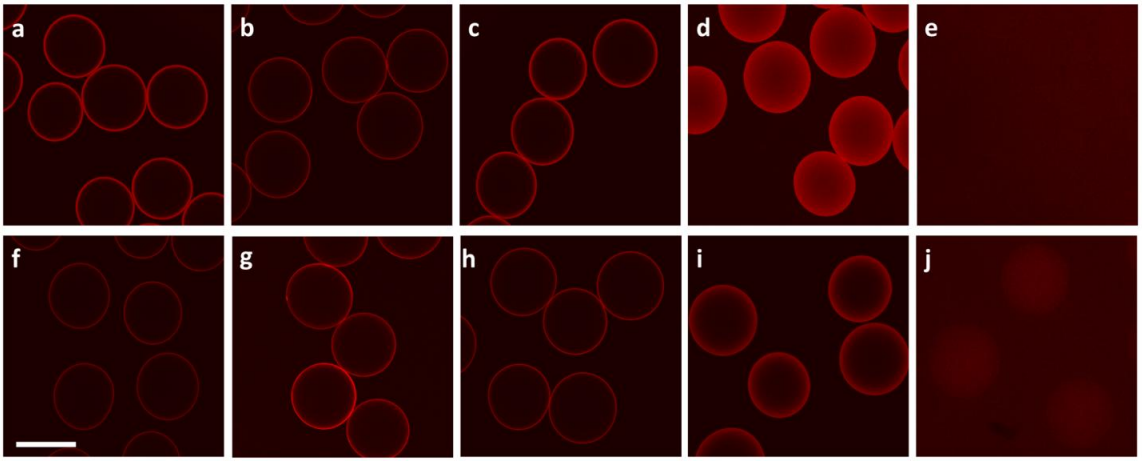

Figure 3A.8. Confocal cross-sectional images showing the distribution of RbITC-labeled polycations in calcium alginate beads coated with: a) PLL 15-30 kDa, b) $pAPM_{75\text{-}15}$, c) $pAPM_{50\text{-}15}$, d) $pAPM_{25\text{-}15}$, e) $pAPM_{10\text{-}15}$, f) PLL 40-60 kDa, g) $pAPM_{75\text{-}40}$, h) $pAPM_{50\text{-}40}$, i) $pAPM_{25\text{-}40}$, j) $pAPM_{10\text{-}40}$. Beads were washed twice with saline after polycation coating. Confocal images were taken at different detector gains. Scale bar is 500 µm.

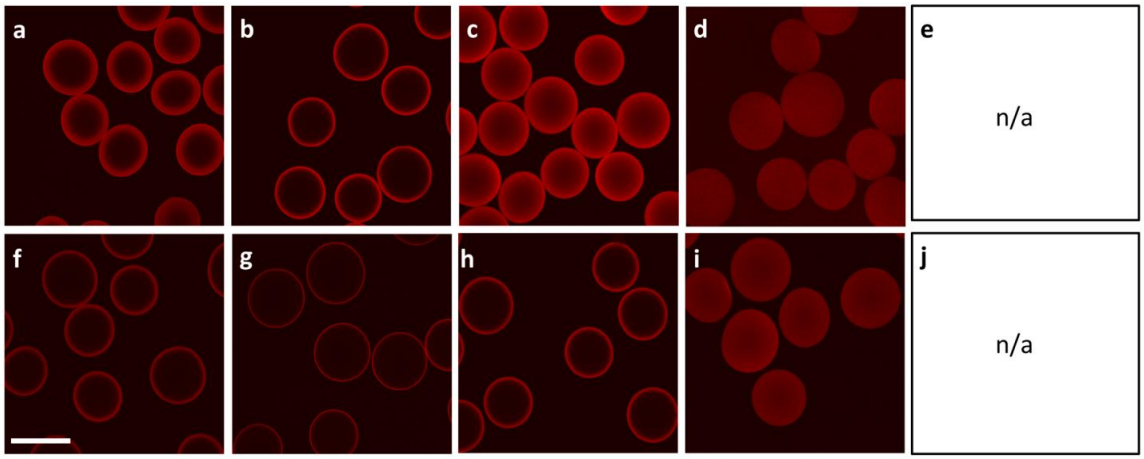

Figure 3A.9. Confocal cross-sectional images showing the distribution of RbITC-labeled polycations in calcium alginate beads: a) PLL 15-30 kDa, b) $pAPM_{75\text{-}15}$, c) $pAPM_{50\text{-}15}$, d) $pAPM_{25\text{-}15}$, e) $pAPM_{10\text{-}15}$, f) PLL 40-60 kDa, g) $pAPM_{75\text{-}40}$, h) $pAPM_{50\text{-}40}$, i) $pAPM_{25\text{-}40}$, j) $pAPM_{10\text{-}40}$. Beads were washed once with gelling bath and once with saline. Confocal images were taken at different detector gains. Scale bar is 500 µm.

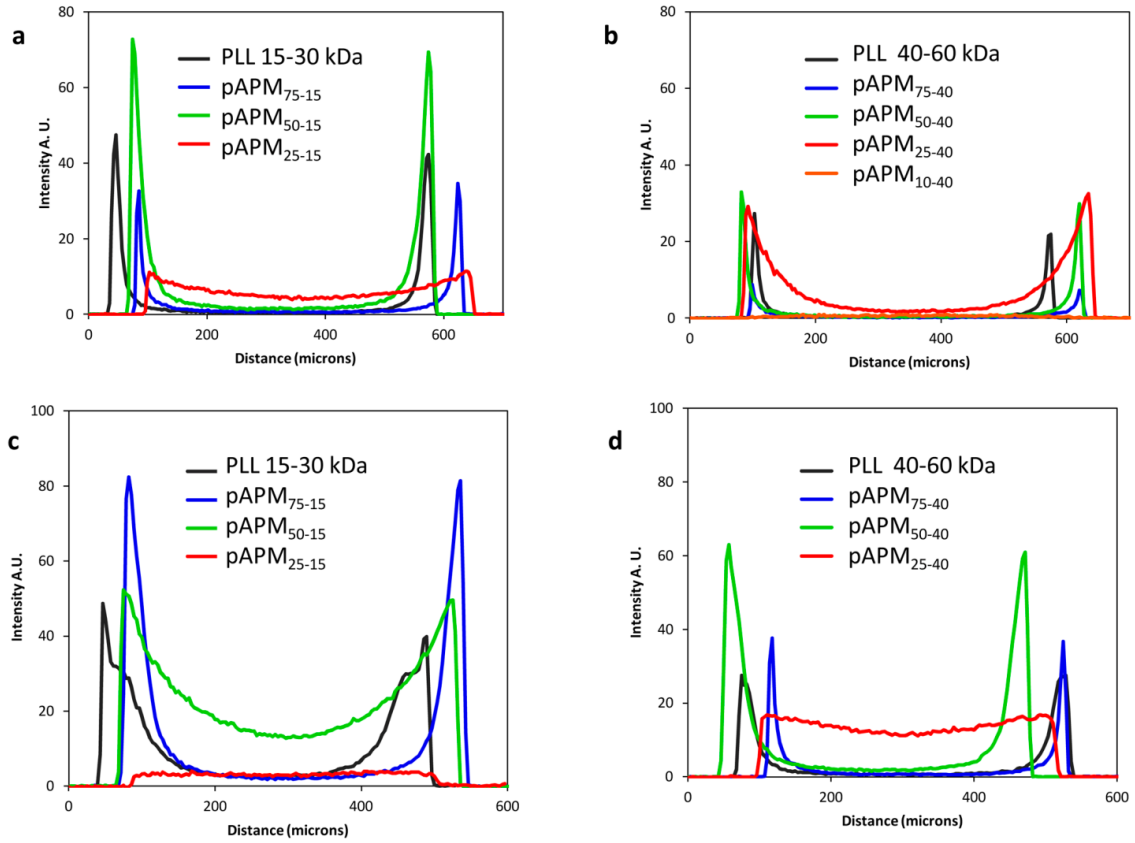

Figure 3A.10. Confocal line profiles (normalized to the same detector gain) showing radial distribution of polycation in alginate beads after washing with **a)**, **b)** saline or **c)**, **d)** gelling bath (100 mM $CaCl_2$, 77 mM NaCl). Results for low MW polycations are shown in **a)** and **c)** and for high MW polycations in **b)** and **d)**.

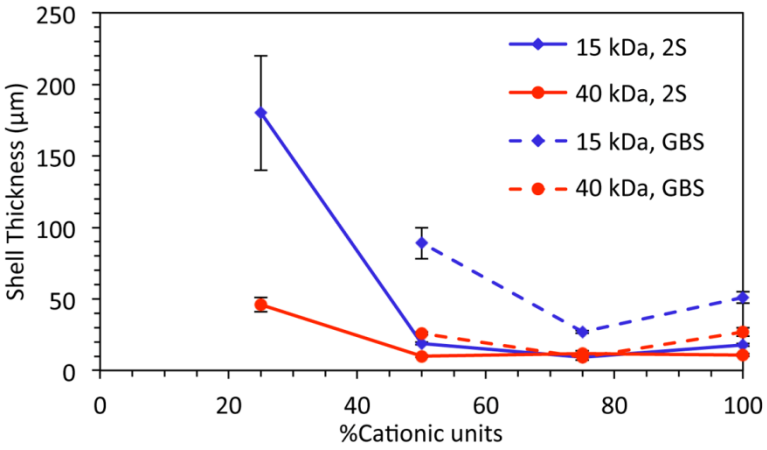

Figure 3A.11. Shell thickness as a function of charge density for calcium alginate beads coated with polycations of MW 15 (blue lines) and 40 kDa (red). Beads were washed twice with saline (solid lines) or once with gel bath and once with saline (dashed).

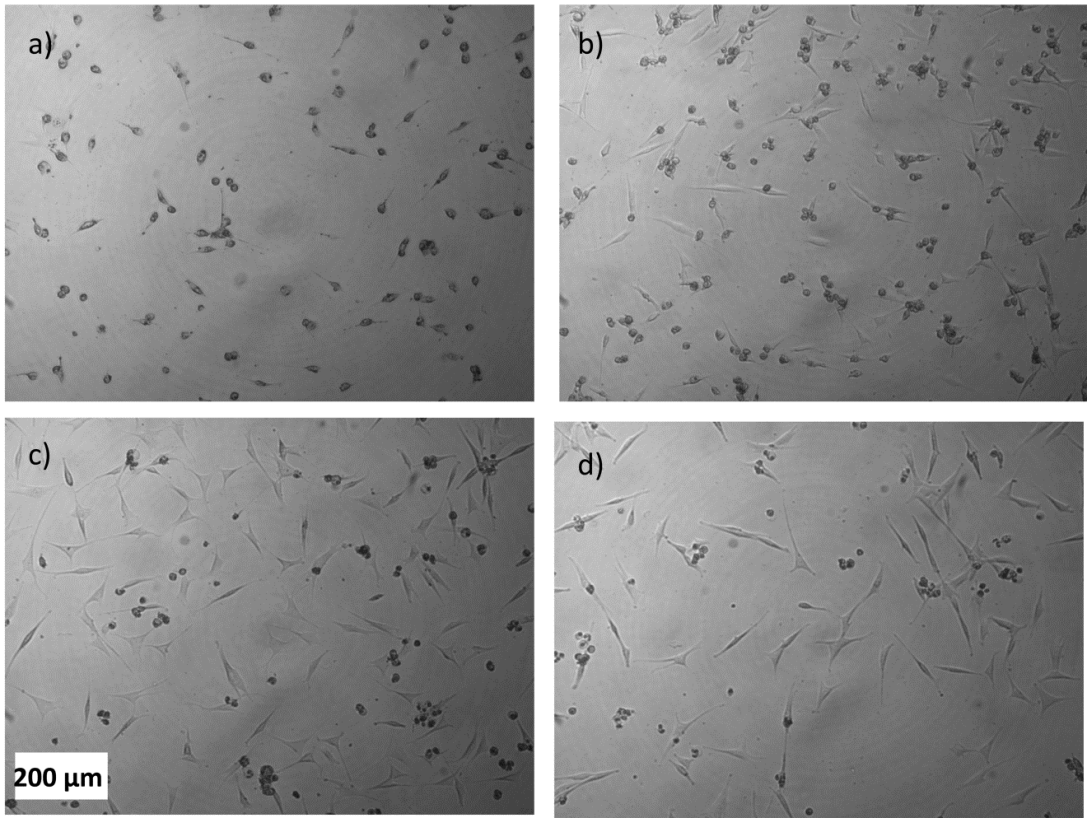

Figure 3A.12. C2C12 Cell morphology on tissue culture treated plate after treatment with 0.1 mg/mL polycation solutions for 20 hrs: a) PLL 15-30 kDa, b) $pAPM_{50\text{-}15}$, c) $pAPM_{25\text{-}15}$ and d) PBS as control.

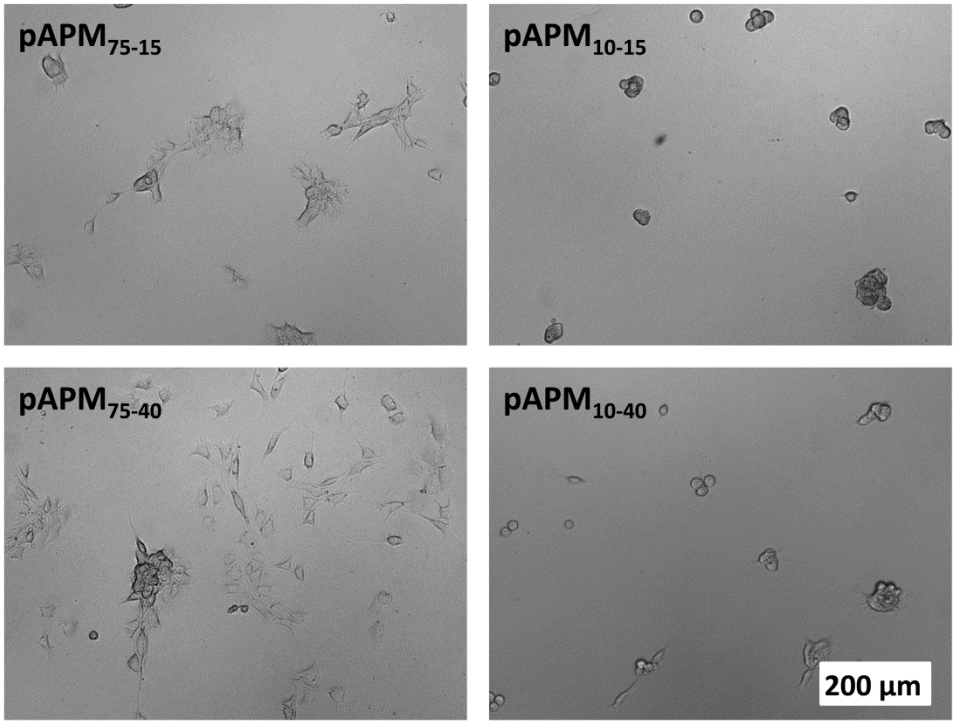

Figure 3A.13. Representative optical microscopy images of NIH/3T3 cells on polycation-modified glass after 3 days of incubation.

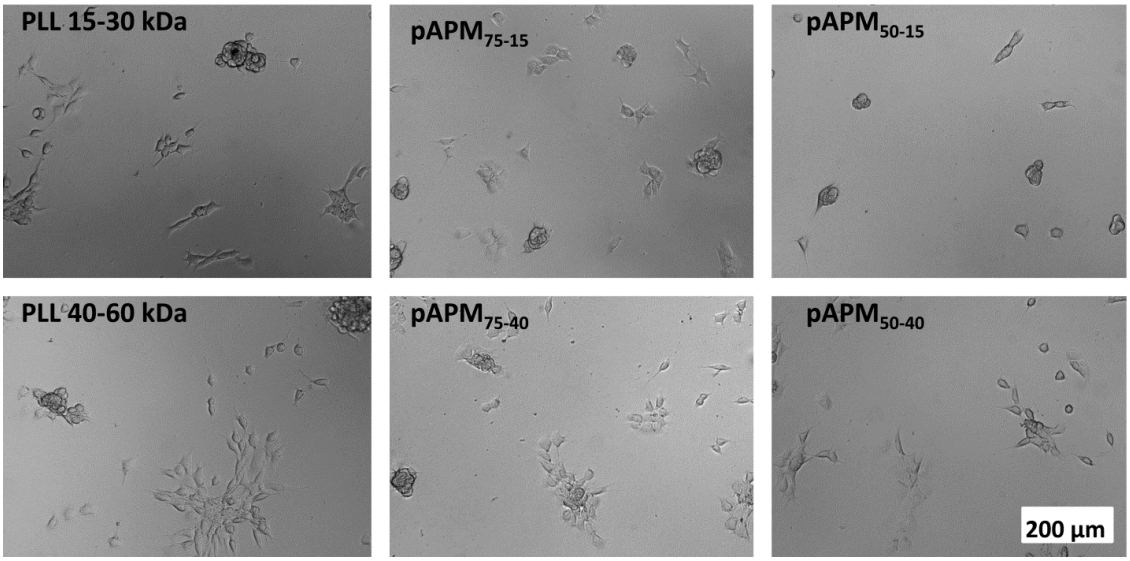

Figure 3A.14. Representative optical microscopy images of NIH/3T3 cells after 3 days incubation on polycation-modified glass coated with alginate.

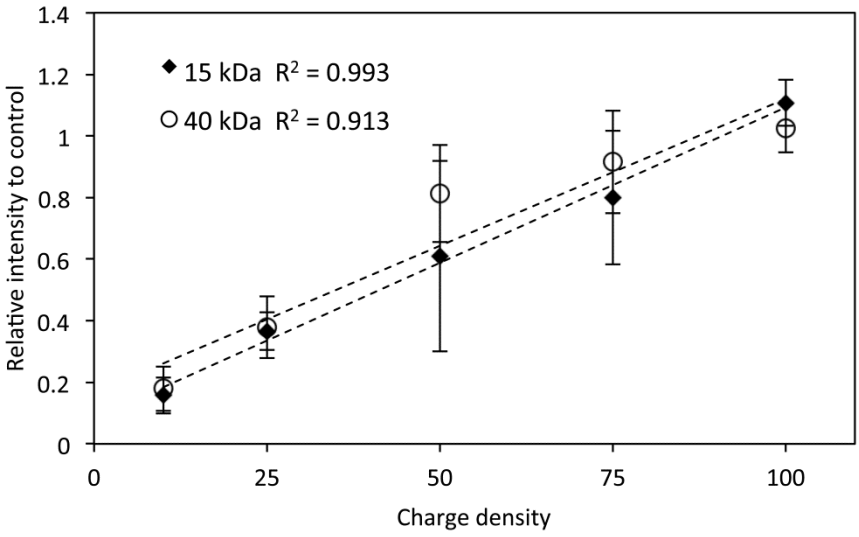

Figure 3A.15. AlamarBlue conversion relative to control of NIH/3T3 cells after 3 days of proliferation on polycation-modified glass as a function of charge density for polycations of 15 kDa (◆) and 40 kDa (O) molecular weight. Data is from 3 individual experiments each done in triplicate (n=9 for all except, $pAPM_{75\text{-}15}$, where n=8).

CHAPTER 4

Cross-linked shells on calcium alginate capsules formed using reduced charge density polycations

Rachelle M. Kleinberger, Nicholas A. D. Burke, Harald D. H. Stöver.
This chapter is being prepared for submission to Materials Science and Engineering C

This chapter reports the capsule properties of alginate based capsules coated with APM/HPM copolymers and cross-linked with temporarily reactive polyanion, PMV60. The ability to effectively covalent cross-link the polycation membrane requires sufficient amount of amine density at the surface of the capsule. Although, covalent cross-linking of the APM/HPM capsule membrane increased the chemical stability and integrity of the membrane, capsules made from the APM/HPM copolymers were significantly more swollen and softer than those made with PLL. Coating capsules with an additional bilayer was able to increase the stiffness of the capsule membrane made with APM/HPM copolymer containing 50% APM of 40 kDa.

Contributions: RMK designed the work for this chapter with help from NADB and HDHS. PMV60 was designed and developed by Dr. Casandra M. Gardner and the modified procedure which RMK used was developed by NADB and Shivanthi Sriskandha. Some of the batches of PMV60 were provided by Shivanti, while other batches were provided by RMK. RMK performed all other experiments. RMK processed and analyzed the data, as well as wrote the manuscript, with edits from NADB and HDHS.

4.1. Abstract

The formation, permeability and stiffness of shells on calcium alginate-based capsules based on charge-reduced polycations are reported. The polycations are formed by copolymerization of N-(3-aminopropyl)methacrylamide hydrochloride (APM) and N-(2-hydroxypropyl)methacrylamide (HPM) in different molar ratios, and coated onto pre-formed calcium alginate capsules. The resulting polyelectrolyte complex shells are more hydrated and hence less robust than comparable poly-L-lysine (PLL)-based shells, but can be covalently cross-linked through coating with a reactive polyanion, poly(methacrylic acid-co-2-vinyl-4,4-dimethylazlactone) (PMV60). Capsule properties were assessed as a function of polycation charge density, molecular weight (MW), and Ca^{2+} facilitated polycation re-distribution within the capsules. Capsules made using copolymers containing 50% APM and MW of 40 kDa were found to be strengthened by treatment with PMV60, showing survival to citrate treatment compared to analogous non cross-linked capsules, in particular when applying multiple coatings. Some formulations show partial stratification of the covalently cross-linked shell, with higher concentration of anionic copolymer on the capsule surface.

4.2. Introduction

Alginate-based hydrogel capsules are useful for many applications in protein delivery,[1] cell encapsulation/protection,[2] and cell delivery/tissue regeneration[3] due to the mild conditions needed for gelation. Hydrogel capsules consisting of polyelectrolyte-

coated calcium alginate beads are promising materials for encapsulation of living cells.[2] Poly-L-lysine (PLL) is most commonly used to tune permeability of the capsules,[4,5] and increase their longevity by creating a polyelectrolyte complex shell resistant to sodium/calcium exchange in the alginate core.[6-8] A final alginate coating is often applied in attempts to provide a more anionic outer surface. These alginate/PLL/alginate (APA) capsules have been explored for, *i.a.*, encapsulation of cells for treatment of diabetes,[2] urea removal due to renal failure,[9] vaccination[10] and large scale anti-body production.[11]

PLL's high charge density leads to strong electrostatic binding to alginate which in turn helps form strong polyelectrolyte complex (PEC) capsule shells, however, such high charge density is associated with cell toxicity and *in vivo* fibrosis, often leading to device failure.[12-14] Efforts to solve this problem include modifying PLL[15-18] or other polycations such as chitosan,[19,20] with PEG, or using synthetic polycations containing neutral,[21] anionic,[22] or charge shifting co-monomers[23] to reduce charge density.

Recently, copolymers of N-(3-aminopropyl)methacrylamide hydrochloride (APM) and N-(2-hydroxypropyl)methacrylamide) (HPM), identified as $pAPM_{X-Y}$ where X is the mol% APM and Y is the molecular weight (MW)**,** were examined as reduced charge density polycations for use as building blocks in biomaterials applications.[21] Not surprisingly, electrostatic binding to alginate weakened as the $pAPM_X$ charge density was reduced, but this was accompanied by reduced cytotoxicity and fouling. A similar effect was seen when the MW of $pAPM_X$ was reduced. Intermediate charge density polycations showed adequate binding to calcium alginate beads, while showing reduced fouling and cytotoxicity compared to PLL for 15 kDa MW.

One concern with the charge-reduced polycations is that the weakened electrostatic binding would give capsules of insufficient strength and stability, especially for long-term applications where slow calcium loss can cause dissolution of the capsule core. Hence, it might be necessary to introduce covalent cross-links, an approach that has been used successfully in several systems using small molecule cross-linkers,[23-26] photo-cross-linking,[27,28] and reactive polyanions.[29-31]

With reactive polyanions the reactive groups can become pre-concentrated in the initially formed polyelectrolyte complex with the polyamine, thus increasing cross-linking efficiency.[32] In addition, immobilized polymeric reactants are less likely to exhibit cytotoxicity than small molecule cross-linkers. In the present work, poly(methacrylic acid-*co*-2-vinyl-4,4-dimethylazlactone) (PMV) was employed as a cross-linking agent to increase capsule strength and stability, for capsule shells formed using charge-reduced polycations. PMV is an example of a temporarily reactive polyanion (TRP)[29,30] containing electrophilic azlactones that can form amide cross-links with the primary amines on the polyamines. This process consumes cationic amine groups, while any azlactones not consumed by cross-linking spontaneously hydrolyze into additional carboxylate groups within minutes. Both aspects reduce the likelihood of electrostatic or covalent protein binding to the capsule surface. PMV has been shown to cross-link PLL coatings on alginate beads leading to increased capsule stability,[29] with the resulting capsules showing improved host compatibility compared to APA capsules, when implanted into immuno-competent mice.[33]

The current paper describes the effect of PMV coatings on alginate-PLL and alginate-pAPM$_X$ capsules, combining the effects of charge-reduced polycations and reactive polyanionic cross-linkers to form capsules of interest for future cell encapsulation work. Capsule properties such as swelling, permeability, and membrane stiffness were measured, and the ability of PMV to covalently cross-link the lower charge density polycation coatings was investigated.

4.3. Experimental

4.3.1. Materials

All materials were used as received unless described otherwise. 2-Vinyl-4,4-dimethylazlactone (VDMA) was purchased from Angene International Limited (Hong Kong, China). Sodium alginate (Pronova UP MVG, batch #: BP-0908-01 and BP-1105-06) was purchased from Novamatrix (Sandvika, Norway). Poly-L-lysine hydrobromide (PLL, 15 kDa and 40 kDa, M_n by viscosity 15-30 and 40-60 kDa, respectively), rhodamine B isothiocyanate (RbITC), 4-(2-hydroxyethyl)piperazine-1-ethanesulfonic acid (HEPES) sodium salt, 2,2-dimethoxy-2-phenylacetophenone (DMPA, 99%), methacrylic acid (MAA, 99%), ethylene carbonate (98%), aminofluorescein (isomer I), fluorescein isothiocyanate conjugated dextran (dextran-FITC 10, 70, 250, 500 kDa), anhydrous tetrahydrofuran (THF, inhibitor free), were purchased from Sigma Aldrich (Oakville, ON Canada). HPLC grade water, reagent grade dioxane, dimethyl sulfoxide (DMSO), anhydrous diethyl ether, sodium chloride and calcium chloride were purchased from Caledon Laboratories (Georgetown, ON). N-(3-Aminopropyl)methacrylamide

hydrochloride (APM) and N-(2-hydroxypropyl)methacrylamide (HPM) were purchased from Polysciences (Warrington, PA). Dextran-FITC (150 kDa) was purchased from Polysciences (Warrington, PA) and was fractionated with ethanol prior to use. DMSO-d6 (99.9% D) was purchased from Cambridge Isotope Laboratories, and ethanol (95%) from Commercial Alcohols (Brampton, ON). Sodium hydroxide (0.1 M) and hydrochloric acid (1 M, 0.1 M) solutions were purchased from Lab Chem (Pittsburgh, PA). Trisodium citrate dihydrate (AnalaR) was from EMD Chemicals (Gibbstown, NJ, USA).

4.3.2. PMV synthesis

PMV60 (nominally 60 mol% VDMA) was prepared in a similar fashion to that previously described,[30] but involving a batch copolymerization based on a 7 wt% total monomer solution of 46:54 VDMA:MAA (initial monomer molar feed ratio), containing 2.8 mol% DMPA photoinitiator and ethylene carbonate as internal standard, in anhydrous THF. Polymerization took place in a home-built photoreactor fitted with two 8 watt black-light bulbs (Ushio F8T5BL). The solution was mixed with a magnetic stirrer and cooled with 10 °C water circulated through a cold finger. The reaction was monitored by ^{1}H NMR, following dilution of an aliquot in DMSO-d6, by comparing the losses of the vinylic signals compared to the internal standard, ethylene carbonate. A typical reaction is as follows:

VDMA (2.78 g, 58%,[34] 11.6 mmol), MAA (1.17g, 13.6 mmol), ethylene carbonate (309 mg, 3.51 mmol), and DMPA (179 mg, 0.698 mmol) were dissolved in 36 mL THF using oven dried glassware. The cold finger was inserted into the reaction

mixture at room temperature and then brought to 10 °C after sealing the reaction with a rubber septum. The photo-reaction proceeded with stirring for 90 mins when a second aliquot of DMPA (170 mg, 0.663 mmol) was added. The reaction was stopped at 40-50% conversion (total irradiation time 115-135 mins) in order to minimize compositional drift, and the polymer isolated by precipitation in diethyl ether and then dried under vacuum, giving typical isolated yields of about 0.508 g (13%). The final polymer was stored in a desiccator and used within 6 weeks (when the degree of azlactone hydrolysis was 10% compared to the initial 3% hydrolysis). Final VDMA content in copolymer is hence estimated to decrease from 56% to about 49% during this time. However, some of this loss of azlactone content is compensated for by formation of also electrophilic acrylic anhydride units elsewhere in the copolymer, as shown previously by Gardner et al.[30] PMV60 was retained as formal name for this reactive copolymer, for convenience.

4.3.3. Synthesis of $pAPM_X$ copolymers

The synthesis by controlled radical polymerization of $pAPM_X$ copolymers with APM/HPM ratios of 75:25, 50:50 and 25:75, and MWs of 15 and 40 kDa with narrow PDI has been previously described.[21] The polymers are identified as $pAPM_{X\text{-}Y}$ where X is mol% APM and Y is the MW in kDa.

4.3.4. Fluorescent labeling of PLL, $pAPM_X$, and PMV60

PLL and $pAPM_X$ copolymers were fluorescently labeled with RbITC as previously described.[21] PMV60 was fluorescently labelled with aminofluorescein (AF)

using a modification of the previously described procedure.[30] For example, PMV60 (0.216 g, 1.04 mmol VDMA) and AF (3.7 mg, 10.7 μmol) were dissolved in 2 mL anhydrous THF and stirred for 4.5 h at room temperature, in the dark. The polymer was precipitated in diethyl ether, isolated by centrifugation and dried under vacuum. The recovered yield was 0.183 g (85%). The amount of reacted AF was determined from a known concentration of hydrolyzed, dialyzed (3.5 kDa MWCO cellulose dialysis tubing, Spectrum Laboratories), and freeze dried PMV60*f* (in sodium salt form) by UV/Vis spectroscopy (Cary 50 Bio). The extinction coefficient of PMV60*f* was 0.179 mL mg^{-1} cm^{-1}, measured at λ_{max} ~ 490 nm in water adjusted to pH 9. The labeling degree of VDMA (0.054 mol%) and labeling efficiency (5.4%) were determined from the absorption coefficient of free AF of 86 000 $M^{-1}cm^{-1}$ at pH 9.[35]

4.3.5. Capsule preparation

Calcium alginate beads (CaAlg beads) were prepared and coated with polycations as previously described.[21] Briefly, CaAlg beads were coated by adding 0.1 wt% PLL or $pAPM_X$ copolymers in saline (pH 7.0-7.5) and occasionally mixing for 6 min. The beads were washed for 2 min with either saline or gelling bath (100 mM $CaCl_2$ and 77 mM NaCl) and then washed again with saline. The beads were then coated with polyanion (0.03 wt% sodium alginate in saline or 0.2 wt% PMV60 in HEPES buffer for 6 min, washed twice with saline to removed excess polyanion and stored in saline at 4 °C, unless indicated otherwise. A standard 3:10 ratio of a dense, sedimeted suspension of beads or capsules to coating or washing solution was used. The 0.2 wt% PMV60 coating solution

was made by diluting a 3% (wt/v) solution of PMV60 in DMSO with 14 parts of 35 mM HEPES-buffered saline at pH 7.8 just prior to capsule coating as previously described. All solutions were pre-cooled to 4°C and coating and washing procedures were performed at room temperature.[33]

The capsule types are denoted with abbreviations such as $ApAPM_{50\text{-}40}PMV60$ (SS) to represent CaAlg beads coated with $pAPM_{50\text{-}40}$ and then PMV60 followed by two saline washes used after the polycation coating. (GS) is used to represent capsules washed once with gelling bath and once with saline after polycation coating.

The standard coating procedure was modified for $ApAPM_{50\text{-}40}PMV60$ (SS) capsules, which became irreversibly aggregated if PMV60 was added to densely packed $ApAPM_{50\text{-}40}$ capsules. Instead, the $ApAPM_{50\text{-}40}$ capsule suspension was diluted with half of the HEPES buffer before being added to 0.4% PMV60 in the other half of the HEPES buffer, to give a final PMV concentration of 0.2%. The suspension was gently mixed for 6 min to prevent the capsules from settling and then the capsules were washed twice with saline.

Doubly-coated $A[pAPM_{50\text{-}40}PMV60]_2$ (SS) capsules were prepared by performing two additional coating steps. $ApAPM_{50\text{-}40}PMV60$ (SS) capsules were diluted with saline, and then transferred to a 0.1% $pAPM_{50\text{-}40}$ solution (final $pAPM_{50\text{-}40}$ concentration of 0.05%) for 6 min, washed twice with saline and then coated with PMV60 as described in the preceding paragraph.

4.3.6. Confocal Microscopy

Confocal microscopy images of fluorescently labeled capsules and/or FITC labelled dextrans were acquired on a Nikon A1 confocal laser scanning microscope, operated using NIKON NIS Elements AR 4.30.02 software, exciting at 561 nm and/or 488 nm. The thickness of PLL*r*, pAPM$_X$*r*, or PMV60*f* coatings was determined using NIKON NIS Elements AR 4.30.02 software to measure the width at half height of 10-pixel (8 μm) wide line profiles, averaged for three capsules each.

4.3.7. Capsule Permeability

Permeability of the as-formed capsules was determined using a method similar to that developed by Vandenbossche based on fluorescently labelled dextrans of different MW.[36] Capsules were analyzed by confocal microscopy after 24 h of exposure at room temperature to 0.001% FITC labelled dextran in saline. The intensity of the fluorescence inside a capsule and in the surrounding solution was determined for three capsules.

4.3.8. Dextran Fractionation

The commercial FITC-labeled dextran samples typically have significant dispersities, however, the 150 kDa sample had a particularly large dispersity showing a considerable fraction of material with MW less than the 70 kDa dextran (Figure 4A.1). The 150 kDa dextran thus was fractionated to remove the lower MW fraction using ethanol, a known non-solvent.[37] Briefly, 93.2 mg of 150 kDa dextran was dissolved in 5 mL of deionized water and phase separated by adding 5 mL of 95% ethanol. The dextran

was collected by centrifugation for 1 hr at 20 °C. The settled viscous liquid was collected and freeze dried, yielding 23.6 mg (25%) of lower dispersity, near 150 kDa, dextran (Figure 4A.1).

4.3.9. Test for Covalent Cross-linking

To test whether the capsule coatings were covalently cross-linked, they were treated with citrate and NaOH.[30] One drop of capsule suspension (~25 μL) was treated with 2-3 drops (~50-75 μL) of 1 M citrate to liquefy the capsule core. Surviving capsules were then washed with 2-3 drops saline followed by exposure to 2-3 drops of 0.1 M NaOH. pH paper was used to confirm that pH ≥12.

4.3.10. Micropipette Aspiration

Micropipette aspiration was performed as previously described,[38] with minor modifications. A borosilicate micropipette (flame pulled from Kimble melting point tube capillaries part no. 34500-99) with an inner diameter of 254 μm and an outer diameter of 305 μm was used. A U-tube filled with water was formed by connecting the micropipette with flexible Tygon tubing to a glass buret (0.5 cm inner diameter, 65 cm length). The height of the water in the column (applied pressure differential) was varied using a syringe pump (Harvard Apparatus Pump 11 Elite Infusion/Withdrawal Programmable Dual Syringe) attached through a Y-shaped connector to the Tygon tubing of the U-tube. Citrate-treated capsules (1-2 drops) were placed in about 0.5-1 mL of saline on a hydrophobic polystyrene dish and imaged during aspiration using a Nikon LV100 upright

optical microscope. The water column was dropped at a rate of 1 inch/min, corresponding to a pressure change of 0.249 kPa/min, for 3, 10 or 15 mins to give a total pressure differential of 0.747, 2.49 or 3.74 kPa, respectively, depending on the stiffness of the capsule. Images of the aspirated capsule were taken every 0.5 or 1 min and the total length of capsule protrusion (x) into the micropipette was measured using NIKON NIS Elements AR 4.30.02 software. The deformation ($x - x_o$, where x_o is the length of the projection of the spherical capsule into the micropipette for a pressure differential of zero) was normalized to the radius of the pipette (R_p). The non-dimensional strain [$(x - x_o/R_p)$] was plotted against the pressure differential and the slope gives the stiffness of the capsule membrane. Any images that showed projection lengths greater than R_p or wrinkling of the capsule surface were not used to determine stiffness. The slope was determined from 5-15 data points, obtained from aspiration of 3 capsules.

4.3.11. Citrate treatment of Capsules for Aspiration Measurements and Capsule Swelling

Two drops (~50 μL) of capsule suspension were treated with 20 drops (~500 μL) of 70 mM sodium citrate for 5 min then washed with 0.5 mL of saline.

4.3.12. Complexation studies

Polycation solutions in saline (0.5 wt %, pH 7.0-7.5) were complexed with PMV60 (0.5 wt%, 43 mM COOH + azlactone). PMV60 solution was prepared by dissolving 15 mg of PMV60 into 0.2 ml of DMSO and adding to 2.8 ml of HEPES buffer

(105 mM, pH 7.8), to obtain final PMV60 solutions at pH 7.0 - 7.5. Different volumes of this PMV60 solution were added to 0.5 mL of polycation solution, in order to achieve a 1:1 ratio of (COO^- + azlactone) to NH_3^+. The phase separated, cross-linked polyelectrolyte complexes formed were observed by optical microscopy the following day. This procedure was also used to form analogous electrostatic complexes formed using fully hydrolyzed PMV (43 mM COOH) in HEPES buffer (105 mM adjusted to pH 7.2). Solutions were filtered through 0.2 μm filters prior to complexation.

4.3.13. GPC

Hydrolyzed PMV was analyzed by aqueous gel permeation chromatography (GPC), consisting of a Waters 515 HPLC pump, Waters 717 plus Autosampler, three Waters Ultrahydrogel columns (-120, -250, -500; 30 cm × 7.8 mm; 6 μm particles), and a Waters 2414 refractive index detector at 30 °C. Hydrolyzed PMV was eluted using 0.5 M $NaNO_3$, 25 mM CHES buffer (pH 10), containing 10 ppm NaN_3 at a flow rate of 0.8 mL/min. FITC labeled dextrans were eluted using a 0.5 M acetic acid/0.5 M sodium acetate buffer pH = 4.8 mobile phase. The MW of PMV (M_n 18.4 kDa) and dispersity (1.3) was determined from a calibration curve of narrow-dispersed PEG standards (Waters, Mississauga, ON).

4.4. Results and Discussion

While APA capsules allow for mild entrapment of living cells, the PLL in their outer coating has often caused problems due to toxicity to some types of encapsulated

cells,[12,39] and in particular due to fibrosis *in vivo*,[12,13] and membrane instability due to protein adhesion and proteolytic degradation.[40] These undesirable interactions with potential guests and hosts are motivating the search for more benign capsule materials for cell-based therapies. In this work we describe the use of reduced charge density $pAPM_X$ polycations as potential replacements for PLL, as some of these polymers had recently shown reduced cytotoxicity and cell adhesion, particularly those of lower charge density and MW.[21] Purely electrostatic capsules were prepared by coating calcium alginate beads with PLL (nominally 15 kDa, where M_n is 15-30 kDa by viscosity), and with $pAPM_X$ having 25, 50 and 75 mol% APM and MWs of 15 or 40 kDa. These capsules were washed using two common procedures involving calcium chloride and saline solutions, respectively, to assess their effects on the polycation shells. Finally, the washed, polycation-coated capsules were further coated with either alginate or PMV60, a reactive polyanion containing about nominally 60 mol% of electrophilic azlactone groups that can covalently cross-link with the polycation coating through amide formation. In addition, the effects of extended and double-layer coatings were explored, and the ability of $pAPM_X$ to complex and covalently cross-link with PMV60 was assessed in model experiments in absence of alginate.

4.4.1. Polycation complexation with PMV60 or hydrolyzed PMV

The nature of the PMV – polycation polyelectrolyte complexes (PEC) formed in the absence of alginate was examined by mixing equivalent mole ratios of selected polycations (PLL 15 kDa, $pAPM_{75\text{-}15}$, $pAPM_{50\text{-}15}$, $pAPM_{50\text{-}40}$, $pAPM_{25\text{-}40}$) with either

PMV60 or fully hydrolyzed PMV60 (PMV0) (Fig. 4.1). In all cases, the mixtures immediately became turbid with phase separated material which settled overtime.

Both direct and microscopic examination revealed that the complexes between polycations and the reactive PMV60 formed solid aggregates. Macroscopically, the optical density for complexes between PMV60 and low MW (15 kDa) polycations increased with APM mol fraction in the polycations, appearing to have less hydrated complexes (Fig. 4.1. 2a-c). Complexes formed between PMV60 and $pAPM_{50\text{-}40}$ (Fig. 4.1. 2d), and in particular those formed with $pAPM_{25\text{-}40}$ (Fig. 4.1. 2e), appear less dense. Microscopic examination showed that all polycations reacted with PMV60 to produced small gel like precipitates, which then combined into larger aggregates. These aggregates were larger if PMV60 was reacted with higher charge density polycations, possibly because these precipitates were more hydrophobic and/or chemically reactive. All complexes formed using PMV60 were found to swell but not dissolve when treated with NaOH, confirming their covalent cross-linking.

In contrast both to the above complexes with reactive PMV60, and to analogous complexes with alginate described earlier,[21] all complexes between polycations and the fully hydrolyzed, non-reactive PMV0 separated out as liquid coacervates (Fig. 4.1.1a-e).

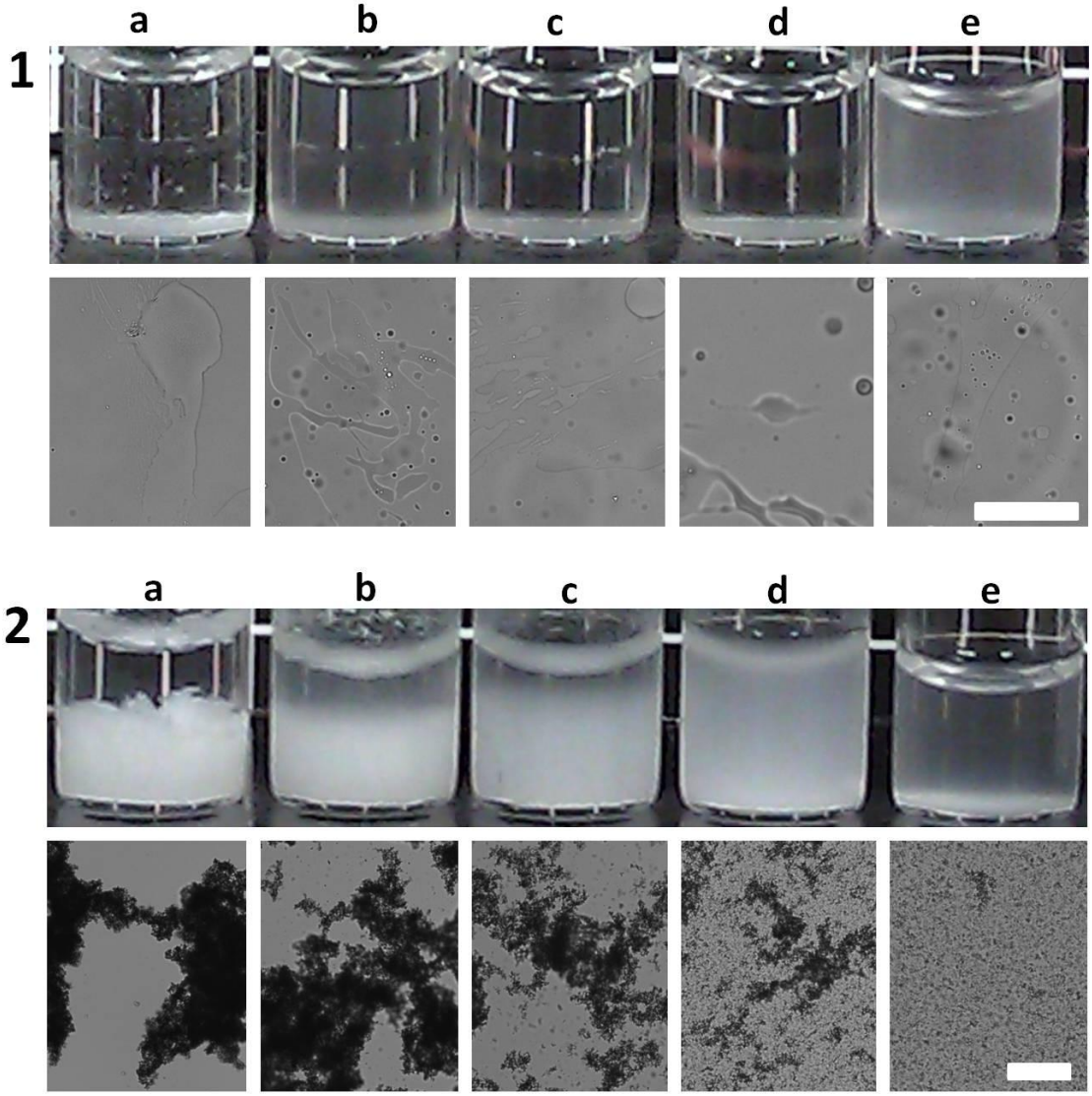

Figure 4.1: Polycation-PMV complexes formed with 1) fully hydrolyzed PMV0 or 2) reactive PMV60 for a) PLL 15 kDa, b) $pAPM_{75\text{-}15}$, c) $pAPM_{50\text{-}15}$, d) $pAPM_{50\text{-}40}$ and e) $pAPM_{25\text{-}40}$. The resulting solutions have pH 7-7.5 in 17-38 mM HEPES buffered saline. Scale bar in 1) is 100 µm and in 2) is 200 µm.

The complexes formed between $pAPM_X$ with PMV0 and PMV60 differ significantly from those described earlier between $pAPM_X$ and alginate,[21] where $pAPM_{75}$ formed solid, dense complexes with alginate, while $pAPM_{25}$ formed transparent gels and

liquid coacervates, in isotonic saline. The results in figure 4.1 show that all complexes between PLL or $pAPM_X$ with PMV0 were liquid coacervates. Thus, the interactions of PLL, $pAPM_{75\text{-}15}$ and $pAPM_{50\text{-}15}$ with PMV0 are weaker than their interactions with alginate, and do not vary significantly with charge density. This is attributed to differences in the polyanions such as the spacing of charge or the lower chain stiffness of acrylates, compared with alginate.[41,42]

Complexes between the polycations and PMV60 appear as irregularly shaped solid precipitates under microscopic observation, thus complexes between $pAPM_{50}$ or $pAPM_{75}$ with PMV60 resemble those with alginate, as described previously.[21] Even $pAPM_{25}$ forms gel or solid precipitates with PMV60, reflecting weak electrostatic interaction that was reinforced by covalent cross-linking. The PLL / PMV60 complexes resemble those for $pAPM_X$, unlike the fibrous PLL/alginate complexes described earlier.[21]

Overall, the electrostatic interactions of both PLL and $pAPM_X$ with hydrolyzed PMV are weaker than those with sodium alginate, leading to more hydrated complexes. Covalent cross-linking introduced by using the reactive PMV60 increases the strength of the total interaction for all $pAPM_X$/PMV60 combinations compared to PMV0.

Below, we explore the formation of corresponding cross-linked $pAPM_X$ / PMV60 shells on preformed calcium alginate beads. It is expected that binding of $pAPM_X$ to the calcium alginate bead, as well as possible dispersal of the $pAPM_X$ within the calcium alginate as consequence of, e.g., washing protocols involving calcium chloride, will reduce the rapid preconcentration by complexation[32] seen in the model solution

experiments, and thus reduce the chances of covalent cross-linking of the electrostatic complexes.

4.4.2. Capsules coated with covalently cross-linked $pAPM_X$ – PMV60 shells, as function of washing protocol.

The ability of capsules coated with $pAPM_X$ copolymers of 15 and 40 kDa to cross-link with PMV60 as a function of washing with saline or gelling bath was assessed.

Calcium alginate beads coated with both 15 or 40 kDa $pAPM_{25}$ copolymers did not show a distinct primary membrane, attributed to the weak electrostatic binding of these polycations to alginate. As a consequence, addition of PMV60 did not lead to effective cross-linking, and the final capsules were soft (Fig. 4A.3, 4A.4) and dissolved on liquefaction of the alginate gel core with 1 M sodium citrate.

Capsules coated with the high MW, high charge density $pAPM_{75\text{-}40}$ tended to aggregate during the PMV60 coating (Fig. 4A.3, image f), creating large defects in the capsule membrane when capsules tore apart. Analogous but less pronounced capsule aggregation was observed for $ApAPM_{75\text{-}15}$PMV60 (SS) and $ApAPM_{50\text{-}40}$PMV60 (SS) capsules during PMV60 coating, but could be mitigated by adding a dispersion of capsules in buffered saline to the PMV60 solution rather than adding the PMV60 solution to the densely packed assembly of capsules.

GS-washed capsules were markedly less prone to aggregation during PMV60 coating (Figure 4A.4, image f), which is attributed to calcium-promoted in-diffusion of $pAPM_X$, leaving a reduced polycation concentration at the capsule surface.[38]

To test for cross-linking after PMV60 coating, the capsules were exposed to sodium citrate to liquefy the capsule core and then to high pH (≥12), which neutralizes the polycations leaving only covalent interactions to hold the membrane together. The presence of intact or broken shells for capsules prepared with PLL, $pAPM_{75}$, and $pAPM_{50}$ (Figs. 4A.5-4A.6) and treated with NaOH is evidence for covalent cross-linking.

Selected PMV60 cross-linked capsules were further compared against non cross-linked analogs coated with alginate instead of PMV60. Considering the aim to reduce amine content at the surface, capsules formed from $pAPM_{75\text{-}15}$, $pAPM_{50\text{-}15}$ and $pAPM_{50\text{-}40}$ were of particular interest, where capsules formed with $pAPM_{75\text{-}15}$ were washed with gelling bath, $pAPM_{50\text{-}15}$ capsules were washed only with saline and $pAPM_{50\text{-}40}$ were washed with either saline or gelling bath.

4.4.3. Capsule Properties

The capsules discussed above were examined by microscopy to determine capsule diameter as function of PLL versus $pAPM_X$ coating, as function of gelling bath/saline (GS) versus saline/saline (SS) washes, and as function of non-cross-linking alginate versus cross-linking PMV60 final coating. Survival of the shells after citrate extraction of calcium from the cores was used as measure of capsule stability and qualitatively described by the ability of the capsules to resist swelling, rupture or disintegration after the alginate core was liquefied. Confocal fluorescent microscopy was used to assess the thickness of coating layers.

4.4.3.1 Capsule Diameters as Function of Composition and Washing Protocols

The data on capsule diameter and layer thickness is summarized in Table 4.1, based on transmission optical and confocal fluorescent microscopy images shown in Figures 4.2 through 4.4 and 4A.7. As seen in previous work,[38] capsules washed with Ca^{2+}-containing gelling bath tend to be smaller and have thicker, more diffuse polyelectrolyte shells, due to more Ca^{2+} being retained in the gel core and due to calcium-assisted polycation redistribution, respectively (Table 4.1). For example, SS-washed $ApAPM_{50\text{-}40}A$ capsules are larger at 688 ± 45 μm than the analogous GS-washed capsules at 501 ± 30 μm, consistent with larger loss of calcium during the two saline washes. Given identical washing procedures, PLL-coated capsules were smaller than any $pAPM_X$-coated ones, indicating stronger binding of PLL to alginate which makes the capsules less susceptible to swelling following calcium loss.

Table 4.1: Size and membrane thickness of polycation/polyanion-coated capsules.

Capsule type	Diameter (μm)	Diameter after citrate (μm)[a]	Polycation layer thickness (μm)[b,c]	PMV60*f* layer thickness (μm)[b]
CaAlg bead	511 ± 15	n/a	n/a	--
APA (SS)	472 ± 13	493 ± 14	15 ± 1	--
APA (GS)	455 ± 19	494 ± 12	27 ± 4	--
$ApAPM_{75\text{-}15}A$ (GS)	476 ± 22	644 ± 25	14 ± 1	--
$ApAPM_{50\text{-}15}A$ (SS)	625 ± 37	Burst	14 ± 2	--
$ApAPM_{50\text{-}40}A$ (SS)	688 ± 45	Burst	7 ± 1	--
$ApAPM_{50\text{-}40}A$ (GS)	501 ± 30	Dissolved	14 ± 1	--
APPMV60 (SS)	473 ± 13	490 ± 16	15 ± 1	8 ± 1
APPMV60 (GS)	482 ± 13	510 ± 16	19 ± 2 (18 ± 2)	13 ± 1
$ApAPM_{75\text{-}15}$PMV60 (GS)	578 ± 16	789 ± 30[d]	12 ± 1 (13 ± 1)	11 ± 1
$ApAPM_{50\text{-}15}$PMV60 (SS)	732 ± 32	861 ± 133[d]	11 ± 1 (13 ± 2)	9 ± 1
$ApAPM_{50\text{-}40}$PMV60 (SS)	685 ± 18	763 ± 15	6 ± 1	5 ± 1
$ApAPM_{50\text{-}40}$PMV60 (GS)	627 ± 22	832 ± 28[e]	13 ± 1	12 ± 1
$A[pAPM_{50\text{-}40}PMV60]_2$ (SS)	706 ± 26[d]	720 ± 32[d]	3 ± 1 (5 ± 2)	3 ± 1
$ApAPM_{50\text{-}40}$PMV60 (SS) longer incubation	672 ± 20	728 ± 16	7 ± 1	n/a

The size was determined from a minimum of 75 capsules and the membrane thickness was determined from 3 capsules

a) In saline after treatment with 70 mM citrate.

b) Layer thickness (full width at half-height) from line profiles of equatorial sections obtained using confocal microscopy on as-formed beads (i.e., before citrate-treatment).

c) Values in brackets are measurements from a separate batch of capsules.

d) Sample contained ruptured, wrinkled and deflated capsules, which were not used to calculate average diameter.

e) Measured in 70 mM citrate as capsules were too fragile to survive subsequent saline wash.

In contrast to the PLL capsules, all three $ApAPM_{50}A$ type capsules burst or dissolved upon citrate treatment, reflecting the low inherent strength of this hydrated polyelectrolyte shell in absence of cross-linking. $ApAPM_{75\text{-}15}A$ (GS) capsules seem to occupy the middle ground between these two types of capsules, in terms of diameter and integrity, attributed in part to their intermediate charge density.

Table 4.1 and Figure 4.3 further show that an outer coating with reactive PMV60 enhances the post-citrate integrity of $pAPM_X$-type capsules, illustrating how covalent cross-linking can mitigate the effect of higher hydration of these PEC shells on capsule integrity.

Capsules coated with PMV60 tended to be larger than those with a final coating of alginate. This is attributed to greater calcium loss from the capsule core because of the higher polymer concentration used during PMV60 coating compared to alginate coating (0.2 *vs*. 0.03 wt%), since all such polyanions can act as chelating agents and strip calcium from the beads during coating. It also indicates that the cross-linking is not extensive enough to give a membrane that resists swelling. Hillberg et. al. showed that an increased cross-linking degree of cross-linked methacrylated glycol chitosan coatings gave capsules better able to resist swelling from calcium loss from the calcium alginate core.[28] In future experiments, small amounts of calcium may be added directly to the PMV60 coating solutions to reduce loss of calcium from the gel beads, or indeed, mixtures of calcium and barium may be used in the cores to strengthen the gel during shell formation.

4.4.3.2. Capsule response to citrate treatment

A stable outer membrane is considered helpful or even essential for most long term encapsulations because Ca^{2+} is slowly lost from the alginate gel core. Capsules were treated with 70 mM citrate to remove calcium from the core as an accelerated aging test. Capsules were also exposed to 1 M citrate, which provides a more severe test of membrane stability because, in addition to liquefying the calcium alginate gel, the high

ionic strength should disrupt all but the strongest electrostatic interactions in the PEC membrane. The capsules were examined by transmission optical microscopy after citrate exposure for signs of swelling, rupture or dissolution of the membrane (Figs. 4.2 & 4.3).

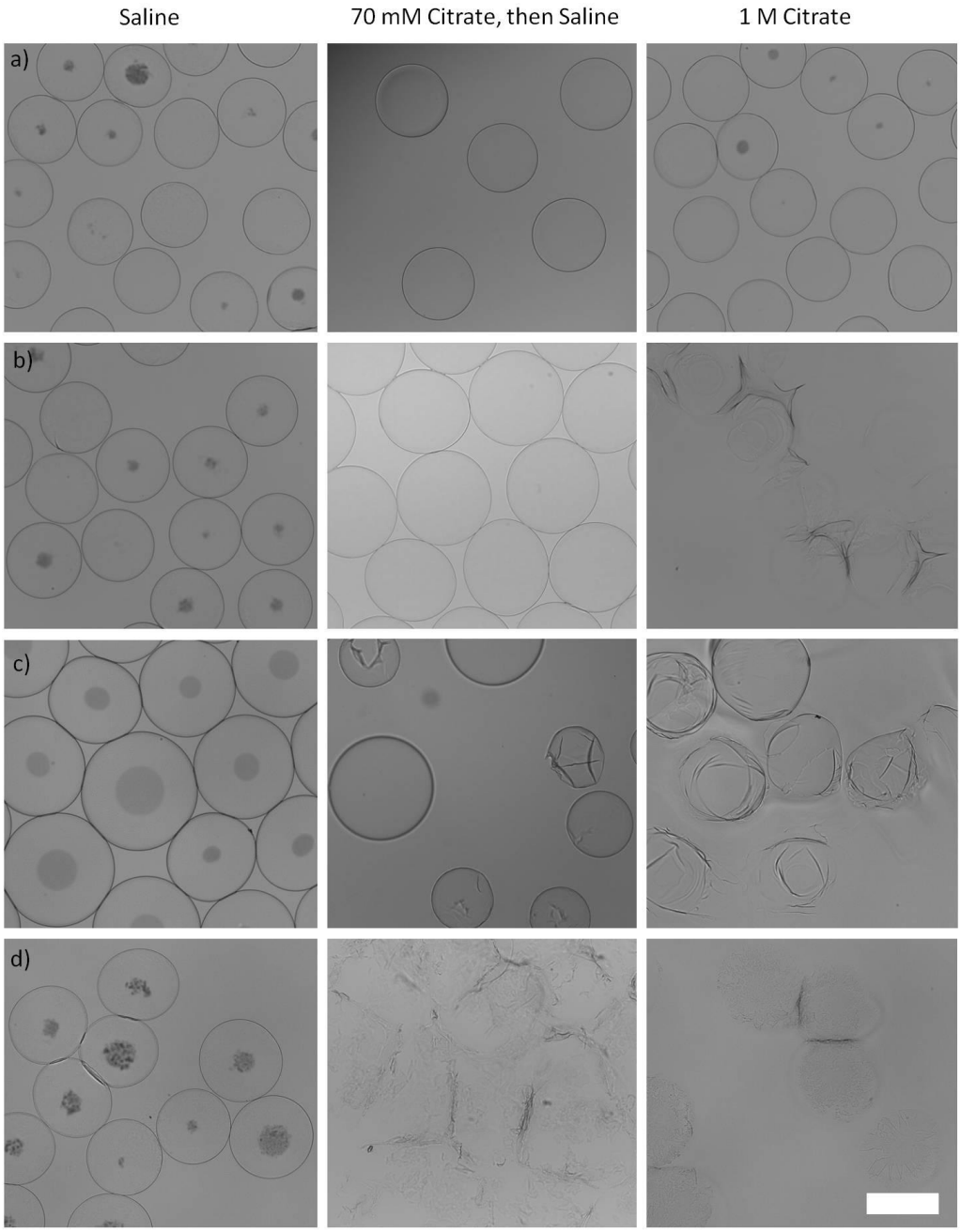

Figure 4.2: Transmission optical microscopy images for alginate-coated capsules in saline (left), in saline after 70 mM citrate treatment (middle) and in 1 M citrate (right) for a) APA (GS), b) ApAPM$_{75\text{-}15}$A (GS) c) ApAPM$_{50\text{-}40}$A (SS) and d) ApAPM$_{50\text{-}40}$A (GS). Image of citrate treated ApAPM$_{50\text{-}40}$A (GS) is taken in the presence of 70 mM citrate without transferring back into saline. Scale bar represents 500 µm. The dark circles in the centre of some capsules come from contact with the air-liquid interface.

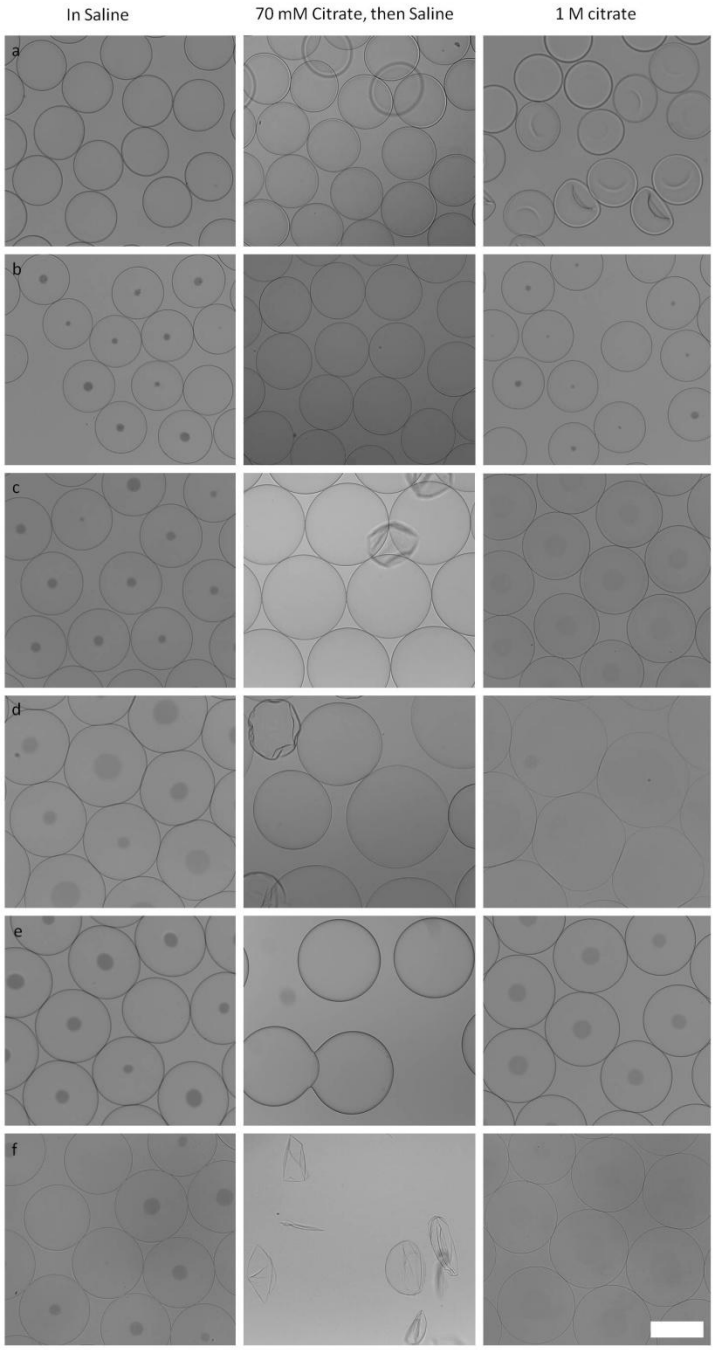

Figure 4.3: Transmission optical microscopy images for PMV60-coated capsules in saline (left), in saline after 70 mM citrate treatment (middle) and in 1 M citrate (right) for a) APPMV60 (SS), b) APPMV60 (GS), c) $ApAPM_{75\text{-}15}PMV60$ (GS), d) $ApAPM_{50\text{-}15}PMV60$ (SS) e) $ApAPM_{50\text{-}40}PMV60$ (SS) and f) $ApAPM_{50\text{-}40}PMV60$ (GS). Scale bar represents 500 µm. The dark circles in the centre of some capsules come from contact with the air-liquid interface.

For alginate-coated capsules, only those prepared with the higher charge density polycations PLL and $pAPM_{75\text{-}15}$ survive exposure to 70 mM citrate, while the others rupture or dissolve (Figure 4.2). The capsules prepared with $pAPM_{75\text{-}15}$ are significantly larger than those prepared with PLL indicating that the PLL/Alginate shell is stronger and better able to withstand the osmotic pressure created after liquefaction of the core. $ApAPM_{50\text{-}15}A$ (SS) (not shown) and $ApAPM_{50\text{-}40}A$ (SS) capsules (Fig. 4.2c) burst in the presence of 70 mM citrate however membrane fragments remained, while $ApAPM_{50\text{-}40}A$ (GS) capsules dissolved in 70 mM citrate showing that this more diffuse alginate/$pAPM_{50\text{-}40}$ membrane is less resistant to high ionic strength. Only APA (SS) and APA (GS) capsules remained intact in 1 M citrate, confirming that the high charge density PLL gave the strongest electrostatic PEC membranes with alginate, of course at the cost of forming a hydrophobic complex.

Fig. 4.3 shows cross-linked PMV-coated capsules after treatment with 70 mM citrate. Capsules made with PLL (APPMV60) were the smallest due to the strong electrostatic interactions of the Alginate/PLL PEC. Capsules made with the $pAPM_X$ copolymers were typically larger than the PLL-coated ones and susceptible to rupture, but unlike the alginate-coated capsules, the cross-linked PMV60-coated capsules showed increased survival on exposure to 70 mM citrate indicating that the PMV60 coating led to improved membrane integrity.

Capsules prepared using $pAPM_{50\text{-}15}$ (SS) showed a minor increase in capsule stability due to PMV60 cross-linking: after treating with 70 mM citrate, all of the $ApAPM_{50\text{-}15}A$ (SS) capsules ruptured while $ApAPM_{50\text{-}15}$PMV60 (SS) showed a mixed

population of ruptured and intact capsules, with the intact capsules having diameters ranging from about 600 μm to above 900 μm.

$ApAPM_{50\text{-}40}PMV60$ (SS) capsules appear to benefit the most from PMV60 coating. They all remain intact and undergo only moderate swelling after treatment with 70 mM citrate, in contrast to $ApAPM_{50\text{-}40}A$ (SS) capsules, in which the majority of capsules ruptured. The higher MW $pAPM_{50\text{-}40}$ may allow more effective covalent cross-linking with PMV60 leading to a more stable membrane compared to $pAPM_{50\text{-}15}$. When the $pAPM_{50\text{-}40}$ layer is made more diffuse by GS washing, the majority of the resulting $ApAPM_{50\text{-}40}PMV60$ (GS) capsules ruptured during handling after 70 mM citrate exposure (Fig. 4.3f), which is attributed to inefficient cross-linking of the more widely distributed $pAPM_{50\text{-}40}$.

Significantly, all of the PMV60-coated capsules survive higher ionic strength of 1 M citrate (Figure 4.3), showing that PMV60 improved the chemical resistance to disintegration of the capsule membrane due to covalent cross-linking. Of these 1 M treated $ApAPM_XPMV60$ capsules, the $ApAPM_{50\text{-}15}PMV60$ (SS) and $ApAPM_{50\text{-}40}PMV60$ (GS) capsules are intact because they were directly observed in 1 M citrate, and were not handled or ruptured by washing with saline. They thus also appear less swollen compared to their saline-washed counterparts.

4.4.3.3. Confocal Study of pAPM$_X$ / PMV60 Shells

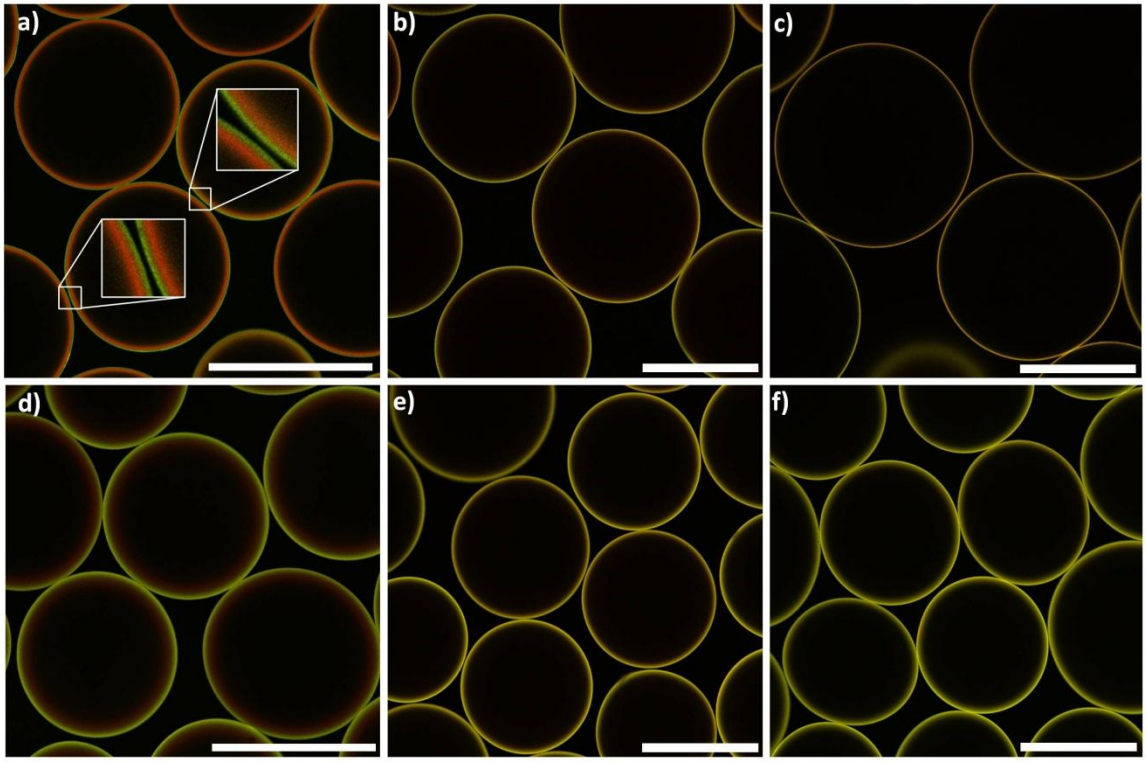

Figure 4.4: Equatorial confocal fluorescence microscopy images of capsules a) AP*r*PMV60*f* (SS), b) ApAPM$_{50\text{-}15}$*r*PMV60*f* (SS), c) ApAPM$_{50\text{-}40}$*r*PMV60*f* (SS), d) AP*r*PMV60*f* (GS), e) ApAPM$_{75\text{-}15}$*r*PMV60*f* (GS), f) ApAPM$_{50\text{-}40}$*r*PMV60*f* (GS). Scale bar is 500 μm.

Confocal fluorescence microscopy was used to assess the thickness and layering of the cross-linked capsule shells, using rhodamine-labelled polycations and fluorescein-labelled PMV60. Fig. 4.4 shows that in all cases, the polycations are concentrated near the surface of the calcium alginate bead, leading to final cross-linked membranes that were about 5-30 μm thick (Table 4.1, Fig. 4.4, 4A.7). The polycation membranes were thicker for lower MW polycations and for GS-washed capsules, where the polycations are more mobile and deposit further into the beads, as seen previously.[21,38,43,44] For example,

capsules formed with ApAPM$_{50\text{-}40}$PMV60 (SS) have a thinner membrane of 6 ± 1 μm compared to analogous capsules prepared with lower MW (ApAPM$_{50\text{-}15}$PMV60 (SS)) or capsules washed with gelling bath (ApAPM$_{50\text{-}40}$PMV60 (GS)), which have a membrane thickness of 11 ± 1 μm and 13 ± 1 μm respectively.

The choice of the final polyanion coating (Alginate or PMV60) did not affect the thickness of the underlying polycation layer. The PMV60*f* was preferentially located at the capsule surface compared to the polycation for PLL (Fig. 4.4a,d; corresponding line profiles in 4A.7), but appeared to have more complete overlap with the pAPM$_X$ polycations. Mixing (overlap) of the polyanion and polycation is often seen in layer-by-layer assemblies on hydrogels. However, the PLL in the APPMV60 (SS and GS) capsules forms a dense highly charged PLL-alginate PEC which seems to limit PMV60*f* in-diffusion. PMV*f* in-diffusion appears to be less limited in APPMV (GS) capsules than APPMV (SS) capsules, likely due to the lower PLL density in the GS washed membranes. Of course, PMV60 can not bind by itself to the anionic calcium alginate, but will only be retained where there is at least some polyamine to offer covalent immobilization. Still, the partial stratification of the two reactive polymers is significant in APPMV (SS) capsules, forming a PLL-PMV layer outer coating and a PLL-alginate inner membrane. Ultimately, this may lead to an inner, mobile PLL layer that may offer undesirable sites for biofouling. Figure 4A.8 shows the confocal images of only the PLL*r* in AP*r*A (SS) and AP*r*PMV60 (SS) capsules. These images show a lower density of PLL in the outer membrane where PMV60 has reacted with PLL. Analogous coating with alginate instead of PMV60, does not show this reduced concentration of PLL at the

surface of the membrane. Indeed, Strand et al.[45] have shown by CLSM that fluorescently labelled alginate coats directly over the PLL layer deposited on Ca Alg beads. In contrast to alginate, PMV60 becomes covalently attached to the PLL deposited on AP (SS) capsules. The resulting conversion of amine to amide, and of residual azlactone to carboxylate anion, is proposed to result in formation of a swollen, net negatively charged covalent network in the outer shell. This net negative charge would limit further indiffusion of anionic PMV60 through the Donnan principle, and thus lead to the observation of a non-homogeneous or stratified membrane, with a reduced PLL density in the outer layer.

4.4.4. Capsule Permeability

Control of permeability is an important function of the PEC membrane on alginate-based capsules, and one where the nature of the polycation, as well as shell cross-linking, can play a key role.[5,46-48]

The permeabilities of APA and ApAPM$_X$A capsules were assessed using in-diffusion of fluorescently labelled dextrans of different MW.[36] Most of the capsules showed permeability profiles that are similar to the standard APA (GS) capsules (Fig. 4.5), and to related AP capsules coated with poly(methyl vinyl ether-alt-maleic acid) described earlier.[49] One advantage of this method is that it allows for visual assessment of individual capsules, which provides an indication of sample heterogeneity.[36] ApAPM$_{50\text{-}15}$A (SS) and ApAPM$_{50\text{-}40}$A (SS) capsules showed significant variability in their permeabilities as noted by the large error bars in Fig 4.5.

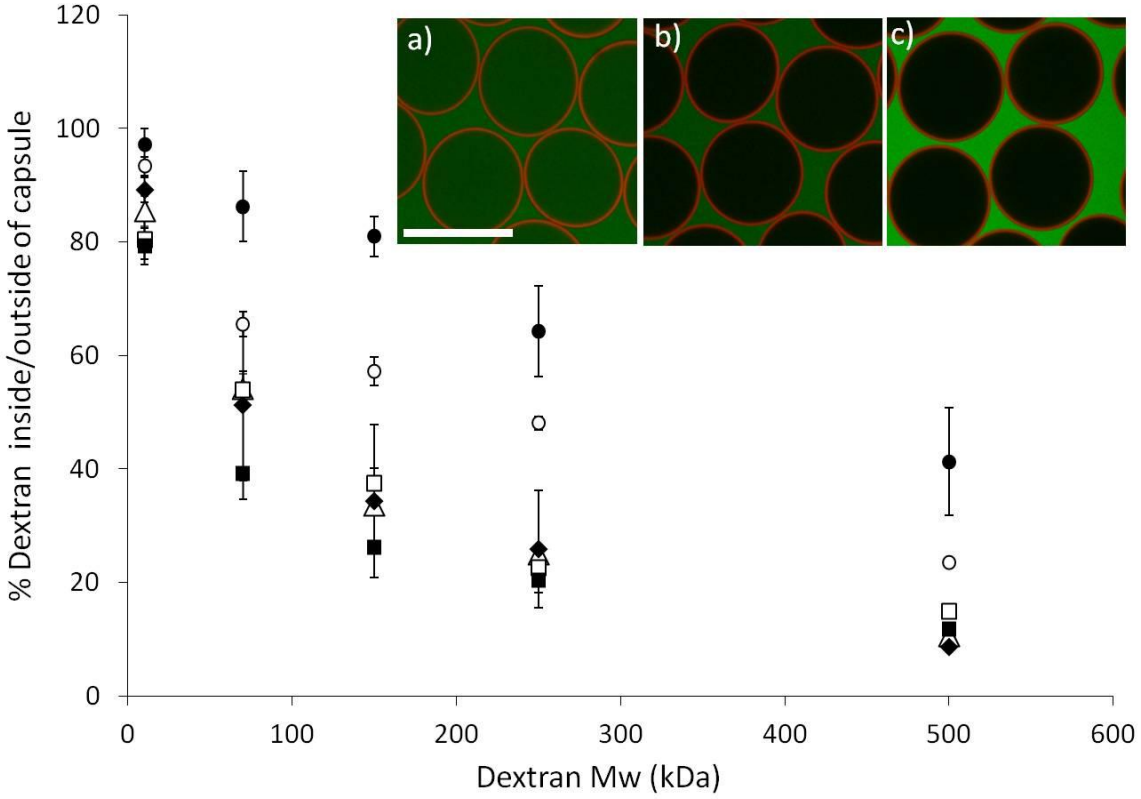

Figure 4.5: Percent ratio of dextran-*f* inside/outside Alginate-coated capsules: (■)APA (SS), (□)APA (GS), (Δ)ApAPM$_{75\text{-}15}$A (GS), (◆)ApAPM$_{50\text{-}15}$A (SS), (●)ApAPM$_{50\text{-}40}$A (SS) and (○)ApAPM$_{50\text{-}40}$A (GS). Inset shows equatorial confocal microscopy images of APA (SS) capsules in a) 10, b) 150 and c) 500 kDa FITC-dextran solution, for illustration. Rhodamine-labelled PLL is shown in red. Scale bar is 500 µm. Inset image was enhanced for visualization of the figure by increasing brightness and contrast by 10% and 20%, respectively. No enhancement was made to images used for analysis. Average and standard deviation is measured from three capsules.

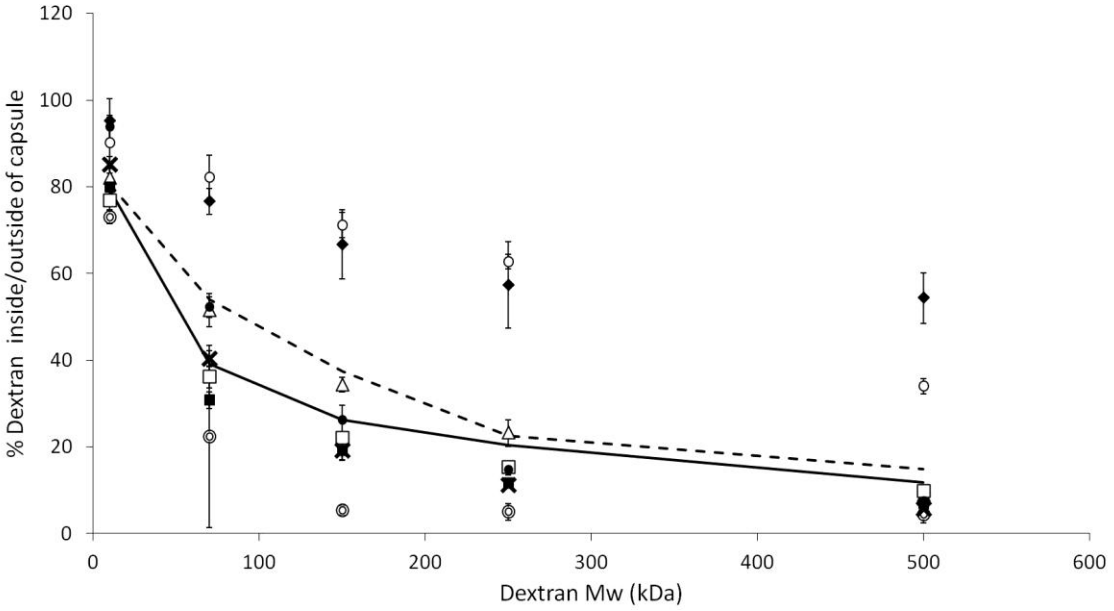

Figure 4.6: Percent ratio of dextran-*f* inside/outside of capsule for (■) APPMV60 (SS), (□) APPMV60 (GS), (Δ) ApAPM$_{75\text{-}15}$PMV60 (GS), (◆) ApAPM$_{50\text{-}15}$PMV60 (SS), (●) ApAPM$_{50\text{-}40}$PMV60 (SS), (○) ApAPM$_{50\text{-}40}$PMV60 (GS), (**x**) ApAPM$_{50\text{-}40}$PMV60 (SS) with longer incubation and (⓪) A[pAPM$_{50\text{-}40}$PMV60]$_2$ (SS). The solid and dashed lines show the permeability profiles of APA (SS) and APA (GS), respectively, from Figure 4.5. Average and standard deviation is measured from three capsules.

Fig. 4.6 shows that outer coatings with a single layer of PMV60 did not strongly affect the membrane permeability, compared to those of APA capsules. However, ApAPM$_{50\text{-}15}$PMV60 (SS) and ApAPM$_{50\text{-}40}$PMV60 (GS) capsules were significantly more permeable to dextran-*f* of all MW, in agreement with the low efficiency of their shell cross-linking described above.

Shell permeability for higher MW dextrans was significantly reduced for A[pAPM$_{50\text{-}40}$PMV60]$_2$ (SS) capsules. The large variation in permeability of this capsule

for the 70 kDa MW dextran is attributed to shell damage from aggregation during the multiple coating steps (Fig. 4.6).

4.4.5. Membrane Stiffness

4.4.5.1. Membrane stiffness of Alginate coated capsules

Micropipette aspiration is a useful method to study the mechanical properties of capsules, quantifying overall capsule stiffness (core plus shell contributions) or, for capsules with liquid cores, the stiffness of the membrane alone. This technique is sensitive to the rate of pressure change because of the permeability and the viscoelastic nature of the capsules, hence the rate of pressure change used in these experiments was constant, and chosen such that an adequate number of data points could be obtained within a reasonable amount of time for the range of capsule stiffnesses tested here.[38]

Figure 4.7 shows a typical plot used to measure the membrane stiffness by capillary aspiration. The length of the protrusion, x, into the capillary was measured for a range of applied pressure differential. The measured total length of x, minus x_o (the natural curvature of the capsule into the capillary at a pressure differential of zero), was then normalized by the radius of the pipette (R_p) to give a non-dimensional strain (x-x_o/R_p). This non-dimensional strain is plotted against the applied pressure differential and the linear slope of the fitted data is used to determine the membrane stiffness.

The alginate coated capsules were treated with citrate (70 mM) prior to analysis so that the effect of polycation ($pAPM_X$ vs. PLL) or polyanion (PMV60 vs. Alginate) coating material on the membrane stiffness could be obtained without contributions from the calcium alginate gel core. As seen previously, APA (GS) membranes are softer than

APA (SS) membranes because they are less dense (Fig. 4.8).[38] ApAPM$_{75\text{-}15}$A (GS) membranes were even softer (Fig. 4.8), which is consistent with the greater swelling of these capsules compared to APA (GS) upon citrate treatment.

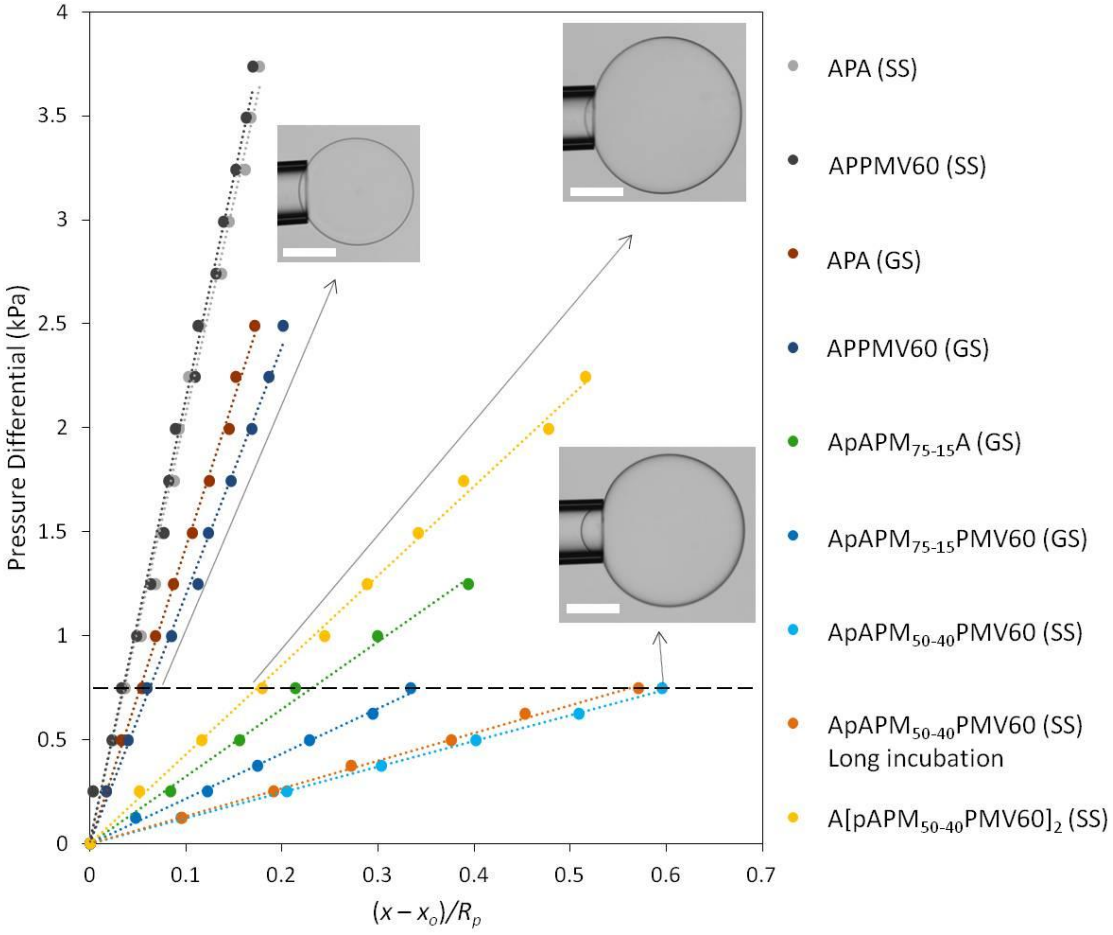

Figure 4.7: Plot of Pressure differential (ΔP) versus normalized deformation $(x - x_o)/R_p$ for each capsule type, showing representative single capsule measurements. The lines are linear fits to the data, where the slope equals membrane stiffness. The inset images show APPMV60 (GS) (left), ApAPM$_{50\text{-}40}$PMV60 (SS) (bottom right) and A[pAPM$_{50\text{-}40}$PMV60]$_2$ (SS) (top right) capsules when ΔP is 0.75 kPa. The scale bar represents 250 μm.

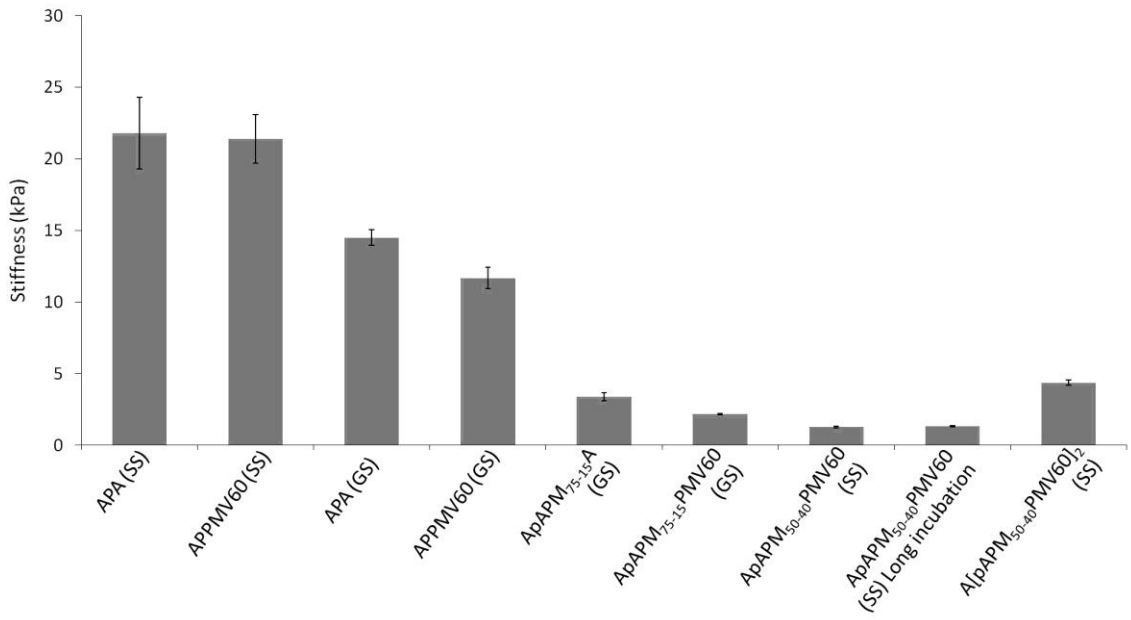

Figure 4.8: Membrane stiffness for citrate-treated PMV60- and Alginate-coated capsules, based on averaging three capsules each.

Alginate coated capsules made with the $pAPM_{50}$ copolymers (15 or 40 kDa) could not be tested by aspiration. Although microscopy showed that the $pAPM_{50}$ copolymers were deposited near the bead surface, they did not form stable membranes once the underlying calcium alginate gel was dissolved as observed by rupture or dissolution. The electrostatic interactions in the $pAPM_{50}$-Alginate PEC that forms the membrane are too weak to maintain the integrity of the membrane.

4.4.5.2.Membrane stiffness of PMV60 coated capsules

Photo-cross-linking of APA capsules has been shown to increase resistance to agitation with glass beads.[27] Cross-linking multi-layer films of PLL and hyaluronan by 1-ethyl-3-(3-(dimethylamino)-propyl)carbodiimide (EDC),[50] and multi-layer films of

alginate-chitosan multi-layers with Genipin,[51] have shown increases in moduli, as did glutaraldehyde cross-linking of poly(allylamine hydrolchloride) / poly(styrene sulfonate) membranes.[52]

Hence, covalently cross-linking the $pAPM_X$ shells with PMV60 was also expected to increase the mechanical properties of the outer capsule membrane. Accordingly, the membrane stiffness was assessed using capillary aspiration for capsules with PMV60 cross-linked membranes after alginate core liquefaction with citrate.

APPMV60 (SS) capsules have the same membrane stiffness of 21.4 ± 1.7 kPa compared to APA (SS) capsules (21.8 ± 2.5 kPa), which have the stiffest membranes tested here. The PMV60 distribution in the APPMV60 (SS) capsule is restricted to the outer surface (Fig. 4.4a, 4A.7) which sits atop an underlying electrostatic PLL-alginate complex, both of which are contributing to the shell stiffness. Surprisingly, APPMV60 (GS) capsules have a slightly lower membrane stiffness of 11.67 ± 0.74 kPa compared to non-cross-linked APA (GS) capsules (14.5 ± 0.55 kPa). A similar trend was observed for $ApAPM_{75\text{-}15}$PMV60 (GS) capsules (2.18 ± 0.04 kPa) compared to $ApAPM_{75\text{-}15}$A (GS) capsules (3.37 ± 0.29 kPa). The membrane stiffness may be affected by its thickness, density, and by the inherent nature of the PEC including hydrophobicity, chain flexibility, secondary structures, and strength of ionic interactions. As shown above, the strength of the PECs of all polycations with PMV0 are weaker than those with alginate and at most equal to complexes with alginate for PMV60.

$ApAPM_{50\text{-}40}$PMV60 (SS) capsules had a membrane stiffness of 1.26 ± 0.06 kPa, whereas $ApAPM_{50\text{-}15}$PMV60 (SS) could not be aspirated under the current rate of

aspiration to acquire sufficient data points before rupture. $ApAPM_{50-40}PMV60$ (GS) capsules were not aspirated because they were too fragile to withstand transfer into saline after citrate treatment. Cross-linking of $pAPM_{50}$–type coated capsules was hence useful only to the $ApAPM_{50-40}PMV60$ (SS) capsules, though they still are soft materials. The MW and (SS) washing procedure limits $pAPM_{50-40}$ to the surface of the microcapsule increasing polymeric concentration allowing for some covalent cross-linking with PMV60. However, the resulting thin membranes on the $pAPM_{50-40}$-PMV60 capsules (Table 4.1), combined with reduced ionic and covalent interactions cannot offer stiffness comparable to the thicker PLL membranes with their strong electrostatic interactions and their tendency to form some α-helices in anionic hydrogels.[53]

Increasing the coating time with $pAPM_{50-40}$ from 6 to 24 mins for $ApAPM_{50-40}PMV60$ had no effect on membrane thickness (Table 4.1), permeability (Fig. 4.6), or membrane stiffness (Fig. 4.7 and 4.8), indicating that additional $pAPM_{50-40}$ binding to the calcium alginate beads during this time is insignificant. Much longer incubation times or higher temperatures might increase the extent of binding and cause differences in capsule properties,[54] however, these conditions might not be suitable for encapsulation of living cells or proteins.

Formation of multi-layered membranes onto alginate capsules has previously been used to enhance permeability,[55,56] biocompatibility[57] and mechanical stability.[29,55-57] This approach was tested here to increase membrane stiffness of $ApAPM_{50-40}PMV60$ (SS). Although forming $A[pAPM_{50-40}PMV60]_2$ (SS) capsules was more difficult due to capsule

aggregation, the membrane stiffness increased from 1.26 ± 0.06 kPa to 4.36 ± 0.18 kPa (Figure 4.7 and 4.8).

As long as the capsules are stable, reduced membrane stiffness may prevent cell adhesion to the surface and potentially unwanted fibrotic overgrowth,[51,58,59] however, the ability to survive *in vivo* needs to tested in an animal model.

The above results show that the nature of the polycation coating can be affected by factors such as charge density, MW and the characteristics of the coating/washing solutions. To benefit from covalent cross-linking using PMV60 there needs to be adequate amine density at the capsule surface while avoiding capsule aggregation. For reduced charge density polycations such as $pAPM_{50}$, this can be accomplished by using saline washes and higher polycation MWs. As mentioned earlier, for higher charge-density polycations like $pAPM_{75\text{-}40}$, GS washing can prevent capsule aggregation.

It is also important to recognize how capsule properties can change with coating protocols, causing variability, a known concern with APA capsules,[60,61] and potentially more concerning for more mobile, reduced charge copolymers such as $pAPM_X$. For example, $ApAPM_{75\text{-}15}$ (SS) and $ApAPM_{50\text{-}15}$ (SS) capsules did not give intact covalently cross-linked membranes when stored for 10 days prior to PMV60 coating. This is likely attributed to continued diffusion of these more mobile polycations further into the capsule, leading to reduced polycation (and amine) concentration at the capsule surface.

The formation of $ApAPM_{50\text{-}40}$PMV60 (SS) capsules appears to straddle an interesting borderline between electrostatic and covalent interactions. In some of the replicate experiments, the $ApAPM_{50\text{-}40}$PMV60 (SS) capsules showed increased swelling

and lower capsule integrity, which could be prevented by doubling the concentration of $pAPM_{50-40}$ in the coating solution. The capsules formed with higher concentration of $pAPM_{50-40}$ had a reduced permeability but only a small increase in membrane stiffness.

Polycation membrane formation and properties are also sensitive to the alginate bead (eg. homogeneity, composition, gelling ion, size).[4,62,63] Future work will explore the use of barium as part of the gelling bath to form more stable core alginate beads.

4.5. Conclusion

Coating of calcium alginate with reduced charge density polycations followed by reactive polyanions results in formation of capsule shells with covalently cross-linked, hydrated shells. These shells have reduced strength compared to classical APA-type capsules, but their higher degree of solvation, together with their lower local cationic charge densities, makes this a promising route to host-compatible capsule shells. The covalent immobilization of PMV60, together with its ability to consume free amine groups and generate negative charges through hydrolysis of unused azlactone groups, may offer an additional route to lower cationic charge density. Future work to increase capsule stiffness will involve use of barium to form more stable primary gel cores, other synthetic polycations with reduced backbone flexibility, and multi-layer capsules.

4.6. Acknowledgments

We would like to thank NSERCs Discovery Grant and CREATE programs for funding, and Shivanthi Sriskandha for providing some of the PMV60 batches.

4.7. References

[1] Wheatly, M. A.; Chang, M.; Park, E.; Langer, R. *J. Appl. Polym. Sci.* **1991,** *43*, 2123 – 2135.
[2] Lim, F.; Sun, A. M. *Science* **1980,** *210*, 908–910.
[3] Draghi, L.; Brunelli, D.; Farè, S.; Tanzi, M. C. *J. Biomater. Sci. Polym. Ed.* **2015,** *15*, 1002–1012.
[4] Thu, B.; Bruheim, P.; Espevik, T.; Smidsrød, O.; Soon-Shiong, P.; Skjåk-Bræk, G. *Biomaterials* **1996,** *17*, 1031–1040.
[5] Goosen, M. F. A.; O'Shea, G. M.; Gharapetian, H. M. ; Chou, S.; Sun, A. M. *Biotechnol. Bioeng.* **1985,** *27*, 146–150.
[6] Saitoh, S.; Araki, Y.; Kon, R.; Katsura, H.; Taira, M. *Dent. Mater. J.* **2000,** *19*, 396–404.
[7] Mørch, Y. A.; Donati, I.; Strand, B. L.; Skjåk-Bræk, G. *Biomacromolecules* **2006,** *7*, 1471–1480.
[8] Wang, X.; Spencer, H. G. *Polymer* **1998,** *39*, 2759–2764.
[9] Prakash, S.; Chang, T. M. S.; *Art. Cells, Blood Sub., and Immob. Biotech.* **1998,** *26*, 35–51.
[10] Gomez-Vargas, A.; Rosenthal, K. L.; McDermott, M. R.; Hortelano, G. *Vaccine* **2004,** *22*, 3902–3910.
[11] Posillico, E. G. *Bio/technology* **1986,** *4*, 114–117.
[12] Strand, B. L.; Ryan, L.; In't Veld, P.; Kulseng, B.; Rokstad, A. M.; Skjåk-Bræk, G.; Espevik, T. *Cell Transplant.* **2001,** *10*, 263–275.
[13] Tam, S. K.; Bilodeau, S.; Dusseault, J.; Langlois, G.; Hallé, J. P.; Yahia, L. H. *Acta Biomater.* **2011,** *7*, 1683–1692.
[14] De Vos, P.; De Haan, B.; Van Schilfgaarde, R. *Biomaterials* **1997,** *18*, 273–278.
[15] Sawhney, A. S.; Hubbell, J. A. *Biomaterials* **1992,** *13*, 863–870.
[16] Wilson, J. T.; Krishnamurthy, V. R.; Cui, W.; Qu, Z.; Chaikof, E. L. *J. Am. Chem. Soc.* **2009,** *131*, 18228–18229.
[17] Wilson JT, Cui W, Kozlovskaya V, ; Kharlampieva, E.; Pan, D.; Qu, Z.; Krishnamurthy, V. R.; Mets, J.; Kumar, V.; Wen, J.; Song, Y.; Tsukruk, V. V.; Chaikof, E. L. *J. Am. Chem. Soc.* **2011,** *133*, 7054–7064.
[18] Spasojevic, M.; Paredes-Juarez, G. A.; Vorenkamp, J.; de Haan, B. J.; Jan Schouten, A.; de Vos, P. Reduction of the inflammatory responses against alginate-poly-L-lysine microcapsules by anti-biofouling surfaces of PEG-b-PLL diblock copolymers. *PLoS ONE* [Online] **2014,** *9*, e109837. http://journals.plos.org/plosone/article?id=10.1371/journal.pone.0109837 (accessed Apr 1, 2015)
[19] Zheng, J. N.; Xie, N. G.; Yu, W. T.; Liu, X. D.; Xie, W. Y.; Zhu, J.; Ma, X. J. *Langmuir* **2010,** *26*, 17156–17164.
[20] Zheng, J. N.; Xie, H.; Yu, W.; Tan, M.; Gong, F.; Liu, X.; Wang, F.; Lv, G.; Liu, W.; Zhen, G.; Yan, Y.; Xie, W.; Ma, X. *Langmuir* **2012,** *28*, 13261–13273.
[21] Kleinberger, R. M.; Burke, N. A. D.; Zhou C.; Stöver, H. D. H. *J. Biomater. Sci. Polym. Ed.* **2016,** *27*,351–369,

[22] Dubey, A.; Burke, N. A. D.; Stöver, H. D. H. *J. Polym. Sci., Part A: Polym. Chem.* **2015,** *53*, 353–365.
[23] Ros, S.; Burke, N. A. D.; Stöver, H. D. H. *Macromolecules* **2015,** *48,* 8958−8970.
[24] Chandy, T.; Mooradian, D. L.; Rao, G. H. R. *Artif. Organs* **1999,** *23,* 894–903.
[25] Chen, H.; Ouyang ,W.; Lawuyi, B.; Prakash, S. *Biomacromolecules* **2006,** *7,* 2091–2098.
[26] Chen, H.; Ouyang, W.; Jones, M.; Metz, T.; Martoni, C.; Haque, T.; Cohen, R.; Lawuyi, B.; Prakash,, S. *Cell Biochemistry and Biophysics* **2007,** *47,* 159–167.
[27] Dusseault, J.; Leblond, F. A.; Robitaille, R.; Jourdan, G.; Tessier, J.; Ménard, M.; Henley, N.; Hallé, J. P. *Biomaterials* **2005,** *26,* 1515–1522.
[28] Hillberg, A. L.; Oudshoorn, M.; Lam, J. B. B.; Kathirgamanathan, K. *J. Biomed. Mater. Res., Part B* **2015,** *103B*, 503–518.
[29] Gardner, C. M.; Burke, N. A. D.; Stöver, H. D. H. *Langmuir* **2010,** *26,* 4916–4924.
[30] Gardner, C. M.; Stöver, H. D. H. *Macromolecules* **2011,** *44,* 7115–7123.
[31] Mazumder, M. A. J.; Shen, F.; Burke, N. A. D.; Potter, M. A.; Stöver, H. D. H. *Biomacromolecules* **2008,** *9,* 2292–2300.
[32] Mohajeri, S.; Burke, N. A. D.; Stöver, H. D. H. *Polym. Degrad. Stab.* **2015,** *114*, 94–104.
[33] Gardner, C.M.; Potter, M. A.; Stöver, H. D. H. *J. Mater. Sci.: Mater. Med.* **2012,** *23*, 181–193.
[34]Buck, M. E.; Schwartz, S. C.; Lynn, D. M. *Chem. Mater.* **2010,** *22,* 6319–6327.
Note: The purity of VDMA decreases during storage due to slow formation of oliogmers as described in the above reference. Thus, the purity and ratio of VDMA added was determined by NMR of the initial comonomer reaction mixture by comparing the mol ratio of VDMA to MAA.
[35] Haugland, R. P. *Handbook of Fluorescent Probes and Research Products,* 6th ed.; Molecular Probes: Eugene, OR, 1996; p 74.
[36] Vandenbossche, G. M. R.; Van Oostveldt, P.; Remon, J. P. *J. Pharm. Pharmacol.* **1991,** *43*, 275–277.
[37] Barrales-Rienda, J. M.; Bello, A.; Bello, P.; Guzmán, G. M. In *Polymer Handbook,* 4th ed.; Brandrup, J.; Immergut, E. H.; Grulke, E. A. Wiley: New York, New York, 1999; p VII/435.
[38] Kleinberger, R. M.; Burke, N. A. D.; Dalnoki-Veress, K.; Stöver, H. D. H. *Mater. Sci. Eng., C* **2013,** *33*, 4295–4304.
[39] Rokstad, A. M.; Holtan, S.; Strand, B. L.; Steinkjer, B.; Ryan, L.; Kulseng, B.; Skjåk-Bræk, G.; Espevik, T. *Cell Transplant.* **2002,** *11,* 313–324.
[40] Van Raamsdonk, J. M.; Cornelius, R. M.; Brash, J. L.; Chang, P. L. *J. Biomater. Sci. Polym. Ed.* **2002,** *12*, 863–884.
[41] Philipp, B.; Dautzenberg, H.; Linow, K. J.; Kotz, J.; Dawydoff, W. *Prog. Polym. Sci.* **1989,***14,* 91–172.
[42] Tsuchida, E.; Abe, K. *Adv. Polym. Sci.* **1982,** *45,* 1–119.
[43] Ma, X.; Vacek, I.; Sun, A. *Artif. Cells, Blood Sub. Biotechnol.* **1994,** *22*, 43–69.
[44] Gåserod, O.; Smidsrød, O.; Skjåk-Bræk, G. *Biomaterials* **1998,** *19,* 1815–1825.

[45] Strand, B. L.; Mørch, Y. A.; Espevik, T.; Skjåk-Bræk, G. *Biotechnol*. *Bioeng*. **2003,** *82,* 386–394.
[46] Polk, A.; Amsden, B.; De Yao, K.; Peng, T.; Goosen, M. F. A. *J*. *Pharm*. *Sci*. **1994,** *83,* 178–185.
[47] Gåserod, O.; Sannes, A.; Skjåk-Bræk, G. *Biomaterials* **1999,** *20,* 773–783.
[48] King, G. A.; Daugulis, A. J.; Faulkner, P.; Goosen, M. F. A. *Biotechnol*. *Prog*. **1987,** *3,* 231–240.
[49] Gardner, C. M.; Burke, N. A. D.; Chu, T.; Shen, F.; Potter, M. A.; Stöver, H. D. H. *J*. *Biomater*. *Sci*. **2011,** *22*, 2127–2145.
[50] Schneider, A.; Francius, G.; Obeid, R.; Schwinté, P.; Hemmerlé, J.; Frisch, B.; Schaaf, P.; Voegel, J.; Senger, B.; Picart, C. *Langmuir* **2006,** *22,* 1193–1200.
[51] Silva, J. M.; Duarte, A. R. C.; Caridade, S. G.; Picart, C.; Reis, R. L.; Mano, J. F. *Biomacromolecules* **2014,** *15,* 3817–3826.
[52] Tong, W.; Gao, C.; Möhwald, H. *Chem*. *Mater*. **2005,** *17,* 4610–4616.
[53] Bysell, H.; Malmsten, M. *Langmuir* **2009,** *25,* 522–528.
[54] Vandenbossche, G. M. R.; Van Oostveldt, P.; Demeester, J.; Remon, J. P. Biotechnol. Bioeng. **1993,** *42,* 381–386.
[55] Schneider, S.; Feilen, P. J.; Slotty, V.; Kampfer, D.; Preuss, S.; Berger, S.; Beyer, J. Pommersheim, R. *Biomaterials* **2001,** *22,* 1961–1970.
[56] Gugerli, R.; Cantana, E.; Heinzen, C.; Von Stockar, U.; Marison, I.W. *J*. *Microencapsul*. **2002,** *19,* 571–590.
[57] Shen, F.; Mazumder, M. A. J.; Burke, N. A. D.; Stöver, H. D. H.; Potter, M. A. *J*. *Biomed*. *Mater*. *Res*. *Part B: Appl*. *Biomater*. **2009,** *90B,* 350–361.
[58] Discher, D. E.; Janmey, P.; Wang, Y. *Science* **2005,** *310,* 1139–1143.
[59] Blakney, A. K.; Swartzlander, M. D.; Bryant, S. J. *J*. *Biomed*. *Mater*. *Res*. *A*. **2012,** *100,* 1375–1386.
[60] De Vos, P.; Bučko, M.; Gemeiner, P.; Navrátil, M.; Švitel, J.; Faas, M.; Strand, B. L.; Skjåk-Bræk, G.; Mørch, Y.A.; Vikartovská, A.; Lacík, I.; Kolláriková, G.; Orive, G.; Poncelet, D.; Pedraz, J. L.; Ansorge-Schumacher, M.B. *Biomaterials* **2009,** *30,* 2559–2570.
[61] Orive, G.; Hernández, M. A.; Gascón, A. R.; Calafiore, R.; Chang, T. M. S.; De Vos, P.; Hortelano, G.; Hunkeler, D.; Lacík, I.; Shapiro, A. M. J.; Pedraz, J. L. Nat. Med. **2003,** *9,* 104–107.
[62] Thu, B.; Bruheim, P.; Espevik,T.; Smidsrød, O.; Soon-Shiong, P.; Skjåk-Bræk, G. *Biomaterials* **1996,** *17,* 1069–1079.
[63] Strand, B. L.; Gåserod, O.; Kulseng, B.; Espevik, T.; Skjåk-Bræk, G. *J*. *Microencapsul*. **2002,** *19,* 615–630.

4.8. Appendix

4.8.1. Fractionation of FITC Dextran (150 kDa)

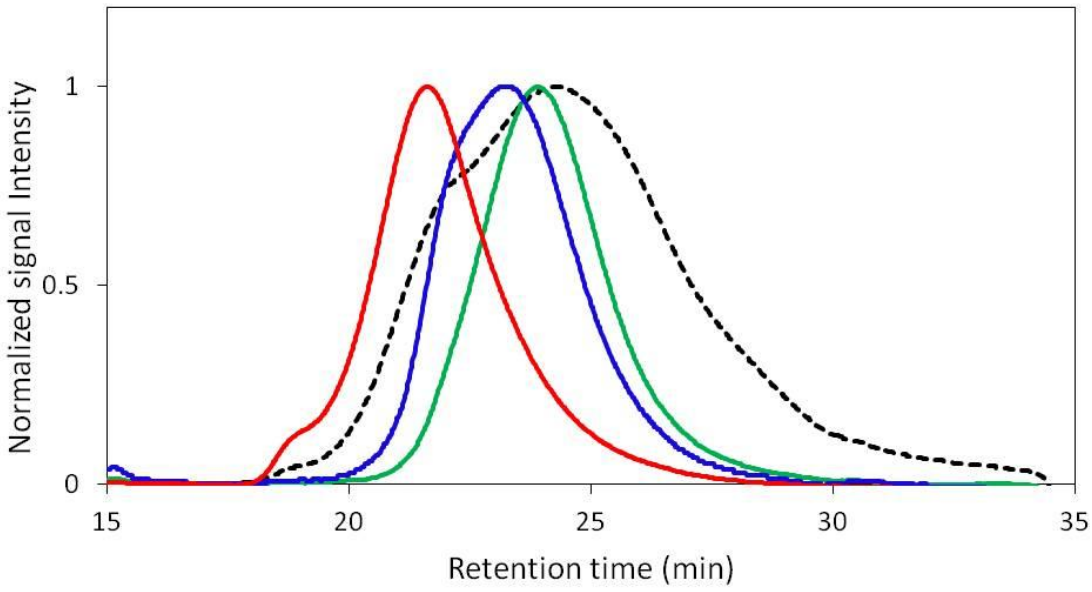

Figure 4A.1: GPC chromatograms of FITC dextran: (dotted black line) 150 kDa as supplied, (blue) 150 kDa after fractionation in ethanol, (green) 70 kDa and (red) 500 kDa.

4.8.2. Preparation of PMV60

PMV60 was prepared by photopolymerization of MAA and VDMA and the reaction was stopped at about 40% conversion to limit compositional drift due to the higher reactivity of VDMA.[1] The PMV60 was found to contain 58 mol% VDMA by ^{1}H NMR spectroscopy (Figure 4A.2). GPC analysis revealed that the PMV60 had a MW (M_n) of about 18.4 kDa with a PDI of 1.3. The relatively narrow PDI for this conventional free radical polymerization was likely due to fractionation during precipitation leading to a loss of lower MW chains and a narrowing of the polydispersity. The azlactone groups of

PMV60 slowly hydrolyze during storage so the polymer was used within six weeks at which point the fraction of hydrolyzed azlactone groups had increased from 3 to 10%.

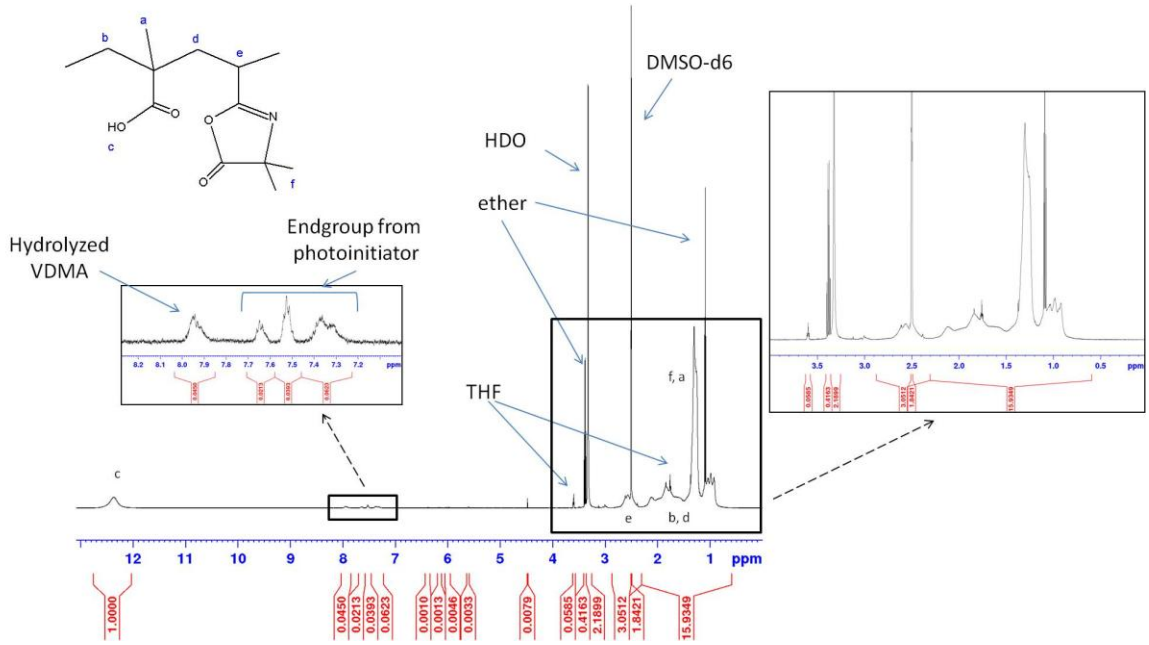

Figure 4A.2: ^{1}H NMR (600 MHz) of PMV60 in DMSO-d6. The sample contains THF (0.4 wt%) and ether (2.8 wt%) used during precipitation of the polymer. The peaks at 7.2–7.7 ppm come from the photoinitiator end-group.

Composition of PMV was determined using the COOH peak at 12.4 ppm to figure out the amount of COOH of MAA by subtracting out the hydrolyzed VDMA at 7.9 ppm. Therefore, the MAA signal (1-0.045 = 0.955) was multiplied by 5 for the number of polymeric backbone peaks contributed by MAA (0.955 x 5 = 4.775). The total contribution of MAA to the polymeric region was subtracted with contributions from ether and THF (15.9349 - [4.775 MAA + 0.0585 THF + 0.6245 ether] = 10.477). The remaining value is due to the contribution from VDMA containing 8 protons in this region (10.477/8 = 1.310). Therefore, the composition of VDMA is 58%

(1.310/[0.955+1.310] x 100 = 58%). Using the calculated ratio of VDMA to the hydrolyzed VDMA signal, the percent of hydrolyzed VDMA was determined to be 3% (0.045/1.310 x 100 = 3%).

4.8.3. PMV60 coated capsules

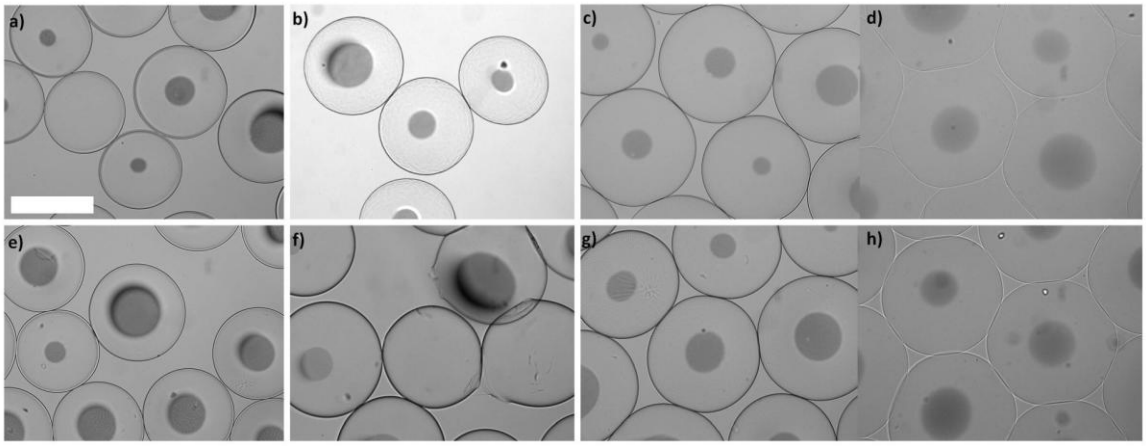

Figure 4A.3: PMV-coated (SS) capsules prepared with two saline washes after polycation coating: a) PLL 15 kDa, b) $pAPM_{75\text{-}15}$, c) $pAPM_{50\text{-}15}$, d) $pAPM_{25\text{-}15}$, e) PLL 40 kDa, f) $pAPM_{75\text{-}40}$, g) $pAPM_{50\text{-}40}$, h) $pAPM_{25\text{-}40}$. Scale bar is 500 µm. The dark circles in the centre of some capsules comes from capsules that touch or breach the air-liquid interface.

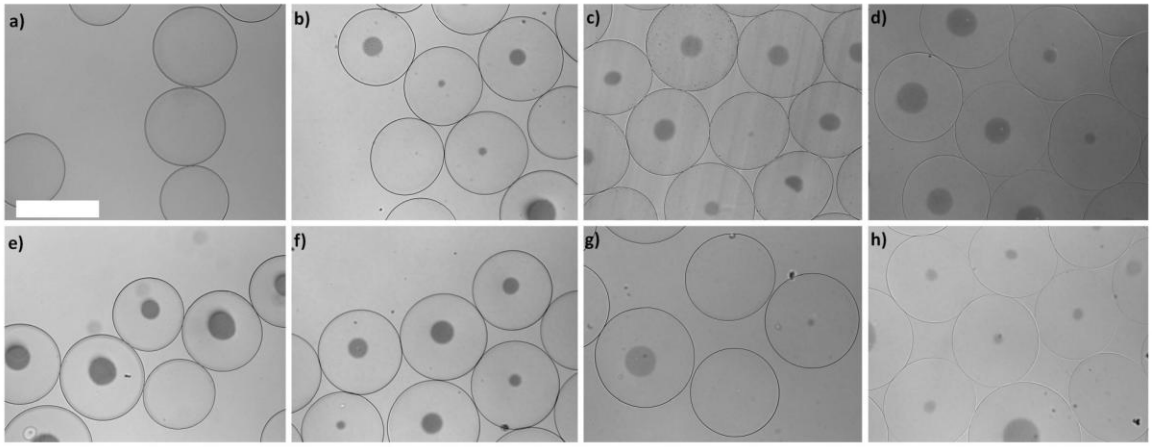

Figure 4A.4: PMV-coated (GS) capsules prepared with one gelling bath and one saline wash after polycation coating: a) PLL 15 kDa, b) $pAPM_{75\text{-}15}$, c) $pAPM_{50\text{-}15}$, d) $pAPM_{25\text{-}15}$, e) PLL 40 kDa, f) $pAPM_{75\text{-}40}$, g) $pAPM_{50\text{-}40}$, h) $pAPM_{25\text{-}40}$. Scale bar is 500 µm. The dark circles in the centre of some capsules comes from capsules that touch or breach the air-liquid interface.

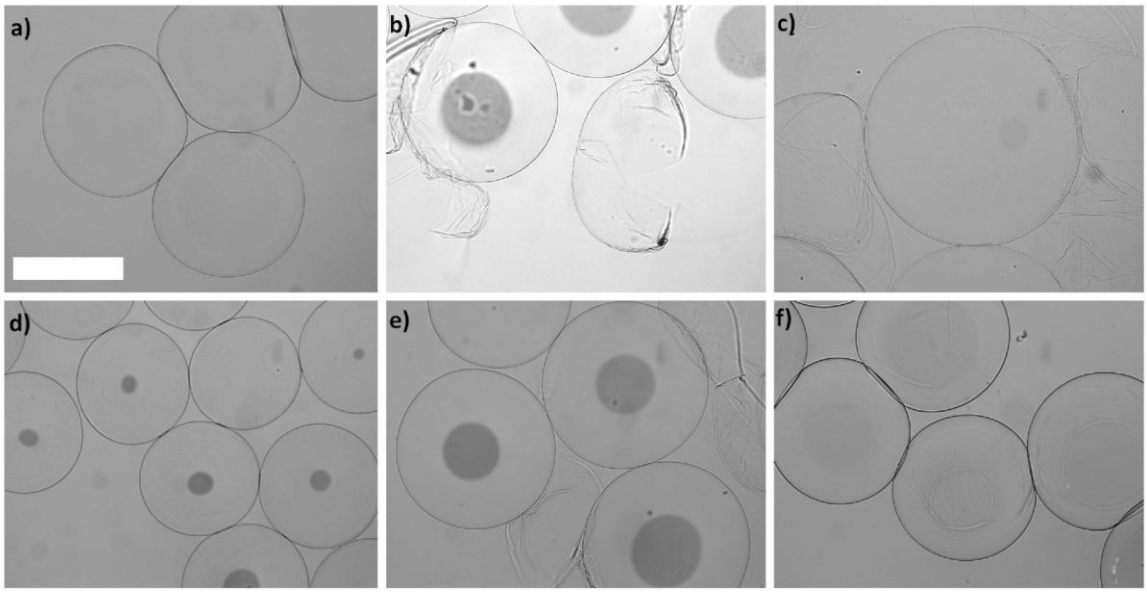

Figure 4A.5: PMV-coated (SS) capsules after treatment with 1 M citrate and 0.1 M NaOH: a) PLL 15 kDa, b) $pAPM_{75\text{-}15}$, c) $pAPM_{50\text{-}15}$, d) PLL 40 kDa, e) $pAPM_{75\text{-}40}$, f) $pAPM_{50\text{-}40}$. Scale bar is 500 µm. The dark circles in the centre of some capsules comes from capsules that touch or breach the air-liquid interface.

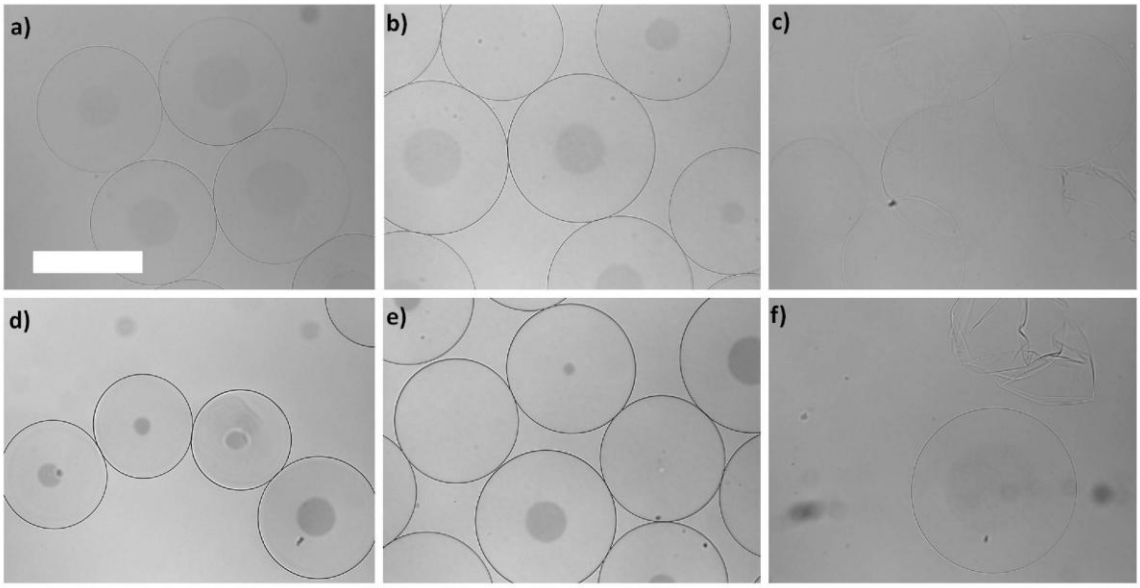

Figure 4A.6: PMV-coated (GS) capsules after treatment with 1 M citrate and 0.1 M NaOH: a) PLL 15 kDa, b) $pAPM_{75\text{-}15}$, c) $pAPM_{50\text{-}15}$, d) PLL 40 kDa, e) $pAPM_{75\text{-}40}$, f) $pAPM_{50\text{-}40}$. Scale bar is 500 µm. The dark circles in the centre of some capsules comes from capsules that touch or breach the air-liquid interface.

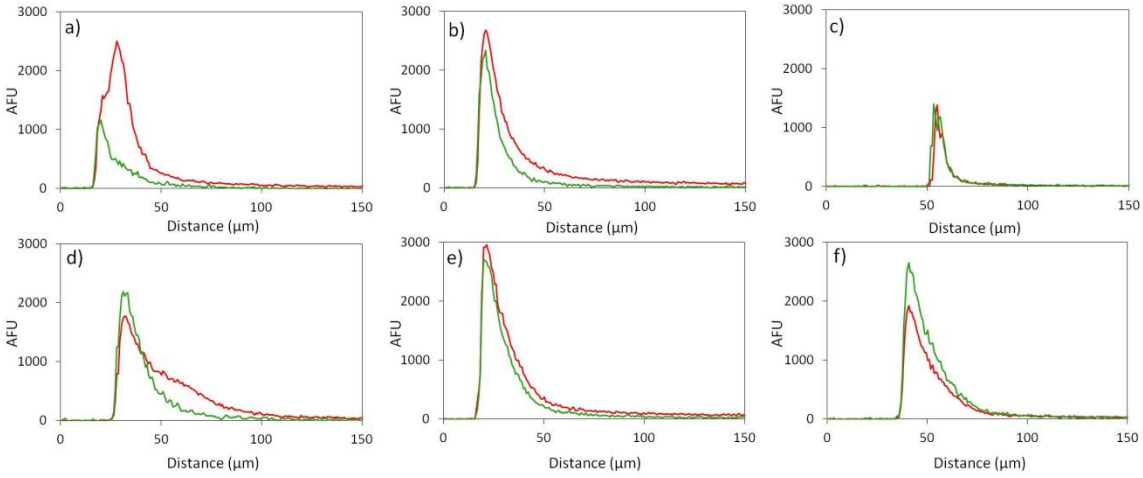

Figure 4A.7: Confocal line profiles taken from confocal images 4.4a-f, a) AP*r*PMV60*f* (SS), b) $ApAPM_{50\text{-}15}$*r*PMV60*f* (SS), c) $ApAPM_{50\text{-}40}$*r*PMV60*f* (SS), d) AP*r*PMV60*f* (GS), e) $ApAPM_{75\text{-}15}$*r*PMV60*f* (GS) and f) $ApAPM_{50\text{-}40}$*r*PMV60*f* (GS) showing the spatial relationship between PMV60*f* (green) and polycation (red) PLL*r*, or $pAPM_X$*r* copolymer, membranes on calcium alginate beads. AFU intensities are comparable within each fluorophore by normalization to the same detector gains.

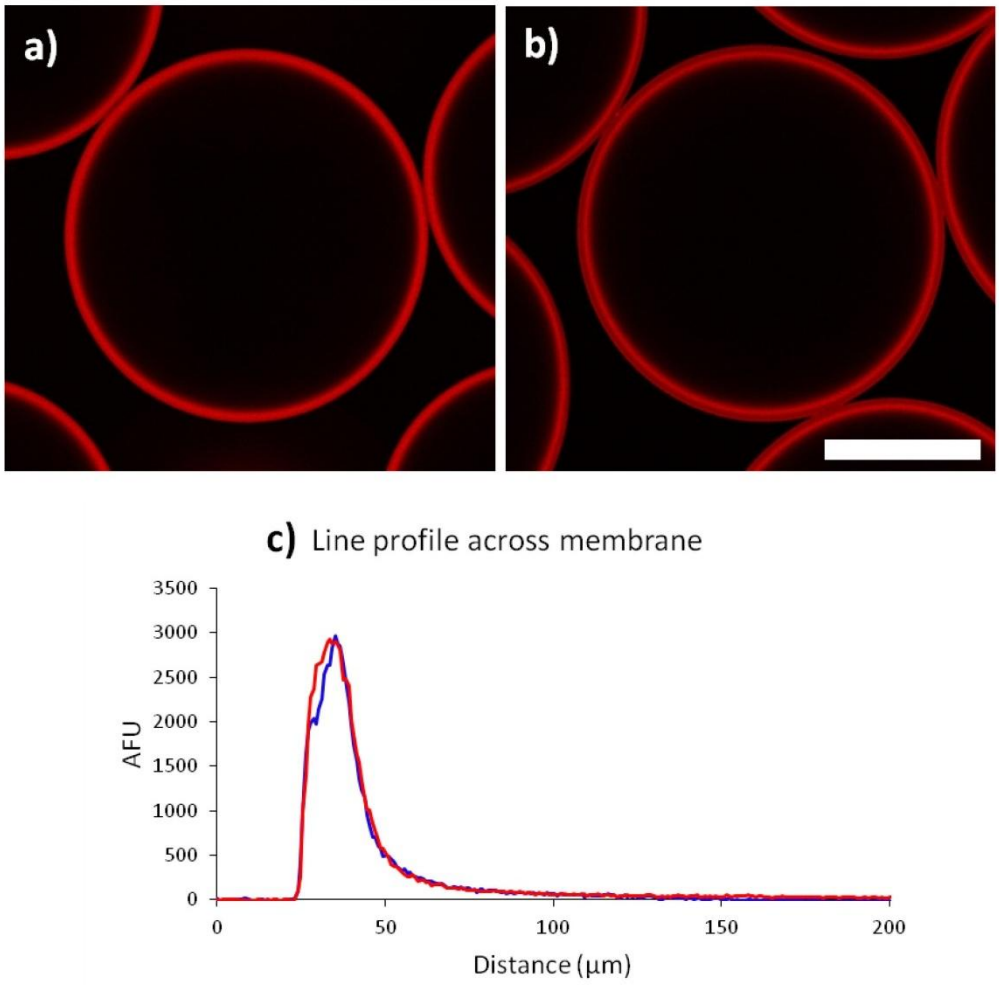

Figure 4A.8: Confocal images of a) AP*r*A (SS), b) AP*r*PMV60 (SS) and c) confocal line profiles showing distribution of PLL*r* membrane for AP*r*A (SS) (red) and AP*r*PMV60 (SS) (blue). Scale bar represents 200 µm.

[1]Gardner, C. M.; Stöver, H. D. H. *Macromolecules* **2011,** *44,* 7115–7123.

CHAPTER 5

Synthesis and study of block copolymer nanoparticles for potential use in controlled drug release

Rachelle M. Kleinberger, Nicholas A. D. Burke, Todd R. Hoare, Harald D. H. Stöver.

This chapter is prepared for submission to Macromolecules

This chapter reports the synthesis and characterization of thermoresponsive block copolymers of poly((NIPAM-*co*-AA)-*b*-HEA). Increasing the temperature above the LCST causes self assembly of the block polymer chains. The decreasing length of the HEA block causes a change from spherical to rod-like micelles. This has been captured by TEM after covalent cross-linking of the micelle core.

Contributions: RMK, with help from NADB, developed the fundamental design. RMK carried out all the experimental work, and wrote the manuscript. TRH helped in designing the block copolymer dimensions and the cross-linking chemistry, and is currently guiding their study for use as controlled release materials. NADB and HDHS helped with interpretation and editing of the manuscript for publication.

5.1. Abstract

Block copolymers of poly((N-isopropylacrylamide-*co*-*tert*-butylacrylate)-*b*-2-hydroxyethylacrylamide), p((NIPAM-*co*-*t*BA)-*b*-HEA), were prepared by RAFT copolymerization. A series of HEA blocks ranging from 2.5 to 20 kDa was grown from 20 kDa p(NIPAM-*co*-*t*BA) macro chain transfer agents. After hydrolysis of the *t*-butylacrylate groups to acrylic acid, the resulting block copolymers were thermally assembled into micelles at 50 °C in aqueous MES buffer, above the LCST of the p(NIPAM-*co*-AA) block, and core-cross-linked *in situ* using adipic acid dihydrazide/EDC. The morphology of the resulting core-cross-linked micelles was studied by TEM, and showed the expected transition from spherical to rod shaped micelles with decreasing HEA block length.

5.2. Introduction

Drug delivery using small nanoparticles has gained interest due to the EPR effect for passive targeted drug delivery to tumours. Particles with 20-200 nm diameter, and stealth properties to permit circulation times greater than six hours, can thus be accumulated at tumour sites.[1] Particles formed with stealthy polymers such as polyethylene glycol (PEG) on the surface are well known to have increased blood circulation half-lifes, and have been investigated in form of polymer drug composites, nanoparticles and micelles as drug delivery vehicles.[2,3,4]

Others have used poly(2-hydroxypropylmethacrylamide) (pHPM) to increase blood circulation time of nanoparticles.[5] Compared to PEG, stealth polymers based on

neutral hydrophilic monomers such as HPM, hydroxyethyl acrylamide (HEA), 2-methyl-2-oxazoline, vinylpyrrolidone often show greater oxidative resistance and better synthetic control over polymer compositions.[6]

Another polymer of interest is poly(*N*-isopropylacrylamide) p(NIPAM), which undergoes a liquid-solid phase transition at its lower critical solution temperature (LCST, 32 °C), due to desolvation of the isopropyl side chains.[7] Micelles formed from double hydrophilic NIPAM/PEG block copolymers have thus become a popular topic for drug delivery systems as they self-assemble into nanoparticles above the LCST.[8,9,10,11,12,13,14,15,16,17,18]

Such NIPAM/PEG block copolymers have been formed by polymer-polymer coupling,[19] free radical polymerizations of NIPAM using either PEG macroazoinitiators,[8,9] a ceric ion redox reaction to generate radicals on PEG-OH,[14,20] or controlled radical copolymerizations such as ATRP[10,11] or RAFT.[12,13,15,21,22,23]

RAFT is a versatile method for making NIPAM block copolymers and has been used to form other double hydrophilic block copolymers of NIPAM with, e.g., dimethylacrylamide (DMA).[24,25,26] HEA is another neutral hydrophilic monomer which can be used to form double hydrophilic block copolymers with NIPAM, and some examples have demonstrated thermo-responsive phase separation of these block polymers synthesized by ATRP.[27,28]

This paper describes the synthesis of NIPAM/HEA block copolymers, using RAFT polymerization to form p(NIPAM) macro-chain transfer agents (macro-CTA) of controlled molecular weight, which are subsequently extended with varying HEA block

lengths, also using RAFT polymerization. Optionally, small amounts of *tert*-butyl acrylate were incorporated into the NIPAM-based macro-CTA to allow for functionalization and core-cross-linking of the final, thermally phase-separated micelles, following hydrolysis of the *t*-BA units to acrylic acid units. The use of a pHEA block over PEG for the second hydrophilic block is intended to allow for future introduction of other comonomers into the pHEA block to help with cellular uptake or cell targeting. Varying the HEA block lengths may also affect self assembly and therefore allow better control over the final micelle morphology.[29,30]

5.3. Experimental

5.3.1. Materials

N-isopropylacrylamide (NIPAM, 97%) was obtained from Sigma-Aldrich, Oakville, ON, and re-crystallized twice from a hexane:toluene mixture. *Tert*-butylacrylate (*t*BA, Sigma-Aldrich, Oakville, ON) was distilled under vacuum or passed over basic alumina. Hydroxyethylacrylamide (HEA, Sigma-Aldrich, Oakville, ON) was separated from MEHQ inhibitor over a silica gel plug by washing out the MEHQ with a 1:1 mixture of ethylacetate and hexanes, followed by HEA elution with a 9:1 mixture of ethylacetate and methanol. Azobisisobutyronitrile (AIBN, DuPont, Mississauga, ON), 2-(dodecylthiocarbonothioylthio)-2-methylpropionic acid (98%, DMP), deuterium chloride solution (35 wt% in D_2O, 99 atom % D), 2-(N-morpholino)ethanesulfonic acid sodium salt (MES), N-ethyl-N-(3-dimethylaminopropyl)-carbodiimide (EDC), Biograde N,N-dimethylformamide (DMF) (Sigma-Aldrich, Oakville, ON) were used as received. All

other solvents were purchased from Caledon Laboratories (Georgetown, ON). Dioxane, DMF, diethylether, ethylacetate were all reagent grade, methanol was HPLC grade, and all were used as received. Adipic acid dihydrazide (ADH, 98%) was obtained from Alfa Aesar (Ward Hill, MA) and was used as received. Ultrapure water was obtained using an Easy Pure II System.

5.3.2. Instrumentation

All ^{1}H NMR spectra were recorded on a Bruker 600 MHz or Bruker 500 MHz.

Polymer molecular weights were estimated using a gel permeation chromatography (GPC) system consisting of a Waters 590 HPLC pump, three Waters Ultrastyragel Linear columns (30 cm x 7.8 mm (i.d.); <10 μm particles) at 35 °C and a Waters 410 refractive index detector at 40 °C. The elutent was 10 or 50 mM LiBr in DMF, and the system was calibrated with narrow molecular weight PEG standards (Waters, Mississauga, ON).

UV-Vis spectra were recorded on Cary 50 Bio spectrophotometer. The extinction coefficient of the DMP endgroup was determined experimentally to be 34.51 $g \cdot cm^{-1} \cdot mg^{-1}$ in MeOH at 310 nm. A Varian Cary 3E spectrophotometer fitted with a temperature-controlled 12-sample cell holder was used to measure cloudpoints.

5.3.3. P(NIPAM-*co*-*t*BA) synthesis

P(NIPAM-*co*-*t*BA) was prepared using RAFT polymerizations modified from procedures previously described for pNIPAM.[31,32,33] A typical procedure for preparing

p(NIPAM-*co*-*t*BA) is as follows: Recrystallized NIPAM (4.438 g, 0.0393 mol), *t*BA (0.556 g, 0.00434 mol), DMP (67.7 mg, 0.186 mmol) and AIBN (6.1 mg, 0.037 mmol) were dissolved in 1,4-dioxane (10 mL) and purged with nitrogen for 30-50 mins, then added to a pre-heated oil bath at 65 °C. The reaction was monitored by removing aliquots using a N_2 purged needle, and assessing conversion using ^{1}H NMR and GPC. The polymerization was stopped by cooling in an ice bath followed by exposure to air. P(NIPAM-*co*-*t*BA) was isolated by precipitation in excess diethylether (x2) and drying the resulting white-light yellow powder under vacuum at room temperature (71% yield, 3.60 g).

5.3.4. P((NIPAM-*co*-*t*BA)-*b*-HEA) synthesis

P((NIPAM-*co*-*t*BA)-*b*-HEA) was prepared in a typical reaction as follows by aiming for a $[M]_o$:$[\text{macro-CTA}]_o$ of 115:1. p(NIPAM-*co*-*t*BA) (3.026 g, 0.138 mmols), AIBN (4.5 mg, 0.0274 mmol) and HEA (2.163 g, 80 wt% in ethylacetate, 15.02 mmol) were dissolved in 10 mL of DMF, separated equally into 3 vials, purged with N_2 for 45-60 mins then added to a pre-heated oil bath at 65 °C. The reaction progress was monitored by ^{1}H-NMR and GPC of the crude reaction mixtures, using aliquots removed with a N_2 purged needle. The polymerization was stopped by cooling in an ice bath at various conversions (20, 40 and 80%) for different HEA chain lengths.

5.3.5. Removal of endgroup

Crude block copolymer polymerization mixtures ($[M]_o$:$[\text{macro-CTA}]_o$ of 113:1) at 80% conversion (0.046 mmol endgroup and residual 23 fold molar excess of HEA) were

aminolyzed similar to previous procedures[34,35] by adding a 5-fold excess of 3-aminopropanol (19 mg, 0.25 mmol) and triethylamine (25 mg, 0.25 mmol) in DMF, pre-purged with N_2. The reaction period ranged from overnight to two days, before checking if the end groups were removed by precipitating aliquots in excess diethyl ether and analysis by ^{1}H NMR. Once the endgroups had been removed, the polymers were isolated by precipitation into excess diethyl ether (twice), dialysis in de-ionized water and freeze-drying.

Crude block copolymer polymerization mixtures (~80% conversion) of HEA block lengths of 20 kDa ($[M]_o$:[macro-CTA]$_o$ of 255:1, 259:1, 205:1), were also aminolyzed by adding a five-fold excess of 3-aminopropanol and triethylamine as above, thus representing a 50-60 fold molar excess of HEA monomer to endgroup.

Crude block copolymer polymerization mixtures of copolymers ($[M]_o$:[macro-CTA]$_o$ of 113:1) at 20 or 40% conversion were worked up by precipitation in excess diethyl ether and then re-dissolved in DMF with a 20 fold molar excess (relative to the endgroups) of HEA, purged with N_2, then aminolyzed as above. Typical recovery of polymer from endgroup removal was about 55-75%.

5.3.6. Hydrolysis of *tert*-butyl ester group

Tert-butyl acrylate units in the block copolymers were hydrolyzed to acrylic acid units by dissolving polymer (200 mg, 0.00132-0.00345 mmol *tert*-butyl groups) into 13.3 mL of cooled de-ionized water. After dissolution, 12 M HCl (0.77 g, 7.76 mmol) was added to the mixture and allowed to react for two weeks at 17 °C, after which, it was

observed that warming to room temperature no longer caused phase separation of the polymers, thus hydrolysis was continued for another 5 days at room temperature.

5.3.7. Cloud point measurements

Cloud point measurements were performed with a Varian Cary 3E spectrophotometer fitted with a temperature-controlled 12-sample cell holder. The polymers were dissolved in 0.1 M MES buffer (pH 4.7) at 5 mg/mL. The temperature was ramped up or down at 1 °C/min, and the solution transmittance at 500 nm was measured at 0.5 °C intervals. The cloud point (soluble to insoluble transition) is defined as the temperature at the onset of decrease in transmittance.

5.3.8. Cross-linking of micelles

A solution of hydrolyzed p((NIPAM$_{172}$-*co*-tBA$_{17}$)-*b*-HEA$_{51}$), nominally p((NIPAM$_{172}$-*co*-AA$_{17}$)-*b*-HEA$_{51}$), was prepared at 6.25 mg/mL by dissolution into 0.1 M MES buffer of pH 4.7 and filtered through a 0.2 μm pore membrane syringe filter. Of this solution, 0.8 mL (5 mg of polymer, 0.0024 mmol AA) was transferred to a glass vial and 0.112 mL (1.68 mg, 0.00966 mmol) of ADH stock solution (15 mg/mL in 0.1 M MES buffer) was added. This solution (0.912 mL at 5.48 mg polymer/mL) was heated to 50 °C for 15 mins in a water bath before 88 μL (4.63 mg, 0.024 mmol) of EDC stock solution (52.9 mg/mL in 0.1 M MES buffer) was added drop-wise at 50 °C. The vial was gently shaken in the water bath to mix the EDC solution and was allowed to react overnight at

50 °C. In all cross-linking reactions, the EDC:COOH:ADH ratio was kept at 10:1:4, with a final polymer concentration of 5 mg/mL unless otherwise noted.

5.3.9. TEM

Cross-linked micelles were prepared for transmission electron microscopy (TEM) by diluting the cross-linked micelle solutions 2000 fold in ultrapure water, adding 5 μL of this solution to Formvar coated copper grids and allowing to dry at room temperature without staining. The samples were imaged on a JEOL 1200EX TEMSCAN TEM with an acceleration voltage of 80 kV. Measurements of aggregates were done using ImageJ Software with the average and standard deviation determined from 50 aggregate measurements.

5.4. Results and discussion

The poly(NIPAM-*co*-*t*BA)-*b*-poly(HEA) block copolymers were synthesized using RAFT polymerization. The commercially available RAFT agent 2-(dodecylthiocarbonothioylthio)-2-methylpropionic acid (DMP) is commonly reported for polymerization of acrylamides such as NIPAM,[31,32,33] and was used here to build a macro-CTA containing 10% *tert*-butyl acrylate (*t*BA). Block lengths of 2.5, 5, 10 and 20 kDa p(HEA) were chain extended from the initially formed 20 kDa p(NIPAM-*co*-*t*BA) macro-CTA. In addition, a p(NIPAM-*b*-HEA) block copolymer with equal block lengths of 20 kDa for both NIPAM and HEA was prepared, as well as analogue block copolymer

containing *t*BA in both NIPAM and HEA blocks to assess the effect of incorporation of *t*BA in the HEA block.

5.4.1. Kinetic studies for the formation of p(NIPAM-*co*-*t*BA)

Reaction aliquots during formation of p(NIPAM-*co*-*t*BA) with $[M]_o$:$[CTA]_o$:$[I]_o$ = 231:1:0.2 were taken at time 0 and every 15 minutes for 90 minutes to monitor the rate of conversion, incorporation of NIPAM and *t*BA, and dispersity (See Figure 5A.1 and 5A.2 for ^{1}H NMR of time 0 and 45 mins aliquots respectively).

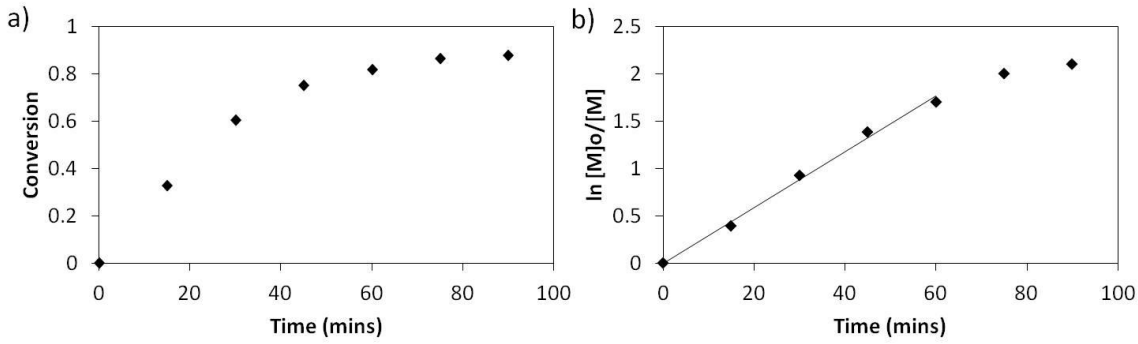

Figure 5.1: a) Conversion over time b) 1st order kinetic plot of monomer consumption with $[M]_o$:$[CTA]_o$:$[I]_o$ = 231:1:0.2.

The reaction proceeds to high conversion and follows first order kinetics up to 80% conversion, where the reaction slows down (Figure 5.1). The reaction also shows a linear increase in molecular weight with conversion and low dispersity (Figure 5.2). These features are typical behavior for a RAFT polymerization proceeding with good control. Interestingly, the M_n determined by GPC is about 2 times smaller than the theoretical M_n (dotted line, Fig 5.2 b) calculated using equation [1]. However, the linear

chain growth and low dispersity suggest that control of polymer growth is in fact achieved, and that rather the PEG standards used to calibrate the GPC are not representative of the M_n of the p(NIPAM-*co*-*t*BA) chains.

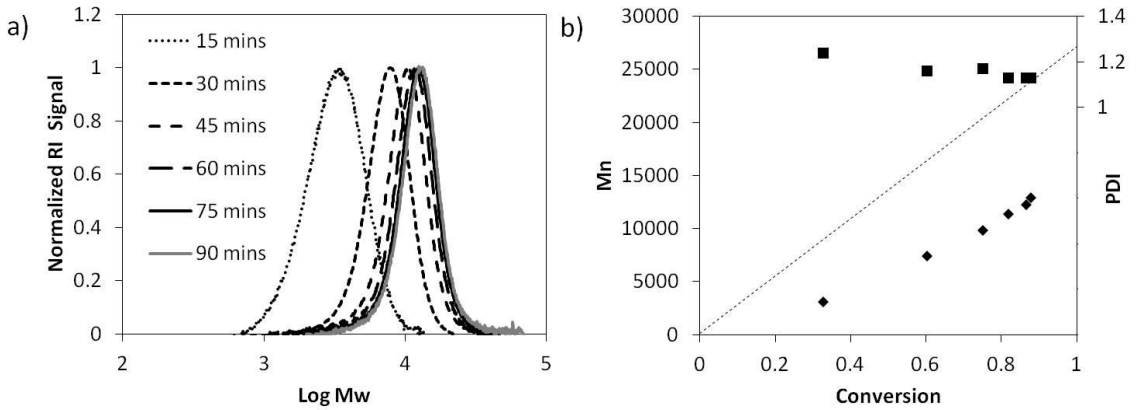

Figure 5.2: a) Normalized GPC chromatograms of p(NIPAM-*co*-*t*BA) sampled at different times during the reaction b) experimental (◆) and theoretical (--) M_n based on equation [1], dispersity (■) for $[M]_o$:$[CTA]_o$:$[I]_o$ = 231:1:0.2.

[1] Theoretical $M_n = [M]_o/[CTA]_o$ x ave MW_m x % conversion + MW of CTA

The incorporation of *t*BA into the copolymer with conversion was monitored (Figure 5.3), using the ^{1}H NMR signals for *t*BA and NIPAM in the residual comonomer pool to determine the amount of *t*BA incorporated during the polymerization. The negligible drift in *t*BA mol fraction in the residual comonomer pool over the course of the copolymerization thus indicates a comparably small drift in copolymer composition during the copolymerization.

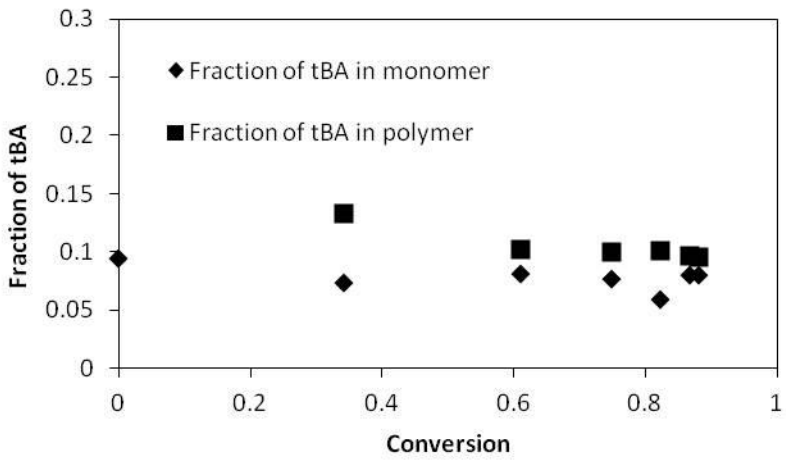

Figure 5.3: Assessment of drift of *t*BA mole fraction in both residual comonomer pool and in the copolymer, from ^{1}H NMR measurements of comonomer ratio in the comonomer pool $[M]_o$:$[CTA]_o$:$[I]_o$ = 231:1:0.2.

5.4.2. Scale up of p(NIPAM-*co*-*t*BA)

P(NIPAM-*co*-*t*BA) of 20 kDa with 10% mol *t*BA was isolated by precipitation in excess diethyl ether (twice) followed by drying under vacuum. The isolated polymer was used to determine the experimental M_n by endgroup analysis, using two methods. The molar ratio of monomer to DMP end group was determined by comparing the integrated DMP signal (deconvoluted terminal CH_3 at 0.9 ppm) to that of the polymeric NIPAM CH group at 4.0 ppm, and found to closely match the theoretically determined M_n (see figure 5A.3 and 5A.4). The M_n determined by this NMR endgroup analysis was confirmed using UV-Vis absorption of the DMP endgroup at 310 nm in MeOH using the extinction coefficient of free DMP in MeOH, which gave similar results (see Table 5.1). The isolated polymers were analyzed for residual NIPAM monomer and solvents used during polymerization and work-up (dioxane, diethylether). Prior to future cell work, these

residual compounds would need to be removed by dialysis or LCST-based purification, followed by freeze drying.

Table 5.1: Scale up results for p(NIPAM-*co*-*t*BA)

Polymer	Conv-ersion [%]	Theoretical Mn[a] (kDa)	Exp Mn (kDa)	PDI[b]	Polymer composition[c]	Residual NIPAM monomer	Residual Solvents: dioxane, ether
p(NIPAM$_{180}$-*co*-*t*BA$_{18}$)	79	21.3	11.0[b] 23.0[c] 22.6[d]	1.17	91% NIPAM 9% *t*BA	1mol%, 2 monomer units per endgroup	4 wt%, 4 wt%
p(NIPAM$_{172}$-*co*-*t*BA$_{17}$)	81	21.4	11.7[b] 22.0[c] 24.3[d]	1.13	91% NIPAM 9% *t*BA	0.3mol%, 0.5 monomer units per endgroup	2 wt%, 0.1 wt%
p(NIPAM$_{155}$)	77	20.3	11.5[b] 17.9[c] 21.9[d]	1.12	100% NIPAM	1.7mol%, 3 monomer units per endgroup	6 wt%, 0.3 wt%

a: determined from equation [1] using CTA to monomer ratio in the NMR of the t=0 aliquot
b: determined from GPC of crude reaction mixtures
c: determined by ^{1}H-NMR of copolymer (1024 scans, 600 MHz)
d: determined by UV-Vis

5.4.3. p((NIPAM-*co*-*t*BA)-*b*-HEA)

Chain extension of HEA or HEA with 10% *t*BA to the p(NIPAM-*co*-*t*BA) was performed in DMF, a non preferential solvent, and proceeded with first order kinetics to about 80% (Figure 5A.5). The reaction showed good chain transfer to the HEA block, as

per the growth of the original macro-CTA (Figure 5.4 and Figure 5A.6, for $[M]_o$:[Macro-CTA]$_o$:$[I]_o$ = 113:1:0.2 and $[M]_o$:[Macro-CTA]$_o$:$[I]_o$ = 215:1:0.2 respectively). The dispersity increases with conversion but remains acceptable at about 1.26 and 1.45 for crude solutions above 80% conversion (Figure 5.5 and Figure 5A.6 for $[M]_o$:[Macro-CTA]$_o$:$[I]_o$ = 113:1:0.2 and $[M]_o$:[Macro-CTA]$_o$:$[I]_o$ = 215:1:0.2, respectively). Incorporation of *t*BA into the growing HEA block also shows little compositional drift during polymerization (Figure 5A.7).

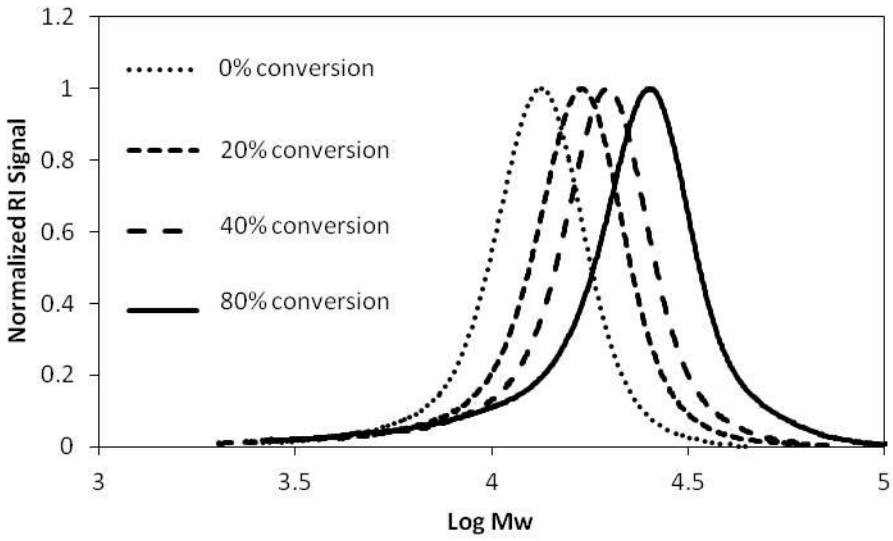

Figure 5.4: GPC chromatograms of the original p(NIPAM-*co*-*t*BA) block, and after chain extension with HEA: 20% conversion, 40% conversion and 80% conversion, for $[M]_o$:[Macro-CTA]$_o$:$[I]_o$ = 113:1:0.2.

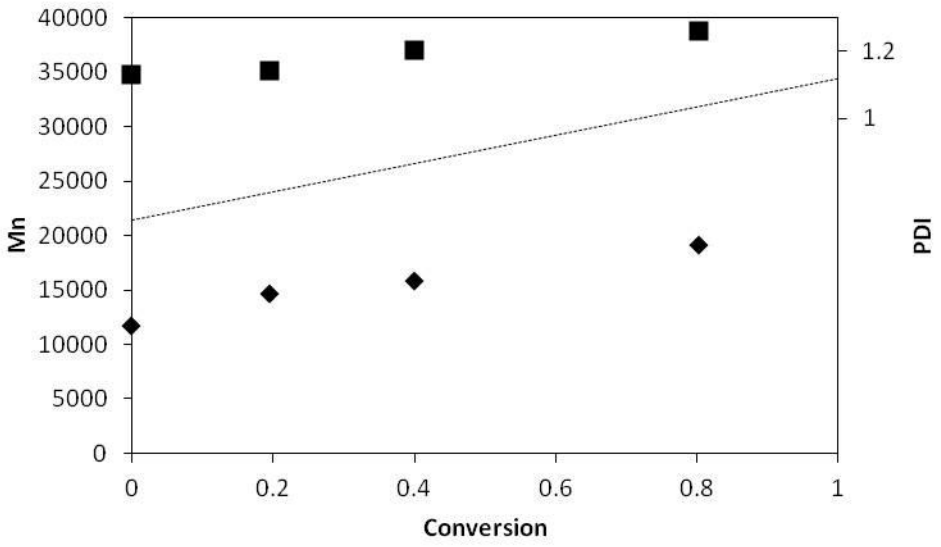

Figure 5.5: Experimental (◆) and theoretical (--) M_n based on equation [2], and Dispersity (■) for $[M]_o$:$[Macro\text{-}CTA]_o$:$[I]_o$ = 113:1:0.2.

5.4.4. Scale up of p((NIPAM-*co*-*t*BA)-*b*-HEA)

Poly(NIPAM) terminated with long alkane chains has been shown to form micelles below LCST even up to NIPAM DP of 98.[36] To avoid such complications of the hydrophobic dodecyl chain at the hydrophilic HEA chain end, this end group was removed. Due to the low efficiency of forced termination with tertiary AIBN radicals with acrylate polymers[37] and hence polyacrylamides, end group removal was performed by aminolysis of the trithiocarbonate in the presence of HEA as Michael acceptor. The trithiocarbonate reacts with amines to form a small molecule thiourea and create a thiol group on the polymer that reacts by Michael addition to HEA. End group removal was confirmed using ^{1}H NMR (Figure 5A.8) on the precipitated polymer. The experimental M_n was calculated from this final polymer by comparing the NIPAM signal to the HEA signal (Figure 5A.9). Chain extension with HEA was targeted for four different molecular

weights of 2.5, 5, 10 and 20 kDa. The lowest three molecular weight HEA blocks were made by aiming for a $[M]_o$:$[macro\text{-}CTA]_o$ of 115:1 and polymerizing to different conversions to acquire different block lengths (Table 5.2, fig 5.4). Another series of three NIPAM/HEA block co-polymers were designed with equal block length of about 20 kDa each ($[M]_o$:$[macro\text{-}CTA]_o$ of 205-259:1), but incorporating *tert*-butyl acrylate in either the NIPAM block, the HEA block or both (Table 5.3).

Table 5.2: Scale up of p((NIPAM-*co*-tBA)-*b*-HEA) for $[M]_o$:$[macro\text{-}CTA]_o$: $[I]_o$= 113:1:0.2

Polymer	Conv [%]	Theor Mn[a] in kDa	Theor length of HEA block in kDa (DP)	Exp Mn in kDa (PDI)[b]	Exp Mn in kDa (PDI) after aminolysis and isolation	Polymer composition[c]	Yield % recovery of polymer formed [%]
p((NIPAM$_{172}$-*co*-*t*BA$_{17}$)-*b*-HEA$_{26}$)	20	24.5	2.5 (22)	14.6 (1.14)	16.5 (1.10)[b] 24.8[c]	80% NIPAM 8% *t*BA 12% HEA	55
p((NIPAM$_{172}$-*co*-*t*BA$_{17}$)-*b*-HEA$_{51}$)	40	27.2	5.2 (45)	15.7 (1.20)	18.5 (1.09)[b] 27.6[c]	72% NIPAM 7% *t*BA 21% HEA	58
P((NIPAM$_{172}$-*co*-*t*BA$_{17}$)-*b*-HEA$_{100}$)	80	32.5	10.5 (91)	19.1 (1.26)	22.1 (1.16)[b] 33.3[c]	60% NIPAM 6% *t*BA 34% HEA	76

a: determined from equation [2]
b: determined from GPC crude reactions mixtures
c: determined by NMR (32 scans, 600 MHz), see supplementary for sample calc.

[2] $M_n(block)=([M]_o/[macro\text{-}CTA]_o \times MW_m \times \%\ conversion_m) + M_n\ (macro\text{-}CTA)$

Table 5.3 : Scale up for p((NIPAM-*co*-*t*BA)-*b*-HEA)

Polymer ($[M]_o$: $[macro\text{-}CTA]_o$: $[I]_o$)	Conv [%]	Theor Mn[a] in kDa	Theor length of HEA block in kDa (DP)	Exp Mn in kDa (PDI)[b]	Exp Mn in kDa (PDI) after aminolysis and isolation	Polymer composition[c]	Yield % recovery of polymer [%]
p(($NIPAM_{180}$-*co*-*t*BA_{18})-*b*-HEA_{230}) (255:1:0.2)	77	45.7	22.6 (196)	26.4 (1.40)	30.4 (1.31)[b] 49.3[c]	42% NIPAM 4% *t*BA 54% HEA	71
p(($NIPAM_{180}$-*co*-*t*BA_{18})-*b*-((HEA_{210}-*co*-tBA_{21})) (259:1:0.2)	77	45.8	23.1 (199)	28.2 (1.30)	30.0 (1.27)[b] 49.7[c]	42% NIPAM 9% *t*BA 49% HEA	70
p($NIPAM_{155}$-*b*-((HEA_{155}-*co*-*t*BA_{13})) (205:1:0.2)	75	35.8	17.9 (154)	24.5 (1.39)	25.1 (1.43)[b] 37.2[c]	48% NIPAM 4% *t*BA 48% HEA	69

a: determined from equation [2]
b: determined from GPC crude reactions mixtures
c: determined by NMR (32 scans, 600 MHz), see supplementary for sample calc.

5.4.5. Hydrolysis of *tert*-butyl groups

The hydrolysis of the *tert*-butyl groups was performed in water containing 0.55 M HCl at 17 ^oC (see Table 5.4). The presence of HCl lowered the LCST of the copolymer below room temperature, causing phase separation with increased turbidity, especially at lower HEA content. Hence, the hydrolysis was performed at 17 ^oC, where all block co-polymer solutions appeared clear. ^1H NMR spectra taken early in the hydrolysis reflect

the reduced solubility of the NIPAM block in 0.55 M DCl in D_2O at room temperature due to the *t*BA in the NIPAM block (Figure 5A.10). Initially, the ratio of NIPAM to HEA appears artificially low in D_2O compared to $MeOD_4$ (a good solvent for both blocks). As the hydrolysis proceeds, the NIPAM peak in D_2O increases to the correct NIPAM to HEA ratio (Figure 5A.10). The exception is the polymer that did not contain *t*BA in the NIPAM block, p(NIPAM$_{155}$-*b*-(HEA$_{155}$-*co*-*t*BA$_{13}$)). At room temperature, this NIPAM block is fully soluble in D_2O and as the hydrolysis of *t*BA proceeds, the ratio of NIPAM to HEA peaks remains constant. Similarly, if p(NIPAM$_{155}$-*b*-(HEA$_{155}$-*co*-*t*BA$_{13}$)) is heated above the LCST of NIPAM, the apparent ratio of NIPAM to HEA decreases when assessed by ^{1}H NMR (Figure 5A.11).

After hydrolysis, all the polymer solutions remained clear at room temperature, regardless of the HEA block length. AA is more hydrophilic than *t*BA and thus increases the LCST of the NIPAM block in the current HCl solution.

Table 5.4: Hydrolysis of *tert*-butyl groups

Hydrolyzed Polymer	Conv [%]	Exp Mn in kDa (PDI)[a]	Polymer composition[b]	Yield [%]
p((NIPAM$_{180}$-*co*-*t*BA$_{18}$)-*b*-HEA$_{230}$)	69	28.2 (1.35)	42% NIPAM 1% *t*BA 3% AA 54% HEA	93
p((NIPAM$_{180}$-*co*-*t*BA$_{18}$)-*b*-(HEA$_{210}$-*co*-*t*BA$_{21}$))	84	24.3 (1.27)	42% NIPAM 1% *t*BA 8%AA 49% HEA	91
p(NIPAM$_{155}$ -*b*-(HEA$_{155}$-*co*-*t*BA$_{13}$))	82	23.0 (1.38)	48% NIPAM 1% *t*BA 3% AA 48% HEA	93
p((NIPAM$_{172}$-*co*-*t*BA$_{17}$)-*b*-HEA$_{26}$)	77	15.0 (1.12)	80% NIPAM 2% *t*BA 6% AA 12% HEA	91
p((NIPAM$_{172}$-*co*-*t*BA$_{17}$)-*b*-HEA$_{51}$)	71	16.6 (1.16)	72% NIPAM 2% *t*BA 5% AA 21% HEA	93
p((NIPAM$_{172}$-*co*-*t*BA$_{17}$)-*b*-HEA$_{100}$)	67	21.6 (1.15)	60% NIPAM 2% *t*BA 4% AA 34% HEA	92

a: determined from GPC
b: determined from conversion of *t*BA to AA

The cloud point in 0.1 M MES buffer pH=4.7 was determined for the final polymers by heating from 20-60 °C at 1 degree per minute. The absorbance at 500 nm was measured every 0.5 mins and converted to % transmittance. Ionization of

comonomers in NIPAM-based copolymers can be used to increase the LCST of the copolymer, thus making the cloud point pH dependent.[38] The pH of 4.7 was chosen as it is useful for subsequent *in situ* EDC coupling. The onset of turbidity for all polymers occurred between 31-35 °C, however, in presence of AA in the NIPAM block the phase separation takes place over a wider temperature range, reflecting a more gradual desolvation of the NIPAM/AA blocks. P(NIPAM-*co*-AA) chains extended with different HEA block lengths show increasing residual transmittance above the LCST with increasing HEA chain length. When the HEA block is greater than 10 kDa, the transmittance plateaus at 80%. The lowest residual transmittance above the LCST was observed for p($NIPAM_{172}$-*co*-AA_{17})-*b*-HEA_{26}) having the shortest HEA block length, which may result from formation of larger and/or more hydrophobic aggregates as well as the greater fraction of p(NIPAM) block (Figure 5.6). Based on the polymer phase transition determined by turbidity as a function of temperature in MES buffer at pH 4.7, the majority of phase separated aggregates seem to stabilize after 46-50 °C (about 10 mins after the onset of phase separation). The phase separation of p(($NIPAM_{172}$-*co*-AA_{17})-*b*-HEA_{51}) seems complete at a higher temperature of about 58 °C, and that of p($NIPAM_{155}$-*b*-(HEA_{155}-*co*-AA_{13})) at a lower temperature of about 39 °C. Based on this information, the block co-polymers were heated in 0.1 M MES buffer at 50 °C for 15 mins before initiating a cross-linking reaction, to determine the nature of the phase separated aggregates. Previously studied p(NIPAM-*b*-HEA) block co-polymers prepared with varying the HEA to NIPAM mole fraction to a total DP of 100 also showed a higher percent transmittance and increased LCST with increasing HEA fractions.[28] The similar

onset and plateau of phase separation seen in Figure 5.6, despite increasing HEA fraction, is likely due to the high molecular weight NIPAM block being less susceptible to endgroup effects on LCST.[39]

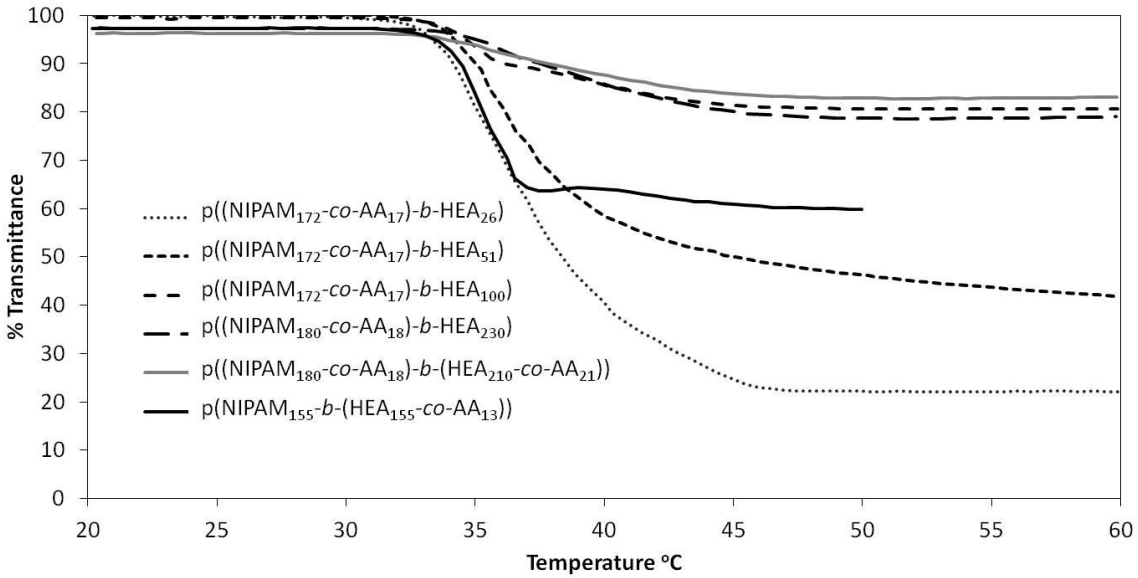

Figure 5.6: Transmittance versus Heating curves for p((NIPAM-*co*-AA)-*b*-HEA), p((NIPAM-*co*-AA)-*b*-(HEA-*co*-AA)) and p(NIPAM-*b*-(HEA-*co*-AA)) block co-polymers (5 mg/mL in 0.1 M MES buffer pH=4.7)

5.4.6. Cross-linking of thermally phase separated block copolymers

To determine if the reduced percent transmittance of p((NIPAM$_{172}$-*co*-AA$_{17}$)-*b*-HEA$_{26}$) and p((NIPAM$_{172}$-*co*-AA$_{17}$)-*b*-HEA$_{51}$) was due to overall increased NIPAM content in solution or larger aggregates, the block co-polymers were covalently core cross-linked after phase separation as a function of increasing HEA block length. Covalent cross-linking of similar micelles made from pNIPAM-*b*-PEG has previously been used to increase micelle stability due to disintegration at lower temperatures, by incorporation of bi-functional vinyl monomers.[11,14] Cross-linking reactions can be also be

accomplished on pre-formed reactive block co-polymers after self-assembly using small molecule cross-linkers.[15,24,26] Previous similar work showed the formation of cross-linkable spherical micelles formed from p((NIPAM-*co*-N-acryloxysuccinimide)-*b*-PEG)[15] made from PEG macro-CTA and p(DMA-*b*-(NIPAM-*co*-3-azidopropylacrylamide))[26] using approximately equal block lengths.

Since NIPAM chains phase separate above the LCST, cross-linking of these micelles allows for formation of hydrophilic particles which remain intact at lower temperatures where both blocks are well solvated. Core cross-linking was performed here to hold the form of the self-assembled micelles and show the micelle morphologies as a function of polymer block length ratio. The block co-polymers will phase separate upon heating above the LCST of the p(NIPAM-*co*-AA) block, and will reversibly return to a soluble state after cooling back to room temperature (Figure 5.7).

The phase separated polymers were chemically cross-linked using EDC chemistry with the carboxylic acids in the p(NIPAM) block being cross-linked with a small molecule adipic acid dihydrazide (ADH) while phase separated at 50 °C. Reactions with EDC and carboxylic acids in water are fast and dependent on pH and temperature,[40] but also known to proceed with undesirable side reactions, such as hydrolysis of the O-acylisourea intermediate, and rearrangement to an unreactive N-acylurea. The likelihood of these reactions increase with temperature of the reaction.[41] A molar ratio of 10:1:4 of EDC:COOH:ADH was selected for p((NIPAM$_{172}$-*co*-AA$_{17}$)-*b*-HEA$_{51}$) after initial screening experiments using other ratios such as 5:1:0.5, 5:1:1, 7.5:1:2. Using lower amounts of ADH led to larger, less cross-linked structures at 25 °C as assessed by DLS

(Table 5A.1). The swollen particle diameter at 25 °C and the volume change of de-swelling, began to level off after COOH:ADH ratio of 1:2 and was the smallest at ratio of 1:4. In a study of micelle cross-linking using oxime formation to core cross-link p(DMA-*b*-diacetone acrylamide), it was found that a stoichiometric amount of a small molecule cross-linker compared to higher ratios led to different rates of cross-linking, with the same degree of conversion of free chains into cross-linked star micelles regardless of the mol ratio of polymeric cross-linkable functional group (ketone) to small molecule cross-linker (O,O'-1,3-propanediylbishydroxylamine) up to 1:3 (1:6 mol ratio ketone to alkoxyamine). However, the reaction was allowed to proceed for 25 hrs for all compositions.[42]

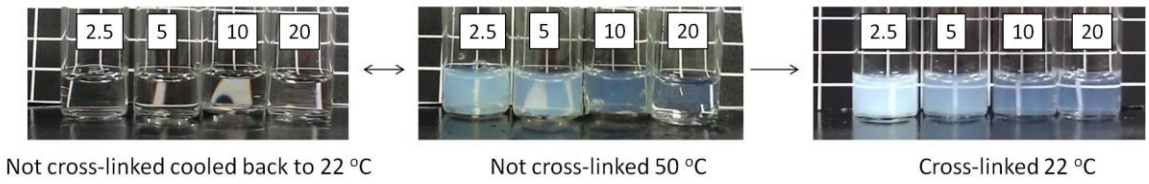

Figure 5.7: Images of solutions of p((NIPAM-*co*-AA)-*b*-HEA) block polymers with HEA block lengths of 2.5, 5, 10 and 20 kDa cooled to room temperature (left) after being heated to 50 °C (middle), and cross-linked at 50 °C and cooled to room temperature (right).

The cross-linking was performed at 50 °C, using 10 mol equivalent EDC and 4 mol equivalent ADH (8 mol equivalent hydrazide) to carboxylic acid, to allow cross-linking to be fast enough to compete with EDC side reactions. The cross-linked suspensions were cooled in a ice bath, allowed to warm to room temperature and

represented in Fig. 5.7. The phase separations still remain after cooling, showing successfully cross-linked structures.

5.4.7. Characterization of cross-linked micelles

The percent transmittance of the block copolymer aggregates above the cloud point, show differences in light scattering which is also affected by particle shape and size. TEM of unstained micelles (Figure 5.8, Table 5.5) show varying micelle morphology as a function of hydrophilic block length. P((NIPAM$_{172}$-*co*-AA$_{17}$)-*b*-HEA$_{26}$) has the lowest fraction of HEA, a HEA block of 2.5 kDa, and shows spherical aggregates of 100 nm. Increasing the HEA block to 5 kDa changes the morphology to Y-shaped rods. P((NIPAM$_{172}$-*co*-AA$_{17}$)-*b*-HEA$_{100}$) (HEA block 10 kDa) has a mixture of morphologies containing both spheres and rods of similar diameter (Table 5.5). Further increase in the HEA block to 20 kDa shows a shift to only spherical micelles.

The transition from sphere to rod with decreasing length of the water soluble block is explained by the volume fraction of each block, guiding self-assembly to reduce the interfacial area of the less soluble block, stretching of chains within the core, and repulsion of the water soluble block in the corona.[29,30,43] P((NIPAM$_{172}$-*co*-AA$_{17}$)-*b*-HEA$_{26}$), with the shortest HEA block length, formed larger spherical aggregates (Table 5.5) of ~100 nm that might appear as phase separated NIPAM nanoparticles instead of HEA- sterically stabilized micellar structures. When aggregates formed from p((NIPAM$_{172}$-*co*-AA$_{17}$)-*b*-HEA$_{26}$) were given more time to anneal from 15 mins to 2 hrs before adding ADH cross-linker, there was no obvious change in particle size, suggesting

that the particle size for this composition is colloidally stable for up to 2 hrs after initial heating above the cloud point.

It is important to note, that aggregates formed for all block polymer compositions were formed by heating the samples quickly by immersion in 50 °C water bath and are speculated to be kinetically trapped. Rate of heating, and concentration, are known to influence particle size for pNIPAM block polymer aggregates[8,27,44] and also influence the morphology of block copolymer assembly.[45] Therefore, the resulting morphologies of these block copolymers are not solely governed by the NIPAM/HEA block lengths but can also be influenced by concentration and rate of desolvation of the NIPAM block, which would be the subject of further investigation. The mixed morphologies of p((NIPAM$_{172}$-*co*-AA$_{17}$)-*b*-HEA$_{100}$) (HEA block 10 kDa) could result from intermediate morphologies trapped during fast heating, or the free energy of the two morphologies are similar such that they co-exist.[45] Regardless, covalent cross-linking of these nanoparticles has locked in the current morphologies shown in Figure 5.8.

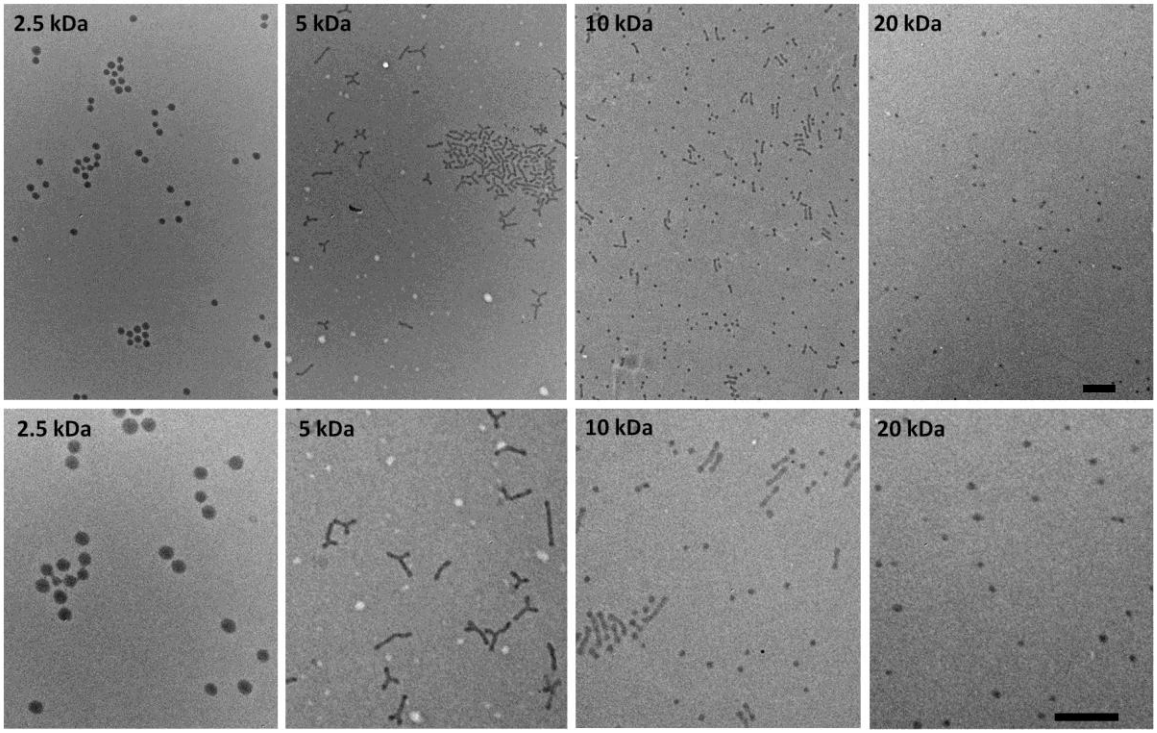

Figure 5.8: TEM of core cross-linked micelles with HEA block lengths of 2.5, 5, 10 and 20 kDa at 25000x (top) and 50000x (bottom) magnification. Scale bar is 500 nm.

Table 5.5: Diameter of spherical micelles and rod micelles measured from 50 aggregates.

Hydrolyzed and Cross-linked polymer	Diameter of spherical micelles (nm)	Diameter of rod-shaped micelles (nm)
p((NIPAM$_{172}$-*co*-*t*BA$_{17}$)-*b*-HEA$_{26}$)	97.5±13.3	n/a
p((NIPAM$_{172}$-*co*-*t*BA$_{17}$)-*b*-HEA$_{51}$)	n/a	29.6±4.3
p((NIPAM$_{172}$-*co*-*t*BA$_{17}$)-*b*-HEA$_{100}$)	39.0±5.5	31.9±4.5
p((NIPAM$_{180}$-*co*-*t*BA$_{18}$)-*b*-HEA$_{230}$)	39.4±8.2	n/a

The cross-linked micelles were investigated by DLS (Table 5A.2) at 25 °C and 50 °C to show the thermoresponsive swelling/deswelling of the cross-linked micelles despite the assumption of spherical shape by DLS. The effective diameter decrease after heating

at 50 °C shows a 1.4-1.8 reduction in volume and low PDI for most polymer compositions. The reduction in volume for cross-linked micelles formed from these block copolymers is small and thus suggests they are highly cross-linked. The degree of cross-linking by this method requires optimization and the volume change could possibly be increased with less cross-linking (Table 5A.1), to provide thermo-responsive cross-linked nanoparticles. The effective diameter of the cross-linked micelles were compared to those of uncross-linked micelles at 50 °C and show similar values (Table 5A.3). The exception is p((NIPAM$_{172}$-*co*-AA$_{17}$)-*b*-HEA$_{100}$), where the effective diameter is higher for the uncross-linked micelles compared to the cross-linked micelles. The difference in size for cross-linked versus uncross-linked p((NIPAM$_{172}$-*co*-AA$_{17}$)-*b*-HEA$_{100}$) may be due to a difference in the distribution of the rods *vs*. spheres in the free acid form compared to those reacted with ADH, affecting the hydrodynamic volume of the NIPAM block and shifting the size or morphology of the micelle. Alternatively, it may be due to a shift in morphology at reduced concentration for the DLS measurement compared to the concentration during cross-linking.

Cross-linking of micellar particles can enhance uptake, and other reactive groups can be incorporated to introduce functional cross-links.[46] Further investigation of the kinetics of formation and evolution of these micelle morphologies at different heating rates, or during addition of co-nonsolvents for NIPAM, are of interest to control architecture/morphology by formation under conditions both close to, as well as far from, equilibrium.

5.5. Conclusions

Well defined NIPAM/HEA block co-polymers were formed using RAFT polymerization creating easy control to increase HEA block length. Thermally induced self assembly of the block copolymers from solution was observed with all HEA block lengths tested. The constant MW thermo-responsive block showed different morphologies for phase separated aggregates as a function of HEA block length.

5.6. Acknowledgements

The authors would like to thank Daryl Sivakumaran and Scott Campbell for help on DLS, and Marcia Reid for help with TEM. The authors thank NSERC for funding of this research through its DG and CREATE programs.

5.7. References

[1] Maeda, H. *Advan*. *Enzyme Regul*. **2001,** *41,* 189–207.
[2] Gref, R.; Domb, A.; Quellec, P.; Blunk, T.; Müller, R. H.; Verbavatz, J. M.; Langer. R. *Adv*. *Drug Deliv*. *Rev*. **2012,** *64,* 316–326.
[3] Kataoka, K.; Kwon, G. S.; Yokoyama, M.; Okano, T.; Sakurai, Y. *J*. *Controlled Release* **1993,** *24*,119–132.
[4] Gaucher, G.; Dufresne, M. H.; Sant, V. P.; Kang, N.; Maysinger, D.; Leroux, J. C. *J*. *Controlled Release*, **2005,** *109,* 169–188.
[5] Kamei, S.; Kopeček, J. *Pharm*. *Res*. **1995,** *12,* 663–668.
[6] Knop, K.; Hoogenboom, R.; Fischer, D.; Schubert, U. S. *Angew*. *Chem*. *Int*. *Ed*. **2010,** *49,* 6288–6308.
[7] Pelton. R. *J*. *Colloid Interface Sci*. **2010,** *348,* 673–674.
[8] Neradovic, D.; Soga, O.; Van Nostrum, C. F.; Hennink, W. E. *Biomaterials* **2004,** *25,* 2409–2418.
[9] Virtanen, J.; Holappa, S.; Lemmetyinen, H.; Tenhu, H. *Macromolecules* **2002,** *35,* 4763–4769.
[10] Zhang, W.; Shi, L.; Wu, K.; An, Y. *Macromolecules* **2005,** *38,* 5743–5747.
[11] Kim, K. H.; Kim, J.; Jo, W. H. *Polymer* **2005,** *46,* 2836–2840.
[12] Yan, J.; Ji, W.; Chen, E.; Li, Z.; Liang, D. *Macromolecules* **2008,** *41,* 4908–4913.
[13] You, Y.; Oupický, D. *Biomacromolecules* **2007,** *8,* 98–105.

[14] Topp, M. D. C.; Dijkstra, P. J.; Talsma, H.; Feijen, J. *Macromolecules* **1997,** *30,* 8518–8520.
[15] Zhang, J.; Jiang, X.; Zhang, Y.; Li, Y.; Liu, S. *Macromolecules* **2007,** *40,* 9125–9132.
[16] He, X.; Wu, X.; Gao, C.; Wang, K.; Lin, S.; Huan, W.; Xie, M.; Yan, D. *React*. *Funct*. *Polym*. **2011,** *71,* 544–552.
[17] Wu, Y.; Lai, Q.; Lai, S.; Wu, J.; Wang, W..; Yuan, Z. *Colloids Surf., B* **2014,** *118,* 298–305.
[18] Wei, H.; Perrier, S.; Dehn, S.; Ravarian, R.; Dehghani, F. *Soft Matter* **2012,** *8,* 9526–9528.
[19] Wang, H.; Chen, W.; Zhu, Y.; Yan, H.; Zhang, J.; Wang, C. *J*. *Disper*. *Sci*. *Technol*. **2016,** *37,* 1341–1348.
[20] Lee, K. K.; Jung, J. C.; Jhon, M. S. *Polym*. *Bull*. **1998,** *40,* 455–460.
[21] Xu, H.; Meng, F.; Zhong, Z. *J*. *Mater*. *Chem*. **2009,** *19,* 4183–4190.
[22] Qin, S.; Geng, Y.; Discher, D. E.; Yang, S. *Adv*. *Mater*. **2006,** *18,* 2905–2909.
[23] Hong, C.; You, Y.; Pan, C. *J*. *Polym*. *Sci*., *Part A: Polym*. *Chem*.**2004,** *42,* 4873–4881.
[24] Li, Y.; Lokitz, B. S.; McCormick, C. L. *Macromolecules* **2006,** *39,* 81–89.
[25] Pascual, S.; Monterio, M. J. *Eur*. *Polym*. *J*. **2009,** *45,* 2513–2519.
[26] Jiang, X.; Zhang, J.; Zhou, Y.; Xu, J.; Liu, S. *J*. *Polym*. *Sci*., *Part A: Polym*. *Chem*. **2008,** *46,* 860–871.
[27] Ashaduzzaman, M.; Kai, S.; Uemura, S.; Kunitake, M. *Chem*. *Lett*. **2011,** *40,* 165–167.
[28] Chen, Y.; Sone, M.; Fuchise, K.; Sakai, R.; Kakuchi, R.; Duan, Q.; Sun, J.; Narumi, A.; Satoh, T.; Kakuchi, T. *React*. *Funct*. *Polym*. **2009,** *69,* 463–469.
[29] Kinning, D. J.; Winey, K. I.; Thomas, E. L. *Macromolecules* **1988,** *21,* 3502–3506.
[30] Zhang, L.; Eisenberg, A. *J*. *Am*. *Chem*. *Soc*. **1996,** *118,* 3168–3181.
[31] Yin, X.; Hoffman, A.S.; Stayton, P.S. *Biomacromolecules* **2006,** *7,* 1381–1385.
[32] Convertine, A.J.; Ayres, N.; Scales, C.W.; Lowe, A.B.; McCormick, C.L. *Biomacromolecules* **2004**, *5,* 1177–1180.
[33] Hermann, A.; Mruk, R.; Roskamp, R. F.; Scherer, M.; Ma, L.; Zentel, R. *Macromol*. *Chem*. *Phys*. **2014,** *215,* 32–43.
[34] Boyer, C.; Granville, A.; Davis, T. P.; Bulmus, V. *J*. *Polym*. *Sci*., *Part A: Polym*. *Chem*. **2009,** *47,* 3773–3794.
[35] Pissuwan, D.; Boyer, C.; Gunasekaran, K.; Davis, T. P.; Bulmus, V. *Biomacromolecules* **2010,** *11,* 412–420.
[36] Fitzgerald, P. A.; Gupta, S.; Wood, K.; Perrier, S.; Warr, G. G. *Langmuir* **2014,** *30,* 7986–7992.
[37] Chen, M.; Moad, G.; Rizzardo, E. *J*. *Polym*. *Sci*., *Part A: Polym*. *Chem*. **2009,** *47,* 6704–6714.
[38] Feil, H.; Bae,Y. H.; Feijen, J.; Kim, S. W. *Macromolecules* **1993,** *26,* 2496–2500.
[39] Xia, Y.; Burke, N. A. D.; Stöver, H. D. H. *Macromolecules* **2006,** *39,* 2275–2283.
[40] Gilles, M. A.; Hudson, A. Q.; Borders, C. L., Jr. *Anal*. *Biochem*. **1990,** *184,* 244–248.
[41] Wang, C.; Yan, Q.; Liu, H.; Zhou, X.; Xiao, S. *Langmuir* **2011,** *27,* 12058–12068.

[42] Mukherjee, S.; Bapat, A. P.; Hill, M. R.; Sumerlin, B. S. *Polym*. *Chem*. **2014,** ***5****,* 6923–6931.
[43] Mayes, A. M.; Olvera de la Cruz, M. *Macromolecules* **1988,** *21*, 2543–2547.
[44] Zhu, P. W.; Napper, D. H. *Langmuir* **2000,** *16,* 8543–8545.
[45] Mai, Y.; Eisenberg, A. *Chem Soc Rev*. **2012,** *41,* 5969–5985.
[46] van Nostrum, C. F. *Soft Matter* **2011,** *7,* 3246–3259.

5.8. Appendix

5.8.1. Polymer characterization

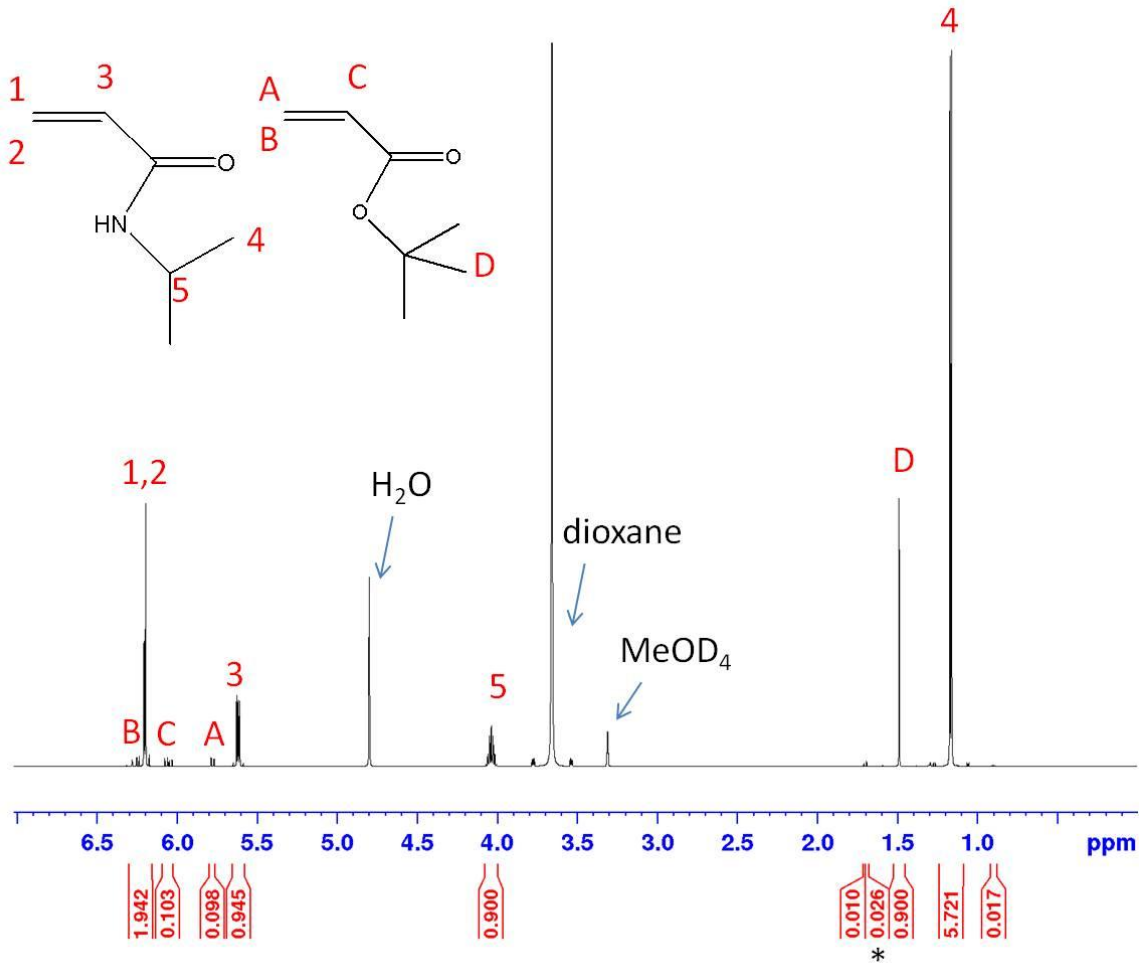

Figure 5A.1: ^{1}H NMR (600 MHz) of t=0 aliquot for p(NIPAM-*co*-*t*BA) polymerization. *Integration of the 6 protons from the 2 equivalent methyl groups of DMP was compared to NIPAM signal 5 and *t*BA signal A. For every 1 mol of DMP (when integration of 0.026 is normalized to 6, there is 208 NIPAM monomer units and 23 *t*BA monomer units, therefore $[M]_o$:$[CTA]_o$= 231:1.

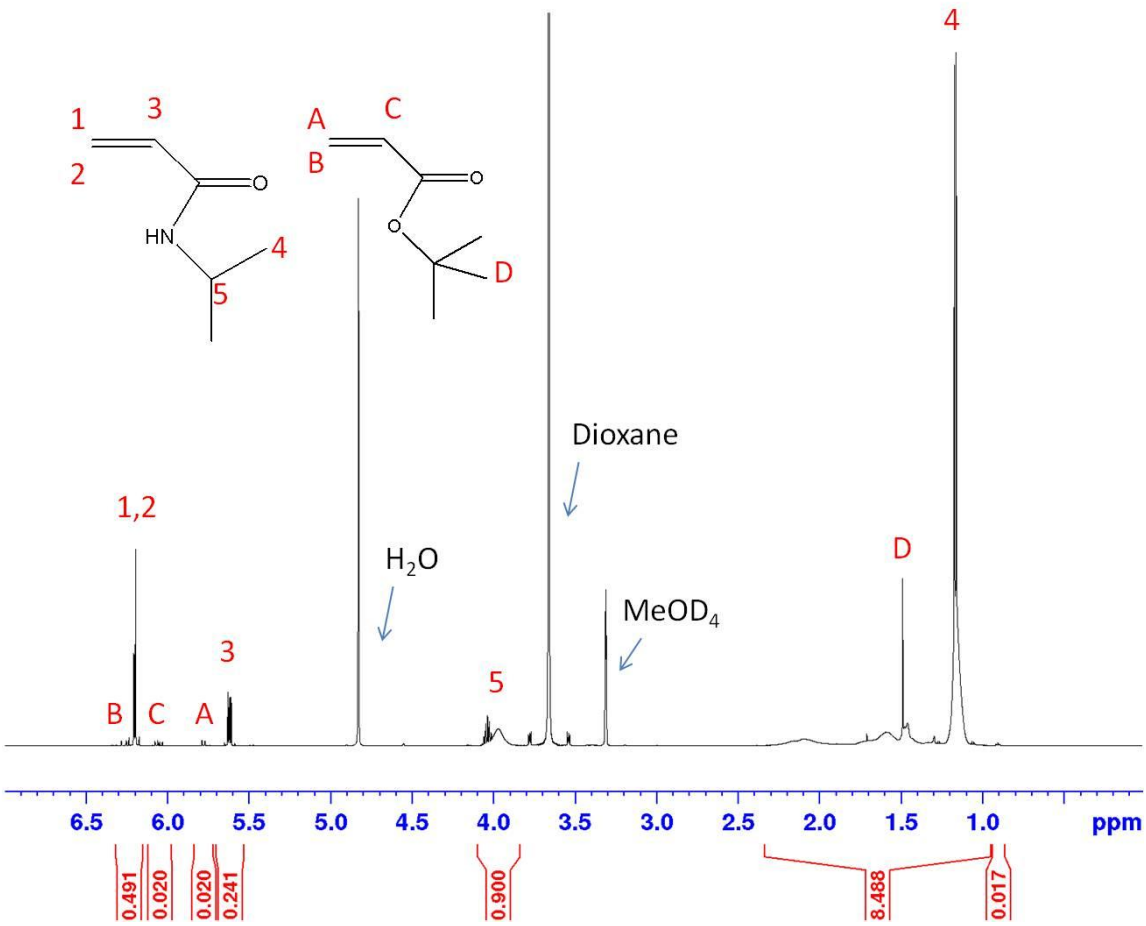

Figure 5A.2: ^{1}H NMR (600 MHz) of aliquot for p(NIPAM-*co*-*t*BA) polymerization taken after 45 mins at 65 °C, showing 75% conversion for $[M]_o$:$[CTA]_o$= 231:1.

Sample calc: = 1-[(sum of A+3 at t=x)/(sum of A+3 at t=0)]*100

=1-[(0.241+0.020)/(0.945+0.098)]*100= 75%

Proton 5 on NIPAM is used as an internal standard since the monomer and polymer peaks show up next to each other. By integrating and calibrating this region (monomer and polymer), the integration of the baseline-resolved vinylic hydrogens for

*t*BA and NIPAM (A and 3) can be used to determine conversion of both monomers compared to t = 0, and thus both instantaneous and cumulative copolymer composition.

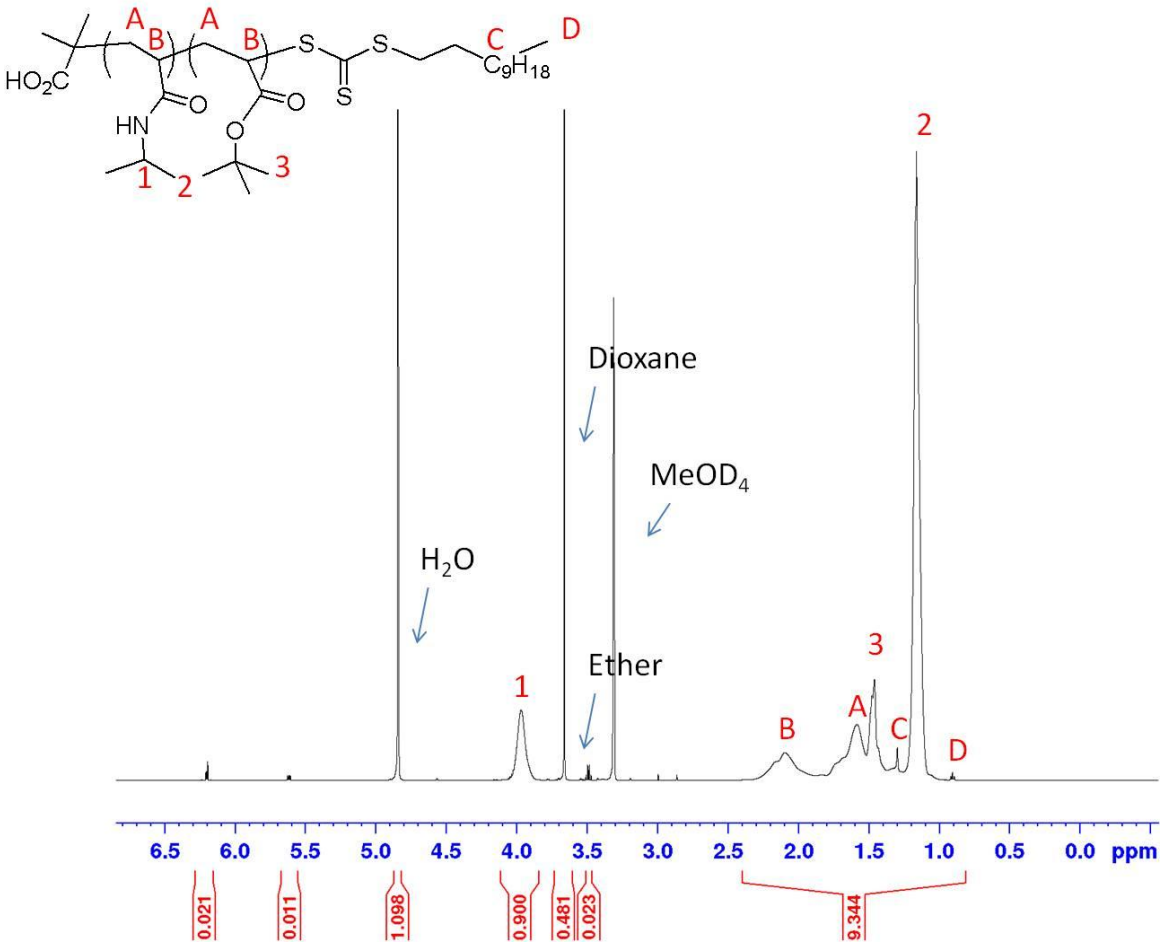

Figure 5A.3: ^{1}H NMR spectra of p(NIPAM-*co*-*t*BA) isolated after preciptiation (1024 scans, 600 MHz). DMP peak at 0.9 ppm has integration of 0.015 determined using deconvolution. DPexp =198 (23.0 kDa) and DP theor= 182 (21.3 kDa).

The amount of *t*BA has to be calculated by subtracting out the polymeric NIPAM and DMP protons from the region between 2.5 – 0.9 ppm.

An example calculation:

9.344 - 0.0349 (ether) - 8.1 (NIPAM) - 0.152 (DMP) = 1.0672/12 (*t*BA)= 0.0889/0.9889= 9% of tBA

The amount of endgroup is calculated by deconvolution of the DMP signal from the shoulder of the NIPAM signal 4. In figure 5A.4, the DMP peak at 0.9 ppm (D) looks well resolved here however, it was common to observe peak D on the tailing end of the NIPAM peak (**2**) and therefore deconvolution was necessary.

Sample calculation for endgroup analysis:

Integrating peak D in Figure 5A.4, and normalizing this signal to 3 protons. This leads to the NIPAM peak at 4 ppm having both an integration and number of NIPAM repeating units of 180 (= 3/0.015 = 200*0.9 = 180). Since NIPAM constitutes 91 mol% of the copolymer then the total degree of polymerization is 198. The average monomer molecular weight is 114.5 g/mol, giving a total molecular weight of 22 671 + 364 (endgroup)= 23 035 g/mol.

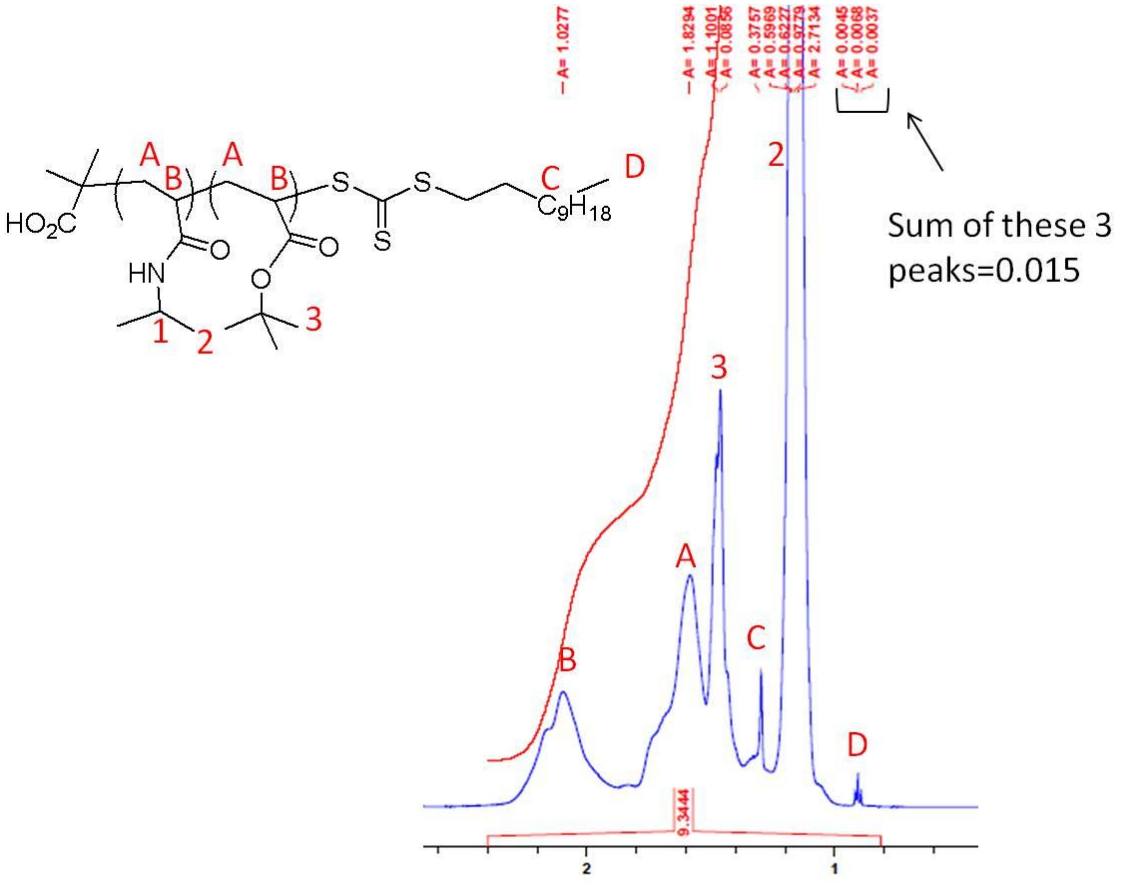

Figure 5A.4: ^{1}H NMR spectra of p(NIPAM-*co*-*t*BA) isolated after preciptiation (1024 scans on 600 MHz) with deconvolution of the peaks between 2.5 – 0.9 ppm.

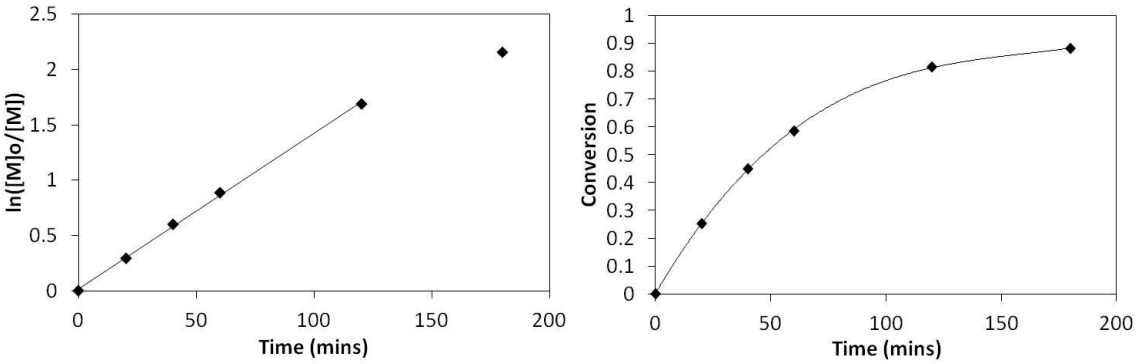

Figure 5A.5: Kinetic study of HEA-co-*t*BA chain extension $[M]_o$:$[Macro\text{-}CTA]_o$:$[I]_o$ = 215:1:0.2.

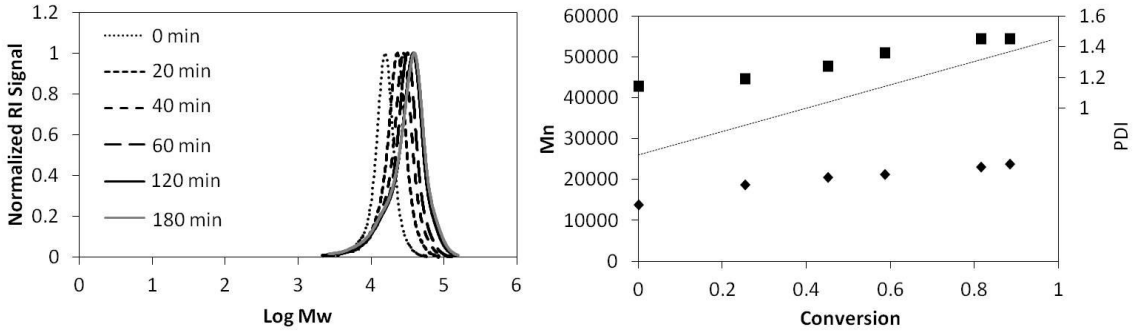

Figure 5A.6: HEA-co-*t*BA chain extension GPC $[M]_o$:$[Macro\text{-}CTA]_o$:$[I]_o$ = 215:1:0.2.

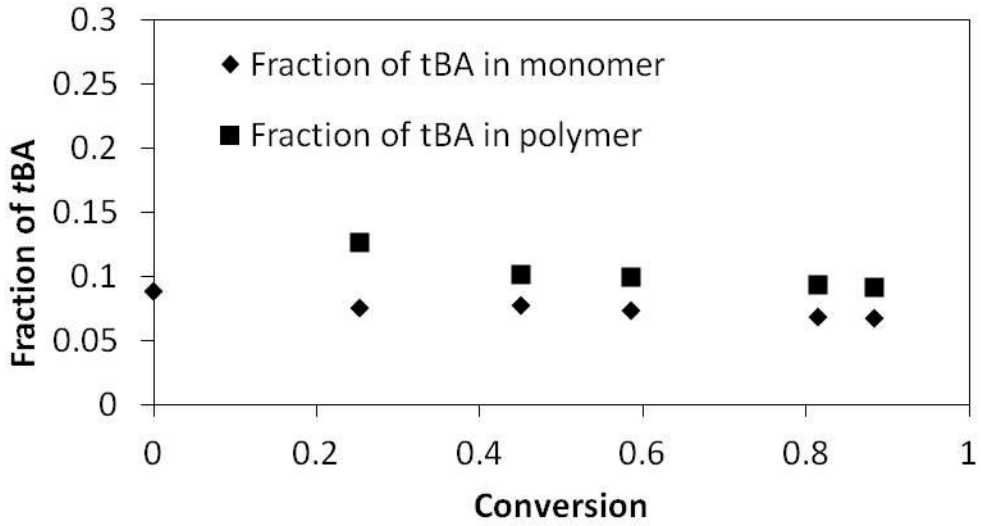

Figure 5A.7: HEA-*co*-*t*BA chain extension $[M]_o$:$[Macro\text{-}CTA]_o$:$[I]_o$ = 215:1:0.2, incorporation of *t*BA

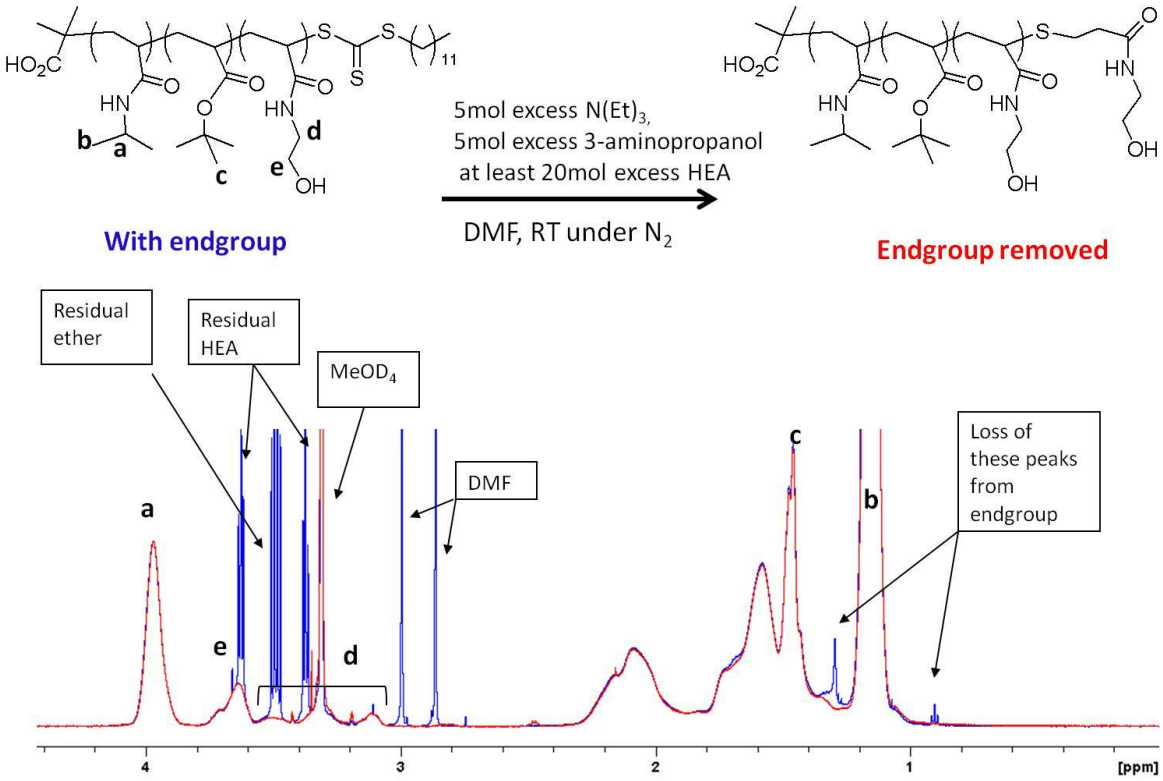

Figure 5A.8: ^{1}H NMR (600 MHz) of p((NIPAM$_{172}$-*co*-*t*BA$_{17}$)-*b*-HEA$_{26}$) before and after endgroup removal.

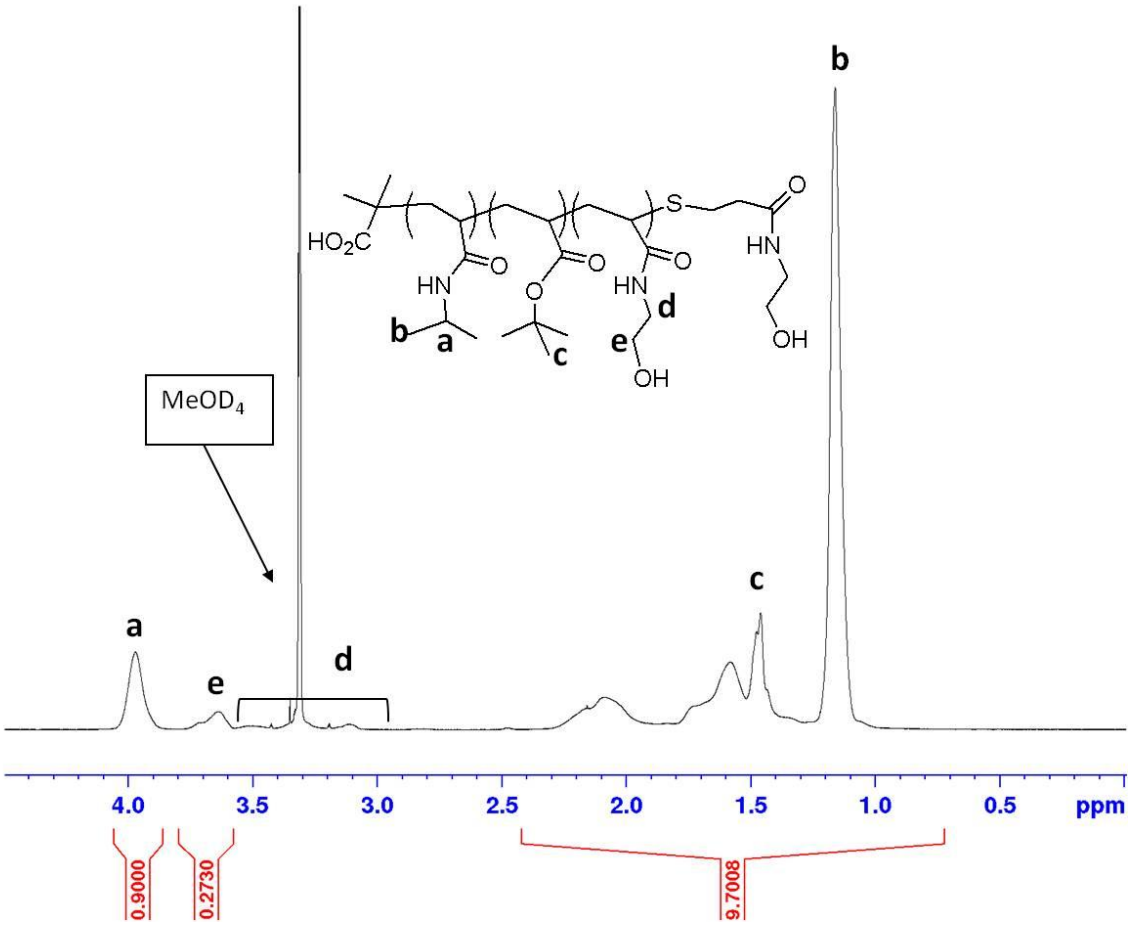

Figure 5A.9: Sample calculation using ^{1}H NMR (600 MHz) of p((NIPAM$_{172}$-*co*-*t*BA$_{17}$)-*b*-HEA$_{26}$) to calculate experimental M_n of the block-copolymer

The HEA (**e**) peak was compared against the NIPAM peak (**a**) to figure out M_n by first figuring out the ratio of NIPAM to HEA.

0.2730/2= 0.1365

Therefore the mol ratio of NIPAM:*t*BA:HEA is 0.9:0.09 (from data of the first block):0.1365 and the mol fraction of the first block is (0.9+0.09)/(0.9+0.09+0.1365)=0.88.

Since the first block has a degree of polymerization of 189, the total degree of polymerization is 215.

The degree of polymerization of the HEA block is 26 (2993 g/mol) therefore the total molecular weight of the polymer is 24 752 kDa.

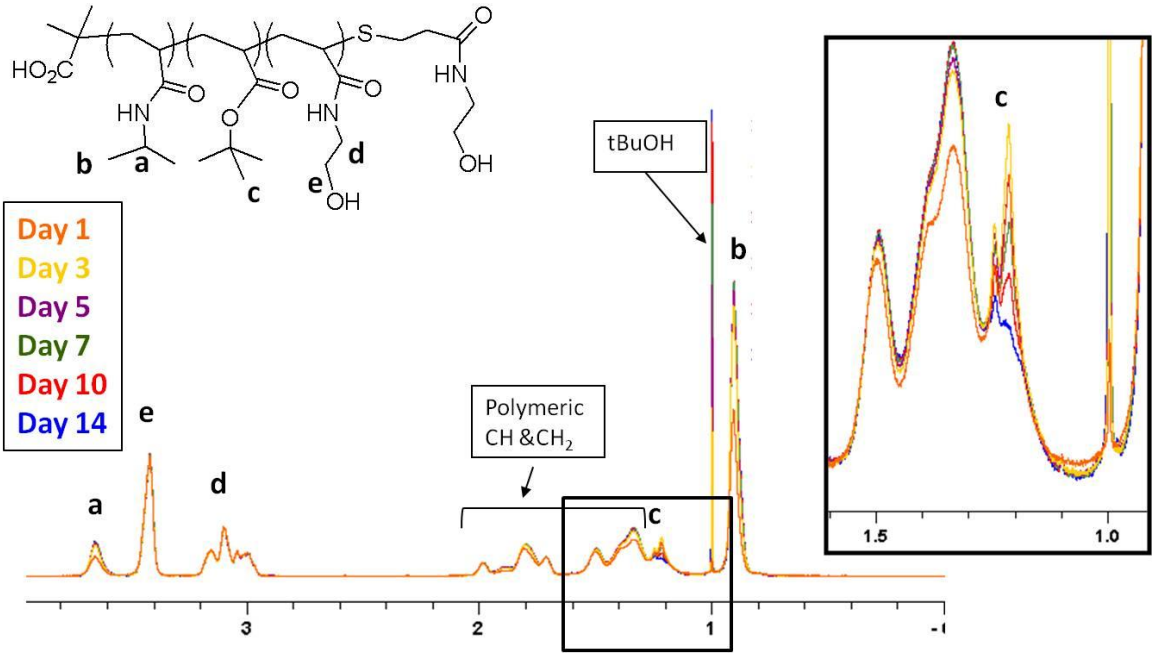

Figure 5A.10: ^{1}H NMR (600 MHz) spectra of p((NIPAM$_{180}$-*co*-*t*BA$_{18}$)-*b*-HEA$_{230}$) hydrolysis over two weeks at 17 °C.

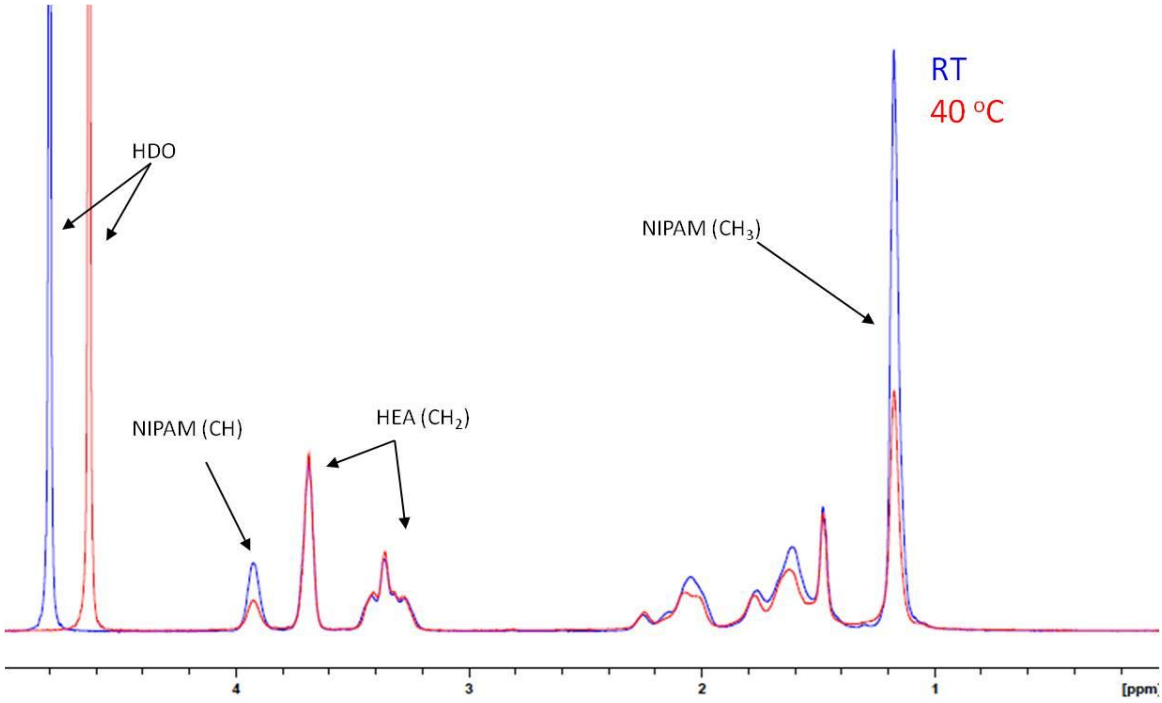

Figure 5A.11: ^{1}H NMR (500 MHz) spectra of p(NIPAM$_{155}$-*b*-(HEA$_{155}$-*co*-*t*BA$_{13}$)) at room temperature (blue) and heated to 40 °C (red)

5.8.2. DLS measurements

Dynamic light scattering was performed on cross-linked micelles by diluting crude samples in 0.1 M MES buffer at pH 4.7 to produce an intensity count between 250-600 kilocounts per second. The solution was syringe filtered using 0.45 µm filters to remove dust prior to measuring at 25 or 50 °C on a Brookhaven 90plus with a laser of 632.8 nm and a 90° angle. Uncross-linked polymer was filtered through 0.2 µm filters at room temperature and analyzed by DLS at 50 °C. The standard deviation is produced from a minimum of 4 replicate measurements, *n*. Due to rod-like and mixed morphologies of cross-linked micelles formed from p((NIPAM$_{172}$-*co*-*t*BA$_{17}$)-*b*-HEA$_{51}$) and p((NIPAM$_{172}$-*co*-*t*BA$_{17}$)-*b*-HEA$_{100}$) (with 10:1:4 [EDC]:[COOH]:[ADH]), DLS measurements were repeated without filtration and produced the same results.

Table 5A.1: Average diameter (nm) of hydrolyzed and cross-linked p((NIPAM$_{172}$-*co*-*t*BA$_{17}$)-*b*-HEA$_{51}$) determined from DLS at 25 °C and 50 °C

Ratio EDC:COOH:ADH (final polymer conc.)	*n*	Diameter (nm) at 25 °C*	PDI at 25 °C*	*n*	Diameter (nm) at 50 °C*	PDI at 50 °C*	ΔV
10:2:1 (4.9 mg/mL)	4	184 ± 3	0.07 ± 0.01	4	109 ± 3	0.03 ± 0.02	4.8
5:1:1 (4.8 mg/mL)	4	162 ± 0.6	0.05 ± 0.02	4	114 ± 0.8	0.07 ± 0.02	2.9
7.5:1:2 (4.2 mg/mL)	8	136 ± 4	0.06 ± 0.05	4	103 ± 0.4	0.06 ± 0.01	2.3
10:1:4 (3.7 mg/mL)	8	131 ± 1	0.04 ± 0.03	4	106 ± 0.6	0.02 ± 0.02	1.9

*Average diameter and PDI shown ± standard deviation for *n* measurements.

Table 5A.2: Average particle diameter (nm) determined by DLS at 25 °C and 50 °C for cross-linked micelles.

Cross-linked Hydrolyzed polymer	*n*	Diameter (nm) at 25 °C*	PDI at 25 °C*	*n*	Diameter (nm) at 50 °C*	PDI at 50 °C*	ΔV
p((NIPAM$_{172}$-*co*-*t*BA$_{17}$)-*b*-HEA$_{26}$)	12	115 ± 1	0.04 ± 0.03	4	94 ± 1	0.05 ± 0.03	1.8
p((NIPAM$_{172}$-*co*-*t*BA$_{17}$)-*b*-HEA$_{51}$)	12 4[#]	128 ± 2 130 ± 2[#]	0.08 ± 0.03 0.05 ± 0.02[#]	12 4[#]	91 ± 14 109 ± 0.9[#]	0.16 ± 0.12 0.03 ± 0.01[#]	2.8 1.7[#]
p((NIPAM$_{172}$-*co*-*t*BA$_{17}$)-*b*-HEA$_{100}$)	8 4[#]	79 ± 0.5 82 ± 0.5[#]	0.10 ± 0.03 0.10 ± 0.01[#]	8 4[#]	67 ± 0.8 69 ± 0.9[#]	0.07 ± 0.03 0.03 ± 0.02[#]	1.7 1.7[#]
p((NIPAM$_{180}$-*co*-*t*BA$_{18}$)-*b*-HEA$_{230}$)	8	81 ± 1	0.04 ± 0.02	8	72 ± 0.5	0.01 ± 0.01	1.4

*Average diameter and PDI shown ± standard deviation for *n* measurements.

[#] Un-filtered sample.

Table 5A.3: Average particle diameter determined by DLS for non-cross-linked aggregates at 50 °C.

Hydrolyzed polymer	*n*	Diameter (nm) at 50 °C*	PDI at 50 °C*
p((NIPAM$_{172}$-*co*-*t*BA$_{17}$)-*b*-HEA$_{26}$)	20	88 ± 11	0.08 ± 0.17
p((NIPAM$_{172}$-*co*-*t*BA$_{17}$)-*b*-HEA$_{51}$)	24	110 ± 17	0.05 ± 0.03
p((NIPAM$_{172}$-*co*-*t*BA$_{17}$)-*b*-HEA$_{100}$)	28	103 ± 3	0.11 ± 0.03
p((NIPAM$_{180}$-*co*-*t*BA$_{18}$)-*b*-HEA$_{230}$)	8	77± 1	0.03 ± 0.02

*Average diameter and PDI shown ± standard deviation for *n* measurements.

CHAPTER 6

Summary and future directions

6.1. Summary of thesis

The current use of encapsulation devices for enzyme deficiency disorders in clinical use has been hampered by inconsistent biocompatibility results of the current go-to technology based on APA capsules.[1] Failure of the APA capsule has been attributed to poor biocompatibility and stability of the PLL-based membrane, causing a foreign body response.[2,3,4] This thesis aims to replace the PLL with alternative polycations of reduced charge density, synthesized from APM and HPM and designed to increase the biocompatibility of alginate based capsules. The resulting effects on capsule formation, stability, and biocompatibility were assessed as a function of charge density and MW of the reduced charge density polycations. Covalent cross-linking of the capsule membranes was also explored as a way to increase the mechanical stability of the capsules. The stiffness of these capsule membranes was assessed by micropipette aspiration, a technique which was scaled and validated for such capsules as part of this thesis.

6.1.1. Summary of chapter 2

This chapter explores the application of micropipette aspiration to alginate gel beads and to APA capsules with a gel or liquid core. Application of Laplace's law does not strictly apply in presence of a gel core or where the membrane is thick enough to contribute stresses from bending. Application of a homogenous half-space model could

not be applied to determine the Young's modulus of the membrane when the membrane is thin and the capillary radius is much larger than the membrane thickness. Thus, micropipette aspiration was adapted in this chapter to report on the total mechanical stiffness of the whole capsule, regardless of whether the core is liquid or a gel. The extent of net protrusion of the capsule into the pipette was plotted against the applied pressure differential (suction force), and revealed a linear increase of deformation with applied suction force, with the slope corresponding to the stiffness of the capsule or bead.

The stiffness determined by aspiration showed softening of alginate beads with increasing saline washes, which was consistent with trends previously seen in the literature due to Na^{+}/Ca^{2+} exchange. Alginate beads coated with PLL were also tested and showed that the stiffness of the PLL/Alg membrane was sensitive to the coating procedure, due to Ca^{2+} facilitated redistribution of PLL within an alginate bead. The presence of Ca^{2+} in the washing solution directly after PLL coating reinforced the underlying alginate gel, initially creating a stiffer capsule. However, once the gel core was liquefied, the resulting membrane was less stiff than capsules exposed only to saline. This was shown by confocal microscopy to be due to a thicker, yet weaker PLL/Alg membrane after Ca^{2+}exposure.

Preliminary results showed that explanted APA capsules were stiffer than capsules incubated *in vitro*, which correlated with overgrowth of the capsules. This may be a useful tool to study the nature and degree of overgrowth on an encapsulation device or production of an extracellular matrix by encapsulated cells.

This chapter shows that this simple and easy set up for micropipette aspiration is a useful technique to study the properties of alginate based capsules. This work demonstrates the sensitivity of the APA capsule properties to small alterations in the procedure. This is a known issue with APA capsules but often underappreciated and it is not always understood how the changes to the procedure could affect the capsule. This paper highlights this aspect of working with APA capsules, in particular with regards to using Ca^{2+} facilitated redistribution of PLL as well as loss of calcium to saline washes.

6.1.2. Summary of chapter 3

In chapter 3, reduced charge density polycations were synthesized with controlled MW using RAFT polymerization of APM and HPM. This chapter explores the uptake of the polycations into alginate beads as a function of MW, charge density and washing procedure using confocal microscopy. Narrow PDI polycations of 10, 25, 50 and 75% APM were synthesized aiming for MWs of 15 and 40 kDa and compared against PLL of 15-30 and 40-60 kDa. It was shown that the APM/HPM polycations would show greater in-diffusion into alginate if the polycation was lower in charge density, MW or washed with a Ca^{2+} containing solution. These factors reduced binding with alginate causing the polycation to be more mobile and diffuse further into alginate beads. Capsules coated with polycations of 50% APM or greater were found to bind well to the alginate beads.

The polycations were also assessed in solution for toxicity against C2C12 myoblast cells and assessed for 3T3 fibroblast cell attachment and proliferation on polycation modified surfaces. The polycations with 25 mol% APM or less were shown to

be non toxic but made poor surfaces for cell attachment. With 75 or greater mol% APM, the polycations were cyto-toxic but made good surfaces for cell attachment and proliferation. When 50% APM was used, the degrees of toxicity and cell attachment depended on the concentration and MW of the polycation. Although polycations with 25% APM or less were biocompatible, they did not form good capsule membranes and thus, polycations containing 50% APM were shown to be a compromise for adequate binding to capsules yet increased biocompatibility, compared to PLL.

This chapter showed the minimum charge density necessary to form capsule membranes using reduced charge density polycations. It also revealed the relationship between the ability of the polycation to bind strongly with anionic surfaces such as alginate or cell membranes and the corresponding toxicity. Thus, the recognition of the need for a compromise between biocompatibility and capsule strength may be the key outcome of these APM/HPM copolymers explored. From this work there were further questions about the mechanical stability of these capsules which were explored in Chapter 4.

6.1.3. Summary of chapter 4

This chapter studies the physical properties of capsules formed with reduced charge density polycations made of 50-75% APM/HPM copolymers compared to APA capsules. This chapter shows that most of the membranes formed with these APM/HPM copolymers had similar permeability to APA capsules but were much less stable. The capsules formed from APM/HPM copolymers were also much more swollen than

analogues APA capsules, showing less resistance to the osmotic pressure of the alginate in the core once calcium begins to be washed away. Most capsules formed with APM/HPM copolymers were not stable to citrate treatment and required a gel core for capsule integrity.

Covalent cross-linking of the APM/HPM capsules using PMV showed some increase in the resistance to citrate treatment, however, covalent cross-linking was shown to only be beneficial to the reduced charge density capsules if there was sufficient amine content at the surface of the capsules. In the case of 50% APM containing polymers, this required that the MW was high enough to form effective bridging cross-links and that the membrane was concentrated at the surface without Ca^{2+} re-distribution.

Testing the citrate treated capsules by aspiration shows that the membranes made with reduced charge density polycations were much softer than those made with PLL. These results also showed that cross-linking due to PMV coating did not increase the stiffness of the capsule membranes, compared to uncross-linked alginate coated capsules.

The capsule membranes thickness formed from PLL was much thicker even though PLL has the highest charge density examined here. Thus, the APM/HPM polycations behave very differently than PLL in APA capsules.

The flexibility of the APM/HPM copolymers may lead to the difference seen in the binding compared to PLL in alginate beads. The stiffness of the capsule membranes made by the APM/HPM copolymers are much softer not only due to the reduced interactions because of the reduced cationic charge, but also due to other factors such as

chain flexibility, hydration and thickness of the membrane. Using PMV to covalently cross-link the membrane, did not result in greater membrane stiffness even though the survival of the membranes exposed to high pH show evidence of covalent cross-linking. Although introducing covalent cross-links would increase the rigidity of the material, substitution of rigid alginate with more flexible PMV may not have strictly additive properties to the membrane stiffness.

Thus, this chapter highlights the challenges in using reduced charge density APM/HPM polycations for stable membranes with this current formulation. Previous work of PEGylated PLL has also shown difficulty in the formation of biocompatible and robust membranes, however the binding of PEGylated PLL to alginate was also limited sterically by PEG.[5] Our system reduced steric interaction by using hydrophilic monomers in the backbone, however the reduced charge density of the APM/HPM polycations still limits binding to alginate, and thus, the overall strength of the these capsules.

6.1.4. Summary of chapter 5

Recent capsule literature gives example of co-encapsulation of anti-inflammatory and other active compounds, sometimes using slow release nanoreservoirs.[6,7] Chapter 5 uses the skills in RAFT copolymerization developed in chapter 3, to prepare thermo-responsive block copolymers by chain extension of p(NIPAM-*co*-*t*BA) macroinitiators with varying lengths of HEA. The self-assembly of these narrow disperse responsive block copolymers above the LCST of the NIPAM-containing block showed reversible formation of phase separated nanoparticles. These nano-particles were covalently cross-

linked to form permanently stable nanoparticles. TEM was used to show that the morphology of these micelles transitions from spheres to rods by decreasing the hydrophilic block length. This behavior is consistent with trends previously observed with other block copolymer systems.

This chapter is significant for showing the morphology of p((NIPAM-*co*-AA)-*b*-HEA) block polymer system can be tuned by varying the HEA block length. Most work in micelle formation from p(NIPAM) block copolymers has directly shown spherical[8,9,10] or vesicle[11,12,13,14,15] morphologies. Observing the transition in morphologies will define boundaries needed to control the self-assembly process for this system. The different morphologies may have different loading capacities and drug release profiles of hydrophobic drugs as well as determine the ability for entrapment in alginate beads.

6.2. Future directions

The results from chapter 4 suggest that the mechanical properties of capsules formed with reduced charge density APM/HPM copolymers and cross-linked with PMV should be additionally reinforced to increase the strength of the capsules. Using Ba^{2+} in the alginate core can help increase the stability of the capsules, by increasing the stability of the underlying network to divalent cation exchange.[16] Thus, the underlying Ba-alginate gel bead will provide the resistance to swelling and the mechanical properties of the capsule, while the hydrophilic membrane of reduced charge density polycations will control the permeability of the capsule.

Building up multi-layer capsules using different MWs of PLL has shown to be useful in controlling the permeability and mechanical properties of capsules.[17,18] Building up multi-layer capsules consisting of different MWs and/or charge densities could lead to capsules with stronger mechanical properties and a biocompatible surface.

The optimized capsules should be tested *in vitro* for biocompatibility prior to assessing biocompatibility *in vivo*. Capsules exposed to whole blood, blood components or peritoneal fluid can be assessed for the binding of proteins, immunoglobulins to the capsule surface and the activation of complement. Attention should be paid to the binding of precursors for inflammation and cellular overgrowth including cell adhesion proteins such as fibronectin and vitronectin, immunoglobulins such as IgG, complement factor C3 and its activation fragments.[4,19,20] The biocompatibility can also be assessed by culture of macrophages in the presence of capsules. The activation of macrophages to release cytokines IL-6, IL-1β and TNF-α will suggest a capsule surface which is not biocompatible.[21] Passing these requirements, the biocompatibility of these capsules could be tested *in vivo* in a small animal model.

It would also be beneficial to characterize the surface of the capsule membrane in accordance with *in vitro* biocompatibility testing. The overall surface charge of membranes from APM/HPM polycations, before and after PMV coating would help understand how the capsule surface charge influences protein adhesion and the biocompatibility of these capsules. This would include zeta potential measurements to determine the surface charge and water contact angle to measure the hydrophilicity.

Capsules should be tested for changes in stiffness after implantation into a host. It was previously observed that the membrane of APA capsules explanted from mice became resistant to NaOH challenge, presumably due to fibrotic overgrowth.[22] It has also be observed that APA capsules which experience proteolytic degradation, were weaker after explanted.[4] Micropipette aspiration performed on capsules with reduced charge density polycations before and after implantation could explain capsule stiffening due to protein and cellular deposits or weakening due to loss of the membrane components.

Other polycations could be synthesized with more rigid backbones or with secondary structures which would increase the rigidity of the polymer and therefore increase the modulus of the membrane material.[23] During complexation, the complementary polyanion can either disrupt or enable the PLL secondary structures (such as an α-helix) in the complex. However, the use of polyelectrolytes with more isotactic content than atactic content are less likely to disrupt these conformations, thus influencing the nature of the polyanion-polycation complex[24] and possibly diffusion into an alginate bead. Tacticity can be controlled in vinylic polymers by optimizing solvent and temperature conditions in the presence of a Lewis acid catalyst.[25] Using isotactic polyelectrolytes with highly regular structures may introduce rigid conformations into a polyelectrolyte membrane, and possibly provide stronger membrane properties.

Further development on drug release from the p(NIPAM) block copolymer micelles synthesized in chapter 5 should be assessed for sustained release of immunosuppressant, dexamethasone, before encapsulating into alginate capsules. Further work could address alternate cross-linking strategies other than EDC, which are not

sensitive to side reactions with higher temperatures such as hydrolysis or conversion to a stable unreactive N-acylurea isomer and can give greater control of the degree of cross-linking.[26] Degradable cross-links could be explored by using cross-linkers containing hydrolysable bonds (esters, hydrazones,[27] acetals,[28] etc.) or reducible di-thiol linkages.[10]

Control over micelle morphology boundaries for polystyrene-polyacrylic acid (PS-PAA) block polymers has been shown to be dependent not only on the ratio of PS to PAA but also on the polymer concentration, rate and total amount of water (non solvent for PS) added to a polymer solution in dioxane (good solvent for both blocks). The thermodynamics and kinetics have been explored, showing reversibility of micelle morphology during thermodynamic control of the phase separation, allowing for the transition of morphologies from spheres to rods to vesicles.[29] The thermodynamic equilibrium/reversibility of the p(NIPAM-*b*-HEA) micelle morphology should analogously be explored at different concentrations, as a function of temperature and the rate of temperature increase. This can be useful to find the conditions necessary (relative block lengths, concentration, temperature) to allow for the formation of all micelle morphologies and polymeric vesicles, which will increase the number of applications for these thermo-responsive materials.

6.3. References

[1] Orive, G.; Hernández, M. A.; Gascón, A. R.; Calafiore, R.; Chang, T. M. S.; De Vos, P.; Hortelano, G.; Hunkeler, D.; Lacík, I.; Shapiro, A. M. J.; Pedraz, J. L. *Nat*. *Med*. **2003,** *9,* 104–107.
[2] Strand, B. L.; Ryan, L.; In't Veld, P.; Kulseng, B.; Rokstad, A. M.; Skjåk-Bræk, G.; Espevik, T. *Cell Transplant*. **2001,** *10*, 263–275.
[3] Tam, S. K.; Bilodeau, S.; Dusseault, J.; Langlois, G.; Hallé, J. P.; Yahia, L. H. *Acta Biomater*. **2011,** *7,* 1683–1692.
[4] Van Raamsdonk, J. M.; Cornelius, R. M.; Brash, J. L.; Chang, P. L. *J*. *Biomater*. *Sci*. *Polym*. *Ed*. **2002,** *13,* 863–884.
[5] Sawhney, A. S.; Hubbell, J. A. *Biomaterials* **1992,** *13,* 863–870.
[6] Bünger, C. M.; Tiedenbach, B.; Jahnke, A.; Gerlach, C.; Freier, Th.; Schmitz, K. P.; Hopt, U. T.; Schareck, W.; Klar, E.; de Vos, P. *Biomaterials* **2005,** *26,* 2353–2360.
[7] Velluto, D.; Manzoli, V.; Tomei, A. A. Development and evaluation of self-assembled biomaterials to maximise the function of conformal encapsulation of pancreatic islets in type 1 diabetes. In *Book of Abstracts*, Proceedings of the 10th World Biomaterials Congress. Montreal, Canada, May 17–22, 2016; P.0259, 1283.
[8] Topp, M. D. C.; Dijkstra, P. J.; Talsma, H.; Feijen, J. *Macromolecules* **1997,** *30,* 8518–8520.
[9] Li, Y.; Lokitz, B. S.; McCormick, C. L. *Macromolecules* **2006,** *39,* 81–89.
[10] Zhang, J.; Jiang, X.; Zhang, Y.; Li, Y.; Liu, S. *Macromolecules*, **2007,** *40,* 9125–9132.
[11] Xu, H.; Meng, F.; Zhong, Z. *J*. *Mater*. *Chem*. **2009,** *19,* 4183–4190.
[12] Li, Y.; Lokitz, B. S.; McCormick, C. L. *Angew*. *Chem*., *Int*. *Ed*. **2006,** *45,* 5792–5795.
[13] Wei, H.; Yu, C.; Chang, C.; Quan, C.; Mo, S.; Chen, S.; Zhang, X.; Zhuo, R. *Chem*. *Commun*. **2008,** *38*, 4598–4600.
[14] Qin, S.; Geng, Y.; Discher, D. E.; Yang, S. *Adv*. *Mater*. **2006,** *18,* 2905–2909.
[15] Wei, H.; Perrier, S.; Dehn, S.; Ravarian, R.; Dehghani, F. *Soft Matter* **2012,** *8,* 9526–9528.
[16]Thu, B.; Bruheim, P.; Espevik,T.; Smidsrød, O.; Soon-Shiong, P.; Skjåk-Bræk, G. *Biomaterials* **1996,** *17,* 1069–1079.
[17] King, G. A.; Daugulis, A. J.; Faulkner, P.; Goosen, M. F. A. *Biotechnol*. *Prog*. **1987,** *3,* 231–240.
[18] Gugerli, R.; Cantana, E.; Heinzen, C.; Von Stockar, U.; Marison, I. W. *J*. *Microencapsul*. **2002,** *19,* 571–590.
[19] Tam, S. K.; de Haan, B. J.; Faas, M. M.; Hallé, J. P.; Yahia, L.; de Vos, P. *J*. *Biomed*. *Mater*. *Res*., *Part A* **2009,** *89A,* 609–615.
[20] Rokstad, A. M.; Brekke, O.; Steinkjer, B.; Ryan, L.; Kolláriková, G.; Strand, B. L.; Skjåk-Bræk, G.; Lacík, I.; Espevik, T.; Mollnes, T. E. *Acta Biomater*. **2011,** *7,* 2566–2578.
[21] Juste, S.; Lessard, M.; Henley, N.; Ménard, M.; Hallé, J. P. *J*. *Biomed*. *Mater*. *Res*., *Part A* **2005,** *72A,* 389–398.
[22] Gardner, C.M.; Potter, M. A.; Stöver, H. D. H. *J*. *Mater*. *Sci*.*: Mater*. *Med*. **2012,** *23*, 181–193.

[23] Schoeler, B.; Delorme, N.; Doench, I.; Sukhorukov, G. B.; Fery, A.; Glinel, K. *Biomacromolecules* **2006,** *7,* 2065–2071.
[24] Tsuchida, E.; Abe, K. *Adv*. *Polym*. *Sci*. **1982,** *45,* 1–119.
[25] Isobe, Y.; Fujioka, D.; Habaue, S.; Okamoto, Y. *J*. *Am*. *Chem*. *Soc*. **2001,** *123,* 7180–7181.
[26] Wang, C.; Yan, Q.; Liu, H.; Zhou, X.; Xiao, S. *Langmuir* **2011,** *27,* 12058–12068.
[27] Shi, Y.; van Nostrum, C. F.; Hennink, W. E. *ACS Biomater*. *Sci*. *Eng*. **2015,** *1,* 393–404.
[28] Huynh, V. T.; Binauld, S.; de Souza, P. L.; Stenzel, M. H. *Chem*. *Mater*. **2012,** *24,* 3197–3211.
[29] Shen, H.; Eisenberg, A. *J*. *Phys*. *Chem*. *B* **1999,** *103,* 9473–9487.